Role of Caveolin-1 for modulating the radiation response in the context of tumor stroma interactions

Inaugural-Dissertation

zur

Erlangung des Doktorgrades

Dr. rer. nat.

der Fakultät für Biologie

an der

Universität Duisburg-Essen

vorgelegt von

Julia Ketteler

aus Velen

August 2019

Die der vorliegenden Arbeit zugrundeliegenden Experimente wurden am Institut für Zellbiologie (Tumorforschung) in der Arbeitsgruppe Molekulare Zellbiologie der Universität Duisburg-Essen durchgeführt.

1. Gutachter: PD Dr. Diana Klein

2. Gutachter: Prof. Dr. Christian Johannes

3. Gutachter: Prof. Dr. Kirsten Lauber

Vorsitzender des Prüfungsausschusses: Prof. Dr. George Iliakis

Tag der mündlichen Prüfung: 07.01.2020

DOI: 10.17185/duepublico/71239
URN: urn:nbn:de:hbz:464-20200805-072031-7

In the context of this doctoral work, the following articles were published:

- Panic A*, **Ketteler J***, Reis H, Sak S, Herskind C, Maier P, Rübben H, Jendrossek V, Klein D. Progression-related loss of stromal Caveolin 1 levels fosters the growth of human PC3 xenografts and mediates radiation resistance. *Scientific Reports* 2017. *equal contribution

- Wiesemann A, **Ketteler J**, Slama A, Wirsdörfer F, Hager T, Röck K, Engel DR., Fischer JW., Aigner C, Jendrossek V, and Klein D. Inhibition of Radiation-Induced Ccl2 Signaling Protects Lungs from Vascular Dysfunction and Endothelial Cell Loss. *Antioxidants & Redox Signaling* 2018.

- **Ketteler J**, Klein D. Caveolin-1, cancer and therapy resistance. *International Journal of Cancer* 2018 doi: 10.1002/ijc.31369 (Epub). Review.

- **Ketteler J**, Panic A, Reis H, Wittka A, Maier P, Herskind C, Yagüe E, Jendrossek V, Klein D. Progression-Related Loss of Stromal Caveolin 1 Levels Mediates Radiation Resistance in Prostate Carcinoma via the Apoptosis Inhibitor TRIAP1. *Jorunal of Clinical Medicine* 2019, *8*, 348.

Manuscript in preparation:

Ketteler J, Leonetti D, Veas Roy V, Wittka A, Estephan H, Maier P, Herskind C, Jendrossek V, Paris F, Klein D. Caveolin 1 dependency of the acid sphingomyelinase/ceramide-mediated radiation-response of endothelial cells in the context of tumor-stroma-interactions.

Table of Contents

1. Summary

The ultimate goal of radiation therapy is to reduce or eliminate tumor burden while sparing normal tissues from long-term injury. However, tumor resistance becomes increasingly aware. In addition, local recurrence of primary tumors and distant metastasis are the leading causes of death in many cancer patients. Herein the high intrinsic sensitivity of normal tissues to ionizing radiation often precludes the application of curative radiation doses. Therefore, further research effort is needed to understand the complex interactions of tumors within their microenvironment and their surrounding (normal) tissue. This is prerequisite for the development of strategies that could either result in normal tissue protection or tumor sensitization to radiation therapy.

Concerning normal tissue protection, the vascular compartment gained attraction, because the endothelial cells were known to be critical determinants of the radiation response and in particular of radiation toxicity in healthy tissues. Own work of the laboratory could show that radiation-induced vascular damage and dysfunction in normal lung tissue supports extravasation of pre-metastatic immune cells and of circulating tumor cells into previously irradiated lung. The pro-invasive cellular activities were accompanied by radiation-induced senescence of bronchial-alveolar epithelial cells and up-regulation of the senescence-associated secretory phenotype (SASP) factor chemokine C-C motif ligand 2 (CCL2), also known as monocyte chemoattractant protein-1 (MCP-1).

In the first work/manuscript, it was hypothesized that this factor with angiogenic activities leads to the stimulation of the hitherto quiescent endothelial cells of the normal tissue upon radiation, which then results in vascular dysfunction (acute effect) and severe endothelial cell loss (late complication). Here, it could be shown that inhibition of CCL2 secreted by irradiated and senescent epithelial cells leads to protection of the vascular components in normal tissue. In more detail, deficiency of the corresponding CCL2 receptor CCR2 or specific inhibition of CCL2 with the inhibitor Bindarit significantly rescued the radiation-induced vascular impairments and subsequent endothelial cell loss. By limiting the radiation-induced endothelial barrier dysfunction, extravasation of circulating immune and tumor cells was significantly reduced and thus inflammation and metastasis were limited. In addition, radiation-induced fibrosis progression was reduced by CCL2 signaling inhibition. Thus, CCL2

signaling inhibition that countered acute and chronic effects of normal tissue toxicity upon radiation treatment is a promising radioprotective strategy.

The vascular compartment is also of potential interest concerning tumor sensitization to radiation therapy. Previous work of the lab revealed that a downregulation of the membrane protein caveolin-1 (CAV1) in endothelial cells resulted in a more activated, angiogenic phenotype which was associated with an increased sensitivity to radiation treatment. In general, CAV1 emerged as a potential biomarker of tumor progression and resistance in numerous solid human tumors and could thus serve as a potential target for sensitizing malignant cells to therapy. Especially, alterations of CAV1 expression in tumor cells and the corresponding microenvironment were shown to be linked to tumor progression and resistance e.g. in prostate cancer.

In the second and third work, it was investigated how a differential CAV1 expression in tumor and stromal cells affected the radiation response of tumors, with a focus on prostate cancer. Whereas a downregulation of CAV1 in radio-resistant CAV1-expressing endothelial and prostate cancer cells resulted in radio-sensitization, CAV1-deficiency in stromal fibroblasts resulted in a more activated, radio-resistant fibroblast phenotype. In particular, CAV1-deficient fibroblasts mediated therapy resistance of prostate cancer xenografts by protecting tumor cells from apoptosis induction. The apoptosis inhibiting protein TP53-regulated inhibitor of apoptosis 1 (TRIAP1), known as p53-inducible cell-survival factor, was identified as a CAV1-dependent secreted factor of activated fibroblast contributing to elevated tumor growth and radiation therapy resistance *in vitro* and *vivo*. Moreover, staining of human prostate cancer tissue revealed an increase in TRIAP1 expression in advanced tumor samples. Conclusively, blocking TRIAP1 activity and avoiding drug resistance may offer a promising drug development strategy to inhibit resistance-promoting CAV1-dependent signals.

In the fourth work, the influence of CAV1 in the radiation response of endothelial cells as well as tumor cells was linked to the ASMase/ceramide pathway. Mechanistically, a reduced CAV1 content of angiogenic and thus more radio-sensitive endothelial cells was linked to increased ceramide levels, in particular to the apoptosis-prone C16 ceramide, resulting from an increased ASMase activity in CAV1-deficient endothelial cells and increased levels of ceramide synthases that were responsible for the generation of C16. The more radio-resistant prostate cancer cells, which were

characterized by a CAV1 upregulation bear more long chain ceramides (C24, C24:1), which were shown to scavenge the apoptosis-inducing effects of C16 ceramide.

Taken together, the present thesis was able to contribute to a better understanding how the tumor-surrounding normal tissue reacts to radiation therapy, and thus provides the basis for the development of radio-protective strategies. Furthermore, mechanistic insights in the stromal-epithelial crosstalk were achieved and molecular targets to possibly improve the outcome of radiotherapy were identified.

2. Zusammenfassung

Das Ziel der Bestrahlungstherapie ist die Reduzierung oder Eliminierung von Tumoren, wobei das Normalgewebe möglichst von Langzeitschäden verschont bleiben soll. Tumor Resistenzen werden jedoch immer häufiger, wobei das Wiederauftreten der Tumore und Metastasten die primäre Todesursache von vielen Krebspatienten ist. Dabei verhindert die hohe intrinsische Sensitivität des Normalgewebes oft die Gabe von einer kurativen Bestrahlungsdosis. Um die komplexen Interaktionen des Tumors innerhalb seiner Mikroumgebung und mit dem umgebenden (normalem) Gewebe zu verstehen, muss die Forschung in diesem Bereich intensiviert werden. Dies ist Voraussetzung für die Entwicklung von Strategien, die in Normalgewebsprotektion oder in Tumorsensibilisierung bei Strahlentherapien resultieren.

Im Hinblick auf die Normalgewebsprotektion ist das vaskuläre System in den Fokus getreten, da Endothelzellen als der bestimmende Faktor der Strahlenantwort, speziell von Strahlungstoxizität im gesunden Gewebe, bekannt sind. Vorherige Arbeiten in unserem Labor haben gezeigt, dass strahlen-induzierte vaskuläre Schäden und Dysfunktionen im Lungengewebe den Ausbruch von pro-metastasierenden Immunzellen und zirkulierenden Tumorzellen in zuvor bestrahlten Lungen fördern. Die pro-invasiven zellulären Aktivitäten gehen mit strahlen-induzierter Seneszenz der bronchial-alveolaren Epithelzellen und einer Hochregulierung von dem Seneszenz-assoziierten sekretorischen Phänotyp (SASP) Faktor Chemokin C-C Motiv Ligand 2 (CCL2), auch bekannt als Monocyte chemoattractant Protein-1 (MCP-1) einher.

Die Hypothese in der ersten Publikation beruht darauf, dass dieser Faktor mit angiogenen Aktivitäten zu der Stimulation durch Strahlung von bisher ruhenden Endothelzellen im Normalgewebe führt, woraus vaskuläre Dysfunktionen (akuter Effekt) und eine schwerwiegende Verminderung von Endothelzellen (späte Komplikation) hervorgehen. Es wurde gezeigt, dass die Inhibition von CCL2, das von bestrahlten und senszenten Epithelzellen sekretiert wird, zu einer Protektion des vaskulären Systems im Normalgewebe führt. Es wird somit, durch das Fehlen des korrespondierenden CCL2 Rezeptors CCR2 oder die spezifische Inhibition von CCL2 mit dem Inhibitor Bindarit, die strahlen-induzierte vaskuläre Schädigung und folglich der Verlust von Endothelzellen kompensiert. Durch die Limitierung der strahlen-induzierten Dysfunktion der endothelialen Blockade, wurde der Ausbruch

zirkulierender Immun- und Tumorzellen signifikant reduziert und dadurch die Inflammation und Metastasen Bildung verringert. Außerdem wurde die strahlen-induzierte Fibrose-Entwicklung durch CCL2-Inhibierung verringert. Die CCL2-Signal Inhibition, die den akuten und chronischen Effekten der Normalgewebstoxizität nach Strahlentherapie entgegenwirkt, ist somit eine potentielle strahlen-protektierende Strategie.

Das vaskuläre System ist bei der Tumor Sensibilisierung mit Hilfe der Strahlentherapie ebenfalls von potentiellem Interesse. Vorherige Arbeiten im Labor zeigten, dass eine Herunterregulierung des Membranproteins Caveolin-1 (CAV1) in Endothelzellen zu einem vermehrt aktivierten, angiogenem Phänotyp führt, was mit einer erhöhten Sensitivität auf die Strahlentherapie einhergeht. Generell zeigte sich, dass CAV1 in vielen soliden humanen Tumoren als ein potentieller Biomarker für Tumor Progression und Resistenz genutzt werde kann. Damit besitzt CAV1 das Potenzial für die Sensibilisierung von malignen Zellen in Therapien. Speziell die Veränderungen der CAV1 Expression in Tumorzellen und dem dazugehörigen Umfeld konnten z.B. im Prostatakarzinom, mit Tumor Progression und Resistenzen in Verbindung gebracht werden.

In der zweiten und dritten Publikation wurde die differentielle CAV1 Expression in den Tumor- und Stromazellen im Hinblick auf die Strahlenantwort im Tumor untersucht. Hierbei wurde sich auf das Prostatakarzinom fokussiert. Die Herunterregulierung von CAV1 führt in Endothel- und Prostatatumorzellen zu einer strahlen-induzierten Sensibilisierung, während ein CAV1-Defizit in stromalen Fibroblasten zu einem aktivierten, strahlenresistenten Phänotyp führt. Insbesondere vermitteln die CAV1-defizienten Fibroblasten eine Resistenz gegenüber der Strahlentherapie an Prostatakarzinom Xenograft Tumoren, wodurch die Apoptose Induktion verringert wird. Das Apoptose inhibierende Protein TP53-regulated inhibitor of apoptosis 1 (TRIAP1), auch bekannt als p53-inducible cell-survival factor, wurde als CAV1-abhängiger sekretierter Faktor in aktivierten Fibroblasten identifiziert, der zu einem erhöhten Tumorwachstum und einer Resistenz gegenüber der Strahlentherapie *in vitro* und *in vivo* beiträgt. Außerdem zeigte die Färbung von humanem Prostatakarzinomgewebe eine erhöhte TRIAP1 Expression in fortgeschrittenen Tumorproben. Dementsprechend würde das Blockieren der TRIAP1 Aktivität und ein Verhindern der Therapieresistenz eine vielversprechende Therapie Strategie darstellen, um die Resistenz-fördernden CAV1-abhängigen Signale zu inhibieren.

Im vierten Manuskript wurde der Einfluss von CAV1 auf die Strahlenantwort der Endothel- und Tumorzellen im Zusammenhang mit dem ASMase/Ceramid Signalweg untersucht. Mechanistisch wurde hierbei gezeigt, dass ein reduzierter CAV1 Gehalt in angiogenen und somit strahlensensitiven Endothelzellen mit erhöhten Ceramid Mengen, speziell mit dem Apoptose-induzierendem C16, in Verbindung steht. Dies basierte auf einer erhöhten ASMase Aktivität in den CAV1-defizienten Endothelzellen und erhöhter Expression von Ceramid Synthasen, die verantwortlich für die Produktion von C16 sind. Die vermehrt strahlenresistenten Prostata Krebszellen, die durch eine Hochregulierung von CAV1 charakterisiert wurden, enthalten eine vermehrte Anzahl an langkettigen Ceramiden (C24, C24:1), die in der Lage sind die Apoptose-induzierenden Effekte von C16 zu neutralisieren.

Zusammenfassend zeigt sich, dass diese Arbeit zu einem verbesserten Verständnis der Strahlenantwort von Tumor-umgebenden Normalgewebe beiträgt und dementsprechend eine Basis für die Entwicklung von strahlen-protektierenden Strategien darstellt. Außerdem wurden mechanistische Erkenntnisse im Zusammenhang mit stromal-epithelialen Crosstalk erreicht und molekulare Targets identifiziert, die ein erhöhtes Potenzial zur Verbesserung des Ergebnisses der Strahlentherapie aufweisen.

3. Introduction

3.1 Radiation Therapy in Cancer Treatment

Cancer is the second leading cause of human death worldwide and cancer incidence is predicted to increase from 18 Million cases in 2018 to almost 30 Million in 2040 (24, 54). Although new treatment strategies have been established during the last decades, overall survival especially for aggressive and therapy resistant cancer entities stays low (24, 54). Therefore, new treatment strategies are needed to overcome resistance and achieve tumor control or even cure.

The standard treatment options to treat cancer are surgery, chemotherapy and radiation therapy (RT). To assure the best treatment outcome and quality of life a combination of these treatment modalities is most often used (100). Herein, more than half of cancer patients receive RT during their treatment schedule (39). Radiation used for cancer therapy (ionizing radiation, IR) is energy that is high enough to form ions (electrically charged particles) in cells of the tissues it passes through (11). The deposited energy then damages genes of a cancer cell (induction of DNA double strand breaks (DSB)), so that it is unable to grow or divide. The induction of DNA DSB was further shown to be responsible for tumor cell death upon IR treatment (115). The energy of e.g. photons generates an ionizing effect leading to the formation of oxygen-free radicals that in turn damage the DNA double strands, either directly or indirectly by interacting with water molecules (145). These radicals than have the capacity to further damage processes in the cell that lead to increased stress response. Thus RT acts predominantly on rapidly dividing cancer cells, but it can also affect dividing cells of normal tissues. Different sources of radiation can be applied: (i) most widely used photons (x-rays and gamma rays), or (ii) particle radiation (electrons, protons, neutrons, alpha/beta particles). These types of radiation bear different energies and thus differ in their ability to penetrate tissues. The main goal of RT is to kill cancer cells and shrink tumors (achieve the best tumor control) while sparing normal tissues (Figure 1).

Although treatment strategies improved during the last decades, normal tissue toxicity still limits the applied dose of RT. Sparing of the normal tissue is achieved by using improved treatment protocols such as fractionated therapy and technically improved imaging devices to monitor the tumor when delivering the dose (15).

However, the radiation dose needed for tumor cure is often greater than the maximum tolerated dose and thus acute and chronic normal tissue toxicities remain as dose limiting factors in RT (100). Therefore, current research aims to increase the therapeutic window (Figure 1).

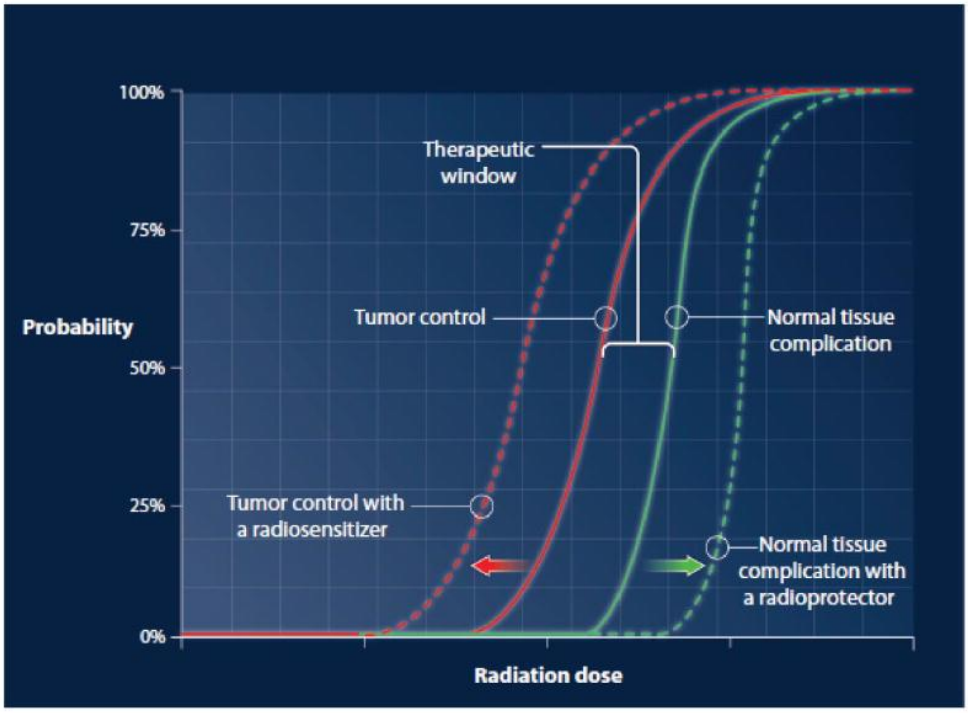

Figure 1: The "therapeutic window" in RT. The radiation dose that is needed to achieve a high probability of tumor control (red line) is inducing normal tissue toxicity (green line). The difference between tumor control probability and normal tissue complication probability is called "the therapeutic window". To broaden this therapeutic window, there are already a number of advances made by technology such as image-guided or intensity-modulated RT to bring the radiation doses precisely and safely to the tumor while the surrounding normal tissue is best preserved. But there are also a number of biological approaches: Such as the modulation of the intrinsic radiation sensitivity of the tumor cells or the modulation of the tumor stroma (to push the red curve further to the left) or just the modulation of the normal tissue by radioprotection (to push the green curve further to the right) Source: Liauw et al., 2013 (100).

One of the hallmarks of cancer is the ability to conquer apoptosis and obtain cell survival that fosters therapy resistance (63). In order to achieve this switch, tumor cells need inhibitors of apoptosis as one possible option to escape cell death. This intrinsic radio-resistance of tumor cells varies widely and can be affected by mutations or tumor hypoxia.

Identification of differentially expressed genetic factors, as well as mircoenvironmental changes compared to normal tissue are one option to succeed in therapy sensitization and protection of normal tissue (13). Accordingly, to widen the therapeutic window, either research on radioprotectors has to be carried out, or new target molecules for radio-sensitization of the tumor cells have to be identified (13).

3.2 The Membrane Protein Caveolin-1

Caveolin-1 (CAV1) is an integral plasma membrane protein that acts as the main component to form caveolae. Caveolae are 50 - 100 nm long invaginated flask shaped parts of the membrane and can be found in almost every cell type (129). They were first described by electron microscopy due to their significant shape and have been shown to play a pivotal role in endocytosis, cholesterol metabolism and signal transduction (92, 104, 105, 185). Caveolae are most frequently found in cells of the stromal compartment, such as endothelial cells, fibroblasts and smooth muscle cells and are heterogeneously distributed in the membrane (124, 154, 156). Next to CAV1 oligo-homodimers, caveolae are rich in sphingolipids, phospholipids, cholesterol and Cavin-1 (72, 129). Caveolae itself are important for membrane heterogeneity and part of the liquid ordered phase in the plasma membrane that marks a platform for signaling molecules. The liquid ordered phase contains planar and non-planar lipid rafts, whereas the non-planar rafts are referred to as caveolae (112). Caveolae-mediated endocytosis can be triggered by mechanical or oxidative stress, as well as several growth factors. This in turn leads to regulation of signaling pathways by the transmission of extracellular signals into intracellular pathways (121, 137, 160, 191). Integrins and glycosphingolipids are examples of molecules internalized by caveolae-dependent endocytosis, whereas also fatty acids can be taken up by binding to CAV1 in caveolae (32, 113).

CAV1 itself can act as a key player in signaling pathways, for example by inhibition of signaling molecules or internalization of growth factors. Herein, the structure of CAV1 plays an important role (Figure 2). CAV1 is a 21 – 24 kDa protein containing 178 amino acids (144). There are three different types of Caveolin: Caveolin 1, 2 and 3 (CAV1, 2, 3), that have common features but are differently distributed in cell types. CAV1 and CAV2 are co-localizing in various cell types, whereas CAV3 is specific for muscle cells (150, 166). CAV1 contains a hydrophobic domain that is inserted into the plasma membrane with a hairpin-shaped conformation. C- and N-terminus of the protein are both directed to the cytosol and contain several functional domains. One highly conserved functional domain of CAV1 is the caveolin-scaffolding domain (CSD; residues 82-101). This domain can bind proteins and thus inhibit signaling. It has been shown that important kinases and receptors as for example SRC, eNOS, HRAS or epidermal growth factor receptor (EGFR) are bound to the CSD, which

in turn blocks their signaling capacity and leads to cell growth inhibition (37, 49, 60, 95). Furthermore, CAV1 is an important cholesterol-binding protein that can intracellularly transport cholesterol between cell organelles, such as Golgi and mitochondria (116, 128). CAV1 contains two distinct phosphorylation sites: tyrosine Y14 and serine S80. Phosphorylation at Y14 (located at the N-terminus) facilitates binding of CAV1 with SH2 domains of proteins, such as SRC and is important for caveolae-mediated endocytosis. Y14 is phosphorylated by cSRC kinase that can bind CAV1 at the C-Terminus where three cysteine residues are subject to palmitoylation (94). Internalization of CAV1 into the cytoplasm results in growth stimulation by EGFR activation or pro-survival signaling via PI3K/AKT pathway (94, 180). S80 phosphorylation (located close to the CSD) enables CAV1 to bind to the endoplasmic reticulum and allows the protein to enter the secretory pathway (180).

Thus, CAV1 either alone or caveolae-dependent alters and regulates many cellular processes, e.g. cell cycle regulation (53, 57), proliferation and cell death induction (49, 114, 169, 184) up to metabolic changes, membrane composition and lipid homeostasis (12, 56, 68).

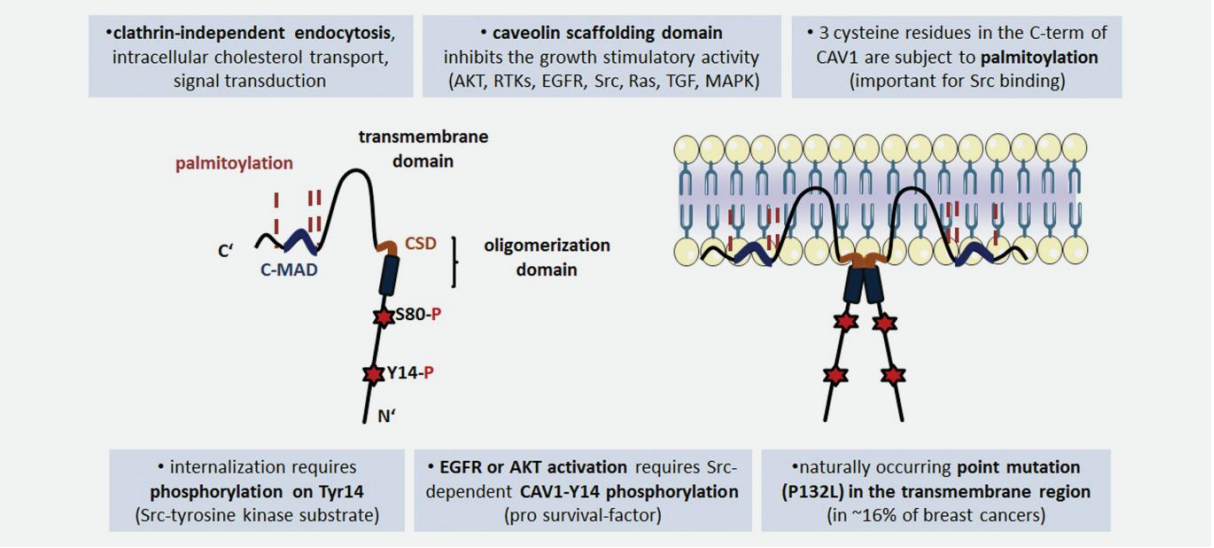

Figure 2: Schematic overview of the CAV1 protein structure (left) and of the homodimer localization in the plasma membrane (right). The CAV1 protein bears several functional domains: CAV1 can be palmitoylated close to the C-terminus or phosphorylated at two distinct sites closer to the N-terminus in the cytoplasm (Serine 80 and Tyrosine 14, stars). Next to the transmembrane domain, the highly conserved caveolin-scaffolding-domain (CSD) is located. The CSD is part of the oligomerization domain that is needed for building up caveolae. Source: Ketteler and Klein, 2018 (83).

3.2.1 CAV1 and Cancer

CAV1 was found to be upregulated or mutated in a variety of solid human tumors and therefore came into focus of cancer research. It was shown to be overexpressed e.g. in pancreatic cancer, glioblastoma, renal cell cancer, esophageal squamous cell carcinoma and prostate cancer (2, 28, 33, 165, 186). Herein, increased CAV1 expressions at advanced tumor stages conferred with poor prognosis, increased metastatic potential and treatment resistance (2, 83, 165, 179). However, the role of CAV1 in cancer remains controversial since the CAV1 expression levels vary widely between different tumor entities (112). In head and neck cancer an upregulation of CAV1 is associated with less aggressive tumors due to suppression of metastasis and growth (187). In contrast, the CAV1 gene is located on a putative tumor suppressor locus (Chromosome 7, q31.1-31.2) which is frequently deleted or mutated in human cancers (50, 141). One example is the rather common P132L mutation of the CAV1 gene in invasive breast carcinoma. The dominant negative mutation P132L is present in around 15% of analyzed breast cancer cases and was shown to activate the mitogen-activated protein-kinase signaling (MAPK) pathway further influencing the invasion activity of breast cancer cells (21, 69). Of note, it has been shown that a CAV1 downregulation in early cancer stages fosters a hyper-proliferative state of the cells, as well as increased angiogenic capacity and tumor progression (30, 177, 178). Therefore, it is hypothesized that early loss of CAV1 contributes to transformation of cells, consequently leading to tumor formation and progression (88). Later on, during tumor progression and in advanced tumor stages the observed (re-)expression of CAV1 is closely connected to metastasis formation and the resistance to chemo- and RT (83). However, the impact of CAV1 in tumor development and prognosis is strongly dependent on the tumor entity, the tumor state, the tumor microenvironment and the cell type.

3.2.2 CAV1 and Prostate Cancer

Prostate cancer is the second most diagnosed cancer and the fifths leading cause of death in men as recently analyzed by the global cancer statistics (GLOBOCAN) in 2018 (24). The incidence of prostate cancer is highest in North America, Europe and Australia, whereas Asian and African countries display a lower

frequency of diagnosis (54). This is presumably due to advanced prevention screenings in high incidence regions. Moreover, incidence of prostate cancer increases significantly with age and reaches an incidence rate of almost 60% in men older than 65 (54, 139). Pathological transformations in the prostate are diagnosed by testing elevated levels of the prostate-specific-antigen (PSA) in the blood. This glycoprotein is usually expressed by prostate tissue, however increased levels (>4 ng/ml) imply prostate cancer. Additionally, a biopsy is taken to ensure a pathological finding. The most common type of prostate cancer is the so-called acinar adenocarcinoma that can be characterized and graded by the Gleason Score (7, 51). The Gleason Score consists of a primary score referring to the dominant pattern in the tumor biopsy, and a secondary score pointing out the second most common pattern. The final Gleason Score is comprised by addition of the two scores (51). The higher the score, the more difficult and extensive treatment strategies are needed to medicate the cancer. In most cases of prostate cancer, radical prostatectomy (removal of the prostatic gland) is used as a first stage treatment. Further on, RT, chemotherapy and surgery are applied (82). Yet, these advanced stages of prostate cancer display an increased resistance to chemo- and RT treatment. Thus, it is important to identify new molecular targets for (re-) sensitizing prostate tumors to therapy.

Prostate cancer is one of the cancer entities, which is characterized by increased CAV1 expression levels upon tumor progression (43, 81). In particular, CAV1 expression is increasing in the malignant epithelial cells during the course of cancer progression and it has even been suggested as a biomarker for prostate cancer progression (81). Of note, it could be shown that CAV1 also plays an important role in the tumor microenvironment.

3.3 CAV1 and the Tumor Microenvironment

The tumor microenvironment plays a pivotal role in tumor progression, tumor growth and therapy resistance (17, 18, 64). Under normal conditions, the stroma can act as a barrier against malignant transformation of cells. On the contrary, during tumor formation malignant epithelial cells form their own environment by modulating/activating and recruiting non-tumoral cells (64). Herein, fibroblasts endothelial cells (EC) and immune cells are the most abundant cells of the tumor stroma. However, the tumor cells also recruit mesenchymal stem cells for maturation

or lymphatic EC for the formation of lymphatic vessels (107). Environmental changes, such as hypoxia or modulation of the extracellular matrix (ECM), further contribute to therapy resistance.

Importantly, the increase of CAV1 expression in malignant epithelial cells, as well as increased survival PI3K/Akt signaling, was paralleled by loss of CAV1 in the stroma of advanced prostate tumors. This further correlated with reduced relapse-free survival (5, 43). In particular, fibroblasts, which are most abundant in the stroma, display a significant switch of CAV1 expression during tumor progression. In low graded Gleason Score tumors, fibroblasts express high CAV1 levels, but as soon as the tumor progresses and reaches higher Gleason Scores CAV1 expression diminishes in stromal fibroblasts (Figure 3) (84). However, the vascular compartment is spared from those CAV1 alterations. It remains elusive how the switch of CAV1 expression is preceded. Although CAV1 is predominantly anchored in the plasma membrane it can also be secreted after phosphorylation. Of note, prostate cancer patients show an upregulated CAV1 secretion in the serum correlating with pro-angiogenic activities and also linking CAV1 secretion to tumor growth and cell survival (162-164).

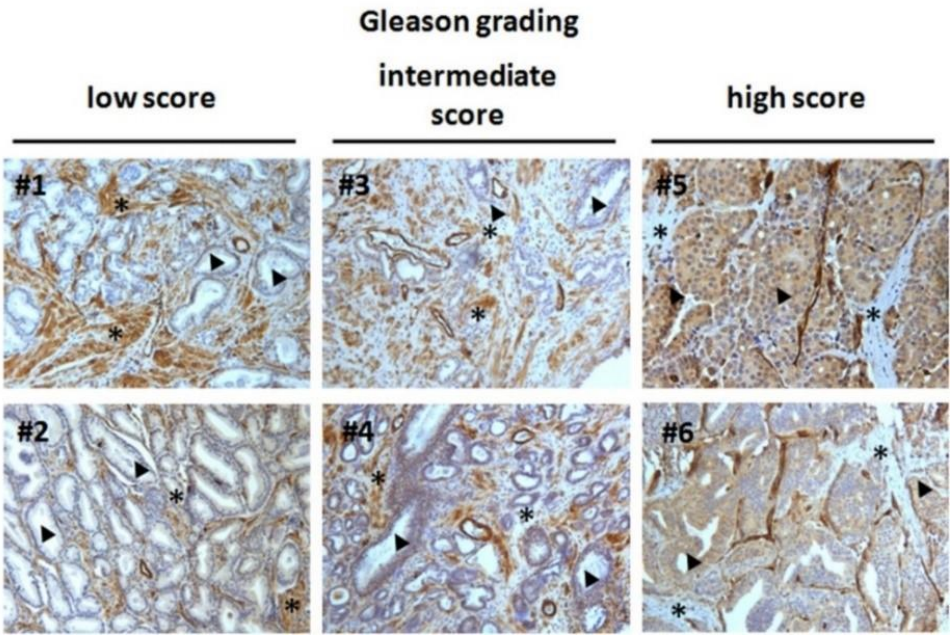

Figure 3: Immunohistochemical staining of CAV1 in different stages of human prostate carcinoma specimen. In the low score Gleason graded tumor CAV1 is highly expressed in the tumor stroma (asterisks), whereas epithelial cells show low or no CAV1 expression levels (arrows). The tissue samples of the high scored Gleason graded tumors show an elevated expression of CAV1 in malignant epithelial cells and moreover a significant downregulation of CAV1 expression in the tumor stroma, particularly in fibroblast rich regions. Source: Klein et al., 2015 (84).

3.3.1 CAV1 and Fibroblasts

Fibroblasts are one of the most abundant type of cells in the tumor stroma and thus have a large impact on the survival and growth of tumorigenic tissue. Fibroblasts are important for the remodeling of connective tissue in the ECM. Depending on their activation status, these cells play different roles in the environment of tumors (148). Although fibroblasts are shown to be beneficial for therapy in early stages of cancer and act as a natural barrier for the tissue, activation of the cells by the tumor can lead to an oppositional effect. Activated fibroblasts in tumors, also called cancer associated fibroblasts (CAFs) can undergo dynamic changes and increase their proliferative potential with tumor progression (16).

CAFs affect tumor progression, development and metastasis by the Reverse Warburg effect that was described by Pavlides et al. (131). Mechanistically, high energy metabolites, such as lactate and pyruvate are transferred from CAFs to neighboring malignant epithelial cells. The tumor cells then undergo metabolic changes towards an increased oxidative mitochondrial metabolism. This in turn leads to increased ATP production, accelerating growth and metastatic potential of the tumor cells (131). Interestingly, the loss of CAV1 in activated fibroblasts is one important step driving the Reverse Warburg effect. Furthermore, it has been shown that the loss of CAV1 in tumor stroma contributes to the formation of CAFs and is associated with poor clinical outcome and therapy resistance. Downregulation of CAV1 and autophagic destruction of mitochondria leads to oxidative stress in fibroblasts that decreases mitochondrial oxidative phosphorylation and increases glycolysis. Moreover, activation of transformation growth factor β (TGFβ) contributes to the induction of a CAF-like phenotype (111). The induced phenotype conclusively drives ECM remodeling to facilitate an angiogenic switch in the tumor allowing invasion and metastasis, as well as an induction of epithelial-mesenchymal transition (EMT) (62, 111, 170). Besides prostate cancer, it was also shown in the stroma of breast cancer that low CAV1 expression levels correlate with aggressive tumor progression and poor clinical outcomes (153, 181, 182). Moreover, the loss of CAV1 in the stroma of gastric cancer and melanoma goes along with reduced relapse-free survival, poor prognosis and tumor aggressiveness (183, 189).

3.3.2 CAV1 and Endothelial Cells

The tumor vasculature is crucial for tumor growth and invasiveness and has to be (re-)build frequently (tumor neovascularization). Therefore, the cells important for vascularization are prominently present in tumor stroma. Endothelial cells (EC) build up the blood vessels and are accordingly most important for tumor-associated vascularization (34, 134). The increasing demands for oxygen and nutrition of the rapidly growing tumor cells thus require new vessel formation, a phenomenon which is called the angiogenic switch. Tumor cells release pro-angiogenic factors, such as vascular-endothelial growth factors (VEGF) and fibroblasts growth factors (FGF) that deactivate the quiescent state of neighboring EC and recruit these cells to its side (angiogenesis). Finally, new vessel formation is a combined process of angiogenesis and post-natal vasculogenesis (87, 117, 174). Subsequently, vascular mural cells are recruited to cover the sprouts; pericytes stabilize the newly generated vessels, and further on smooth muscle cells maintain the construct (27, 78).

The role of CAV1 in EC for tumor progression and therapy survival is not fully understood. It is known that CAV1 is expressed in normal EC and does not change during tumor progression in tumor associated EC of the microenvironment (84). Of note, a downregulation of CAV1 was shown to induce a de-regulated tumor vascularization and furthermore to sensitize EC to apoptosis after IR. Thus, CAV1 downregulation contributes to an improved outcome of RT in pre-clinical model (prostate cancer xenograft model) (84). Moreover, CAV1-deficient mice tend to display an increased tumor growth that goes along with angiogenesis and microvascular permeability (103). Dewever et al. showed in a melanoma mouse model that tumor vessel maturation is dependent on CAV1. In $CAV1^{(-/-)}$ mice mural cells fail to stabilize the newly generated blood vessel and thus reduce tumor vessel maturation (42).

Conclusively, there is much evidence that the interaction between malignant epithelial cells, stromal cells and the components of the ECM largely supports tumor formation and therapy resistance. Therefore, the complete tumor microenvironment and the stromal-epithelial crosstalk has to be considered for developing new therapeutic strategies (63, 64).

3.4 CAV1 and Radiation Therapy

Therapy resistance and in particular RT resistance in advanced tumor stages is one of the biggest challenges in cancer treatment nowadays. The impact of CAV1 on therapy resistance has been studied extensively during the last years, but the complete molecular mechanisms behind CAV1-induced/dependent resistance remain elusive. Several studies could show that CAV1 expression is upregulated after treatment with IR and confers with radio-resistance. Therefore a downregulation of CAV1 in tumor cells was hypothesized to sensitize these cells to RT and indeed a downregulation was shown to overcome radiation resistance of e.g. pancreatic cancer cells, prostate cancer cells and breast cancer cells (10, 35, 70, 84, 194). Of note, CAV1 expression could also be a sensor for chemotherapy resistance. Again a downregulation of CAV1 was shown to overcome resistance against chemotherapeutics in a variety of tumor types, e.g. renal carcinoma, non-small cell lung carcinoma (NSCLC) or colorectal cancer (73, 83, 98, 126).

Moreover, radiation was shown to induce phosphorylation of the CAV1 protein going along with EGFR signaling and internalization to the nucleus (46). CAV1 can be phosphorylated by cSRC on Tyr14, leading to activation of EGFR. It has been shown that this process can be induced by IR in squamous cell carcinoma and human bronchial cells and conversely inhibition of SRC is reversing these effects (46). The CAV1-dependent EGFR shuttling to the cell nucleus induces phosphorylation of the major repair pathway protein DNA-PK (46). CAV1 is even participating in DNA double strand break repair which is the most frequent IR-induced damage in cells. Zhu et al. showed that CAV1 is involved in both major pathways of DNA damage repair: Non homologous end joining (NHEJ) and homologous recombination (HR) (190). Hereby, CAV1 silencing led to a reduced phosphorylation of DNA-PK which affects the onset of NHEJ. Furthermore, they could depict that downregulation of CAV1 also leads to reduced activation of HR. Moreover, it was demonstrated that CAV1 expression in brain metastasis of lung cancer patients has an impact on RT resistance (48). Upregulated CAV1 predicted a worse RT outcome and decreased overall survival. A similar finding was presented by Rodel et al., where low CAV1 expression levels in colorectal cancer favored beneficial therapy outcome and increased overall survival of patients (142). Recently, an underlying mechanism was identified that could be linked again to DNA damage response. The tyrosine kinase receptor TIE2 is able to recruit the proto-oncogene ABL1, which in turn leads to onset of the DNA repair pathway

machinery. Furthermore, TIE2 can build a complex with CAV1 leading to caveolae-dependent endocytosis and nuclear translocation of the complex further increasing DNA damage response and therefore radiation resistance (75, 76).

Besides sensitization of malignant epithelial cells by CAV1 downregulation, it was as well hypothesized that a reduction of CAV1 expression in stromal EC leads to radio-sensitization of the stromal compartment, since EC are spared from differential CAV1 expression levels during tumor progression (84). Of note, xenograft tumors grown on a CAV1-deficient background ($CAV1^{-/-}$ mice) showed a pronounced effect after RT in comparison to wildtype (WT) mice. A similar effect was also observed *in vitro*, where CAV1 downregulation in EC resulted in an increased apoptosis induction and decreased clonogenic survival (84). However, the CAV1-deficient background in mice led to elevated growth of those tumors hinting to a potential risk of targeting CAV1, possibly due to the fibroblastic compartment (84, 122). Thus, a treatment strategy of simply targeting CAV1 to promote sensitization may not be a promising alternative. A better understanding of CAV1-mediated signaling between tumor and stroma in the context of radiation resistance is urgently needed to identify molecular targets for secure treatment strategies of those tumors.

3.5 Radiation-induced Normal Tissue Complications

3.5.1 Radiation-induced Vascular Damage

Although radiation for cancer treatment is carefully measured and highly controlled, current RT techniques expose not only tumors to the energy of radiation, but even substantial amounts of normal tissue are potentially irradiated (14, 61, 100). Radiation of normal tissues in turn can lead to severe side complications, which are the basis for radiation-induced secondary malignancies, e.g. local recurrence of primary tumors and distant metastasis (23, 152, 172). Thus, radiation-induced normal tissue damage in particular of tissues with a high intrinsic radio-sensitivity can be distinguished into acute and late effects that limit the application of curative radiation doses. The lung is a very radiation sensitive tissue. Lung irradiation induces inflammation and fibrosis as dose limiting side effects of breast irradiation in the RT of thoracic associated cancers, or whole body irradiation in preparation for bone marrow transplantation (85, 86). Here, the underlying molecular mechanisms are not well

understood yet and there is no effective or radioprotective treatment option. Therefore, it is important to understand the underlying mechanisms of normal tissue toxicity in order to establish treatment strategies that can rationally minimize late effects and maximize a survivor's quality of life (4, 23, 130).

The homeostasis between infiltrating immune cells and cells of the vascular compartment is carefully maintained upon normal or healthy conditions. The current perspective is that RT response of the normal tissue leads to a deregulated and disturbed homeostasis between the resident parenchymal, mesenchymal and vascular cells as well as penetrating immune cells (1, 25, 146). Increasing evidence suggests that radiation-induced normal tissue damage is closely associated with damage to the vascular system and its dysfunction (8, 36, 74, 125, 138). EC apoptosis plays a major role in late tissue toxicity while acute EC damage influences vascular leakage and infiltration of immune cells. This in turn fosters radiation-induced injuries and secondary malignancies (8, 90, 125). Especially in radiation-induced normal tissue toxicity in the lung, RT activates EC resulting in vascular dysfunction (acute phase) and severe EC loss (late tissue complication), thus leading to radiation-induced senescence of lung resident epithelial cells (85, 86). Herein, chemokines and their receptors evolved as important mediators of EC activation and dysfunction finally leading to acute leukocyte attraction and extravasation at damaged tissue sites (143, 193). Increased levels of chemokines can further contribute to chronic inflammation as well as cancer development (192). The tumor and its microenvironment produce elevated levels of chemokines in order to alter proliferation signaling and invasion. The chemokine C-C motif ligand 2 (CCL2) came into focus of cancer research due to its role in cancer progression and metastasis (93, 101). CCL2 is expressed by many cells of the tumor such as epithelial, EC or fibroblasts and is among the factors of the senescence-associated secretory phenotype (SASP) (41). It has been shown that increased tumoral CCL2 levels confer with metastasis and migration in several solid human tumors such as prostate and colorectal cancer by promoting tumor growth, angiogenesis and invasion (77, 188). Interestingly, CCL2 has the ability to recruit stromal cells to tumor sites. Therefore, inhibition of CCL2 signaling by targeting CCL2 directly or its corresponding receptor CCR2 could be a potential target to limit metastasis formation and tumor growth. Furthermore, CCL2 is upregulated in senescent normal tissue lung epithelial cells after radiation. Accompanied radiation-induced vascular dysfunction and severe EC loss could be normalized by applying mesenchymal stem cells as radioprotective strategy (85, 86). Therefore, inhibition of

CCL2 signaling could in addition be used to limit radiation-induced normal tissue toxicity.

3.5.2 Radiation-induced Signaling Mechanism in EC

One critical factor of normal EC is to ensure quiescence of the homeostasis between inflammatory response and immune control by preventing signaling for leukocyte attraction (79, 159). Upon activation, EC are able to influence leukocyte recruitment into tissues by the expression of adhesion molecules and chemokine release. Various processes are sufficient to activate EC directly or indirectly, such as circulating inflammatory cytokines, e.g. tumor necrosis factors (TNF) and interleukins (IL). Further on, reactive oxygen species (ROS) and therefore radiation induce activation of EC, whereas also oxidized low density lipoproteins, autoantibodies and environmental risk factors influence this process (159). A continuing activation of the endothelium over time can be linked to dysfunction of microvascular barrier integrity, resulting in vascular injury and can finally end with a progression to EC apoptosis (87, 99).

One essential signaling mechanism in the cellular response to stress stimuli is the p38/MAPK signaling pathway (118). This pathway plays a particular role in EC as a major target of radiation. In addition, the p38/MAPK pathway was linked to the ceramide pathways especially in IR treated EC. Bioactive sphingolipid ceramide generated by acid sphingomyelinase (ASMase) contributes to stress induced EC apoptotic death (Figure 4) (118). In general, the family of sphingolipids has been shown to act as bioactive lipids and second messenger molecules regulating several cellular processes and signal transduction in human cells (67, 157, 158). Herein, the sphingolipid ceramide came into focus of research since it influences apoptosis, proliferation and differentiation of cells after stress induction (66, 67). Ceramide is generated by cleavage of sphingomyelin by the enzyme ASMase or *de novo* synthesis by metabolizing serine and palmitoyl-CoA (89, 132). Pro-apoptotic activity of ceramide is well known. Therefore, application of exogenous ceramide derivative or its endogenous suppression is used to impair cancer progression. (65, 102, 120). However, the tumor itself suppresses the function of ceramide generation by inhibiting ASMase activity, lowering ceramide generation and hereby escapes apoptosis induction (147).

In contrast, ASMase is highly abundant in EC and has been shown to play a role in radiation-induced cellular stress response and EC apoptosis after single dose radiation (20, 108, 125). Apoptosis induction in EC has already been shown to be CAV1-dependent. Additionally, apoptosis can be mediated by ASMase/ceramide pathway that in turn can affect either the radiation response of tumors, and/or of normal tissues (58, 125). Under physiological conditions ASMase is located in lysosomes. Upon stress induction, e.g. radiation, ASMase is translocated to the plasma membrane, where it cleaves its target sphingomyelin and produces ceramide. Ceramide itself then generates large lipid raft formations that act as a major platform for signal transduction at the plasma membrane (Figure 4) (118). Although, this pathway takes place at the plasma membrane and includes the need of lipid rafts up to date only a single publication could link caveolae and CAV1 to the ASMase/ceramide pathway. Zundel et al. showed that ceramide-dependent recruitment of CAV1 to large lipid platforms impaired survival signaling of the PI3K kinase. Inhibition of CAV1 counteracted the impairment and PI3K signaling was subsequently increased (195).

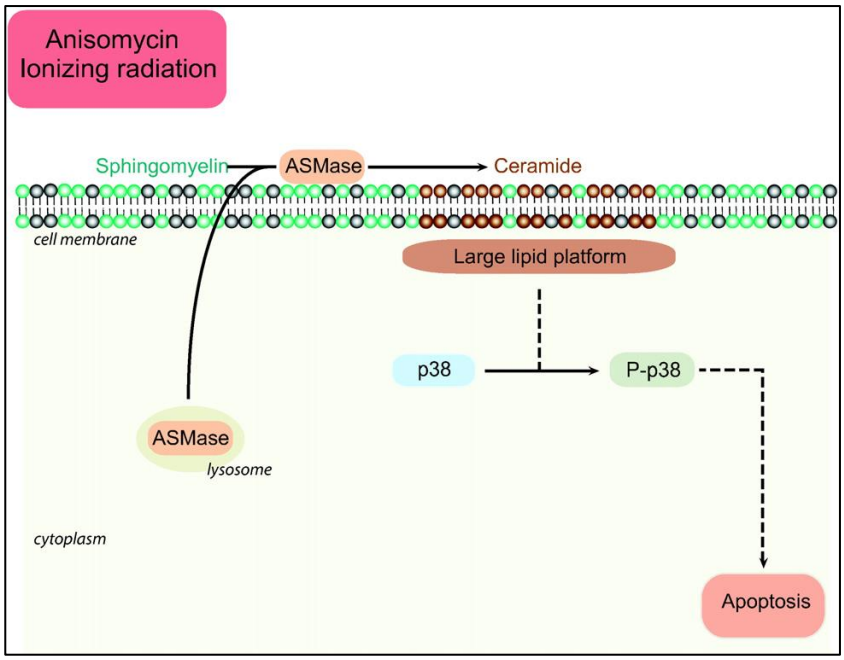

Figure 4: Overview of the stress-induced ASMase/ceramide pathway in EC. Upon stress induction of e.g. IR or anisomycin, ASMase is translocated from lysosomes to the plasma membrane. Here, it can act out its enzymatic function and cleave sphingomyelin to generate ceramide. Further on, ceramide accumulation leads to the formation of large lipid platforms that are capable to alter signaling of the p38/MAPK pathway in EC resulting in apoptosis induction. Source: modified after Niaudet et al., 2017 (118).

4. Aims

Tumor resistance to cancer therapy and in particular to RT limits the effectiveness of current cancer treatments. Herein, increasing evidence indicates that apart from cancer cells, the heterogeneous tumor stroma supports therapy resistance at multiple levels. Within this scenario, the membrane protein CAV1 came into focus. High CAV1 expression levels in tumor cells, as well as downregulation of stromal and in particular fibroblastic CAV1 were shown to correlate with cancer progression, invasion, metastasis and therapy resistance and thus a worse clinical outcome, e.g. in prostate cancer. However, the role of CAV1 for the outcome of RT in the context of tumor-stroma interactions remains elusive.

Downregulation of CAV1 in different tumor cells turned out to be a promising option to re-sensitize cells to the toxic effects of IR. EC were spared from the observed loss of stromal CAV1 at advanced tumor stages. Previous work in the own lab showed that CAV1 downregulation in EC resulted in a more activated, angiogenic phenotype and contributed to the observed radio-sensitizing effect of RT, particularly in prostate cancer. However, a loss of CAV1 in stromal fibroblasts pointed towards growth- and resistance-promoting tumor-stroma interactions during prostate cancer progression.

Thus, the main aim of the present thesis was to analyze the role of altered stromal CAV1 for radiation response of prostate cancer, focusing on the impact of stromal fibroblasts. To further gain insight in the potential mechanism of CAV1-dependent and resistance-promoting tumor-stroma interactions, fibroblast-derived target molecules mediating prostate cancer radio-resistance were supposed to be identified and characterized. Identification of CAV1-dependent factors of the tumor-stroma and malignant epithelial cells could help to specify new molecular targets for sensitizing advanced prostate cancer to RT.

Here, syngeneic prostate tumor and stroma (fibroblasts and endothelial) cells were investigated, either proficient or deficient for CAV1 and analyzed either alone or in combination for their radiation response *in vitro* and *in vivo*.

In contrast to the suggested radio-resistance-promoting interactions of CAV1-low and/or –deficient stromal fibroblasts, CAV1-deficient stromal EC were shown to radio-sensitize the tumor blood vessels or EC in the tumor and thus to improve the efficiency of RT. CAV1-deficient EC were characterized by a more immature

angiogenic phenotype which is in general more sensitive to IR. But on the other hand, protection of EC in the normal tissue during irradiation is necessary to minimize the risk of radiation-induced normal tissue damage. Thus, the role of radiation-induced EC activation and vascular dysfunction of normal tissues was studied in an animal model of radiation-induced normal tissue toxicity (subordinate aim). Here it was hypothesized that radiation-induced microenvironmental changes of normal tissues, in particular cytokines and growth factors secreted from senescent bronchial epithelial cells (following thoracic irradiation) could activate the hitherto quiescent endothelium and result in vascular dysfunction (acute phase) as well as severe EC loss (late tissue complication).

Last but not least, the already known CAV1-dependent radiation response of EC finally leading to EC apoptosis should be characterized. As a transmembrane protein, CAV1 is supposed to be involved in plasma membrane reorganization. Therefore, CAV1-dependency of the ASMase/ceramide to p38/MAPK pathways in EC apoptosis was investigated.

5. Results

5.1 Publication overview

Inhibition of Radiation-Induced Ccl2 Signaling Protects Lungs from Vascular Dysfunction and Endothelial Cell Loss.

Wiesemann A, Ketteler J, Slama A, Wirsdörfer F, Hager T, Röck K, Engel DR, Fischer JW, Aigner C, Jendrossek V, Klein D.

Antioxidants and Redox Signaling 2019;30(2):213-231. doi: 10.1089/ars.2017.7458. Epub 2018 Apr 2.

Progression-related loss of stromal Caveolin 1 levels fosters the growth of human PC3 xenografts and mediates radiation resistance.

Panic A*, Ketteler J*, Reis H, Sak S, Herskind C, Maier P, Rübben H, Jendrossek V, Klein D.

Scientific Reports 2017;7:41138. doi: 10.1038/srep41138

* shared first authorship/equal contribution

Progression-Related Loss of Stromal Caveolin 1 Levels Mediates Radiation Resistance in Prostate Carcinoma via the Apoptosis Inhibitor TRIAP1.

Ketteler J, Panic A, Reis H, Wittka A, Maier P, Herskind C, Yagüe E, Jendrossek V, Klein D.

Jorunal of Clinical Medicine 2019; 8(3). pii: E348. doi: 10.3390/jcm8030348.

Caveolin 1 dependency of the acid sphingomyelinase/ceramide-mediated radiation-response of endothelial cells in the context of tumor-stroma-interactions.

Ketteler J, Leonetti D, Veas Roy V, Wittka A, Estephan H, Maier P, Herskind C, Jendrossek V, Paris F, Klein D.

Manuscript in preparation/close to submission

5.2 Inhibition of Radiation-Induced Ccl2 Signaling Protects Lungs from Vascular Dysfunction and Endothelial Cell Loss.

Cumulative thesis of Ms Julia Ketteler

Author contributions

Title of publication: Inhibition of Radiation-Induced Ccl2 Signaling Protects Lungs from Vascular Dysfunction and Endothelial Cell Loss.

Authors: Wiesemann A, Ketteler J, Slama A, Wirsdörfer F, Hager T, Röck K, Engel DR, Fischer JW, Aigner C, Jendrossek V, Klein D.

Antioxidants and Redox Signaling 2018, http://doi.org/10.1089/ars.2017.7458

Credit to Mary Ann Liebert, Inc.; New Rochelle, NY.

Contributions:

- Conception – 5 – 10 %: addition of *in vitro* cultures of EC and DNA damage repair
- Experimental work – 10 %: experiments for Figure 5 a and b, Figure S4 b - d
- Data analysis – 10 %: Figure 5 b, Figure S4 b - d
- species identification: not applicable
- Statistical analysis -10 %: Figure 5 b, Figure S4 b - d
- Writing the manuscript – 5 %: proof reading, contribution to Material and Methods (EC culture), respective figure legends
- Revising the manuscript – 10 %: critical proofreading

Unterschrift Doktorand/in

Unterschrift Betreuer/in

ANTIOXIDANTS & REDOX SIGNALING
Volume 30, Number 2, 2019

DOI: 10.1089/ars.2017.7458

Therapeutics

ORIGINAL RESEARCH COMMUNICATION

Inhibition of Radiation-Induced Ccl2 Signaling Protects Lungs from Vascular Dysfunction and Endothelial Cell Loss

Alina Wiesemann,[1] Julia Ketteler,[1] Alexis Slama,[2] Florian Wirsdörfer,[1] Thomas Hager,[3] Katharina Röck,[4] Daniel R. Engel,[5] Jens W. Fischer,[4] Clemens Aigner,[2] Verena Jendrossek,[1,*] and Diana Klein[1,*]

Abstract

Aims: Radiation-induced normal tissue toxicity often precludes the application of curative radiation doses. Here we investigated the therapeutic potential of chemokine C-C motif ligand 2 (Ccl2) signaling inhibition to protect normal lung tissue from radiotherapy (RT)-induced injury.
Results: RT-induced vascular dysfunction and associated adverse effects can be efficiently antagonized by inhibition of Ccl2 signaling using either the selective Ccl2 inhibitor bindarit (BIN) or mice deficient for the main Ccl2 receptor CCR2 (KO). BIN-treatment efficiently counteracted the RT-induced expression of Ccl2, normalized endothelial cell (EC) morphology and vascular function, and limited lung inflammation and metastasis early after irradiation (acute effects). A similar protection of the vascular compartment was detected by loss of Ccl2 signaling in lungs of CCR2-KO mice. Long-term Ccl2 signaling inhibition also significantly limited EC loss and accompanied fibrosis progression as adverse late effect. With respect to the human situation, we further confirmed that Ccl2 secreted by RT-induced senescent epithelial cells resulted in the activation of normally quiescent but DNA-damaged EC finally leading to EC loss in *ex vivo* cultured human normal lung tissue.
Innovation: Abrogation of certain aspects of the secretome of irradiated resident lung cells, in particular signaling inhibition of the senescence-associated secretory phenotype-factor Ccl2 secreted predominantly by RT-induced senescent epithelial cells, resulted in protection of the endothelial compartment.
Conclusions: Radioprotection of the normal tissue *via* Ccl2 signaling inhibition without simultaneous protection or preferable radiosensitization of tumor tissue might improve local tumor control and survival, because higher doses of radiation could be used. *Antioxid. Redox Signal.* 30, 213–231.

Keywords: radiation-induced normal tissue toxicity, vascular damage, Ccl2, radiotherapy, senescence

Introduction

RADIOTHERAPY (RT) IS A treatment for cancer that uses carefully measured and controlled high-energy X-rays. However, current RT techniques expose not only tumors to a wide range of dose size and fractionation, even substantial amounts of normal tissue are potentially irradiated as well (7, 23, 40). Thus, acute and late effects in normal tissues following RT often limit the application of curative radiation doses, which in turn can foster local recurrence of primary tumors and distant metastasis, as well as mutagenesis in normal tissues, which are the basis for radiation-induced secondary malignancies (10, 59, 67). The challenge for scientists therefore is to understand the underlying mechanisms of normal tissue toxicity and to provide mechanistic bases for targeted therapies that can rationally minimize

[1]Institute of Cell Biology (Cancer Research), University of Duisburg-Essen, University Hospital, Essen, Germany.
[2]Department of Thoracic Surgery and Surgical Endoscopy, Ruhrlandklinik-University Clinic Essen, Essen, Germany.
[3]Institute of Pathology, University Clinic Essen, University of Duisburg-Essen, Essen, Germany.
[4]Institute for Pharmacology, University Hospital, Heinrich-Heine-University, Düsseldorf, Germany.
[5]Department Immunodynamics, Institute of Experimental Immunology and Imaging, University Duisburg-Essen, University Hospital Essen, Essen, Germany.
*Shared senior authorship.

Innovation

Blood vessels are critical determinants of the radiation response. Acute vascular damage and dysfunction on radiation therapy, as well as endothelial cell (EC) loss, are particularly prominent in the radiation response of tumors and of normal tissues. Herein, radiation-induced normal tissue toxicity often precludes the application of curative radiation doses. In this study, we show that chemokine C-C motif ligand 2 (Ccl2) signaling inhibition limits radiation-induced normal lung tissue toxicity in particular with respect to the vascular compartment, strongly arguing for Ccl2 signaling inhibition as potential radioprotective strategy.

late effects and maximize a survivor's quality of life (3, 10, 54).

The contemporary view of the tissue response to RT is that radiation perturbs the homeostatic network linking resident parenchymal, mesenchymal, and vascular cells within tissues with infiltrating immune cells (2, 11, 56). Among these cells, the endothelial cell (EC) have been shown to be critical determinants of radiation toxicity in healthy tissues (4, 14, 29, 53, 55). RT treatments generally foster EC apoptosis, increased vascular permeability, and acquisition of a proinflammatory and pro-coagulant phenotype (37). These alterations strongly participate in the development of radiation-induced damage in tissues with high intrinsic sensitivity, notably in the lung (12, 20, 37, 75). We recently provided evidence for an endothelium-dependent mechanism in radiation-induced normal tissue injury in the lung (33, 35).

Investigations in preclinical models revealed the importance of cytokine-driven pathways in radiation damage. Moreover, there is growing evidence for their relevance to radiation-induced disease in humans (11, 27, 30). RT exposures trigger cascades of cytokines in the irradiated tissues and released mediators perpetuate and augment the inflammatory response for long time periods, potentially supporting the development of chronic inflammation and progressive obliterate fibrosis. Among these cytokines, interleukin (IL)-1, IL-A, IL-6, tumor necrosis factor-α, and transforming growth factor beta (TGF-β) were shown to be major cytokines involved in the radiation response of normal lung tissue with complex and multifaceted roles in the regulation of tissue homeostasis, adaptive immune responses, inflammation, inflammatory resolution, and repair (31, 44, 45, 60). A better understanding of the signaling networks of cytokines is expected to reveal novel targets for protecting or mitigating radiation injury.

Using a murine model of radiation-induced pneumopathy, we recently showed that radiation-induced vascular damage and dysfunction in normal lung tissue support extravasation of premetastatic immune cells and of circulating tumor cells into previously irradiated lungs (33). The proinvasive cellular activities were accompanied by RT-induced senescence of bronchial-alveolar epithelial cells and up-regulation of the senescence-associated secretory phenotype (SASP) factor Ccl2 (chemokine C-C motif ligand 2), also known as monocyte chemoattractant protein-1 (MCP-1), by these cells. We further showed that adoptive transfer of mesenchymal stem cells (MSCs) during the early phase after irradiation efficiently counteracted epithelial senescence as well as vascular dysfunction (33). Furthermore, adoptive transfer of MSCs during the early phase after irradiation had the potential to provide a long-term protection of pulmonary EC from radiation-induced damage, preventing EC loss as long-term complication (35).

However, the detailed mechanism of the protective paracrine action of therapeutically applied MSCs especially on the vascular compartment remains elusive, but strongly suggests a central role of RT-induced Ccl2, since the protective effects of MSCs were associated with normalized Ccl2 levels. Here we investigated whether the specific inhibition of Ccl2 signaling is suited to mimic the protective MSC effects on RT-induced normal tissue damage with respect to the vascular compartment and unraveled the mechanism behind.

Results

Ccl2 inhibitor treatment does not prevent radiation-induced senescence of bronchial-alveolar epithelial cells but counteracts Ccl2 induction and recruitment of inflammatory cells

To investigate the therapeutic potential of Ccl2 signaling inhibition to prevent radiation-induced vascular dysfunction (acute effect), we first analyzed the effect of the Ccl2-inhibitor bindarit (BIN) treatment in our mouse model of radiation-induced pneumopathy (Fig. 1). C57BL/6 mice were left untreated, received a 15 Gy whole thorax irradiation (WTI), or received a 15 Gray (Gy) WTI and were subsequently treated by intraperitoneal injection with the Ccl2-inhibitor BIN three times a week within the first 3 weeks postirradiation. Induction of epithelial senescence was analyzed by determining senescence-associated beta-galactosidase (SA-betagal) activity in frozen lung tissue sections at 21 days postirradiation (Fig. 1A). Interestingly, increased SA-betagal activity was detected in bronchial-alveolar epithelial cells in lungs after WTI when compared with lung sections from control animals, and BIN treatment did not affect senescence induction.

Induction of senescence was further confirmed on the protein level by Western blot and on mRNA level by real-time reverse transcription polymerase chain reaction (qRT-PCR) quantification of the cellular senescence mediator cyclin-dependent kinase inhibitor 1 (Cdkn1a/p21) (Fig. 1B, C, and Supplementary Fig. S1; Supplementary Data are available online at www.liebertpub.com/ars). Notably, Cdkn1a expression levels were significantly increased in lungs of irradiated animals but were not affected by BIN treatment. qRT-PCR quantification was further used to confirm the increased *Ccl2* mRNA expression levels in total lung RNA isolates of irradiated lungs (Fig. 1D). Of note, BIN treatment efficiently reduced expression levels of *Ccl2* in lungs of irradiated animals. No significant effect on the main Ccl2-receptor *CCR2* expression levels was detected.

Since Ccl2 has been linked to immune modulation, we further investigated whether the associated recruitment of myeloid cells was affected by BIN treatment (Fig. 1E). Therefore, we analyzed the composition of the myeloid cell compartment by flow cytometry. The percentages of CD11b(+) myeloid cells of CD45(+) leukocytes, particularly of Ly6C(+) cells, were significantly increased and of Ly6G(+) cells by tendency after WTI, whereas BIN therapy antagonized infiltration of these cells. These findings indicated that BIN treatment did not alter WTI-induced senescence of bronchial-alveolar epithelial cells, but was able to reduce an aspect of the SASP, namely increased Ccl2 expression and associated inflammation.

Ccl2 inhibitor treatment normalizes EC morphology and vascular function and limits seeding of lung metastasis after thorax irradiation

Next, we explored whether inhibition of Ccl2 signaling limits radiation-induced vascular dysfunction and the associated risk of increased seeding of metastatic tumor cells in previously irradiated lungs (Fig. 1F–J). Electron microscopy of lung blood vessels demonstrated severe impaired morphology of arterial EC (numerous vacuoles, partially degraded mitochondria) in irradiated lungs but revealed a reconstitution of a regular vessel structure and EC morphology in irradiated lungs of BIN-treated animals (Fig. 1F). To confirm these results, the regular content of EC was analyzed by Western blot analysis (Fig. 1G and Supplementary Fig. S1).

The total amount of VE-cadherin (VE-Cad) was not altered after WTI and BIN treatment. Furthermore, flow cytometry analysis of the relative number of PECAM1/CD31 expressing cells confirmed a regular amount of EC at 3 weeks after WTI (Fig. 1H). Interestingly, the CD31-expressing EC upregulated the angiogenic growth factor receptor, vascular endothelial growth factor receptor 2 (VEGFR2), by tendency, whereas BIN treatment normalized these levels. Furthermore, RT-induced increased vascular permeability/dysfunction resulted in increased albumin leakage (Fig. 1I), thereby corroborating our earlier findings (33). Importantly, RT-induced impairment of EC function as determined by Evans blue dye (EBD) extravasation was restored 21 days after irradiation in BIN-treated animals. To investigate a potential protective effect of BIN treatment on metastasis-promoting effect of RT, we studied seeding and growth of intravenously injected syngeneic tumor cells in previously irradiated lung tissue (Fig. 1J). For this, B16F10 melanoma cells were injected into the tail vein at 21 days postirradiation and BIN treatment. Metastasis formation was significantly increased in irradiated lungs 14 days after tumor cell injection, whereas BIN treatment significantly reduced seeding of circulating tumor cells and subsequent metastasis formation.

Ccl2 signaling inhibition early after irradiation does not prevent chronic senescence and associated radiation-induced expression of Ccl2, nor radiation-induced EC loss and fibrosis as adverse late effects

To investigate if acute inhibition of Ccl2 signaling has the potential to prevent RT-induced chronic adverse late effects, we first confirmed prevailing RT-induced senescence and accompanied Ccl2 expression in lungs from mice at 25 weeks after WTI (Fig. 2). As revealed by SA-betagal activity stainings in frozen lung tissue sections, Cdkn1a protein, as well as *Cdkn1a* and *Ccl2* mRNA expression levels, BIN treatment in the early phase after irradiation was not sufficient to reverse the senescent phenotype of bronchial-alveolar epithelial cells and associated increased *Ccl2* expression levels after WTI in the long-term follow up (Fig. 2A–C and Supplementary Fig. S1). Next, we analyzed the effect of early BIN treatment on the EC compartment in lungs 25 weeks after WTI. The amount of

FIG. 1. Ccl2 inhibitor treatment does not prevent senescence of bronchial-alveolar epithelial cells but counteracts radiation-induced Ccl2 expression (acute effect), recruitment of inflammatory myeloid cells, and vascular dysfunction. C57BL/6 mice were left untreated (Ctrl), received a 15 Gy WTI, or received a 15 Gy WTI and were subsequently Ccl2-inhibitor treated by intraperitoneal injection with BIN three times a week within the first 3 weeks postirradiation. **(A)** SA-betagal activity was assessed using frozen sections of lung tissue at 21 days after irradiation. Photomicrographs depict representative pictures of three independent experiments. Scale bar = 100 μm. **(B)** Cdkn1a/p21 protein expression was analyzed in whole lung protein lysates using Western blot analysis. *p*-Values were indicated: $*p \leq 0.05$ by one-way ANOVA with Bonferroni correction ($n = 6$ for each group); ns, not significant. **(C, D)** *Cdkn1a* **(C)** as well as *Ccl2* and *Ccr2* **(D)** mRNA expression levels were further analyzed in total lung RNA isolates using real-time reverse transcription polymerase chain reaction. Data are presented as mean ± SEM measured in duplicates each (0 Gy Ctrl, 15 Gy Ctrl and 15 Gy BIN: $n = 6$ per group; 0 Gy BIN: $n = 7$). *p*-Values were indicated: $*p \leq 0.05$, $**p \leq 0.01$, $***p < 0.005$, $****p < 0.001$ by one-way ANOVA (*Cdkn1a*) or by two-way ANOVA (*Ccl2* and *Ccr2)* with *post hoc* Tukey multiple comparison test. **(E)** Leukocytes in crude cell extracts of freshly isolated lung tissue were identified using CD45 expression and flow cytometry analysis. Myeloid cells were further characterized using CD11b, Ly6C, and Ly6G antibodies. Data are presented as mean ± SEM ($n = 5$–6 for each group). *p*-Values were indicated: $*p \leq 0.05$, $**p \leq 0.01$, $***p < 0.005$ as analyzed by one-way ANOVA with Bonferroni correction. **(F)** Morphological analysis of lung blood vessels was done using electron microscopy at 3 weeks postirradiation. Scale bar 5 μm (*left panel*), 2 μm (*right panel*). A regular vessel structure as well as EC morphology was present in the lungs of BIN-treated animals. *Arrows* point toward EC. **(G)** Endothelial VE-Cad expression was analyzed in whole protein lysates using Western blot analysis. **(H)** EC in crude cell extracts of freshly isolated lung tissue were identified using CD31/PECAM1 as well as VEGFR2 expression and FACS analysis. Data are presented as mean ± SEM ($n = 5$–6 for each group). **(I)** Three weeks postirradiation, vascular leakage was determined by EBD extravasation from the blood stream to the lung interstitium. Dye concentrations in the isolated lungs were quantified by absorption measurements and related to the weight of lung tissue. Data are presented as mean ± SEM from three independent experiments (0 Gy Ctrl: $n = 17$, 0 Gy BIN: $n = 10$, 15 Gy Ctrl: $n = 15$, 15 Gy BIN: $n = 10$). *p*-Values were indicated: $*p \leq 0.05$, $**p \leq 0.01$ as analyzed by one-way ANOVA with Bonferroni correction. **(J)** Seeding of circulating tumor cells into the lungs was analyzed 21 days after irradiation and BIN treatment. Sham-irradiated and BIN-treated animals served as controls (0 Gy BIN). After 14 days of tumor cell injection, animals were sacrificed, lungs were isolated and subjected for lung histology (scale bar = 100 μm). Lung metastasis formation was quantified in whole lung sections. Shown are mean values from one of three independent experiments (0 Gy Ctrl: $n = 6$, 0 Gy BIN: $n = 5$, 15 Gy Ctrl: $n = 5$, 15 Gy BIN: $n = 6$). *p*-Values were indicated: $**p \leq 0.01$, $***p \leq 0.001$ by one-way ANOVA with Bonferroni correction. BIN, bindarit; Ccl2, chemokine C-C motif ligand 2; Cdkn1a/p21, cellular senescence mediator cyclin-dependent kinase inhibitor 1; cT, connective tissue; EBD, Evans blue dye; EC, endothelial cell; FACS, fluorescent activated cell sorting; Gy, Gray; Lu, lumen; SA-betagal, senescence-associated beta-galactosidase; SEM, standard error of the mean; SMC, smooth muscle cell; VE-Cad, VE-cadherin; VEGFR2, vascular endothelial growth factor receptor 2; WTI, whole thorax irradiation. To see this illustration in color, the reader is referred to the web version of this article at www.liebertpub.com/ars

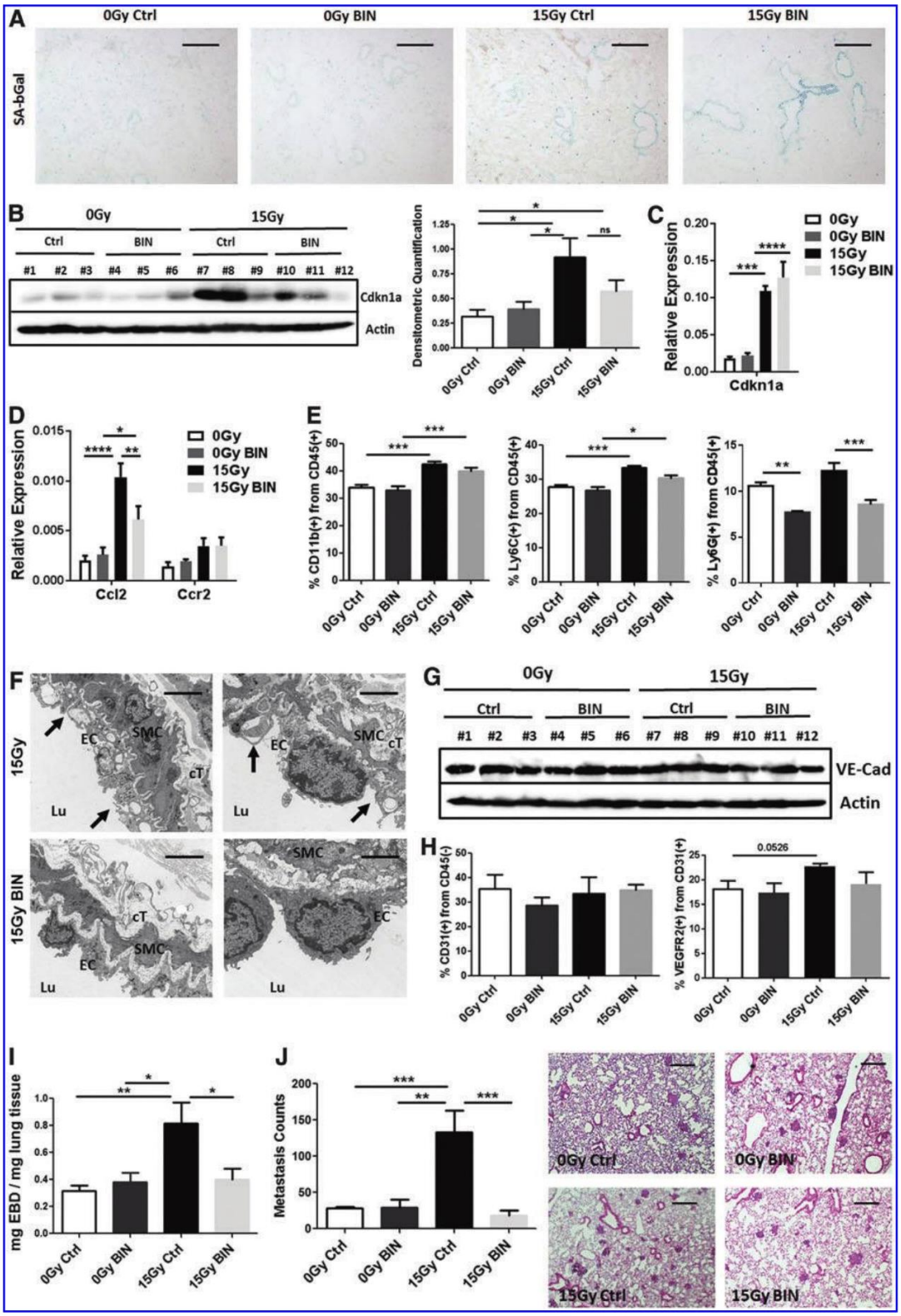
A
0Gy Ctrl
0Gy BIN
15Gy Ctrl
15Gy BIN
SA-bGal
B
0Gy
15Gy
Ctrl
BIN
Ctrl
BIN
#1 #2 #3 #4 #5 #6 #7 #8 #9 #10 #11 #12
Cdkn1a
Actin
Densitometric Quantification
0Gy Ctrl
0Gy BIN
15Gy Ctrl
15Gy BIN
C
Relative Expression
0Gy
0Gy BIN
15Gy
15Gy BIN
Cdkn1a
D
Relative Expression
0Gy
0Gy BIN
15Gy
15Gy BIN
Ccl2
Ccr2
E
% CD11b(+) from CD45(+)
% Ly6C(+) from CD45(+)
% Ly6G(+) from CD45(+)
0Gy Ctrl
0Gy BIN
15Gy Ctrl
15Gy BIN
F
15Gy
15Gy BIN
EC
SMC
cT
Lu
G
0Gy
15Gy
Ctrl
BIN
Ctrl
BIN
#1 #2 #3 #4 #5 #6 #7 #8 #9 #10 #11 #12
VE-Cad
Actin
H
% CD31(+) from CD45(-)
% VEGFR2(+) from CD31(+)
0.0526
0Gy Ctrl
0Gy BIN
15Gy Ctrl
15Gy BIN
I
mg EBD / mg lung tissue
0Gy Ctrl
0Gy BIN
15Gy Ctrl
15Gy BIN
J
Metastasis Counts
0Gy Ctrl
0Gy BIN
15Gy Ctrl
15Gy BIN

VE-Cad as well as of the smooth muscle cell marker transgelin (Tagln) was quantified in whole protein lysates by Western blot and qRT-PCR analysis in 0 or 15 Gy WTI mice, which received BIN treatment within the first 3 weeks postirradiation or vehicle control (Fig. 2D, E, and Supplementary Fig. S1).

BIN treatment in the early phase after irradiation was not sufficient to limit the EC loss in lungs after WTI in the long-term follow-up. Radiation-induced EC loss at 25 weeks after WTI was accompanied by the development of significant fibrosis, as revealed by Masson–Goldner's trichrome histological stainings of lung sections and immunohistochemistry (IHC) of the major extracellular matrix glycosaminoglycan hyaluronan, Western blot analysis for increased expression levels of the profibrotic cytokine TGF-β, and qRT-PCR quantifications of the significantly increased extracellular matrix components collagen Col1A2, Col3A1, and fibronectin 1 in total lung isolates (Fig. 2F–G and Supplementary Fig. S1). BIN treatment in the early phase after irradiation was also not sufficient to limit fibrosis development and progression in lungs after WTI in the long-term follow-up.

Inhibition of Ccl2 signaling by CCR2 deficiency normalizes vascular function and limits seeding of lung metastasis after WTI without reducing RT-induced senescence and accompanied increased Ccl2 secretion

Since short-term Ccl2 suppression was not sufficient to provide long-term protection of the vascular compartment, we investigated the genetic inhibition of Ccl2 signaling by using mice deficient for the main Ccl2 chemokine receptor CCR2 (CCR2-KO) (Fig. 3). Therefore, C57BL/6 and CCR2-KO mice were left untreated or received a 15 Gy WTI. Three weeks postirradiation, vascular function/dysfunction was determined by EBD extravasation (Fig. 3A), metastasis formation (Fig. 3B), and immune cell extravasation with subsequent inflammation (Fig. 3C). Similar to the effects observed on BIN treatment, genetic abrogation of Ccl2 signaling in CCR2-KO mice reduced RT-induced vascular dysfunction as shown by the normalization of EBD leakage, metastasis formation, and immune cell recruitment. Again, a relative number of CD31-expressing EC showed a regular amount despite CCR2 deficiency. Of note, a RT-induced upregulation of VEGFR2 expression levels on CD31-expressing cells was not detected in CCR2-deficient EC (Fig. 3C).

These results demonstrate that an inhibition of Ccl2 signaling has a high potential to counteract RT-induced vascular dysfunction by preventing an activated ''angiogenic'' EC phenotype as an acute effect early after irradiation. In the long-term follow-up, CCR2 deficiency did not reverse the senescent phenotype and associated increased *Ccl2* expression levels at 25 weeks after WTI (Fig. 3D–F and Supplementary Fig. S1). Interestingly, increased expression levels of the proliferation marker cyclin D1 (Ccnd1) were detected in lungs of irradiated WT mice, which were partially normalized in lungs of irradiated CCR2-KO mice (Fig. 3E). These data indicate that RT-induced Ccl2 expression can induce proliferation of resident lung cells, presumably lung EC.

Deficiency in the main Ccl2 receptor CCR2 limits EC loss and radiation-induced lung fibrosis

We then analyzed whether long-term Ccl2 signaling inhibition limits radiation-induced EC loss. Therefore, untreated

FIG. 2. Ccl2 inhibitor treatment early after irradiation does not prevent senescence and associated radiation-induced expression of Ccl2, EC loss, and fibrosis progression as adverse late effect. C57BL/6 mice were left untreated (Ctrl), received a 15 Gy WTI, or received a 15 Gy WTI and were subsequently Ccl2-inhibitor treated by intraperitoneal injection with BIN three times a week within the first 3 weeks postirradiation. **(A)** SA-betagal activity was assessed using frozen sections of lung tissue at 25 weeks after irradiation. Photomicrographs depict representative pictures of three independent experiments. Scale bar = 50 μm. **(B)** Cdkn1a protein expression was analyzed in whole lung protein lysates using Western blot analysis. Representative blots are shown. *p*-Values were indicated: $*p \le 0.05$ by one-way ANOVA with Bonferroni correction ($n = 5$–6 for each group). **(C)** *Cdkn1a* and *Ccl2* mRNA expression levels were further analyzed in total lung RNA isolates using qRT-PCR. Data are presented as mean ± SEM from three independent experiments ($n = 6$ per group). *p*-Values were indicated: $*p \le 0.05$, $**p < 0.01$ by one-way ANOVA with Bonferroni correction; ns, not significant. **(D)** Endothelial VE-Cad expressions as well as the smooth muscle cell marker transgelin (Tagln) were analyzed in whole protein lysates using Western blot analysis at 25 weeks postirradiation. *p*-Values were indicated: $**p \le 0.01$, $***p \le 0.001$, by one-way ANOVA with Bonferroni correction ($n = 5$ per group). **(E)** *VE-Cad* mRNA expression levels were further analyzed in total lung RNA isolates using qRT-PCR. Data are presented as mean ± SEM from three independent experiments measured in duplicate each ($n = 5$ per group). *p*-Values were indicated: $*p \le 0.05$ by one-way ANOVA with Bonferroni correction. **(F)** Histological staining with Masson–Goldner's trichrome on sections of paraffin-embedded lung tissue was performed at 25 weeks after WTI. Sham-irradiated (0 Gy) animals that received BIN treatment were included as control. The major extracellular matrix glycosaminoglycan HA was further analyzed in lung section using DAB staining (brown). Nuclei were counterstained with hemalaun (*blue*). Shown are representative light microscopy images (scale bar = 100 μm). Quantification of lung fibrosis was done by determining the Ashcroft scores blinded to the genotype and treatment conditions. Data are presented as mean ± SEM. $*p \le 0.05$ by one-way ANOVA with Bonferroni correction (0 Gy Ctrl: $n = 5$, 0 Gy BIN: $n = 6$, 15 Gy Ctrl: $n = 5$, 15 Gy BIN: $n = 6$); ns, not significant. **(G)** The profibrotic cytokine TGF-β known to be associated with fibrosis development was further analyzed in whole protein lysates using Western blot analysis at 25 weeks postirradiation ($n = 5$–6 per group). $*p \le 0.05$ by one-way ANOVA with Bonferroni correction. **(H)** qRT-PCR quantifications of the extracellular matrix components Col3A1 and Fn1 were performed and shown as relative expression to actin at ≥25 weeks postirradiation. Shown are mean values ± SEM from independent samples ($n = 5$–6 per group and gene) measured in duplicate each. $*p \le 0.05$, $**p \le 0.01$ by one-way ANOVA with *post hoc* Tukey multiple comparison test; ns, not significant. DAB, 3,3′-diaminobenzidine; Fn1, fibronectin 1; HA, hyaluronan; qRT-PCR, real-time reverse transcription polymerase chain reaction; TGF-β, transforming growth factor beta. To see this illustration in color, the reader is referred to the web version of this article at www.liebertpub.com/ars

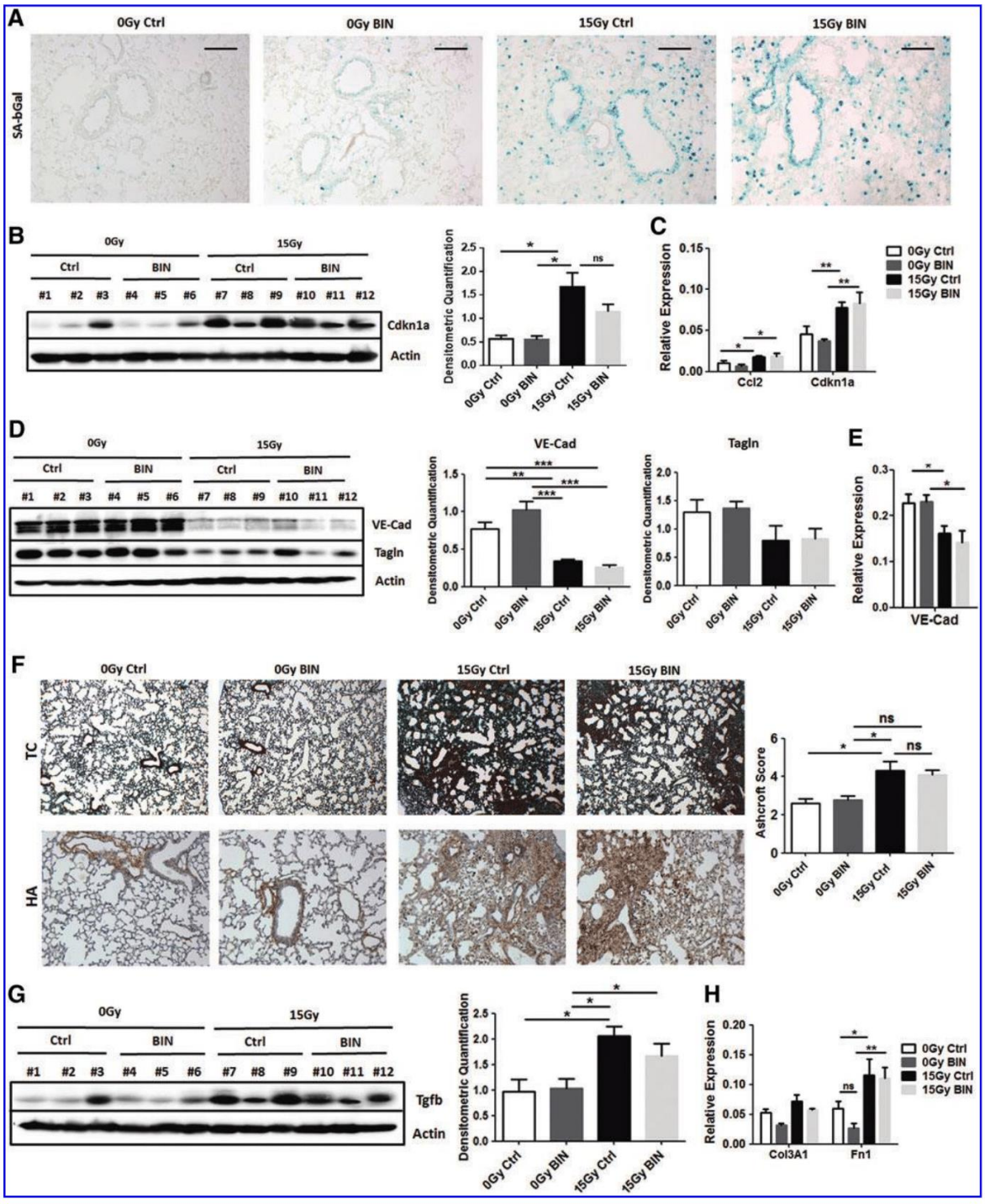

or 15 Gy WTI-treated WT and CCR2-deficient mice after WTI were used (Fig. 4A and Supplementary Fig. S2). Here endothelial VE-Cad and associated smooth muscle cell (SMC) characteristic Tagln expression levels were normalized in irradiated lungs of CCR2-KO mice compared with the RT-induced increased levels of WT controls. In line with qRT-PCR analysis, *VE-Cad* mRNA levels were not reduced on radiation in CCR2-KO mice (Fig. 4B). In addition, we quantified the number of EC in crude cell extracts of freshly isolated lung tissue using endothelial-specific PECAM1/CD31

expression by flow cytometry (Fig. 4C). WTI induced a significant reduction of VE-Cad expression levels, whereas the reduction in lungs of CCR2-KO mice was less pronounced. The RT-induced upregulation of VEGFR2 expression levels on CD31-expressing cells was significantly decreased in CCR2-deficient EC. Intensive morphological analysis of lungs from WT and CCR2-deficient mice at 25 weeks after WTI using electron microscopy further demonstrated a more regular vessel structure as well as EC morphology, which was present in the lungs of CCR2-KO animals (Fig. 4D). In contrast, WTI induced multiple signs of severe morphological impairment in EC such as partially degraded mitochondria and numerous vacuoles. Of note, abrogation of Ccl2 signaling *via* the CCR2 receptor significantly limited fibrosis development as adverse late effect on treatment with 15 Gy WTI in CCR2-deficient mice (Fig. 4E–G and Supplementary Fig. S2). These results suggest that a long-term inhibition of Ccl2 *via* CCR2 signaling has a high potential to counteract RT-induced normal tissue damage by preventing EC loss as an adverse late effect after irradiation.

Exogenous Ccl2 stimulation increases radiation-induced EC death and decreases survival of clonogenic EC

Up to now, our data indicated that radiation-induced increase in Ccl2 secretion of predominantly senescent bronchial-alveolar epithelial cells (33) activates the hitherto quiescent RT-damaged EC resulting in EC death/loss. To corroborate the assumed stimulating action of Ccl2 on EC, we exposed cultured AS-M5 cells as a model for EC to irradiation with 15 Gy, and subsequently cultured these cells in normal growth media (NGM) or NGM supplemented with 20 ng/mL CCL2. We used the documented potent angiogenic growth factor 10 ng/mL VEGF as a control for EC activation (Fig. 5). Radiation fostered a downregulation of VE-Cad expression levels as well as of the associated junctional proteins beta-catenin and occludin in cultured EC, while the major angiogenic receptor KDR/VEGFR2 was upregulated on growth factor stimulation with CCL2 and VEGF (Fig. 5A, Supplementary Figs. S3 and S4A). Expression levels of the proliferation marker proliferating-cell-nuclear-antigen (PCNA) and Cyclin D1 (CCND1) were furthermore increased in CCL2 and VEGF-stimulated EC (Fig. 5A and Supplementary Fig. S4). We then investigated the signaling pathways activated on irradiation and growth factor treatment in cultured EC in more detail (Fig. 5A and Supplementary Fig. S3).

CCL2 and VEGF activated mitogen-activated protein kinase (MAPK) pathways, including extracellular signal-regulated kinases 1 and 2 (ERK1/2) and p38 MAPK, suggesting that both contribute to the onset of proliferation in irradiated EC. In parallel, an increased phosphorylation of the cell cycle regulating and as tumor suppression functioning p53 was detected in irradiated EC (Fig. 5A and Supplementary Fig. S3). Expression levels of the survival protein Akt/protein kinase B showed that the phosphorylation at T308 was increased on radiation, whereas phosphorylation at S473 was slightly decreased. Total AKT levels were clearly decreased after radiation irrespective of growth factor treatment. Consequently, angiogenic growth factor treatment, in particular CCL2, caused an upregulation of KDR/VEGFR2 and increased proliferation of cultured EC, and thus an angiogenic phenotype (Supplementary Figs. S4 and S5).

The kinetics of DNA double-strand breaks repair was analyzed by γ-H2A.X-immunofluorescence (Fig. 5B). Interestingly, treatment with the respective factors did not alter the RT-induced DNA damage response as revealed by a similar number of total γ-H2A.X foci. However, the analysis revealed that even after 48 h, similar high γ-H2A.X foci numbers were still detectable in irradiated AS-M5 EC indicating a very slow or even no repair capacity. Of note, angiogenic growth factor stimulation in particular stimulation with CCL2 resulted in an increased sensitivity of EC to radiation-induced apoptosis as shown by the pronounced increase in the subG1-fraction (Supplementary Fig. S4). In line with these findings, a long-term assay measuring the surviving fraction after irradiation revealed that the number of EC able to regrow and form a colony was considerably diminished in CCL2-treated AS-M5 EC (Fig. 5C). Based on these observations, we speculate that

FIG. 3. Ccl2 signaling inhibition *via* CCR2 deficiency limits vascular dysfunction (acute effect), whereas senescence and associated radiation-induced expression of Ccl2 are not prevented. C57BL/6 (WT) and CCR2-deficient (KO) mice were left untreated (Ctrl) or received a 15 Gy WTI. **(A)** Three weeks postirradiation, vascular leakage was determined by EBD extravasation from the blood stream to the lung interstitium. Data are presented as mean ± SEM from at least three independent experiments (0 Gy WT: $n=11$, 15 Gy WT: $n=6$, 0 Gy KO: $n=9$, 15 Gy KO: $n=7$). p-Values were indicated: $*p \le 0.05$, $**p \le 0.01$ as analyzed by one-way ANOVA with Bonferroni correction. **(B)** Seeding of circulating tumor cells into the lungs was analyzed 21 days after irradiation. After an additional 14 days, lungs were subjected to lung histology and metastasis formation was quantified in whole lung sections. Shown are mean values from one of three independent experiments (0 Gy WT: $n=6$, 15 Gy WT: $n=6$, 0 Gy KO: $n=8$, 15 Gy KO: $n=7$). p-Values were indicated: $*p \le 0.05$, $**p \le 0.01$ by one-way ANOVA with Bonferroni correction; ns, not significant. **(C)** Myeloid cells in crude cell extracts of freshly isolated lung tissue were identified using CD45 together with CD11b and Ly6C expression and FACS analysis. EC were identified using CD31/PECAM1 and VEGFR2 antibodies. Data are presented as mean ± SEM ($n=6$–7 for each group). p-Values were indicated: $*p \le 0.05$, $**p \le 0.01$, $****p \le 0.001$ as analyzed by two-way ANOVA with *post hoc* Tukey multiple comparison test. **(D)** SA-betagal activity was assessed using frozen sections of lung tissue at 25 weeks after irradiation. Photomicrographs depict representative pictures of three independent experiments. Scale bar = 50 μm. **(E)** *Cdkn1a*, as well as *Ccl2* mRNA expression levels were analyzed in total lung RNA isolates using qRT-PCR. Data are presented as mean ± SEM from at least three independent experiments ($n=6$ per group). p-Values were indicated: $*p \le 0.05$, $**p < 0.01$, $***p < 0.005$ by two-way ANOVA with Bonferroni correction. **(F)** Cdkn1a as well as the proliferation marker Ccnd1 protein expression was further analyzed in whole lung protein lysates using Western blot analysis. p-Values were indicated: $*p \le 0.05$, $**p \le 0.01$ by one-way ANOVA with Bonferroni correction ($n=6$ for each group); ns, not significant. CCND1, Cyclin D1. To see this illustration in color, the reader is referred to the web version of this article at www.liebertpub.com/ars

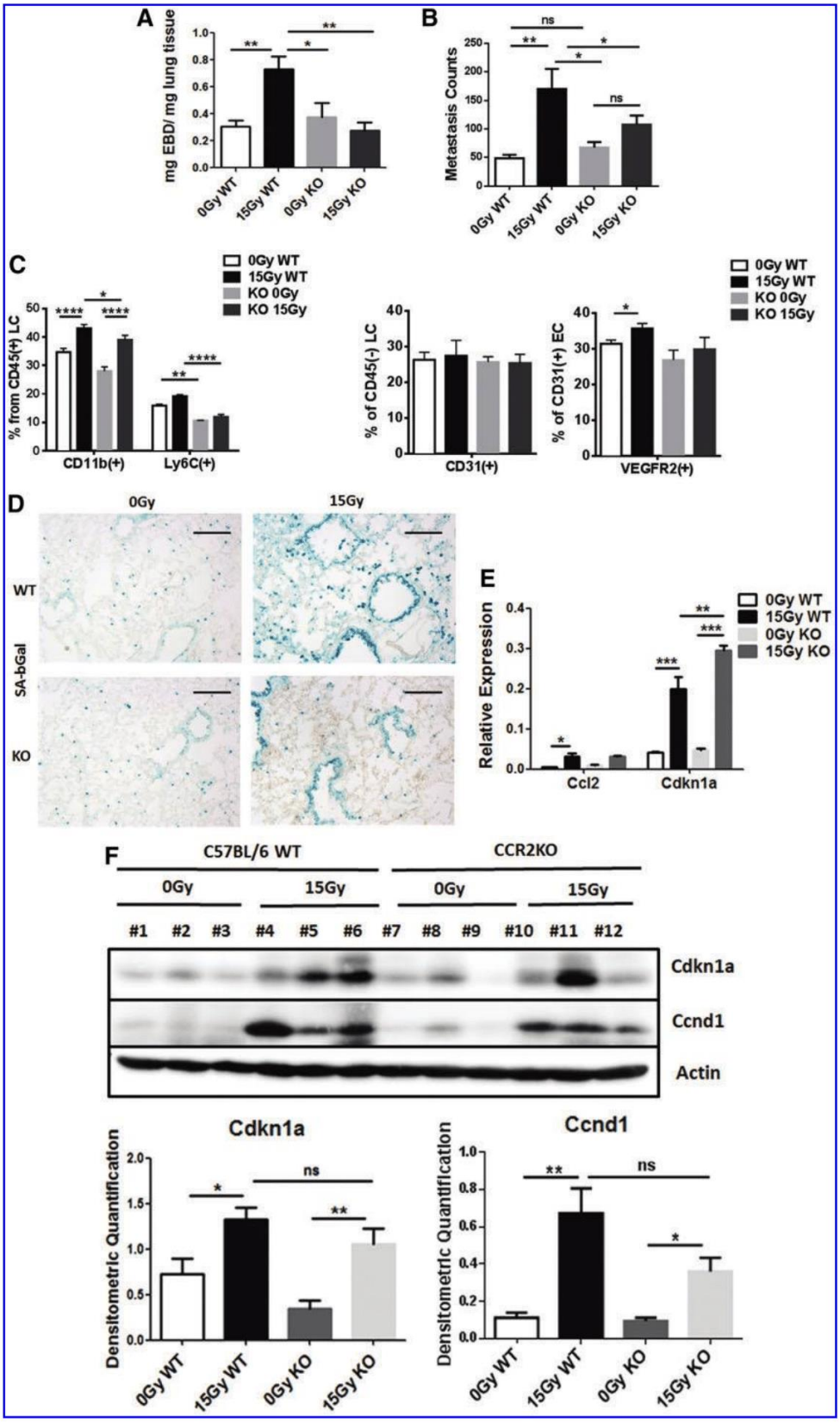
A
mg EBD/ mg lung tissue
0Gy WT
15Gy WT
0Gy KO
15Gy KO
B
Metastasis Counts
ns
C
0Gy WT
15Gy WT
KO 0Gy
KO 15Gy
% from CD45(+) LC
CD11b(+)
Ly6C(+)
% of CD45(-) LC
CD31(+)
% of CD31(+) EC
VEGFR2(+)
D
0Gy
15Gy
WT
SA-bGal
KO
E
Relative Expression
Ccl2
Cdkn1a
F
C57BL/6 WT
CCR2KO
0Gy
15Gy
#1 #2 #3 #4 #5 #6 #7 #8 #9 #10 #11 #12
Cdkn1a
Ccnd1
Actin
Densitometric Quantification
ns

the SASP-factor CCL2 secreted by RT-induced senescent epithelial cells (33) results in the activation of normally quiescent but DNA-damaged EC. This activation then leads to endothelial apoptosis induction resulting in EC loss (Supplementary Fig. S5).

Radiation-induced senescence of bronchial-alveolar epithelial cells and associated increased expression of Ccl2 induced an angiogenic phenotype in EC of ex vivo *cultured human lung tissues*

To corroborate our findings about the CCL2 action on lung endothelium as well as about the therapeutic potential of CCL2 signaling inhibition with respect to the human situation, we used *ex vivo* tissue cultures of human normal lung tissue obtained during surgery embedded in growth factor-reduced Matrigel (Fig. 6). Fresh lung specimens were dissected and embedded in Matrigel prior irradiation with 15 Gy with or without subsequent CCL2 and VEGF stimulation for an additional 5 days. Radiation fostered a downregulation of VE-Cad expression levels in cultured lung tissues, while the KDR/VEGFR2 was upregulated on radiation alone or in combination with CCL2 and VEGF growth factor stimulation (Fig. 6A and Supplementary Fig. S6). Expression levels of the proliferation marker PCNA were slightly increased on radiation and in CCL2 and VEGF-stimulated tissue pieces. Further examination of the expression levels of the apoptosis-mediating protein caspase 3, as well of its cleaved form, showed that radiation induced apoptosis in the cultured lung tissue. To investigate then the therapeutic potential of CCL2 signaling inhibition to prevent radiation-induced and CCL2-mediated EC activation as well as radiation-induced EC loss, we analyzed the effect of the selective CCL2-inhibitor BIN in these tissue cultures. Induction of epithelial senescence was analyzed by determining SA-betagal activity in frozen lung tissue cultures at 5 days postirradiation (Fig. 6B). Interestingly, increased SA-betagal activity was detected in bronchial-alveolar epithelial cell in lungs after irradiation when compared with nonirradiated lung tissue cultures, and BIN treatment did not affect senescence induction. A radiation-induced upregulation of endothelial CD34, indicating angiogenic activation, was further blocked in BIN-treated *ex vivo* lung cultures (Fig. 6B). A similar finding was detected for the proliferation marker KI-67: radiation induced a KI-67-immunoreactivity in lung EC, indicating EC proliferation that was blocked in BIN-treated *ex vivo* lung cultures (Fig. 6B and Supplementary Fig. S7). Induction of senescence was further confirmed on the protein level by Western blot (Fig. 6A and Supplementary Fig. S6) and on mRNA level by qRT-PCR quantification of CDKN1A/P21 (Fig. 6C). Respective radiation-induced CCL2 expression levels, as well as increased expression levels of KDR/VEGFR2, were significantly reduced in mRNA isolates of BIN-treated normal lung cultures. Western blot analysis of respective protein isolates confirmed these findings (Fig. 6D and Supplementary Fig. S6). Although CCL2 is the best-characterized target of BIN, it also inhibits other MCP family members, namely CCL7 (MCP-3) and CCL8 (MCP-2) (49, 50). Therefore, and in addition to CCL2, we quantified CCL7 and CCL8 mRNA expression levels, as well as their potential receptors (17), in *ex vivo* isolated human normal lung tissue and normal lung cultures (Supplementary Fig. S7). As demonstrated by the high expression levels of CCL2 in normal lung tissue, which were significantly inhibited by BIN treatment in normal lung tissue cultures, compared with CCL7 and CCL8, these results strongly argue for the fact that indeed CCL2 is the most prominent factor involved in radiation-induced lung disease. Consequently, radiation and in particular radiation-induced CCL2 caused and increased activation of lung EC, and thus, an angiogenic phenotype that could be antagonized by CCL2 signaling inhibition using the inhibitor BIN.

FIG. 4. Ccl2 signaling inhibition *via* CCR2 deficiency limits endothelial cell loss and fibrosis progression as adverse late effect. C57BL/6 (WT) and CCR2-deficient (KO) mice were left untreated (Ctrl) or received a 15 Gy WTI. **(A)** Endothelial VE-Cad and Tagln expression was analyzed in whole protein lysates using Western blot analysis at 25 weeks postirradiation. *p*-Values were indicated: $*p \le 0.05$, $**p \le 0.01$, $***p \le 0.001$ by one-way ANOVA with Bonferroni correction ($n = 6$–8 per group). **(B)** *VE-Cad* mRNA expression levels were further analyzed in total lung RNA isolates using qRT-PCR. Data are presented as mean ± SEM from at least three independent experiments ($n = 6$ per group). *p*-Values were indicated: $**p \le 0.01$ by one-way ANOVA with Bonferroni correction. **(C)** EC were further quantified using FACS analysis and CD31 as well as VEGFR2 expression in the absence of CD45 expression [CD45(−)CD31(+) cells]. Data are presented as mean ± SEM from three independent experiments ($n = 6$–8 mice per group). *p*-Values were indicated: $**p \le 0.01$, $****p \le 0.001$ by two-way ANOVA with Bonferroni correction. **(D)** Morphological analysis of lung blood vessels was done using electron microscopy 25 weeks postirradiation ($n = 3$ per group). Partially degraded mitochondria and numerous vacuoles present in EC are predominant in WTI lungs (emphasized by *arrows*) compared to sham controls (0 Gy). A regular vessel structure as well as EC morphology was present in the lungs of CCR2-KO animals. SMC, cT, Lu. Scale bar 2 μm (*left panel*), 5 μm (*middle*), 10 μm (*right*). **(E)** Histological staining with Masson–Goldner's trichrome on sections of paraffin-embedded lung tissue was performed at 25 weeks after WTI. Sham-irradiated (0 Gy) animals were included as control. HA was further analyzed in lung section using DAB staining (brown). Nuclei were counterstained with hemalaun (*blue*). Shown are representative light microscopy images (scale bar = 100 μm). Quantification of lung fibrosis was done by determining the Ashcroft scores blinded to the genotype and treatment conditions. Data are presented as mean ± SEM. $***p \le 0.001$ by one-way ANOVA with Bonferroni correction (0 Gy WT: $n = 14$, 15 Gy WT: $n = 13$, 0 Gy KO: $n = 17$, 15 Gy KO: $n = 21$). **(F)** The TGF-β expression was further analyzed in whole protein lysates using Western blot analysis at 25 weeks postirradiation ($n = 6$–8 per group). $*p \le 0.05$ by one-way ANOVA with Bonferroni correction. **(G)** qRT-PCR quantifications of Col1A2, and Fn1 were performed and shown as relative expression to actin ($n = 6$) at ≥25 weeks postirradiation. Shown are mean values ± SEM from three independent samples per group measured in duplicate each. $***p \le 0.005$ by two-way ANOVA with *post hoc* Tukey multiple comparison test; ns, not significant. Tagln, transgelin. To see this illustration in color, the reader is referred to the web version of this article at www.liebertpub.com/ars

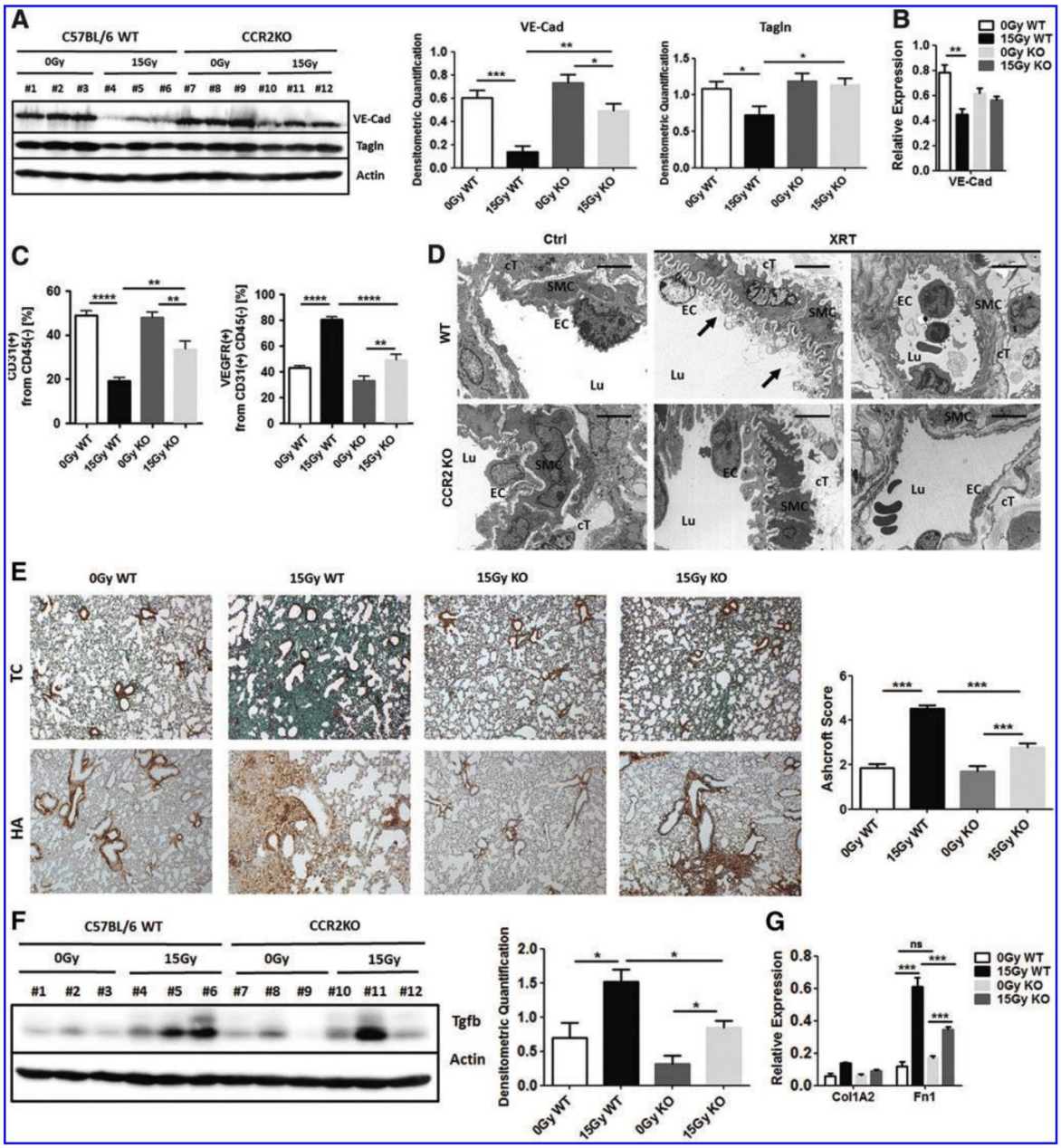

Discussion

Normal tissue toxicity remains a dose-limiting factor for RT treatment. Acute side effects can complicate tissue regeneration or necessitate treatment interruptions, which then might compromise tumor control or cure. Moreover, long-term adverse effects can result in permanently debilitating organ dysfunction such as cardiovascular diseases (1, 37). Therefore, it is hoped that by counteracting biological mediators of radiation-induced tissue damage or deregulated repair may be suited to prevent these unwanted side effects of RT.

We and others already showed that radiation-induced Ccl2 is closely linked with normal tissue toxicity (5, 33, 46). This proinflammatory factor was shown to be expressed by cells of the immune system as well as by senescent fibroblasts and epithelial cells (13, 58). In addition, cancer-associated fibroblasts, which have the potential to modulate the microenvironment by altering epithelial homeostasis and proliferative quiescence, were shown to characteristically express Ccl2 (26, 64). In addition and with respect to fibrotic lung diseases, Ccl2 was already shown to play an important role in idiopathic pulmonary fibrosis as the activated pulmonary epithelium was identified as an

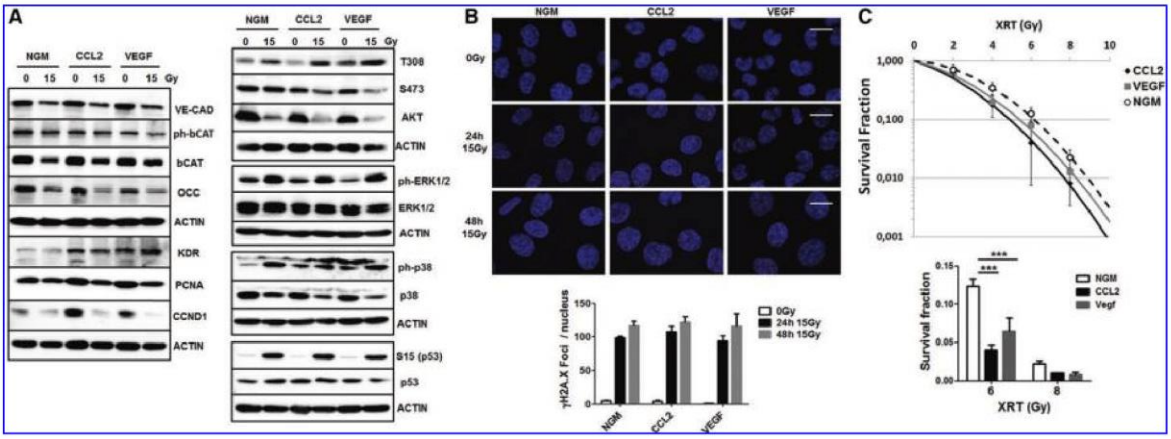

FIG. 5. Exogenous CCL2 stimulation increases radiation-induced EC death and decreases survival of clonogenic ECs. Cultured AS-M5 EC were exposed to irradiation with 15 Gy and subsequently cultured in NGM or NGM supplemented with 20 ng/mL CCL2 or 10 ng/mL VEGF and fixed at the indicated time points for protein or immunofluorescence analysis. **(A)** Expression levels of the indicated proteins were analyzed in whole protein lysates using Western blot analysis at 96 h after radiation and subsequent growth factor treatment. Representative blots from four different experiments are shown ($n=4$). **(B)** Representative photomicrographs of the γ-H2A.X assay with nuclei dyed in *blue* and phosphorylated H2A.X in *magenta*. The kinetics of DNA double-strand breaks repair was followed by counting the amount of γ-H2A.X foci. Data show mean ± SEM ($n=3$) or representative photomicrographs out of three independent experiments (scale bar = 25 μm). **(C)** AS-M5 cells were plated for colony formation assay, irradiated with indicated doses, and subsequently further incubated for additional 10 days in NGM or the presence of CCL2 and VEGF. Data show the surviving fractions from three independent experiments (mean ± SEM). $^{***}p<0.005$ by one-way ANOVA with Bonferroni correction; NGM, normal growth media. To see this illustration in color, the reader is referred to the web version of this article at www.liebertpub.com/ars

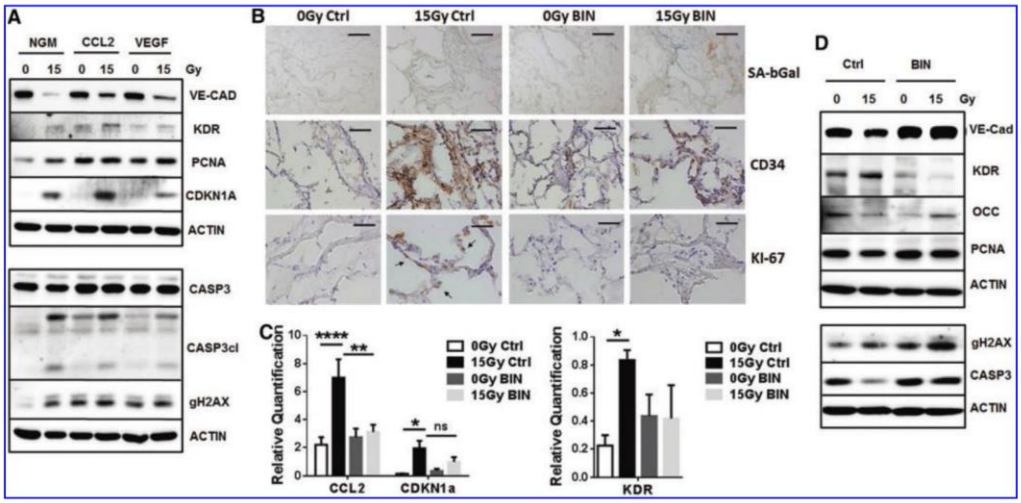

FIG. 6. Exogenous CCL2 stimulation as well as radiation induces a downregulation of endothelial VE-Cad, while upregulating the angiogenic KDR in *ex vivo* cultured lung tissue pieces. Cultured normal lung tissue fragments embedded in growth factor-reduced Matrigel were exposed to irradiation with 15 Gy and subsequently cultured in NGM or NGM supplemented with 20 ng/mL CCL2 or 10 ng/mL VEGF and fixed at the indicated time points for protein or immunofluorescence analysis. **(A)** Expression levels of the indicated proteins were analyzed in whole protein lysates using Western blot analysis at 5 days after radiation and subsequent growth factor treatment. Additional lung tissue pieces were exposed to irradiation with 15 Gy and subsequently treated with BIN (200 μM) or vehicle control. **(B)** SA-betagal activity was assessed using frozen sections of lung tissue pieces at 5 days after irradiation. Photomicrographs depict representative pictures of three independent experiments. Scale bar = 100 μm. Immunohistological stainings with antibodies for the angiogenic EC marker CD34 and for the cell proliferation marker KI-67 on cryostat sections were performed. Sham-irradiated (0 Gy) lung tissue pieces were included as control. Scale bar = 50 μm. **(C)** *CDKN1A*, *CCL2*, as well as *KDR/VEGFR2* mRNA expression levels were further analyzed in total lung piece RNA isolates using qRT-PCR. Data are presented as mean ± SEM from four independent experiments ($n=5$–6 per group). *p*-Values were indicated: $^{*}p\le0.05$, $^{**}p\le0.01$, $^{****}p\le0.005$ by one-way ANOVA with Bonferroni correction; ns, not significant. **(D)** Expression levels of the indicated proteins were analyzed in whole protein lysates using Western blot analysis at 5 days after radiation and subsequent growth factor treatment. To see this illustration in color, the reader is referred to the web version of this article at www.liebertpub.com/ars

important source of (proteinase-activated receptor-1-inducible) Ccl2 (47, 48). We previously reported upregulation of Ccl2 after WTI, which was predominantly induced in bronchial-alveolar epithelial cells and contributed to pneumonitis and fibrosis as distinct features of the lung's response to radiation damage (33). In line with our findings, it was recently reported that lung epithelial cells represent the major source of Ccl2 after influenza A virus infection and that BIN treatment efficiently reduced Ccl2 expression in these cells (73).

Here we show that a timely and spatially defined inhibition of Ccl2-CCR2 signaling represents a potential therapeutic approach for protecting adjacent EC from Ccl2-induced activation and accompanied side effects such as increased immune cell extravasation (acute effect) and EC loss as long-term complication. Ccl2 has already been described to act on the vascular system, for example, by disrupting the blood–brain barrier (21, 61, 74). In general, Ccl2 promotes recruitment, proliferation, as well as vascular dysfunction, for example, increased vascular permeability of EC (28, 41). Endothelial barrier dysfunction in turn was shown to be mediated by activation of the p38 MAPK in inflammation-induced acute lung injury (39). Of note, p38 activation in EC has been demonstrated to be both anti- and proangiogenic: p38 could depress AKT levels resulting in apoptotic signaling; in contrast VEGF-induced VEGFR2-dependent p38 phosphorylation fostered EC migration as well as tube formation (22).

Conformingly we present here that radiation-induced Ccl2 activated MAPK pathways in angiogenic EC *via* CCR2, including ERK1/2 and p38 MAPK, both contribute to the onset of proliferation. p38 MAPK in contrast could also contribute to apoptosis through phosphorylation of p53. As a consequence, the irradiated and thus DNA-damaged and further Ccl2-activated EC start to proliferate, which subsequently results in apoptosis induction and EC loss occurs as long-term complication. Thus, EC express CCR2 and can be activated in response to Ccl2. Mechanistically, Ccl2 induced p42/44 MAPK (ERK1/2) phosphorylation in EC *via* activated CCR2, while the candidate receptors CCR3/5 were not induced by Ccl2, further stressing that Ccl2 exhibits a particular affinity for CCR2 (63). In addition, Ccl2-CCR2 signaling as a mediator of neovascularization has been previously demonstrated in several *in vitro* and *in vivo* models of angiogenesis (57, 62, 69).

As a small synthetic indazolic derivative that preferentially inhibits transcription of Ccl2, BIN has shown clinical efficacy in a broad array of experimental inflammatory, autoimmune, and especially vascular disorders (25, 42, 49, 66). The Ccl2-CCR2 pairing appears to be the prevalent interaction *in vivo* as mice deficient in Ccl2 share similar phenotypes to those deficient in CCR2 (9, 43). Increased levels of Ccl2 were described to effect the recruitment of CCR2-positive Ly6C(+) monocytes. Herein, tumor cell-derived Ccl2 activated the CCR2-positive endothelium to increase vascular permeability and thus fostered tumor cell extravasation and metastasis *in vivo*, whereas CCR2 deficiency prevented the endothelium from activation (72). Of note, endothelial CCR2 re-expression restored extravasation and metastasis, but reduction of CCR2 expression on myeloid cells only decreased, but did not prevent metastasis (72).

Besides its central role in inflammation, a protumorigenic function for Ccl2 in favoring cancer development and subsequent metastasis has also been described and Ccl2 has been associated with poor clinical outcomes in several cancers (15, 41). In particular, the Ccl2-induced recruitment of Ly6C(+) myeloid cells can promote cancer cell metastasis to the lung (65). Myelomonocytic cells were also shown to be essential for the establishment of a premetastatic niche and survival of metastatic cells (24). We show here that in parallel to the restoration of proper vascular function, BIN treatment efficiently counteracted the recruitment of tumor-promoting myeloid cells to the previously irradiated lungs.

Targeting the radiation-induced upregulation of Ccl2 and respective signaling in combination with conventional RT was shown to block undesired radiation-induced immune cell infiltration in an orthotopic mouse model of non-small-cell lung carcinoma (NSCLC) (68). Preventing of Ccl2 signaling can further efficiently inhibit tumor growth of primary and metastatic disease in animal models of NSCLC and prostate cancer. Interestingly, these mechanisms of retarded tumor growth include a significant decrease in microvascular density (19).

Thus, specific targeting of the Ccl2-CCR2 axis presents an attractive therapeutic strategy in several clinical settings (41). Here we now demonstrate that abrogation of certain aspects of the secretome of irradiated resident lung cells, in particular signaling inhibition of the SASP-factor Ccl2, results in protection from RT-induced lung injury, in particular with respect to the endothelial compartment (Fig. 7). In the healthy situation, EC are usually quiescent and thus normal lung capillaries provide an efficient barrier to circulating blood stream components. Radiation induces epithelial cell senescence, which in turn leads to increased production and secretion of Ccl2. Secreted Ccl2 in turn acts as a mediator and stimulates the hitherto quiescent endothelium resulting in endothelial activation toward an angiogenic phenotype (acute effect). The increased endothelial permeability in turn leads to increased leakage of liquids or circulating immune and/or tumor cells into the lung interstitium and thus fosters inflammation and/or metastasis. As long-term complication, the radiation-induced DNA damage, together with the Ccl2-induced EC activation, leads to proliferation of these damaged cells resulting in apoptotic cell death and severe EC loss.

Thereby our findings highlight the contribution of radiation-induced damage to the vascular compartment within the processes of radiation-induced adverse late effects, including fibrosis development. Importantly, our novel data indicate that therapeutic inhibition of radiation-induced Ccl2 signaling protects lungs from vascular dysfunction and EC loss. In addition, reconstitution of proper vascular function may support a microenvironment, for example, through normalization of immune cell infiltration, which favors both prevention of and recovery from radiation injury to vascular cells and other resident lung cells. Conclusively, this study provides novel insight into the mechanisms of radiation-induced inflammation-promoting effects (acute effect) and EC loss (adverse late effect) and strongly argues for Ccl2 signaling inhibition as potential radioprotective strategy. Radioprotection of the normal tissue without affecting the radiosensitization of the tumor tissue has important implications in oncology, because higher doses of radiation might improve both local control and survival.

Materials and Methods

Whole thorax irradiation

Wild-type C57BL/6 (WT) and CCR2-deficient (CCR2-KO) mice (C57BL/6 background) were bred and kept under

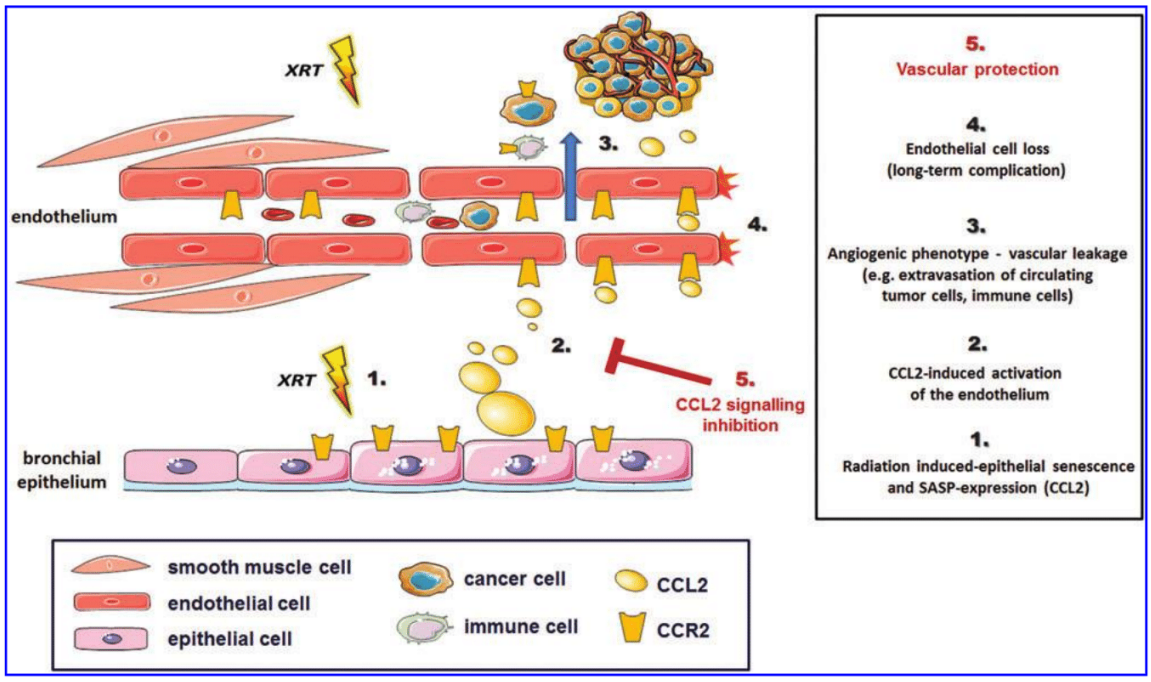

FIG. 7. Radiation-induced normal tissue toxicity is closely linked to vascular EC damage and dysfunction of the blood–air barrier. In the healthy state, EC are usually quiescent and thus normal lung capillaries provide an efficient barrier to liquids or cell extravasation. Radiation-induced epithelial senescence leads to increased SASP factor production (in particular Ccl2) by senescent bronchial-alveolar epithelial cells **(1)**. Secreted Ccl2 stimulates the quiescent endothelium resulting in an activated and/or ''angiogenic'' phenotype (acute effect) **(2)**. The increased endothelial permeability leads to increased leakage of blood stream components into the lung interstitium and thus fosters inflammation and/or metastasis formation by increased extravasation of circulating immune and tumor cells **(3)**. EC loss occurs as long-term complication because the radiation-induced and thus DNA-damaged and further Ccl2-activated EC start to proliferate, subsequently resulting in apoptosis induction **(4)**. Inhibition of radiation-induced Ccl2 signaling protects lungs from radiation-induced vascular dysfunction and EC loss **(5)**. This study provides novel insight into the mechanisms of radiation-induced inflammation-promoting effects (acute effect) and EC loss (adverse late effect) and strongly augments for Ccl2 signaling inhibition as potential protective strategies. SASP, senescence-associated secretory phenotype. To see this illustration in color, the reader is referred to the web version of this article at www.liebertpub.com/ars

specific pathogen-free conditions (18, 38). Mice (mixed gender) received 15 Gy of WTI in a single dose as previously described (33, 70). All procedures involving mice were approved by the local Animal Care Committee (Regierungspräsidium Düsseldorf Az-84-02.04.2012.A137, Az-84-02.04.2015.A446). Within combined treatment, WT mice were exposed to WTI and subsequently treated three times a week (starting within 24 h after WTI) within the first 3 weeks postirradiation by intraperitoneal injection of 100 mg/kg BIN (Selleckchem, Houston, TX) in 0.5% aqueous methylcellulose or methylcellulose alone (vehicle control). Seeding of circulating tumor cells into the lungs was analyzed 21 days after irradiation. Therefore, 0.5×10^6 tumor cells were intravenously transplanted and 14 days later lungs were subjected for IHC. At respective time points, animals were narcotized using isoflurane and killed by transcardial perfusion. Lungs were isolated and directly subjected (isolation time: <5 min) for IHC (PFA fixation), RNA or protein isolation (freshly frozen material in liquid nitrogen), or fluorescent activated cell sorting (FACS) analysis to keep the *ex vivo* postsampling processing time to a minimum (8).

Vascular leakage

Twenty-one days after irradiation, vascular leakage was determined by EBD (Sigma-Aldrich, St. Louis, MO) extravasation from the blood stream into the lung interstitium. Therefore, 100 μg EBD/100 μL phosphate-buffered saline (PBS) were intravenously injected (33). Two to 4 h after injection, anesthetized animals were killed by transcardial perfusion with PBS to remove the vascular blood. Lung pieces were weighted and EBD exuded in the lung interstitium was extracted by incubating tissues in 200 μL formamide for 24 h at 65°C, and dye concentrations were measured by absorption at 620 nm and related to the weight of lung tissue.

Real-time reverse transcription polymerase chain reaction

RNA was isolated using the RNeasy Mini Kit (Qiagen, Hilden, Germany) according to the manufacturer's instruction and qRT-PCR was carried out as previously described (33, 35). Expression levels were normalized to the reference gene (beta actin; set as 1) and were shown as relative quantification.

SA-betagal activity

SA-betagal activity, detectable at pH6, was detected as previously described using frozen sections of lung tissue (16, 33). In brief, slides were rinsed with PBS for 4×5 min and incubated with X-gal staining solution (0.1% X-gal, 5 m*M* potassium ferrocyanide, 5 m*M* potassium ferricyanide, 150 m*M* NaCl, and 2 m*M* $MgCl_2$ in 40 m*M* citric acid/sodium phosphate solution, pH 6; all chemicals were from Sigma-Aldrich) for more than 1 h in a 37°C (light impermeable) incubator. Slides were washed with PBS 3×5 min prior embedding.

Flow cytometry

Crude cell extracts of freshly isolated lungs were generated, and flow cytometry was performed as previously described (33, 70). Lung cell suspensions were stained with fluorochrome-labeled anti-mouse CD45 (30-F11; BioLegend, San Diego, CA), anti-mouse CD31 (390; eBioscience Frankfurt, Germany), and anti-mouse CD11b (M1/70; BioLegend). Flow cytometric measurements were performed on a BD LSRII flow cytometer using FACS DIVA software (BD Bioscience, Franklin Lakes, NJ). For quantification of apoptotic DNA fragmentation (sub-G1 population), trypsinized cells (including respective cells from the cell culture supernatants) were incubated for 15–30 min with 50 μg/mL propidium iodide in 0.1% (w/v) sodium citrate/0.05% (v/v) Triton X-100 (v/v) and subsequently analyzed (BD FACS Calibur) (34, 52).

Western blot

Protein samples (50–100 μg total protein) were subjected to sodium dodecyl sulfate/polyacrylamide gel electrophoresis, and Western blots were done as previously described (33, 35). Unless otherwise indicated, representative blots from three different experiments are shown. For quantification, blots were analyzed by densitometry and respective signals were related to beta-actin. p21 (F8, sc271610), Col1A1 (D13, sc-25974), and VE-Cad (C19, sc6458) antibodies were from Santa Cruz (Santa Cruz, CA), TGF-β-1 antibody (MA5-16949) was from Thermo Scientific (Dreieich, Germany), and beta-actin (AC-74, A2228) antibody was from Sigma-Aldrich. Phospho-β-catenin (Ser33/37/Thr41), phospho-p53 (Ser15), phospho-p44/42 MAPK (Erk1/2) (Thr202/Tyr204), phospho-p38 MAPK (Thr180/Tyr182), and respective non-phosphorylated antibodies were from Cell Signaling Technology (Danvers, MA).

Lung histopathology

For lung histology, mice were narcotized using isoflurane and killed by transcardial perfusion with PBS as previously described (33, 35). In brief, whole inflation fixed lungs were embedded in paraffin. Three micrometer longitudinal cross sections were taken per mouse lung at the midpoint through the lung block depth. Sections were stained with Masson–Goldner's trichrome (Carl Roth, Karlsruhe, Germany) for histological evaluation. Sections were scored blinded to the genotype and treatment group using a 0–8-point Ashcroft scale (35, 70). The mean scores (five per section) were averaged to yield the final score for each specimen. Depicted data represent the mean values of all mice per group as indicated. Metastatic lesions/foci were quantified in hematoxylin and eosin-stained sections by counting numbers of nodules in at least three whole cross sections per mice lung, and averages for individual animals were calculated. IHC and electron microscopy were done as previously described (33, 35).

Cell cultures

The human microvascular EC line AS-M5 was cultured in endothelial cell growth (ECG) medium (PromoCell). Radiation with indicated doses was performed using the Isovolt-320-X-ray machine (Seifert-Pantak, East Haven, CT) at 320 kV, 10 mA with a 1.65-mm aluminum filter. γ-H2A.X foci were stained for 1 h at room temperature with Alexa Fluor®647-anti-H2A.X(pS139) (BD Biosciences). γ-H2A.X foci were analyzed by fluorescence microscopy and counted with the Focinator software (51). For clonogenic survival, 200–1600 cells/well were plated in six-well plates as previously described (34). After radiation with indicated doses, plates were incubated for 10 days to allow growth of single colonies. Cells were then fixed and subsequently stained with 0.05% Coomassie brilliant blue. Colonies (≥50 cells/colony) were counted under the microscope. The survival curves were established by plotting the log of the surviving fraction against the treatment dose.

Cell viability assay

The number of living cells was determined on staining of the cells with the vital dye trypan blue. For this, cells were harvested with trypsin-EDTA, resuspended in fresh medium, diluted with Trypan blue, and counted using a Neubauer chamber.

Tissue material

Normal lung tissue samples were obtained during surgery according to local ethical and biohazard regulations and provided from the Department of Thoracic Surgery and Surgical Endoscopy, Ruhrlandklinik, University Hospital Essen for our institute. All experiments were approved by the local ethics committee. Written informed consent (17-7454-BO) was obtained from the Ethikkommission of the University Medical Faculty, Essen, Germany.

Ex vivo *lung tissue culture*

The *ex vivo* arterial ring or sprouting assay basically used to study angiogenesis was modified for the culture of human lung tissue specimen (6, 32). The benefit of this assay is that the tissue-resident cells can be studied within their own *in situ* microenvironment. Therefore, fresh lung specimens were dissected and transferred directly into sterile PBS on ice. Lung tissue pieces were cut into 5–10 mm squares using a surgical scalpel. A first layer of Matrigel (150 μL) was plated per well, using 48-well cluster tissue culture plates, and incubated at 37°C in a humidified atmosphere with 5% CO_2 for 30 min. Afterward, the lung tissue pieces were placed into the first layer of gel and reincubated in a 37°C, 5% CO_2 humidified incubator for 10 min. After addition of the second layer of Matrigel (150 μL), lung pieces were reincubated for one hour, before they were seeded with 300 mL ECG medium. Embedded pieces were irradiated with indicated doses and incubated at 37°C, 5% CO_2 and further incubated in NGM alone or supplemented with BIN (200 μ*M*) for 5 days.

Statistical analysis

If not otherwise indicated (n = biological replicates), data were obtained from at least from three independent experiments. Individual mice numbers (n) were also indicated in the respective figure legends. Data analysis was performed with Prism 5.0 software (GraphPad, La Jolla, CA). Statistical significance was evaluated by one- or two-way ANOVA followed by multiple comparisons post-test. Statistical significance was set at the level of $p \leq 0.05$.

Acknowledgments

We thank L. Lüdemann and M. Groneberg for support with the irradiation of mice, Holger Jastrow for help in ultrastructural analysis, and Mohamed Benchellal, Inge Spratte, and Eva Gau for their excellent technical assistance. The work was supported by grants of the DFG (GRK1739/1; GRK1739/2), the BMBF (ZISS 02NUK024-D), and the UK Essen/IFORES (D/107-81040).

Authors' Contributions

A.W., J.K., A.S., K.R., F.W., T.H., and D.K. performed experiments; D.K. supervised and analyzed results and made the figures; J.F., D.E., and C.A. provided materials; V.J. and D.K. designed the research and wrote the article. All authors read and approved the article.

Author Disclosure Statement

No competing financial interests exist.

References

1. Aleman BM, van den Belt-Dusebout AW, De Bruin ML, van 't Veer MB, Baaijens MH, de Boer JP, Hart AA, Klokman WJ, Kuenen MA, Ouwens GM, Bartelink H, and van Leeuwen FE. Late cardiotoxicity after treatment for Hodgkin lymphoma. *Blood* 109: 1878–1886, 2007.
2. Almeida C, Nagarajan D, Tian J, Leal SW, Wheeler K, Munley M, Blackstock W, and Zhao W. The role of alveolar epithelium in radiation-induced lung injury. *PLoS One* 8: e53628, 2013.
3. Anscher MS, Chen L, Rabbani Z, Kang S, Larrier N, Huang H, Samulski TV, Dewhirst MW, Brizel DM, Folz RJ, and Vujaskovic Z. Recent progress in defining mechanisms and potential targets for prevention of normal tissue injury after radiation therapy. *Int J Radiat Oncol Biol Phys* 62: 255–259, 2005.
4. Baker DG and Krochak RJ. The response of the microvascular system to radiation: a review. *Cancer Invest* 7: 287–294, 1989.
5. Balli D, Ustiyan V, Zhang Y, Wang IC, Masino AJ, Ren X, Whitsett JA, Kalinichenko VV, and Kalin TV. Foxm1 transcription factor is required for lung fibrosis and epithelial-to-mesenchymal transition. *EMBO J* 32: 231–244, 2013.
6. Bellacen K and Lewis EC. Aortic ring assay. *J Vis Exp* 33: 1564, 2009.
7. Bentzen SM. Preventing or reducing late side effects of radiation therapy: radiobiology meets molecular pathology. *Nat Rev Cancer* 6: 702–713, 2006.
8. Bohackova E and Dankova P. Human peripheral blood cells mRNA levels are highly sensitive to duration of ex vivo post-sampling conditions prior to RNA isolation. *Clin Lab* 63: 1929–1933, 2017.
9. Boring L, Gosling J, Chensue SW, Kunkel SL, Farese RV, Jr., Broxmeyer HE, and Charo IF. Impaired monocyte migration and reduced type 1 (Th1) cytokine responses in C-C chemokine receptor 2 knockout mice. *J Clin Invest* 100: 2552–2561, 1997.
10. Braunstein S and Nakamura JL. Radiotherapy-induced malignancies: review of clinical features, pathobiology, and evolving approaches for mitigating risk. *Front Oncol* 3: 73, 2013.
11. Brush J, Lipnick SL, Phillips T, Sitko J, McDonald JT, and McBride WH. Molecular mechanisms of late normal tissue injury. *Semin Radiat Oncol* 17: 121–130, 2007.
12. Cappuccini F, Eldh T, Bruder D, Gereke M, Jastrow H, Schulze-Osthoff K, Fischer U, Kohler D, Stuschke M, and Jendrossek V. New insights into the molecular pathology of radiation-induced pneumopathy. *Radiother Oncol* 101: 86–92, 2011.
13. Contrepois K, Coudereau C, Benayoun BA, Schuler N, Roux PF, Bischof O, Courbeyrette R, Carvalho C, Thuret JY, Ma Z, Derbois C, Nevers MC, Volland H, Redon CE, Bonner WM, Deleuze JF, Wiel C, Bernard D, Snyder MP, Rube CE, Olaso R, Fenaille F, and Mann C. Histone variant H2A.J accumulates in senescent cells and promotes inflammatory gene expression. *Nat Commun* 8: 14995, 2017.
14. Corre I, Guillonneau M, and Paris F. Membrane signaling induced by high doses of ionizing radiation in the endothelial compartment. Relevance in radiation toxicity. *Int J Mol Sci* 14: 22678–22696, 2013.
15. Craig MJ and Loberg RD. CCL2 (Monocyte Chemoattractant Protein-1) in cancer bone metastases. *Cancer Metastasis Rev* 25: 611–619, 2006.
16. Debacq-Chainiaux F, Erusalimsky JD, Campisi J, and Toussaint O. Protocols to detect senescence-associated beta-galactosidase (SA-betagal) activity, a biomarker of senescent cells in culture and in vivo. *Nat Protoc* 4: 1798–1806, 2009.
17. Deshmane SL, Kremlev S, Amini S, and Sawaya BE. Monocyte chemoattractant protein-1 (MCP-1): an overview. *J Interferon Cytokine Res* 29: 313–326, 2009.
18. Engel D, Dobrindt U, Tittel A, Peters P, Maurer J, Gutgemann I, Kaissling B, Kuziel W, Jung S, and Kurts C. Tumor necrosis factor alpha- and inducible nitric oxide synthase-producing dendritic cells are rapidly recruited to the bladder in urinary tract infection but are dispensable for bacterial clearance. *Infect Immun* 74: 6100–6107, 2006.
19. Fridlender ZG, Kapoor V, Buchlis G, Cheng G, Sun J, Wang LC, Singhal S, Snyder LA, and Albelda SM. Monocyte chemoattractant protein-1 blockade inhibits lung cancer tumor growth by altering macrophage phenotype and activating CD8+ cells. *Am J Respir Cell Mol Biol* 44: 230–237, 2011.
20. Garcia-Barros M, Paris F, Cordon-Cardo C, Lyden D, Rafii S, Haimovitz-Friedman A, Fuks Z, and Kolesnick R. Tumor response to radiotherapy regulated by endothelial cell apoptosis. *Science* 300: 1155–1159, 2003.
21. Ge S, Shrestha B, Paul D, Keating C, Cone R, Guglielmotti A, and Pachter JS. The CCL2 synthesis inhibitor bindarit targets cells of the neurovascular unit, and suppresses experimental autoimmune encephalomyelitis. *J Neuroinflammation* 9: 171, 2012.
22. Gee E, Milkiewicz M, and Haas TL. p38 MAPK activity is stimulated by vascular endothelial growth factor receptor 2

activation and is essential for shear stress-induced angiogenesis. *J Cell Physiol* 222: 120–126, 2010.
23. Ghafoori P, Marks LB, Vujaskovic Z, and Kelsey CR. Radiation-induced lung injury. Assessment, management, and prevention. *Oncology (Williston Park)* 22: 37–47; discussion 52–53, 2008.
24. Gil-Bernabe AM, Ferjancic S, Tlalka M, Zhao L, Allen PD, Im JH, Watson K, Hill SA, Amirkhosravi A, Francis JL, Pollard JW, Ruf W, and Muschel RJ. Recruitment of monocytes/macrophages by tissue factor-mediated coagulation is essential for metastatic cell survival and premetastatic niche establishment in mice. *Blood* 119: 3164–3175, 2012.
25. Grassia G, Maddaluno M, Guglielmotti A, Mangano G, Biondi G, Maffia P, and Ialenti A. The anti-inflammatory agent bindarit inhibits neointima formation in both rats and hyperlipidaemic mice. *Cardiovasc Res* 84: 485–493, 2009.
26. Heneberg P. Paracrine tumor signaling induces transdifferentiation of surrounding fibroblasts. *Crit Rev Oncol Hematol* 97: 303–311, 2016.
27. Higo T, Naito AT, Sumida T, Shibamoto M, Okada K, Nomura S, Nakagawa A, Yamaguchi T, Sakai T, Hashimoto A, Kuramoto Y, Ito M, Hikoso S, Akazawa H, Lee JK, Shiojima I, McKinnon PJ, Sakata Y, and Komuro I. DNA single-strand break-induced DNA damage response causes heart failure. *Nat Commun* 8: 15104, 2017.
28. Hiratsuka S, Ishibashi S, Tomita T, Watanabe A, Akashi-Takamura S, Murakami M, Kijima H, Miyake K, Aburatani H, and Maru Y. Primary tumours modulate innate immune signalling to create pre-metastatic vascular hyperpermeability foci. *Nat Commun* 4: 1853, 2013.
29. Holler V, Buard V, Gaugler MH, Guipaud O, Baudelin C, Sache A, Perez Mdel R, Squiban C, Tamarat R, Milliat F, and Benderitter M. Pravastatin limits radiation-induced vascular dysfunction in the skin. *J Invest Dermatol* 129: 1280–1291, 2009.
30. Kim JH, Jenrow KA, and Brown SL. Mechanisms of radiation-induced normal tissue toxicity and implications for future clinical trials. *Radiat Oncol J* 32: 103–115, 2014.
31. Kim JY, Kim YS, Kim YK, Park HJ, Kim SJ, Kang JH, Wang YP, Jang HS, Lee SN, and Yoon SC. The TGF-beta1 dynamics during radiation therapy and its correlation to symptomatic radiation pneumonitis in lung cancer patients. *Radiat Oncol* 4: 59, 2009.
32. Klein D, Meissner N, Kleff V, Jastrow H, Yamaguchi M, Ergun S, and Jendrossek V. Nestin(+) tissue-resident multipotent stem cells contribute to tumor progression by differentiating into pericytes and smooth muscle cells resulting in blood vessel remodeling. *Front Oncol* 4: 169, 2014.
33. Klein D, Schmetter A, Imsak R, Wirsdorfer F, Unger K, Jastrow H, Stuschke M, and Jendrossek V. Therapy with multipotent mesenchymal stromal cells protects lungs from radiation-induced injury and reduces the risk of lung metastasis. *Antioxid Redox Signal* 24: 53–69, 2016.
34. Klein D, Schmitz T, Verhelst V, Panic A, Schenck M, Reis H, Drab M, Sak A, Herskind C, Maier P, and Jendrossek V. Endothelial Caveolin-1 regulates the radiation response of epithelial prostate tumors. *Oncogenesis* 4: e148, 2015.
35. Klein D, Steens J, Wiesemann A, Schulz F, Kaschani F, Rock K, Yamaguchi M, Wirsdorfer F, Kaiser M, Fischer JW, Stuschke M, and Jendrossek V. Mesenchymal stem cell therapy protects lungs from radiation-induced endothelial cell loss by restoring superoxide dismutase 1 expression. *Antioxid Redox Signal* 26: 563–582, 2017.
36. This reference has been deleted.
37. Korpela E and Liu SK. Endothelial perturbations and therapeutic strategies in normal tissue radiation damage. *Radiat Oncol* 9: 266, 2014.
38. Kuziel WA, Morgan SJ, Dawson TC, Griffin S, Smithies O, Ley K, and Maeda N. Severe reduction in leukocyte adhesion and monocyte extravasation in mice deficient in CC chemokine receptor 2. *Proc Natl Acad Sci USA* 94: 12053–12058, 1997.
39. Li L, Hu J, He T, Zhang Q, Yang X, Lan X, Zhang D, Mei H, Chen B, and Huang Y. P38/MAPK contributes to endothelial barrier dysfunction via MAP4 phosphorylation-dependent microtubule disassembly in inflammation-induced acute lung injury. *Sci Rep* 5: 8895, 2015.
40. Liauw SL, Connell PP, and Weichselbaum RR. New paradigms and future challenges in radiation oncology: an update of biological targets and technology. *Sci Transl Med* 5: 173sr2, 2013.
41. Lim SY, Yuzhalin AE, Gordon-Weeks AN, and Muschel RJ. Targeting the CCL2-CCR2 signaling axis in cancer metastasis. *Oncotarget* 7: 28697–28710, 2016.
42. Lin J, Zhu X, Chade AR, Jordan KL, Lavi R, Daghini E, Gibson ME, Guglielmotti A, Lerman A, and Lerman LO. Monocyte chemoattractant proteins mediate myocardial microvascular dysfunction in swine renovascular hypertension. *Arterioscler Thromb Vasc Biol* 29: 1810–1816, 2009.
43. Lu B, Rutledge BJ, Gu L, Fiorillo J, Lukacs NW, Kunkel SL, North R, Gerard C, and Rollins BJ. Abnormalities in monocyte recruitment and cytokine expression in monocyte chemoattractant protein 1-deficient mice. *J Exp Med* 187: 601–608, 1998.
44. Maebayashi T, Ishibashi N, Aizawa T, Sakaguchi M, Sato T, Kawamori J, and Tanaka Y. Radiation pneumonitis changes over time after stereotactic body radiation therapy for lung tumors: post-treatment cavity (Sunny-side-up Egg-like) Changes. *Anticancer Res* 36: 5563–5570, 2016.
45. Martin M, Lefaix J, and Delanian S. TGF-beta1 and radiation fibrosis: a master switch and a specific therapeutic target? *Int J Radiat Oncol Biol Phys* 47: 277–290, 2000.
46. Maus UA, Waelsch K, Kuziel WA, Delbeck T, Mack M, Blackwell TS, Christman JW, Schlondorff D, Seeger W, and Lohmeyer J. Monocytes are potent facilitators of alveolar neutrophil emigration during lung inflammation: role of the CCL2-CCR2 axis. *J Immunol* 170: 3273–3278, 2003.
47. Mercer PF, Johns RH, Scotton CJ, Krupiczojc MA, Konigshoff M, Howell DC, McAnulty RJ, Das A, Thorley AJ, Tetley TD, Eickelberg O, and Chambers RC. Pulmonary epithelium is a prominent source of proteinase-activated receptor-1-inducible CCL2 in pulmonary fibrosis. *Am J Respir Crit Care Med* 179: 414–425, 2009.
48. Mercer PF, Williams AE, Scotton CJ, Jose RJ, Sulikowski M, Moffatt JD, Murray LA, and Chambers RC. Proteinase-activated receptor-1, CCL2, and CCL7 regulate acute neutrophilic lung inflammation. *Am J Respir Cell Mol Biol* 50: 144–157, 2014.
49. Mirolo M, Fabbri M, Sironi M, Vecchi A, Guglielmotti A, Mangano G, Biondi G, Locati M, and Mantovani A. Impact of the anti-inflammatory agent bindarit on the chemokinome: selective inhibition of the monocyte chemotactic proteins. *Eur Cytokine Netw* 19: 119–122, 2008.
50. Mora E, Guglielmotti A, Biondi G, and Sassone-Corsi P. Bindarit: an anti-inflammatory small molecule that modulates the NFkappaB pathway. *Cell Cycle* 11: 159–169, 2012.
51. Oeck S, Malewicz NM, Hurst S, Rudner J, and Jendrossek V. The Focinator—a new open-source tool for

high-throughput foci evaluation of DNA damage. *Radiat Oncol* 10: 163, 2015.
52. Panic A, Ketteler J, Reis H, Sak A, Herskind C, Maier P, Rubben H, Jendrossek V, and Klein D. Progression-related loss of stromal Caveolin 1 levels fosters the growth of human PC3 xenografts and mediates radiation resistance. *Sci Rep* 7: 41138, 2017.
53. Paris F, Fuks Z, Kang A, Capodieci P, Juan G, Ehleiter D, Haimovitz-Friedman A, Cordon-Cardo C, and Kolesnick R. Endothelial apoptosis as the primary lesion initiating intestinal radiation damage in mice. *Science* 293: 293–297, 2001.
54. Paulino AC, Constine LS, Rubin P, and Williams JP. Normal tissue development, homeostasis, senescence, and the sensitivity to radiation injury across the age spectrum. *Semin Radiat Oncol* 20: 12–20, 2010.
55. Rannou E, Francois A, Toullec A, Guipaud O, Buard V, Tarlet G, Mintet E, Jaillet C, Iruela-Arispe ML, Benderitter M, Sabourin JC, and Milliat F. In vivo evidence for an endothelium-dependent mechanism in radiation-induced normal tissue injury. *Sci Rep* 5: 15738, 2015.
56. Rube CE, Uthe D, Wilfert F, Ludwig D, Yang K, Konig J, Palm J, Schuck A, Willich N, Remberger K, and Rube C. The bronchiolar epithelium as a prominent source of pro-inflammatory cytokines after lung irradiation. *Int J Radiat Oncol Biol Phys* 61: 1482–1492, 2005.
57. Salcedo R, Ponce ML, Young HA, Wasserman K, Ward JM, Kleinman HK, Oppenheim JJ, and Murphy WJ. Human endothelial cells express CCR2 and respond to MCP-1: direct role of MCP-1 in angiogenesis and tumor progression. *Blood* 96: 34–40, 2000.
58. Sasaki M, Miyakoshi M, Sato Y, and Nakanuma Y. Modulation of the microenvironment by senescent biliary epithelial cells may be involved in the pathogenesis of primary biliary cirrhosis. *J Hepatol* 53: 318–325, 2010.
59. Sherborne AL, Davidson PR, Yu K, Nakamura AO, Rashid M, and Nakamura JL. Mutational analysis of ionizing radiation induced neoplasms. *Cell Rep* 12: 1915–1926, 2015.
60. Sohn SH, Lee JM, Park S, Yoo H, Kang JW, Shin D, Jung KH, Lee YS, Cho J, and Bae H. The inflammasome accelerates radiation-induced lung inflammation and fibrosis in mice. *Environ Toxicol Pharmacol* 39: 917–926, 2015.
61. Stamatovic SM, Keep RF, Kunkel SL, and Andjelkovic AV. Potential role of MCP-1 in endothelial cell tight junction ''opening'': signaling via Rho and Rho kinase. *J Cell Sci* 116: 4615–4628, 2003.
62. Stamatovic SM, Keep RF, Mostarica-Stojkovic M, and Andjelkovic AV. CCL2 regulates angiogenesis via activation of Ets-1 transcription factor. *J Immunol* 177: 2651–2661, 2006.
63. Sun RL, Huang CX, Bao JL, Jiang JY, Zhang B, Zhou SX, Cai WB, Wang H, Wang JF, and Zhang YL. CC-Chemokine Ligand 2 (CCL2) Suppresses High Density Lipoprotein (HDL) Internalization and Cholesterol Efflux via CC-Chemokine Receptor 2 (CCR2) Induction and p42/44 Mitogen-activated Protein Kinase (MAPK) activation in human endothelial cells. *J Biol Chem* 291: 19532–19544, 2016.
64. Trimboli AJ, Cantemir-Stone CZ, Li F, Wallace JA, Merchant A, Creasap N, Thompson JC, Caserta E, Wang H, Chong JL, Naidu S, Wei G, Sharma SM, Stephens JA, Fernandez SA, Gurcan MN, Weinstein MB, Barsky SH, Yee L, Rosol TJ, Stromberg PC, Robinson ML, Pepin F, Hallett M, Park M, Ostrowski MC, and Leone G. Pten in stromal fibroblasts suppresses mammary epithelial tumours. *Nature* 461: 1084–1091, 2009.
65. van Deventer HW, Palmieri DA, Wu QP, McCook EC, and Serody JS. Circulating fibrocytes prepare the lung for cancer metastasis by recruiting Ly-6C+ monocytes via CCL2. *J Immunol* 190: 4861–4867, 2013.
66. Vangilder RL, Rosen CL, Barr TL, and Huber JD. Targeting the neurovascular unit for treatment of neurological disorders. *Pharmacol Ther* 130: 239–247, 2011.
67. Vilalta M, Rafat M, Giaccia AJ, and Graves EE. Recruitment of circulating breast cancer cells is stimulated by radiotherapy. *Cell Rep* 8: 402–409, 2014.
68. Wang X, Yang X, Tsai Y, Yang L, Chuang KH, Keng PC, Lee SO, and Chen Y. IL-6 mediates macrophage infiltration after irradiation via up-regulation of CCL2/CCL5 in non-small cell lung cancer. *Radiat Res* 187: 50–59, 2017.
69. Weber KS, Nelson PJ, Grone HJ, and Weber C. Expression of CCR2 by endothelial cells: implications for MCP-1 mediated wound injury repair and In vivo inflammatory activation of endothelium. *Arterioscler Thromb Vasc Biol* 19: 2085–2093, 1999.
70. Wirsdorfer F, de Leve S, Cappuccini F, Eldh T, Meyer AV, Gau E, Thompson LF, Chen NY, Karmouty-Quintana H, Fischer U, Kasper M, Klein D, Ritchey JW, Blackburn MR, Westendorf AM, Stuschke M, and Jendrossek V. Extracellular adenosine production by ecto-5′-nucleotidase (CD73) enhances radiation-induced lung fibrosis. *Cancer Res* 76: 3045–3056, 2016.
71. This reference has been deleted.
72. Wolf MJ, Hoos A, Bauer J, Boettcher S, Knust M, Weber A, Simonavicius N, Schneider C, Lang M, Sturzl M, Croner RS, Konrad A, Manz MG, Moch H, Aguzzi A, van Loo G, Pasparakis M, Prinz M, Borsig L, and Heikenwalder M. Endothelial CCR2 signaling induced by colon carcinoma cells enables extravasation via the JAK2-Stat5 and p38MAPK pathway. *Cancer Cell* 22: 91–105, 2012.
73. Wolf S, Johnson S, Perwitasari O, Mahalingam S, and Tripp RA. Targeting the pro-inflammatory factor CCL2 (MCP-1) with Bindarit for influenza A (H7N9) treatment. *Clin Transl Immunol* 6: e135, 2017.
74. Yao Y and Tsirka SE. Truncation of monocyte chemoattractant protein 1 by plasmin promotes blood-brain barrier disruption. *J Cell Sci* 124: 1486–1495, 2011.
75. Zeng L, Ou G, Itasaka S, Harada H, Xie X, Shibuya K, Kizaka-Kondoh S, Morinibu A, Shinomiya K, and Hiraoka M. TS-1 enhances the effect of radiotherapy by suppressing radiation-induced hypoxia-inducible factor-1 activation and inducing endothelial cell apoptosis. *Cancer Sci* 99: 2327–2335, 2008.

Address correspondence to:
Dr. rer. nat. Diana Klein
Institute of Cell Biology (Cancer Research)
University of Duisburg-Essen
University Hospital Essen
Virchowstr. 173
Essen Ger-45147
Germany

E-mail: diana.klein@uk-essen.de

Date of first submission to ARS Central, November 27, 2017; date of final revised submission, February 3, 2018; date of acceptance, February 20, 2018.

Abbreviations Used

Akt = protein kinase B
BIN = bindarit
Ccl2 = chemokine C-C motif ligand 2
CCND1 = Cyclin D1
Cdkn1a/p21 = cellular senescence mediator cyclin-dependent kinase inhibitor 1
cT = connective tissue
DAB = 3,3′-diaminobenzidine
EBD = Evans blue dye
EC = endothelial cell
ECG = endothelial cell growth
ERK1/2 = extracellular signal-regulated kinases 1 and 2
FACS = fluorescent activated cell sorting
Fn1 = fibronectin 1
Gy = Gray
HA = hyaluronan
IHC = immunohistochemistry
IL = interleukin
Lu = lumen
MAPK = mitogen-activated protein kinase
MCP = monocyte chemoattractant protein
MSCs = mesenchymal stem cells
NGM = normal growth media
NSCLC = non-small-cell lung carcinoma
PBS = phosphate-buffered saline
PCNA = proliferating-cell-nuclear-antigen
qRT-PCR = real-time reverse transcription polymerase chain reaction
RT = radiotherapy
SA-betagal = senescence-associated beta-galactosidase
SASP = senescence-associated secretory phenotype
SMC = smooth muscle cell
Tagln = transgelin
TGF-β = transforming growth factor
VE-Cad = VE-cadherin
VEGFR2 = vascular endothelial growth factor receptor 2
WTI = whole thorax irradiation

Supplemental Material

Supplemental Figures

Figure S1

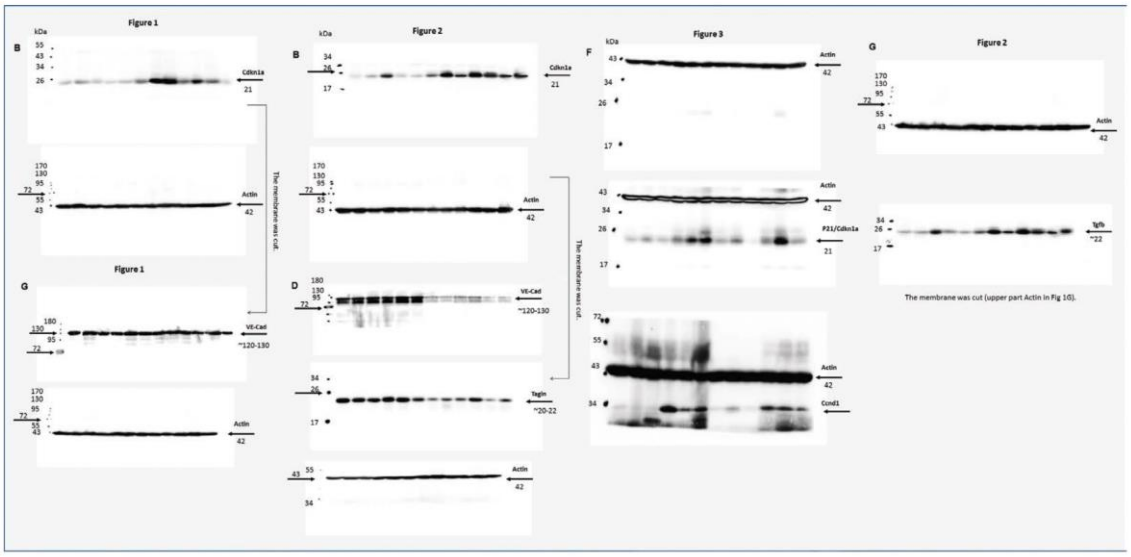

Supplementary Figure S1. Full gels of cropped gels as shown in Figure 1B,G, 2B, D, G and 3F. Equal protein amounts (100 µg, whole cell lysate) were loaded. Beta-actin was included as a loading control.

Figure S2

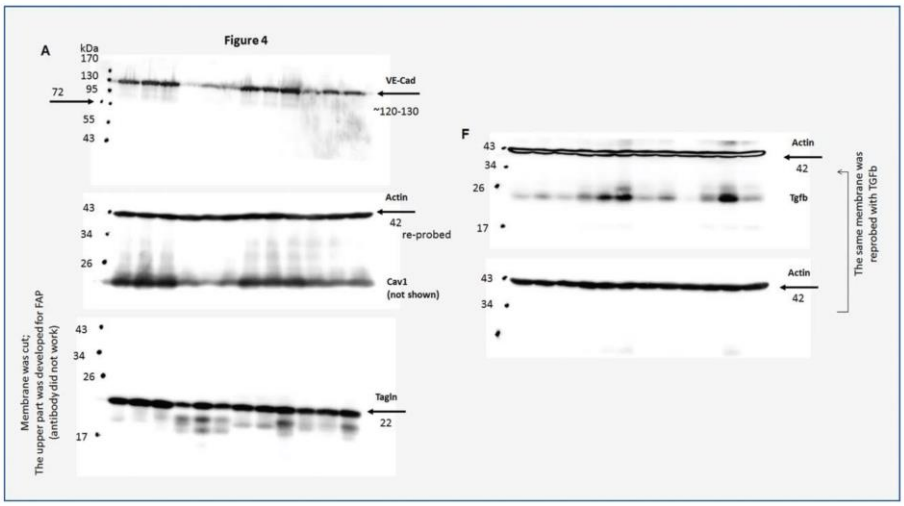

Supplementary Figure S2. Full gels of cropped gels as shown in Figure 4A and F. Equal protein amounts (100 µg, whole cell lysate) were loaded. Beta-actin was included as a loading control.

Figure S3

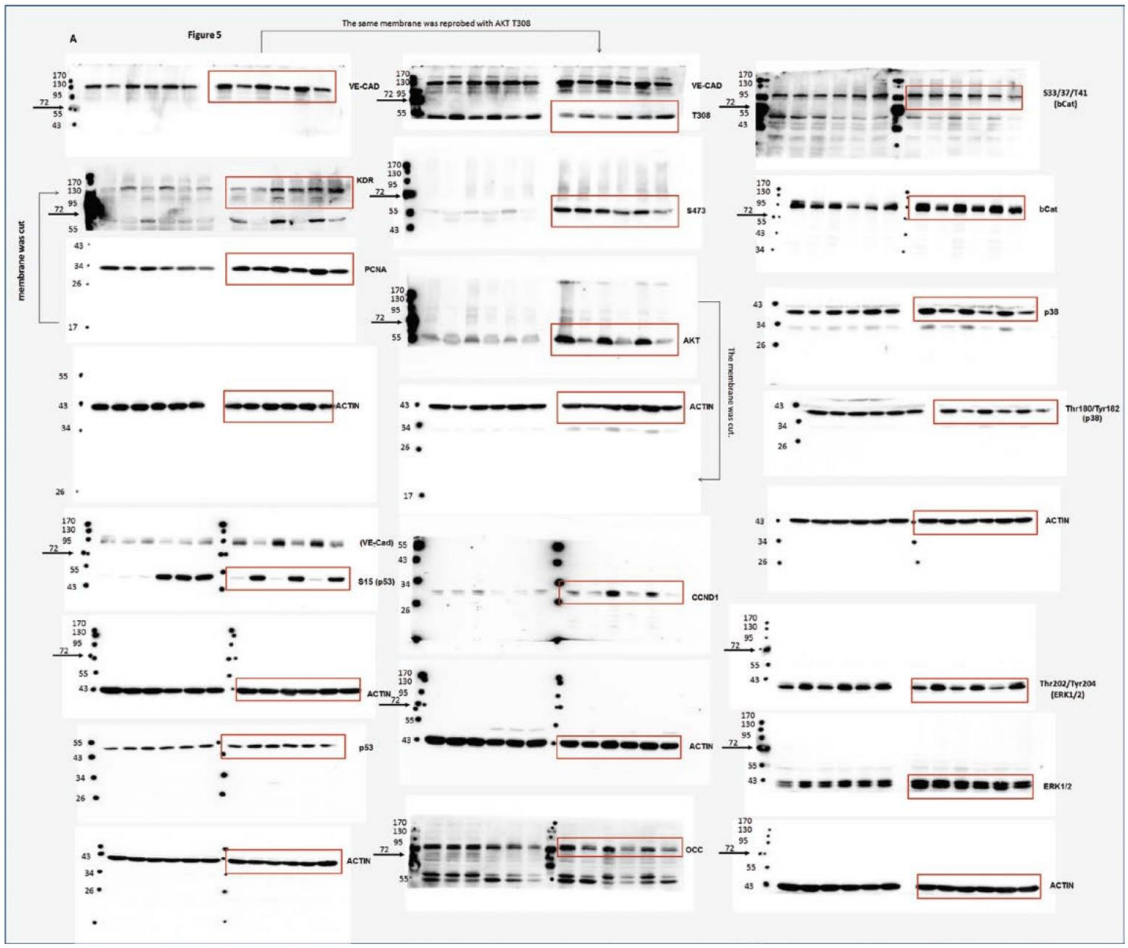

Supplementary Figure S3. Full gels of cropped gels (emphasized by a red rectangle) as shown in Figure 5A. Equal protein amounts (100 µg, whole cell lysate) were loaded. Beta-actin was included as a loading control.

Figure S4

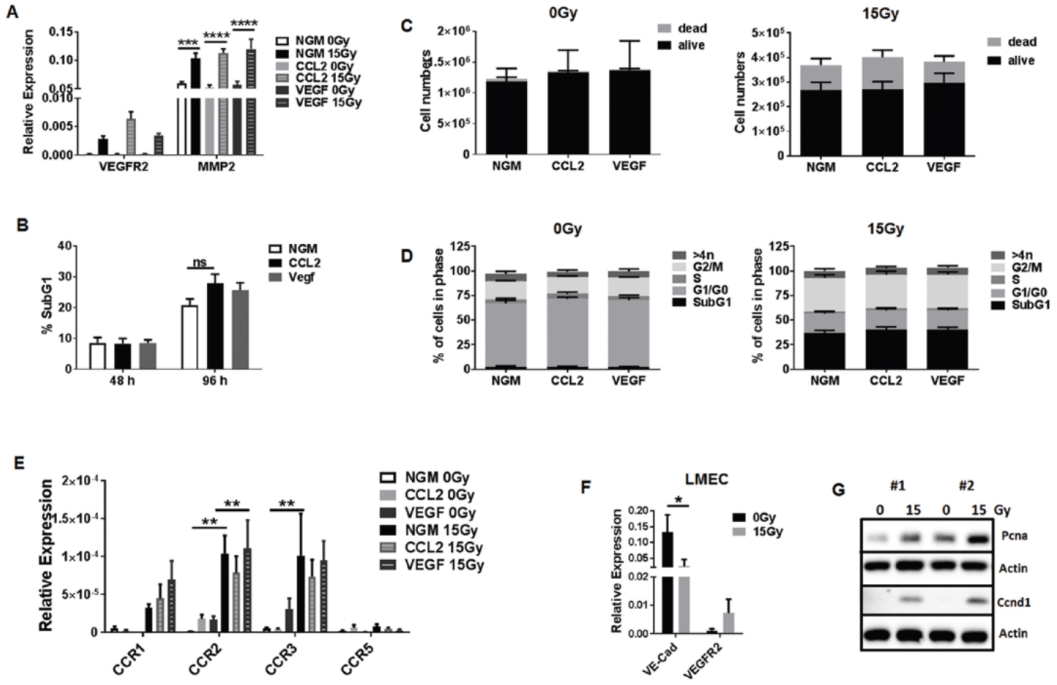

Supplementary Figure S4. Exogenous CCL2 stimulation induces an activated/ angiogenic endothelial phenotype, increases proliferation as well as radiation-induced endothelial cell death. Cultured AS-M5 endothelial cells were exposed to irradiation with 15 Gy, subsequently cultured in normal growth media (NGM) or NGM supplemented with 20 ng/ml CCL2 or 10 ng/ml VEGF and harvested after 96 hours for the respective analysis. (**A**) *KDR/VEGFR2* as well as the angiogenic endothelial matrix metalloproteinase *MMP2* mRNA expression levels were analyzed in total AS-M5 RNA isolates using qRT-PCR. Data are presented as mean ± SEM from four independent experiments (n=5 per group). P-values were indicated: ***$P \leq 0.005$, ****$P < 0.001$ by two-way ANOVA with post-hoc Tukey multiple comparison test. (**B**) The degree of apoptosis was quantified measuring the SubG1 fraction after radiation by flow cytometry analysis. SubG1 levels were related to the 0Gy (control) value (set as 1). Data are presented as means ± SEM from three independent experiments. (**C**) Cell proliferation was analyzed by cell counting of Trypan blue-stained 15Gy irradiated and control (0Gy) irradiated AS-M5 cells (96 hours after irradiation). Counted Trypan-blue-positive cells were depicted as dead cells. Data are shown as means ± SEM of four independent experiments. (**D**) Cell cycle analysis was performed by determining the proportion of cells in different phases of the cell cycle in the DNA histogram of 7-Aminoactinomycin D (7-AAD)-stained AS-M5 cells 96 hours after irradiation and subsequent growth factor treatment. (**E**) Beside the main CCL2 receptor *CCR2* the potential CCL2 receptors *CCR1, CCR3* and *CCR5* mRNA expression levels were analyzed in total AS-M5 RNA isolates by qRT-PCR. Data are presented as mean ± SEM from three independent experiments (n=3-5 per group). P-values were indicated: **$P \leq 0.01$ by two-way ANOVA with post-hoc Tukey multiple comparison test. (**F**) To corroborate the radiation-induced activated endothelial cell phenotype we purified lung microvascular EC (LMEC) from *ex vivo* isolated crude lung cell extracts (C57BL/6 mice) by PECAM1/CD31 antibody and immunomagnetic separation and quantified the *VE-Cad* and *VEGFR2* expression levels by qRT-PCR. Data are presented as mean ± SEM from three independent experiments (n=4 per group). *$P < 0.05$ by two-way ANOVA with Bonferroni correction. Induced endothelial cell proliferation was further assessed in whole protein lysates using Western blot analysis of the proliferation markers Pcna and Ccnd1. Representative blots from three different experiments are shown (n=3).

Figure S5

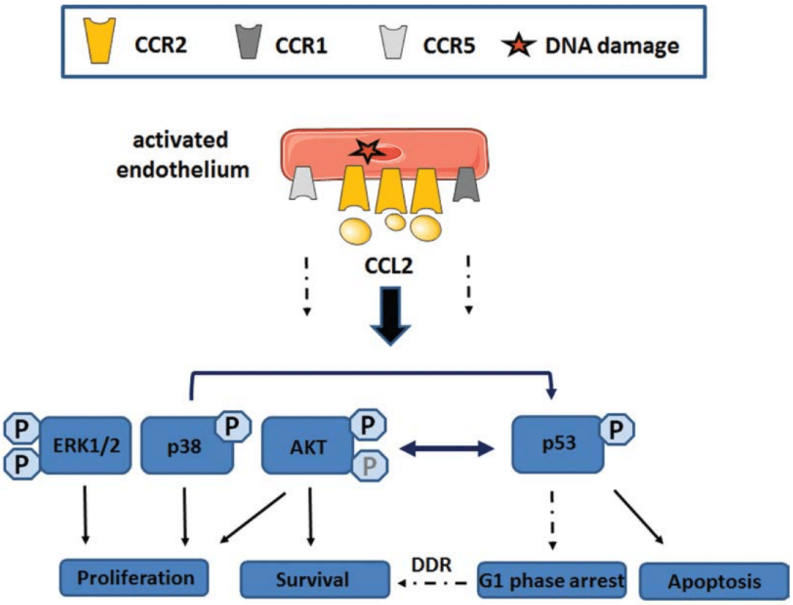

Supplementary Figure S5. Proposed model for the impact of CCL2 on the regulatory mechanism in irradiated endothelial cells. The radiation-induced SASP factor CCL2 (secreted from senescent bronchial epithelial cells) binds to CCR2 in activated endothelial cells , and activates MAPK pathways including extracellular signal-regulated kinases 1 and 2 (ERK1/2) and p38 MAPK that both contribute to the onset of proliferation. p38 MAPK in turn can regulate apoptosis through specific phosphorylation of downstream mediators of apoptosis, including p53. The p53 surveillance system, which is responsive to cell stress (e.g. DNA damage) from external sources such as irradiation, can induce cell cycle arrest while the DNA damage is repaired or can drive the cell into p53-induced apoptosis if the damage is too severe. Irradiation of endothelial cells results further in protein kinase B (PKB)/AKT activation fostering cell survival.

Figure S6

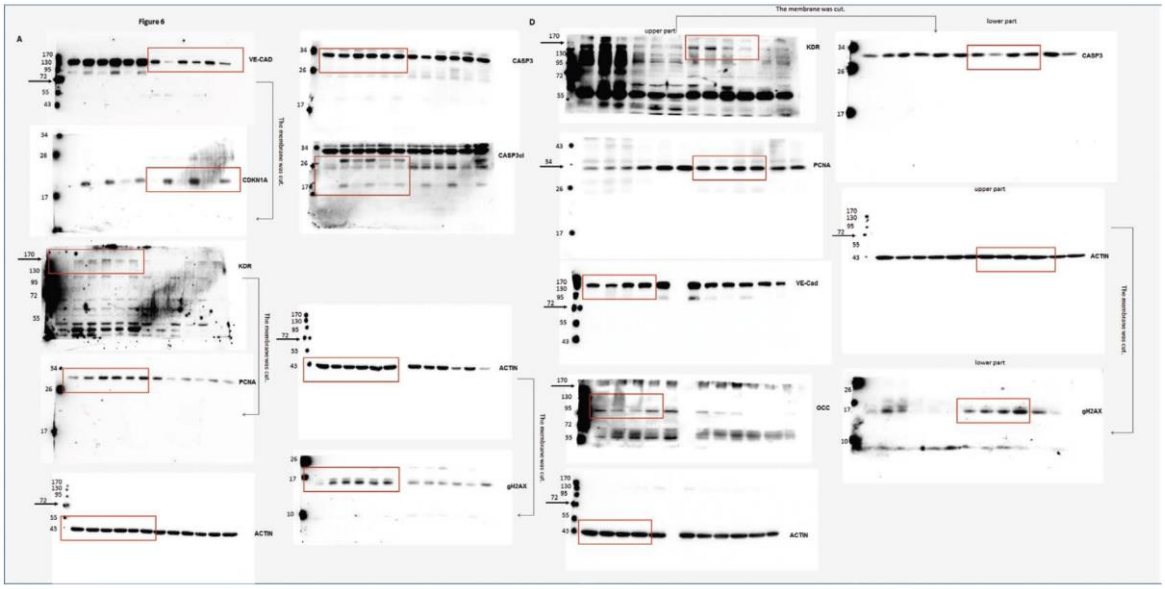

Supplementary Figure S6. Full gels of cropped gels as shown in Figure 6A,D. Equal protein amounts (100 µg, whole cell lysate) were loaded. Beta-actin was included as a loading control.

Figure S7

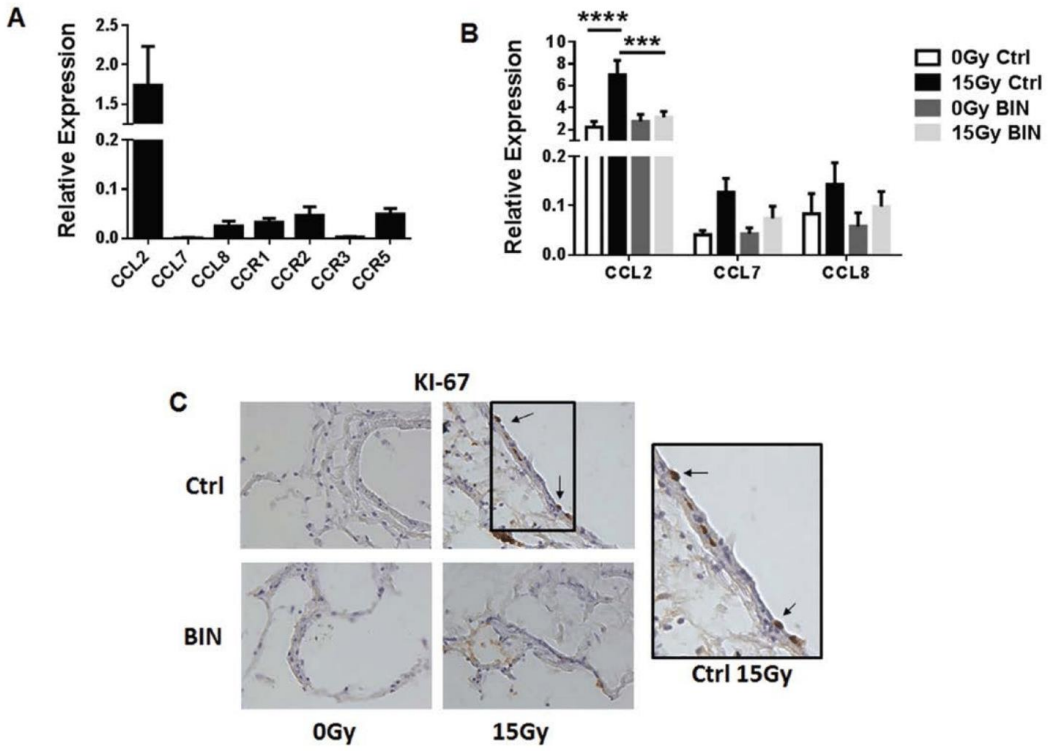

Supplementary Figure S7. Radiation-induced CCL2 expression in *ex vivo* cultured human lung tissues induces endothelial cell proliferation. Although CCL2 is the best characterized target of bindarit, it also inhibits other inflammatory mediators, such as CCL8, CCL7. (**A**) In order to highlight the central role of CCL2 contributing to radiation-induced normal tissue damage, *CCL2, CCL7* and *CCL8* as well as their potential receptors were quantified directly in normal lung specimens which were obtained during surgery and directly apart from embedding into matrigel (ex vivo lung tissue culture). mRNA expression levels of indicated genes were analyzed in total lung pieces RNA isolates using qRT-PCR. Data are presented as mean ± SEM from six independent experiments measured in duplicates each (n=6 per gene). P-values were indicated: **P* ≤ 0.05, **P < 0.01 by one-way ANOVA with Bonferroni correction. (**B**) Cultured normal lung tissue fragments embedded in growth factor reduced matrigel were exposed to irradiation with 15 Gy, subsequently treated with bindarit (200 µM) or vehicle control for 5 days. mRNA expression levels of CCL2 (as shown in Figure 6C) as well as of CCL7 and CCL8 were analyzed in total lung pieces RNA isolates using qRT-PCR. Data are presented as mean ± SEM from four independent experiments (n=5-7 per group). P-values were indicated: **P* ≤ 0.05, **P < 0.01 by ****P* ≤ 0.005, ****P < 0.001 by two-way ANOVA with post-hoc Tukey multiple comparison test. (C) Immunohistological stainings for the cell proliferation marker KI-67 on cryostat sections were performed (as shown in Figure 6B). The higher magnification was included in order to visualize proper nuclear KI-67 staining.

5.3 Progression-related Loss of Stromal Caveolin 1 Levels Fosters the Growth of Human PC3 Xenografts and Mediates Radiation Resistance.

Cumulative thesis of Ms Julia Ketteler

Author contributions

Title of publication: Progression-related loss of stromal Caveolin 1 levels fosters the growth of human PC3 xenografts and mediates radiation resistance.

Authors: Panic A*, Ketteler J*, Reis H, Sak S, Herskind C, Maier P, Rübben H, Jendrossek V, Klein D.

Scientific Reports 2017, doi: 10.1038/srep41138

* Equal contribution

Contributions:

- Conception – 20 %: planning experiments
- Experimental work – 40 %: Figure 1c, 5c, experiments for Figure 7 a-f, Figure S4, Figure S6, Figure S7
- Data analysis – 40 %: Figure 1c, 5c, Figure 7 c and d, Figure S4, S6 and S7, figure preparation and panel selection
- species identification: not applicable
- Statistical analysis – 30 %: Figure 1c, 5c, 7 c and d
- Writing the manuscript – 20 %: Material and Methods, respective figure legends, proof reading
- Revising the manuscript – 50 %: critical proofreading and adjustments of figures/text, additional experiments required for revision

Unterschrift Doktorand/in

Unterschrift Betreuer/in

SCIENTIFIC REPORTS

OPEN

Progression-related loss of stromal Caveolin 1 levels fosters the growth of human PC3 xenografts and mediates radiation resistance

Received: 13 September 2016
Accepted: 15 December 2016
Published: 23 January 2017

Andrej Panic[1,2,*], Julia Ketteler[1,*], Henning Reis[3], Ali Sak[4], Carsten Herskind[5], Patrick Maier[5], Herbert Rübben[2], Verena Jendrossek[1,#] & Diana Klein[1,#]

Despite good treatment results in localized prostate tumors, advanced disease stages usually have a pronounced resistance to chemotherapy and radiotherapy. The membrane protein caveolin-1 (Cav1) functions here as an important oncogene. Therefore we examined the impact of stromal Cav1 expression for tumor growth and sensitivity to ionizing radiation (IR). Silencing of Cav1 expression in PC3 cells resulted in increased tumor growth and a reduced growth delay after IR when compared to tumors generated by Cav1-expressing PC3 cells. The increased radiation resistance was associated with increasing amounts of reactive tumor stroma and a Cav1 re-expression in the malignant epithelial cells. Mimicking the human situation these results were confirmed using co-implantation of Cav1-silenced PC3 cells with Cav1-silenced or Cav1-expressing fibroblasts. Immunohistochemically analysis of irradiated tumors as well as human prostate tissue specimen confirmed that alterations in stromal-epithelial Cav1 expressions were accompanied by a more reactive Cav1-reduced tumor stroma after radiation and within advanced prostate cancer tissues which potentially mediates the resistance to radiation treatment. Conclusively, the radiation response of human prostate tumors is critically regulated by Cav1 expression in stromal fibroblasts. Loss of stromal Cav1 expression in advanced tumor stages may thus contribute to resistance of these tumors to radiotherapy.

The clinical relevance of the tumor microenvironment in modulating the response of solid tumors to chemotherapy and radiotherapy has been documented[1–5]. Herein, the membrane protein caveolin-1 (Cav1) came into focus as it is overexpressed or mutated in many solid human tumors[6–11]. Although Cav1 acts as tumor suppressor in non-transformed cells, its overexpression has been linked to tumor progression and poor prognosis[12–15]. As an example, overexpression of Cav1 has been identified as a marker for breast, lung and prostate cancer (PCa) progression that is associated with increased resistance to chemotherapy, metastatic disease and poor prognosis[16,17]. Furthermore, patients with advanced PCa had also increased serum levels of Cav1 suggesting a secretion of Cav1 from PCa cells that may contribute to the tumor-promoting effects of Cav1[18]. Interestingly, though levels of Cav1 increased in epithelial cancer cells during PCa progression, Cav1 expression was decreased in the tumor stroma in advanced and metastatic PCa, an effect that was found to be functionally relevant to tumor progression and to correlate with reduced relapse-free survival[10,19]. It is assumed that regulated Cav1 expression in the cancer cells is a prerequisite for their hyperproliferative stage and that Cav1 might regulate tumor-promoting epithelial-mesenchymal transition (EMT) of the transformed epithelial cells, tumor angiogenesis and metastasis[20]. Regulation of Cav1 function was further related to signaling by receptor-independent tyrosine kinases (Src, Abl) or oncogenes (c-myc, v-Abl, H-Ras), to the inactivation of tumor suppressor genes (p53), as well as to

[1]Institute of Cell Biology (Cancer Research), University of Duisburg-Essen, University Hospital, Virchowstrasse 173, 45122 Essen, Germany. [2]Department of Urology and Urooncology, University of Duisburg-Essen, University Hospital, Essen, Hufelandstr. 55, 45122 Essen, Germany. [3]Institut of Pathology, University of Duisburg-Essen, University Hospital, Hufelandstr. 55, 45122 Essen, Essen, Germany. [4]Department of Radiotherapy, University of Duisburg-Essen, University Hospital, Hufelandstr. 55, 45122 Essen, Germany. [5]Department of Radiation Oncology, University Hospital, Medical Faculty Mannheim, Heidelberg University, Theodor-Kutzer-Ufer 1-3, 68167 Mannheim, Germany. *These authors contributed equally to this work. #These authors jointly supervised this work. Correspondence and requests for materials should be addressed to D.K. (email: Diana.Klein@uk-essen.de)

posttranslational modifications such as phosphorylation or palmitoylation[21]. Altogether these observations demonstrate that in the context of the altered genetic background of transformed cells Cav1 mediates altered cellular functions such as apoptosis resistance and metastasis[22]. Studies in other cancer types further implicated Cav1 as a pro-survival factor mediating resistance e.g. in pancreatic and lymphoblastoid cancer cells to the cytotoxic action of ionizing radiation (IR) *in vitro*. Silencing of Cav1 in pancreatic cancer cell lines resulted in the disruption of its interactions with beta1-integrin and focal adhesion kinase leading to reduced cell adhesion, proliferation and survival after exposure to IR[23–25]. Similarly, Cav1 expression also protected lymphoblastoid TK6 from radiation-induced apoptosis[26].

For PCa therapy radical prostatectomy, hormone ablation therapy, percutaneous radiotherapy and interstitial radiation methods are available today for treatment of localized stages[27–30]. Radiotherapy (RT) is also an integral part of treatment protocols for inoperable locally advanced PCa. However, resistance to chemotherapy and RT remains a major obstacle in the successful treatment of high-risk PCa patients. Herein the role of Cav1 for the outcome of RT in the context of tumor-stroma interactions is still largely unknown.

Consistent with earlier findings we recently demonstrated that increased expression of Cav1 in epithelial cancer cells of advanced human PCa tissue specimens was paralleled by a reduction of Cav1 in the tumor stroma which is well known to have a more reactive phenotype in advanced prostate carcinoma[19,31–33]. Importantly alterations in stromal Cav1 levels did not include the tumor vasculature because independent of the tumor stages Cav1 was highly expressed in tumor endothelial cells, even in advanced prostate carcinomas. Cav1 may therefore constitute a valuable therapeutic target to overcome therapy resistance by sensitizing both, radioresistant tumor cells and the radioresistant tumor vasculature, to the cytotoxic effects of IR[19]. Nevertheless, the accelerated growth of untreated prostate tumors in the Cav1-deficient background hinted to a potential risk of treatment strategies targeting endothelial Cav1 for radiosensitization in these tumors making careful validation of such treatment strategies with respect to adverse growth promoting effects absolutely necessary[19].

Therefore it has to be elucidated whether Cav1-dependent resistance-promoting signals from endothelial cells (EC) can be separated from Cav1-dependent stromal signals that restrict tumor growth and may thus allow a safer targeting of Cav-1 mediated radiation resistance. Here we investigated the role of stromal Cav1 for growth- and resistance-promoting tumor-stroma interactions during PCa progression with a focus on the impact of stromal fibroblasts.

Results

Reduction of Cav1 levels decreased survival of clonogenic epithelial cells *in vitro*. To investigate whether reduced Cav1 expressions might alter the radiation response of malignant prostate epithelial cells we performed *in vitro* experiments using the human prostate carcinoma cell line PC3 in combination with shRNA knock-down of Cav1 expression (Fig. 1). Using long-term assays measuring the surviving fraction after irradiation revealed that the number of epithelial PC3 cells able to re-grow and form a colony after irradiation was considerably diminished in shCav1 PC3(−) cells as compared to the shCtrl PC3(+) cells with normal Cav1 expression (Fig. 1A). The reduction of Cav1 levels resulted in a slight but not significant increase in epithelial cell proliferation (Fig. 1B). Radiation further fostered a significant upregulation of Cav1 expression levels in shCtrl PC3(+) but not in shCav1 PC3(−) (Fig. 1C). Expression levels of the proliferation marker cyclin D1 (Ccnd1) were furthermore significantly increased in shCav1 PC3(−) upon radiation. Further examination of the expression levels of the survival protein Akt/ Protein kinase B showed that the more radio-sensitive shCav1 PC3(−) showed significantly decreased expression levels of Akt as compared to Cav1- expressing shCtrl PC3(+). Consequently lowering Cav1 levels specifically in tumor epithelial cells may be suited to increase the efficiency of IR in PCa.

Single dose irradiation decreased growth of PC3 xenograft tumors more efficiently in Cav1-expressing PC3 tumors which was accompanied by a less reactive tumor stroma. To examine the role of epithelial Cav1 in prostate tumor radiosensitivity *in vivo*, we next compared the response to a single high dose irradiation in PC3(−) tumor xenografts to that of Cav1-expressing PC3(+) cells, because the above *in vitro* data suggested that the Cav1-silenced PC3 cells are more sensitive to IR (Fig. 2). For this, subcutaneous PC3 prostate xenografts were implanted onto the hind limb of NMRI nude mice and were irradiated locally with a single dose of 10 Gy when the tumor reached a size of about 100 mm^3 (around day 3). Tumor growth was determined by measuring the tumor volume 3 times a week (Fig. 2A). PC3(−)-derived tumors showed a significantly increased tumor growth when compared to PC3(+)-derived tumors as demonstrated by the reduced time to reach a four-fold tumor volume (Fig. 2A). Moreover, tumor growth delay after radiation was significantly decreased in shCav1 PC3(−)-derived tumors as demonstrated by the reduced time to reach a four-fold tumor volume (PC3(+) 0 Gy: 10,80 ± 0,49d, n = 5; PC3(+) 10 Gy: 14,60 ± 0,60d, n = 5; PC3(−) 0 Gy: 7,50 ± 0,33d, n = 8; PC3(−) 10 Gy: 9,14 ± 0,55d, n = 7). Because of this discrepancy in radiosensitivity between the *in vitro* and *in vivo* findings we investigated the levels of the proliferation marker Ccnd1 in whole tumor lysates by Western blot analysis (Fig. 2B). In line with the observed *in vitro* findings shCav1 PC3-derived tumors showed significantly higher protein levels of Ccnd1. Ccnd1 expression levels were even significantly increased in irradiated shCav1 PC3(−)-derived tumors as compared to irradiated PC3(+)-derived tumors. We further examined the expression levels of the survival protein Akt (Fig. 2B). Significantly increased expression levels of Akt were detected in PC3(−)-tumors. Surprisingly the Cav1 expression levels were not significantly reduced in tumors grown from Cav1-silenced PC3(−) cells (Fig. 2C). Together with the fact that *in vitro* PC3(−) cells showed an increased proliferation rate and a significantly increased sensitivity to IR we speculate that differences in the stromal compartment between tumors grown from PC3(−) and Cav1-expressing PC3(+) cells may contribute to the observed findings. We therefore investigated the expression levels of the reactive stroma markers fibroblast activating protein (FAP) and transgelin (Tagln), as well as c-Src, a non-receptor tyrosine kinase that regulates a complex

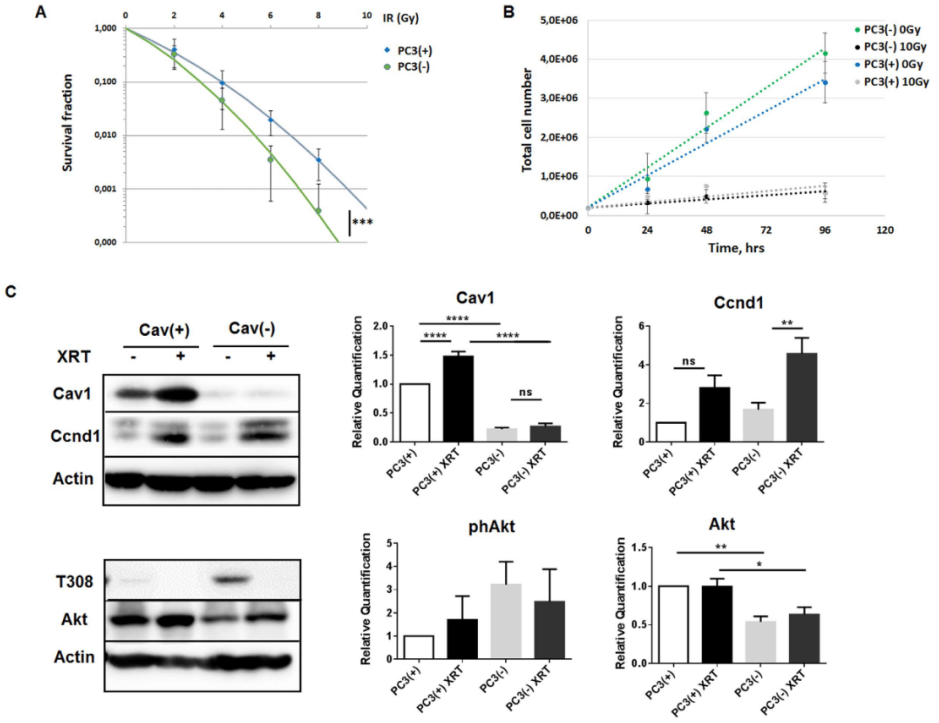

Figure 1. Reduction of Cav1 levels decreased survival of clonogenic epithelial PC3 while proliferation was increased *in vitro*. (**A**) PC3 (shCav1-transfected tumor cells [PC3(−)] as well as PC3 shCtrl control cells [PC3(+)] with normal Cav1 expression) cells were plated for colony formation assay, irradiated with indicated doses (0–8 Gy) and subsequently further incubated for additional 10 days. Data show the surviving fractions from three independent experiments measured in triplicates each (means ± SD). $^{***}P \leq 0.005$ by two-tailed students T-test. (**B**) Cell proliferation was analyzed by cell counting in cultured shCav1-transfected PC3(−) and control-transfected PC3(+) epithelial cells at the indicated time points after irradiation with 10 Gy. Data are shown as means ± SEM of three independent experiments. (**C**) Expression levels of the indicated proteins were analyzed in whole protein lysates of cultured PC3 cells (+/−Cav1) with or without radiation (48 hours after XRT with 10 Gy) using Western blot analysis. Representative blots are shown. For quantification blots were analyzed by densitometry and the respective signal was related to beta-actin (n = 4–5 for each group). For determination of the Akt phosphorylation status the obtained phospho-specific signal was related to the signal of the total protein (phAkt/Akt). P-values were indicated: $^{*}P \leq 0.05$, $^{**}P \leq 0.01$, $^{****}P \leq 0.001$, by one-way ANOVA followed by post-hoc Tukey test.

signaling network and that has been implicated in both epithelial and stromal mechanisms of disease progression (Fig. 2D). Interestingly higher expression levels of these proteins were detected in PC3(−)-tumors indicating the presence of a more reactive tumor stroma. In particular after irradiation the presence of a more reactive tumor stroma might account for the observed reduced sensitivity to IR *in vivo*.

Immunohistological analysis of experimental PC3 prostate xenografts confirmed the presence of a more reactive tumor stroma which potentially caused the radiation resistance. To corroborate the findings of a more reactive tumor stroma in Cav1-silenced PC3(−)-tumors tissues derived from PC3(−) cells as well as from Cav1-expressing PC3(+) cells were subjected to immunohistochemistry for Cav1, FAP and Tagln (Fig. 3A). As expected nearly no epithelial Cav1 expression was detected in tumors derived from Cav1-silenced PC3(−) cells. As compared to Cav1-expressing PC3(+)-tumors, PC3(−)-tumors contain a more collagenous tumor stroma as revealed by the increased blue-green stromal compartment after a Masson's Goldner Trichrome staining. After radiation there was markedly increased Cav1 expression detectable in these PC3(−)-derived tumors which was paralleled by an increased immunoreactivity to FAP and Tagln in the stromal compartment (Supplemental Figure S1). This confirmed our Western blot results that tumors derived from PC3(−) cells have higher amounts of stromal marker proteins and that in particular after radiation treatment the more radioresistant PC3(−)-tumors are characterized by a more reactive tumor stroma. In line with the observed increase in tumor growth of shCav1 PC3-derived tumors we further detected an increased immunoreactivity to the universal proliferation marker proliferating cell nuclear antigen (Pcna) in these tumors (Fig. 3A). Immunofluorescence analysis further confirmed that the increase in proliferation was mainly caused by the

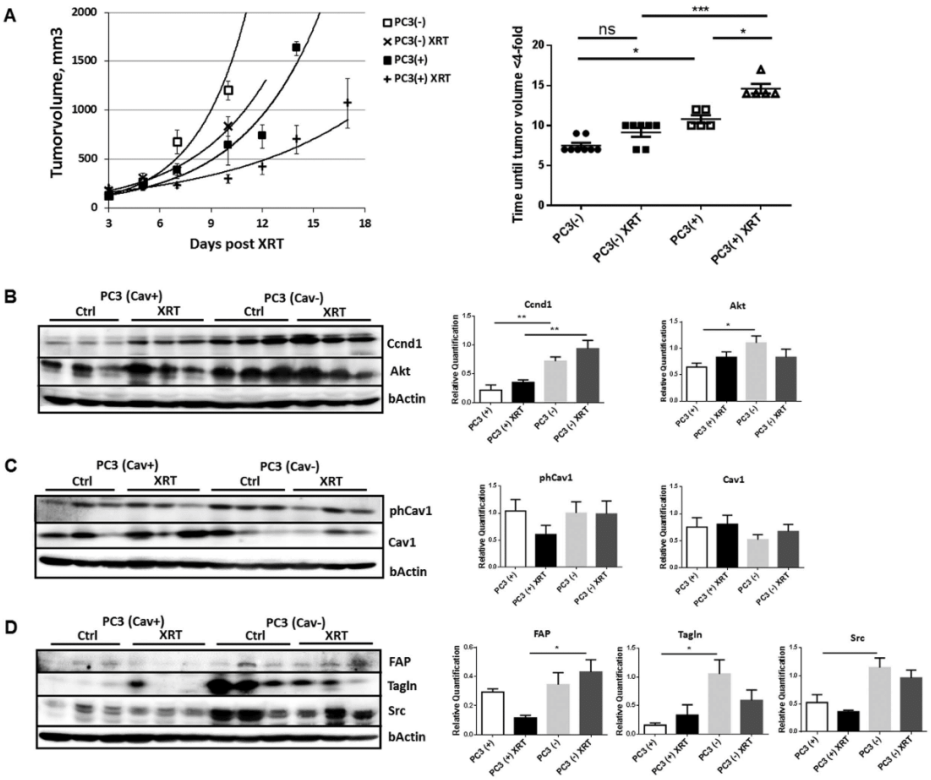

Figure 2. Single dose irradiation (10 Gy) decreased growth of PC3 xenograft tumors more efficiently in Cav1-expressing PC3 tumors which was accompanied by a less reactive tumor stroma. (**A**) PC3 shCav1 tumor cells [PC3(−)] as well as PC3 shCtrl control cells [PC3(+)] with normal Cav1 expression ($0.5*10^6$ cells each) were subcutaneously transplanted onto the hind limb of NMRI nude mice. One set of animals from each group received a single radiation dose of 10 Gy to the tumor after manifestation of the tumor at day 3. Tumor volume was determined at indicated time points using a sliding caliper (left diagram). Data are presented as mean ± SEM from 3 independent experiments (25 mice in total: PC3(+) 0 Gy n = 5; PC3(+) 10 Gy n = 5; PC3(−) 0 Gy n = 8; PC3(−) 10 Gy n = 7). Tumor growth and respective computed median growth delay was determined as time (days) until a four-fold tumor volume was reached (right diagram). *$p < 0.05$, ***$p < 0.005$ by one-way ANOVA followed by post-hoc Tukey's test. (**B**–**D**) Expression levels of the indicated proteins were analyzed in whole protein lysates using Western blot analysis. Representative blots are shown. For quantification blots were analyzed by densitometry and the respective signal was related to beta-actin (at least n = 4 for each group). When the phosphorylation status was determined the obtained phospho-specific signal was related to the signal of the total protein (phCav1/Cav1). P-values were indicated: **$P \leq 0.01$, ***$P \leq 0.01$, by one-way ANOVA followed by post-hoc Tukey test.

malignant epithelial cells itself as nearly no Pcna-immunoreactivity was detectable in Tagln-positive stromal cells (Supplemental Figure S2). Immunofluorescent analysis of the stromal marker protein smooth muscle actin (ACTA2) together with Cav1 further revealed that in PC3(−)-derived tumors some Cav1 expressing epithelial cells can be detected close to fibroblast-enriched tumor regions, which led us speculate that the recruited stromal cells might mediate partially Cav1 re-expression in the prostate epithelial PC3 cells which because of the phenotype of implanted stable transduced PC3(−) cells must be due to a Cav1 substitution (Fig. 3B, arrows). Radiation further seemed to induce an increase in Cav1 re-expression in tumors of Cav1-silenced PC3(−) cells (Supplemental Figure S1). These results suggested that close to the human situation an increase in epithelial Cav1 (re-) expression together with a more reactive tumor stroma may account for the observed increase of radiation resistance.

In order to corroborate these findings and to mimic the human situation more precisely we implanted Cav1-silenced PC3 cells as well as Cav1-expressing control cells directly into the right and left dorsolateral lobe of the prostate of NMRI nude mice (Fig. 4). In line with the results obtained above PC3(−)-derived tumors showed a significantly increased tumor growth when compared to PC3(+)-derived tumors as demonstrated by the significantly increased tumor weight and volume 14 days after tumor cell implantation (Fig. 4A). Akt expression levels were also increased in shCav1 PC3(−)-derived tumors as compared to PC3(+)-derived tumors (Fig. 4B). The Cav1 expression levels were reduced in tumors grown from Cav1-silenced PC3(−) cells but the lower Cav1

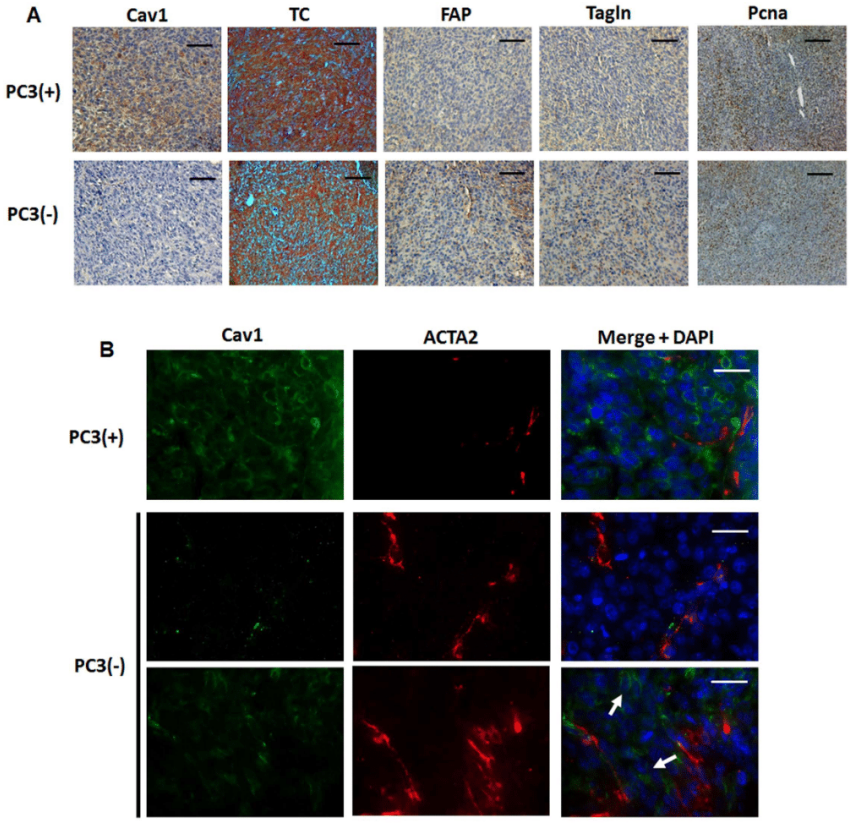

Figure 3. Prostate tumors grown from Cav1-silenced PC3 cells were accompanied by a more reactive tumor stroma. (**A**) Tumors derived from shCav1 PC3 cells [PC3(−)] as well as from PC3 shCtrl control cells [PC3(+)] with normal Cav1 expression were removed when tumor volumes reached a critical size (8–14 days after implantation) and were then subjected to immunohistochemistry with the indicated antibodies. Masson´s Goldner Trichrome (TC) was performed in order to visualize the collagenous stroma. Representative images are shown. Sections were counterstained using hematoxylin. Magnification Cav1, TC, FAP, Tagln 20x; Pcna 10x. (**B**) Subcutaneously grown tumors were further analyzed by immunofluorescence and confocal microscopy. Tumor stroma was stained for smooth muscle actin (ACTA2; red) and Cav1 (green). Arrows point towards Cav1-positive PC3(−) epithelial cells which were supposed to become immunoreactive for Cav1 upon tumor progression. Representative images from at least three independent experiments are shown. Magnification 63x (scale bar 50 μm).

expression levels varied between the different shCav1 PC3(−)-derived tumors. Interestingly we found a variable upregulation of the EMT promoting growth factor transforming growth factor beta 1 (TGFb) within these tumors. Also, higher expression levels of the reactive stroma markers FAP and Tagln were detected in PC3(−)-tumors confirming the presence of a more reactive tumor stroma (not shown). Immunohistochemical analysis of Cav1 further showed that in PC3(−)-derived tumors some areas with Cav1-expressing epithelial cells can be detected (Fig. 4C). These Cav1-immunoreactive PC3 cells were again localized within fibroblast-enriched tumor regions (Fig. 4D).

Reduction of Cav1 levels increased survival of clonogenic fibroblasts *in vitro*. To investigate whether reduced Cav1 expressions might alter the radiation response of stromal fibroblasts we performed *in vitro* experiments using the human fibroblast cell line HS5 as model in combination with shRNA knock-down of Cav1 expression (Fig. 5). According to the experiments with the PC3 cells as described above a long-term assays measuring the surviving fraction after irradiation revealed that the clonogenic survival of Cav1-silenced HS5(−) cells was significantly increased after irradiation as compared to the Cav1-expressing HS5(+) cells (Fig. 5A). Furthermore HS5(−) fibroblasts showed a decreased proliferation rate (Fig. 5B). Radiation further fostered a downregulation of Cav1 expression levels in shCtrl HS5(+) by tendency but not in shCav1 HS5(−) (Fig. 5C). Expression levels of the proliferation marker cyclin D1 (Ccnd1) were furthermore significantly decreased in shCav1 HS5(−). Further examination of the Akt expression levels revealed that the more radio-resistant shCav1 HS5(−) showed significantly increased expression levels of Akt as compared to Cav1-expressing shCtrl HS5(+).

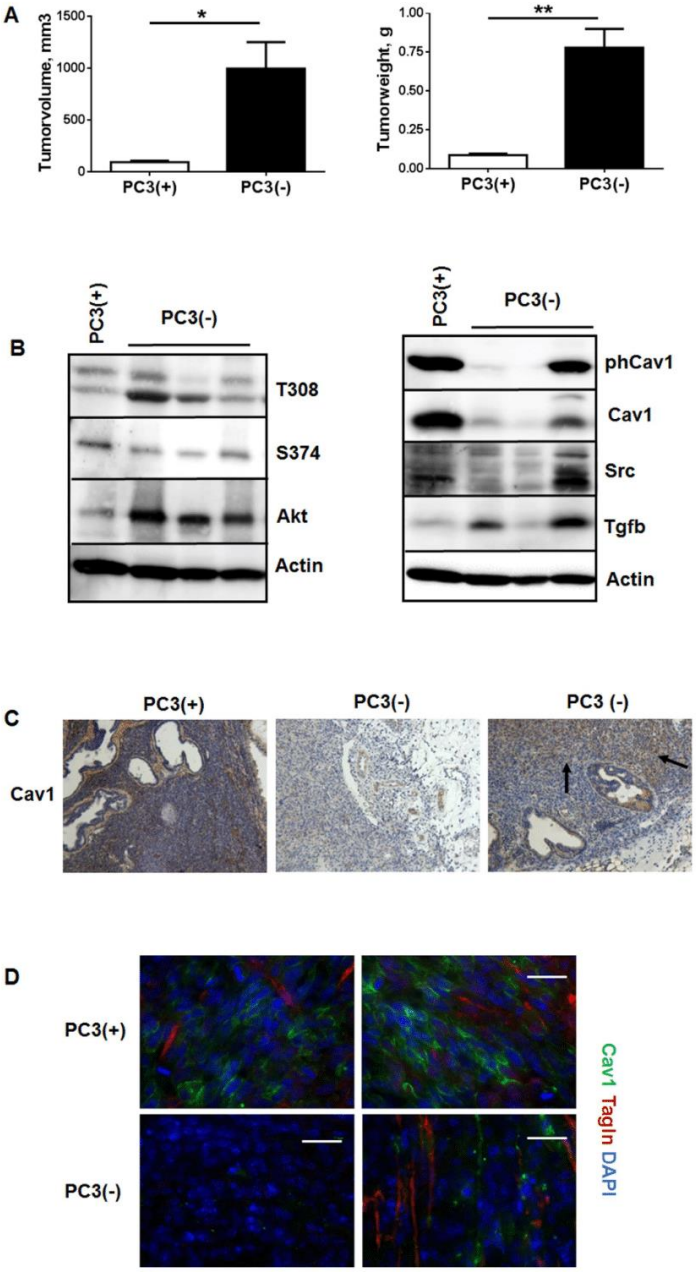

Figure 4. Orthotopic tumors derived from Cav1-silenced PC3(−) cells showed a significantly increased tumor growth and epithelial Cav1 (re-) expressions. (**A**) PC3 (+/−Cav1) cells were injected into the right and left dorsolateral lobe (0.5×10^5 cells per lobe) of the prostate of NMRI nude mice. Tumor weight and volume was determined 14 days after tumor cell implantation. Data are presented as mean ± SEM from 3 independent experiments (16 mice in total: PC3(+) n = 7; PC3(−) n = 9); *P ≤ 0.05, **P ≤ 0.01 by two-tailed t-tests with Welch's correction. (**B**) Expression levels of the indicated proteins were analyzed in whole protein lysates using Western blot analysis. Representative blots are shown. (**C**) Tumors derived from shCav1 PC3 cells as well as from shCtrl control cells with normal Cav1 expression were subjected to immunohistochemistry with Cav1 antibody. Representative images are shown. Sections were counterstained using hematoxylin. Arrows point towards Cav1-positive epithelial cells within tumors derived from implanted PC3(−) cells. Magnification 20x. (**D**) Orthotopic grown tumors were further analysed by immunofluorescence and confocal microscopy. Tumor stroma was stained for Tagln (red) and Cav1 (green). Representative images from at least three independent experiments are shown. Magnification 63x (scale bar 50 μm).

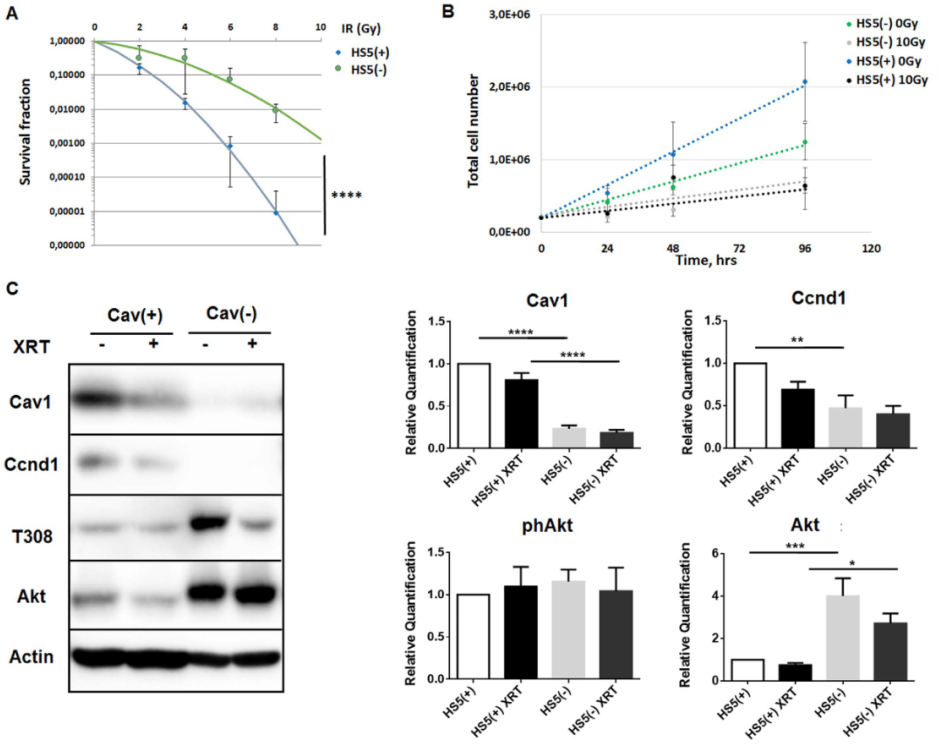

Figure 5. Reduction of Cav1 levels increased survival of clonogenic epithelial PC3 and stromal HS5 cells while proliferation was decreased *in vitro*. (**A**) Lentiviral expression of a Cav1-specific siRNA (shCav1) in stromal HS5 fibroblasts resulted in an efficient and sustained down-regulation of Cav1 expression compared to control-transduced (shCtrl) cells as shown by Western blot analysis. β-actin (bActin) was included as loading control. Representative blots of at least three different experiments are shown. (**A**) HS5 (shCav1-transfected fibroblasts [HS5(−)] as well as shCtrl control cells [HS5(+)] with normal Cav1 expression) cells were plated for colony formation assay, irradiated with indicated doses (0–8 Gy) and subsequently further incubated for additional 10 days. Data show the surviving fractions from three independent experiments measured in triplicates each (means ± SD). $^{****}P \leq 0.001$ by two-tailed students T-test. (**B**) Cell proliferation was analyzed by cell counting in cultured shCav1-transfected HS5(−) and control-transfected HS5(+) fibroblasts cells at the indicated time points after irradiation with 10 Gy. Data are shown as means ± SEM of three independent experiments. (**C**) Expression levels of the indicated proteins were analyzed in whole protein lysates of cultured HS5 cells (+/−Cav1) with or without radiation (48 hours after XRT with 10 Gy) using Western blot analysis. Representative blots are shown. For quantification blots were analyzed by densitometry and the respective signal was related to beta-actin (n = 4–5 for each group). For determination of the Akt phosphorylation status the obtained phospho-specific signal was related to the signal of the total protein (phAkt/Akt). P-values were indicated: $^{*}P \leq 0.05$; $^{**}P \leq 0.01$; $^{***}P \leq 0.005$ $^{****}P \leq 0.001$; by one-way ANOVA followed by post-hoc Tukey test.

Conclusively the impact of the increased survival of Cav1-deficient fibroblasts on the radiation treatment outcome remains to be determined but argues against a general approach for Cav1-silencing in PCa.

Cav1-deficient stromal fibroblasts mediated radiation resistance. We then aimed to test whether a more reactive fibroblastic tumor stroma with presumably reduced Cav1 expression accounts for the increased radiation resistance observed in PC3(−) xenograft tumors. To mimic the human situation we performed co-implantations of Cav1-silenced PC3(−) tumor cells in combination with Cav1-silenced or Cav1-expressing HS5 fibroblasts by subcutaneous transplantations onto the hind limb of NMRI nude mice and irradiation treatment after manifestation of the tumor (Fig. 6). In line with the results presented above co-implantation of PC3(−) prostate epithelial cells with HS5 fibroblasts showed that Cav1-silenced HS(−) fibroblasts promoted tumor growth of PC3(−) cells stronger than Cav1-expressing HS5(+) fibroblasts (Fig. 6A). Importantly, the response of PC3(−) xenograft tumors to radiation treatment was significantly less pronounced when they were co-implanted with Cav1-silenced HS5(−) fibroblasts compared to co-implantation with Cav1-expressing HS5(+) fibroblasts as demonstrated by the increased time to reach a four-fold tumor volume (Fig. 4A) (PC3(−)HS5(+) 0 Gy: 13, 9 ± 0,

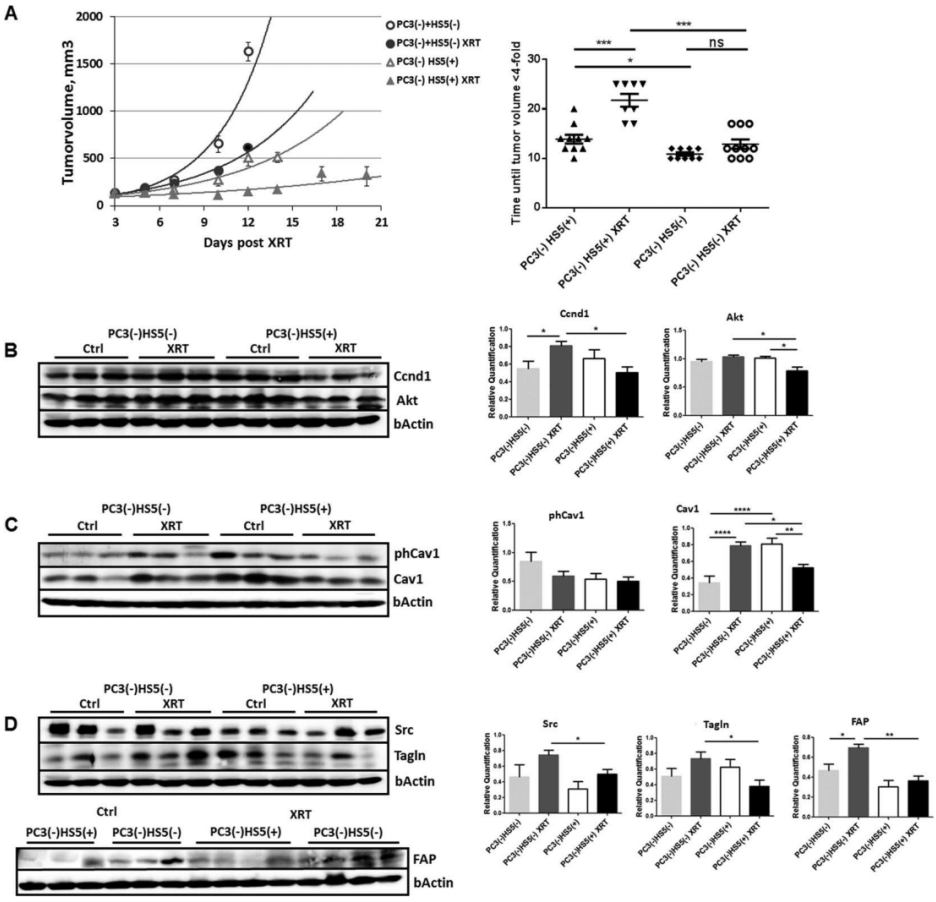

Figure 6. Cav1-deficient stromal fibroblasts mediated radiation resistance. (**A**) Co-implantations of PC3 tumor cells ($0.5*10^6$ cells each) after Cav1 silencing [shCav1, PC3(−)] in combination HS5 Cav1-silenced fibroblasts [shCav1, HS5(−)] ($0.5*10^6$ cells each) or control fibroblasts [shCtrl, HS5(+)] were performed by subcutaneously transplanted onto the hind limb of NMRI nude mice. One set of animals from each group received a single radiation dose of 10 Gy to the tumor after manifestation of the tumor at day 3. Tumor volume was determined at indicated time points using a sliding caliper (left diagram). Data are presented as mean ± SEM from 3 independent experiments (37 mice in total: PC3(−)HS5(+) 0 Gy n = 10; PC3(−)HS5(+) 10 Gy n = 8; PC3(−)HS5(−) 0 Gy n = 9; PC3(−)HS5(−) 10 Gy n = 10). Tumor growth and respective computed median growth delay was determined as time (days) until a four-fold tumor volume was reached (right diagram). *p < 0.05, ***p < 0.005 by one-way ANOVA followed by post-hoc Tukey's test. (**B**–**D**) Expression levels of indicated proteins were analyzed in whole protein lysates using Western blot analysis. Representative blots are shown. For quantification blots were analyzed by densitometry and the respective signal was related to beta-actin (at least n = 4 for each group). When the Cav1 phosphorylation status was determined the obtained phospho-specific signal was related to the signal of the total Cav1 protein [phCav1/Cav1]. P-values were indicated: *p < 0.05, **$p \leq 0.01$, ***$p \leq 0.005$, ****$P \leq 0.001$ by one-way ANOVA followed by post-hoc Tukey test.

90 d, n = 10; PC3(−)HS5(+) 10 Gy: 21, 75 ± 1.29 d, n = 8; PC3(−)HS5(−) 0 Gy: 10, 89 ± 0, 35 d, n = 9; PC3(−)HS5(−) 10 Gy: 12, 90 ± 0, 94 d, n = 10).

We investigated again the levels of the proliferation marker Ccnd1 in whole tumor lysates by Western blot analysis (Fig. 6B). Protein levels of Ccnd1 were not altered in HS5(−) co-implanted PC3(−) tumors. After radiation treatment Ccnd1 expression levels were significantly decreased in irradiated shCav1 PC3-derived tumors containing HS5(+) fibroblasts as compared to irradiated shCav1 PC3-derived tumors containing HS5(−) fibroblasts corroborating the data that Cav1-silenced fibroblasts were more radioresistant in respective tumors. We further examined the expression levels of the survival protein Akt and Cav1. Significantly reduced expression levels of Akt were detected in PC3(−)HS5(+)-derived tumors after radiation in line with reduced expression levels of Cav1 (Fig. 6C). Radiation of PC3(−)HS5(−)-derived tumors resulted in significantly upregulated Cav1

levels, which might implicate that epithelial Cav1 re-expression in the prostate epithelial PC3 could contribute to the observed radiation resistance.

Because we speculated that differences in the stromal compartment between PC3 tumors may contribute to the observed findings, we again investigated the expression levels of the reactive stroma markers c-Src, Tagln and FAP as performed above (Fig. 6D). Importantly significant higher expression levels of these proteins were detected in irradiated PC3(−)HS5(−)-derived tumors supporting that a more reactive tumor stroma mediated radiation resistance. We further performed immunohistochemistry analysis to confirm our findings (Supplemental Figure S3). In tumors of Cav1-silenced PC3(−) cells in combination with Cav1-silenced HS5(−) fibroblasts Cav1 immunoreactivity was clearly reduced whereas the reactive stromal markers FAP and Tagln showed a more prominent and intensive staining (Supplemental Figure S3A). And in particular after radiation treatment the more radioresitant PC3(−)HS5(−)-derived tumors displayed an increased immunoreactivity to FAP and Tagln in the stromal compartment, which demonstrated a more reactive tumor stroma after radiation as well as a more prominent staining of epithelial Cav1 (Supplemental Figure S3B). Immunohistochemistry using the Pcna antibody further confirmed the Western blot results because a more intensive staining of the proliferation marker was detected in the more radioresitant PC3(−)HS5(−)-derived tumors and in particular after radiation treatment (Supplemental Figure S3). These results revealed that loss of stromal Cav1 is paralleled by an increase in epithelial Cav1 expression and further suggests again that loss of stromal Cav1 can presumably foster epithelial Cav1 expression and thereby promoting increased of radiation resistance.

Supernatants derived from Cav1-silenced HS5 fibroblasts fostered radiation resistance of cultured malignant epithelial cells. Next, to confirm our *in vivo* data mechanistically, *in vitro* analysis of the radiation response of cultured PC3 (+/−Cav1) and Cav1-deficient LNCaP prostate cancer cells were performed in the presence of supernatants (SN) derived from cultured Cav1-silenced HS5(−) or control transduced Cav1-expressing HS5(+) fibroblasts with or without radiation treatment (+/−XRT with 10 Gy) (Fig. 7). Interestingly, SN of Cav1-silenced HS5(−) cells induced a marked upregulation of Cav1 expression levels in cultured PC3(+) cells with and without radiation (Fig. 7A). A similar but less prominent increase in Cav1 was detected in Cav1-silenced PC3(−) cells. No real differences were detected in Akt expression levels upon radiation in combination with HS5 SN treatment. Expression levels of the proliferation marker Ccnd1 were furthermore slightly increased in cultured PC3(+) cells upon treatment with SN of Cav1-silenced HS5(−) cells. The increase of Ccnd1 was more prominent in HS5(−) SN cultured PC3(−) cells. The HS5(−) SN induced upregulation of Cav1 expression levels in cultured PC3(+) cells with and without radiation were paralleled by an upregulation of the mesenchymal marker smooth muscle actin (Acta2). In androgen receptor-expressing and naturally Cav1-deficient LNCaP cells, HS5(+) SN treatment induced a slight upregulation of Cav1 expression levels (Fig. 7B). Again, no real differences were detected in Akt expression levels upon radiation in combination with HS5 SN treatment. A trend of higher Akt phosphorylation levels at threonine 308 (T308) was observed upon HS5(+) SN treatment. Expression levels of Ccnd1 were again slightly increased cultured LNCaP cells upon treatment with SN of Cav1-silenced HS5(−) cells. Interestingly, the HS5(+) SN induced upregulation of Cav1 expression levels were paralleled by an upregulation of Acta2. To further investigate how Cav1 levels might be altered in cultured Cav1-deficient tumor cells Cav1 expression and localization was analyzed in LNCaP cells co-cultured with GFP-expressing (shCtrl)-transfected HS5 fibroblasts by immunofluorescence (Supplemental Figure S4). Direct co-culture of both cell types can lead to an up-regulation of Cav1-immunoreactivity in LNCaP cells suggesting a transfer of Cav1 between the cells (Supplemental Figure S4A). In contrast increased Cav1-immunoreactivity can even be observed in some LNCaP cells upon radiation. Similar findings were observed in Cav1-silenced and GFP-expressing (shCav1-transfected) PC3 cell co-cultures with normal (non-transfected) HS5 fibroblasts (Supplemental Figure S4B). Cav1 secretion was further confirmed by the presence of Cav1 in cell culture supernatants derived from HS5(+/−Cav1) fibroblasts with or without radiation treatment (Supplemental Figure S4C).

The resistance-promoting effect of Cav1-deficient HS5(−) fibroblasts was further analyzed by determining the degree of apoptosis (SubG1 fraction) after radiation in PC3 (+/−Cav1) and Cav1-deficient LNCaP prostate cancer cells in the presence of HS5 SN (Fig. 7C,D). Conformingly SN of Cav1-silenced HS5(−) significantly reduced apoptosis induction in cultured PC3(+) and in the *in vitro* more radiosensitive PC3(−) (Fig. 7C). A similar but less prominently reduced apoptosis rate was detected in LNCaP cells upon radiation and HS5(−) SN treatment (Fig. 7D). Quantitative Real Time RT-PCR analysis of the reactive fibroblasts markers Acta2, Tagln as well as the tumor-promoting factors Vegf (vascular endothelial growth factor), Tgfb and Mmp2 (matrix metalloproteinase 2) in total RNA isolates of HS5 fibroblasts (+/−Cav1 and +/−XRT) further confirmed the more reactive phenotype of Cav1(−) HS5 fibroblasts (Fig. 7E). A general upregulation of the most prominent angiogenic growth factor Vegf in Cav1(−) HS5 fibroblasts was detected, whereas a significant upregulation of the EMT promoting growth factor Tgfb was detected in Cav1(−) HS5 fibroblasts upon radiation. Furthermore reduced Mmp2 mRNA expression levels were detected in HS5(−) fibroblasts which is in line with the findings stated above as reduced expressions of collagenases may also contribute to increased collagen deposition and thus the presence of a more reactive tumor stroma. QRTPCR analysis further confirmed significantly increased mRNA expression levels of the Tgfb receptors TGFBR1 and TGFBR2 as well as the epithelial cadherin repressing EMT gene Snai2 in PC3(+) cells (Fig. 7F). Conclusively the resistance-promoting effect of Cav1-deficient HS5(−) fibroblasts coincided with upregulations of Cav1 expression levels in malignant epithelial cells and further suggests that EMT might contribute to the observed radiation resistance.

Loss of stromal Cav1 in advanced PCa is accompanied by a more reactive tumor stroma indicating radiation resistance. To confirm that loss of stromal Cav1 is paralleled by a radiation-resistance promoting reactive tumor stroma, human prostate tissue specimens were analyzed for Cav1 and Tagln protein expressions. Therefore, formalin fixed paraffin-embedded tissue slides of human prostate

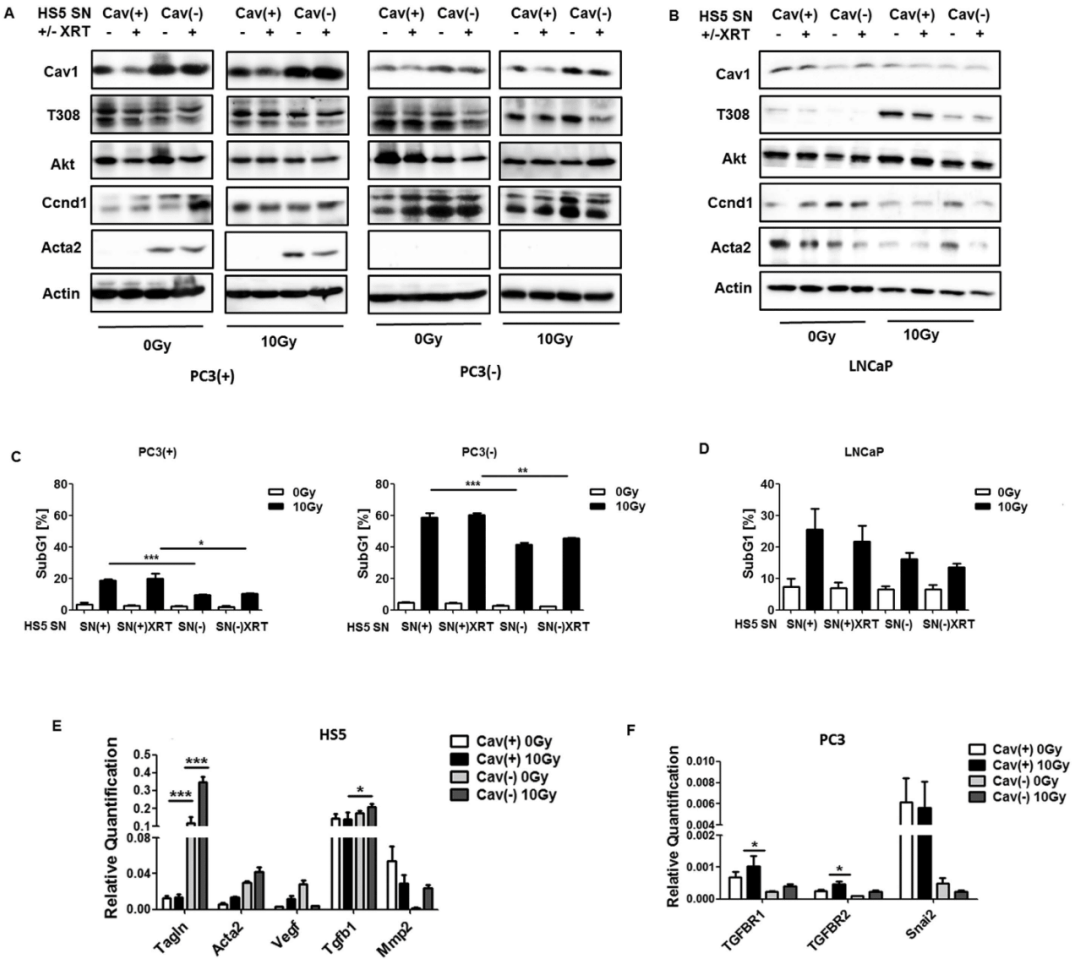

Figure 7. Treatment of cultured PC3 (+/−Cav1) or Cav1-deficient LNCaP malignant epithelial cells with supernatants derived from Cav1-silenced HS5 fibroblasts fostered radiation resistance. (**A**,**B**) PC3 (shCav1-transfected tumor cells [PC3(−)] as well as PC3 shCtrl control cells [PC3(+)] with normal Cav1 expression) and Cav1-deficient LNCaP cells were irradiated with 10 Gy and subsequently treated with supernatants (SN) derived from cultured Cav1-silenced HS5(−) or control transfected Cav1-expressing HS5(+) fibroblasts with or without radiation treatment (+/−XRT with 10 Gy). Western blot analysis of whole protein lysates was performed after 48 hours of treatment using the indicated antibodies. (**C**,**D**) The degree of apoptosis was quantified by measuring the SubG1 fraction 48 hours after radiation by flow cytometry analysis. Therefore, PC3cells (+/−Cav1) and Cav1-deficient LNCaP cells were left non-irradiated (white bars) or irradiated with 10 Gy (black bars) and subsequently treated with SN derived from cultured Cav1-silenced HS5(−) or Cav1-expressing HS5(+) fibroblasts with or without radiation treatment (+/−XRT with 10 Gy). (**E**) Quantitative Real Time RT-PCR (qRT-PCR) analysis of the reactive fibroblasts markers Acta2, Tagln as well as the tumor-promoting factors Vegf (vascular endothelial growth factor), Tgfb and Mmp2 (matrix metalloproteinase 2) were performed in total RNA isolates of Cav1-silenced HS5(−) or control transfected Cav1-expressing HS5(+) fibroblasts with or without radiation treatment (+/−XRT with 10 Gy) and were shown as relative expression to actin (set as 1) at 96 hours post irradiation. Shown are mean values ± SEM from 4 independent samples per group measured in duplicates each. $^{*}P \leq 0.05$, $^{***}P \leq 0.005$, by one-way ANOVA followed by post-hoc Tukey's test. (**F**) Expression levels of the Tgfb receptors TGFBR1 and TGFBR2 as well as the E-cadherin repressing EMT gene Snai2 were analyzed in whole RNA isolates of cultured PC3 cells (+/−Cav1) with or without radiation (48 hours after XRT with 10 Gy) using qRT-PCR analysis. Shown are mean values ± SEM from 4 independent samples per group measured in duplicates each. $^{*}P \leq 0.05$ by one-way ANOVA followed by post-hoc Tukey's test.

adenocarcinomas with distinct Gleason Scores were immunostained for Cav1, phosphoCav1, Src and Tagln (Fig. 8, Supplemental Figure S5). In line with previous reports we found that benign prostate epithelia were negative for Cav1 but that Cav1 expression in prostate epithelial cells increased with higher Gleason scores, i.e. lower

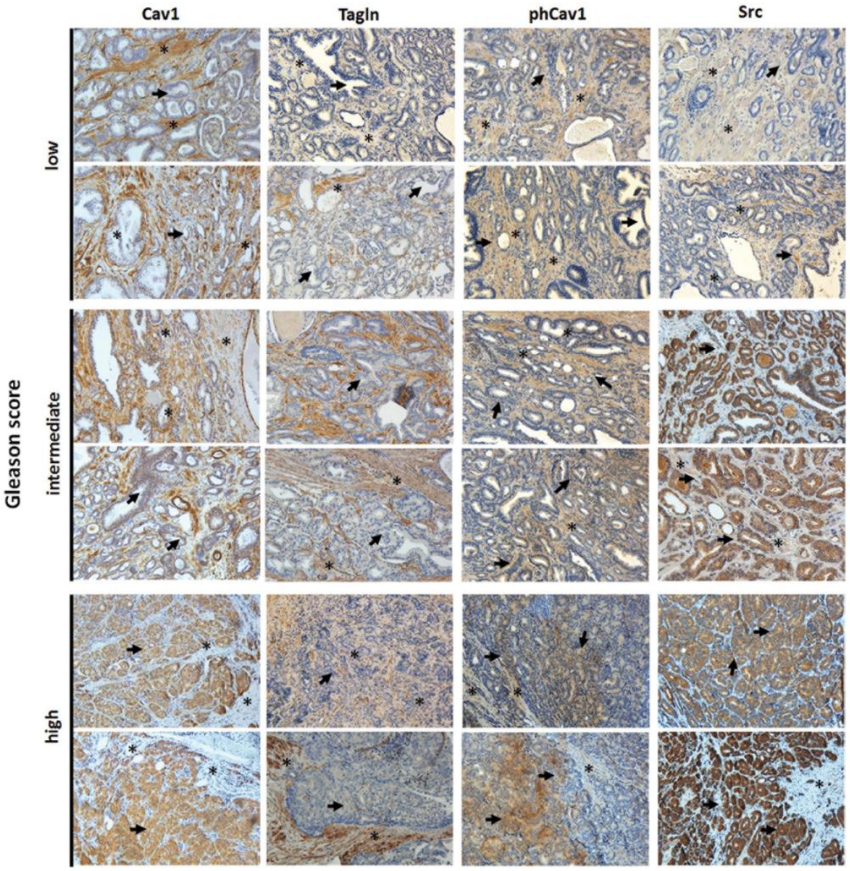

Figure 8. Immunohistological analysis of Cav1 expressions in human prostate tumor tissues. Paraffin-sections of human prostate tumors were stained for the indicated antibodies. Gleason grading scores used to evaluate prognosis of men with prostate cancer were divided into low (1 + 1, 2 + 2), intermediate (3 + 3, 4 + 3) and high scores (4 + 5) according to the sum of the primary and secondary Gleason patterns in whole resection specimens. The observed patterns of the tumor specimen were assigned based on current WHO and updated ISUP criteria: the primary grade - assigned to the dominant pattern of the tumor (has to be greater than 50% of the total pattern seen) as well as a secondary grade - assigned to the next-most frequent pattern (has to be less than 50%, but at least 5%, of the pattern of the total cancer observed). Asterisks mark stromal compartments and bold arrows point to epithelial structures. Sections were counterstained using hematoxylin. Representative images are shown. Magnification 20x.

tumor differentiation (Fig. 8, bold arrows). In contrast, stromal cells of tumor samples tended to be less intensively stained or even negative in cases with higher Gleason grade (Fig. 8, asterisks). The increase in stromal Tagln expression in higher Gleason score specimen confirmed the more reactive tumor stroma phenotype. Similar to the Cav1-alterations differences were found for phosphoCav1 and the Cav1 (on Tyr14) phosphorylating kinase Src expressions. Whereas both proteins were more intensively stained in the stromal compartment of tumor specimen with lower Gleason scores, immunoreactivity clearly increased in the malignant epithelial cells of higher Gleason grade tumor specimen. These results indicated that Src-mediated regulations of Cav1 phosphorylation have implications for prostate carcinoma progression and therapy resistance because Src-dependent Cav1 phosphorylation is required for Cav1 signaling prior our suggested potentially stromal-epithelial Cav1 substitution.

Discussion

Understanding the role of stromal cells in tumor responses to RT and chemotherapy is essential to improve treatment strategies and to reduce the rate of resistant tumors. We recently demonstrated that stromal Cav1 levels in the tumor microvasculature are important to the outcome of RT[19]. Within that previous study murine prostate MPR31–4 tumors grown in Cav1-deficient mice showed significantly increased tumor progression, but upon radiation treatment a more pronounced tumor growth delay, because loss of stromal Cav1 enhanced the sensitivity of microvascular EC to radiation-induced apoptosis[19]. Therefore we concluded that Cav1 might be a promising therapeutic target for combinatorial therapies to counteract radiation resistance of PCa at the level of the tumor

vasculature. Accordingly we used cultured PC3 cells and confirmed that loss of Cav1 expression increased sensitivity of PC3 cells to radiation and reduces their clonogenic survival after irradiation, which further supports the idea of Cav1 being a valuable therapeutic target. This is inline with the work from other groups which already demonstrated in other cancer types that Cav1 acts as a pro-survival factor mediating resistance. In particular silencing of Cav1 in pancreatic cancer cell lines and lymphoblastoid cancer cells resulted in reduced cell adhesion, proliferation and survival after exposure to IR[23–25].

In vivo, silencing of Cav1 expression in PC3 cells resulted in an increased tumor growth and reduced growth delay after IR when compared to tumors generated by Cav1-expressing PC3 cells, which was accompanied by increasing amounts of reactive tumor stroma and potentially by a Cav1 re-expression in the malignant epithelial cells. The importance of stromal fibroblasts for the progression and radiation response of prostate tumors was further highlighted after co-implantation of Cav1-silenced PC3 cells with Cav1-proficient or -deficient HS5 fibroblasts as model. We show here for the first time that HS5 fibroblasts with reduced Cav1 levels resulted in increased radioresistance to IR. We further demonstrated for the first time that the decreased radiation-induced growth delay of tumors with co-implanted Cav1-silenced HS5 cells was associated with an increased reactive tumor stroma. Thus, normal Cav1-positive stroma might inhibit tumor progression and improve the efficiency of radiation therapy, whereas a Cav1-dependend transformed and more reactive tumor stroma fosters tumor growth and contributes to therapy resistance. Together with the accelerated growth of untreated prostate tumors when Cav1-silenced fibroblasts were implanted the presented results hint to a potential risk of treatment strategies targeting Cav1 for radiosensitization in these tumors making careful validation of such treatment strategies with respect to adverse growth promoting effects absolutely necessary.

Today it is widely accepted that stroma changes play a functional role during neoplastic transformation and also a key role in cancer cell invasiveness and progression and potentially therapy resistance[34,35]. Herein the reactive tumor stroma significantly contributes to therapy resistance at multiple levels[36–41]. In particular therapy-induced DNA damage of the stromal compartment can lead to the activation of secretory programs which in turn influence the growth and survival of tumor cells[42]. On the one hand transcriptional alterations in primary prostate fibroblasts following DNA damage resulted in potential paracrine effects on adjacent tumor cells[43]. Here we now show that tumors from Cav1-silenced PC3 cells were characterized by increasing amounts of reactive tumor stroma and a reduced growth delay after IR and that these tumors displayed significantly higher levels of the survival protein Akt. Similar results were obtained in tumors with co-implanted Cav1-silenced HS5 cells and thus an increased reactive tumor stroma and increased Akt levels. Elevated Akt levels and aberrant activation of PI3K-Akt pathway was already suggested to contribute to increased cell invasiveness and facilitate PCa progression[44].

As it is not possible to target Cav1 specifically in tumor cells it is important to dissect the molecular details of Cav1-mediateded radiation response modulation. One potential candidate as suggested by the presented results is the non-receptor tyrosine kinase Src. Src has already been implicated in PCa development, progression and metastasis[45]. Accordingly, we show here for the first time that both untreated and irradiated tumors grown from Cav1-silenced PC3 cells after orthotopic or subcutaneous implantation displayed significantly higher Src levels which were in parallel with the observed significantly higher levels of reactive stroma markers. Furthermore, using the co-implantation model, the more radioresitant tumors which contained Cav1-deficient HS5 fibroblasts at the implantation time point, showed significantly higher Src levels in response to IR which again was in parallel with the observed significantly higher levels of reactive stroma markers. Therefore treatment with Src inhibitors might be a potential treatment option for radiosensitizing advanced prostate carcinomas which were characterized by a Cav1-deficient reactive tumor stroma. This is of particular interest since work from another group already demonstrated that the Src inhibitor dasatinib treatment impaired the metastatic phenotypes of the human PCa cell lines PC-3, DU-145, and LNCaP, by significantly reducing migration and invasion[46]. Dasatinib treatment of athymic nude mice resulted in impaired growth of PC3 cell xenograft tumors. Herein, dasatinib also had direct effects on the ability of microvascular EC to form tubes *in vitro* and impaired the ability of PC-3 cells to induce angiogenesis *in vivo*[46].

In general, Src-mediated Cav1 phosphorylation on Tyr14 has been demonstrated to be essential for Cav1 signaling and Cav1 endocytosis because phosphorylation of Cav1 leads to separation of neighboring negatively-charged N-terminal phospho-tyrosine residues, promoting swelling of caveolae followed by their release from the plasma membrane[47,48]. Hereby Src has also been shown to play an important role in PCa development and progression because Src can signal through focal adhesion kinase (FAK) in response to integrin activation, which has been implicated in many aspects of tumor biology, such as cell proliferation, metastasis and angiogenesis[49,50]. Therefore Src inhibition represents a valid therapeutic strategy for investigation[46]. Src was further shown to contribute to increases in Cav1 expressions[51]. Furthermore, upregulations of epithelial Cav1 expression followed the induction of EMT and was preceded by increased activation of FAK and Src, two known tyrosine kinases also involved in EMT[51]. Cav1 was already shown to regulate tumor-promoting EMT of transformed epithelial cells and thereby promoting invasive phenotypes e.g. in bladder or gastric cancers[20,52]. Herein positive Cav1 expression was significantly correlated with negative E-cadherin expression in malignant epithelial cells[52]. Mechanistically EMT might result from an increased internalization of TGFBRI and Cav1 from lipid rafts which in turn results in an increased TGFb signaling[53]. In line with these findings we show here for the first time that Cav1-deficient fibroblasts foster an upregulation of prostate cancer cell Cav1 expression levels *in vitro* and *in vivo* and furthermore in response to IR treatment and thereby might contribute to the observed radiation resistance.

In a very recently published study DeRita *et al.* demonstrated that Src is packaged into exosomes and released from PCa cells[50]. Furthermore the authors showed that Src- containing exosomes can be isolated in higher amounts from the plasma of prostate tumor-bearing TRAMP mice than wildtype littermates, suggesting that Src signaling network may provide useful biomarkers detectable by liquid biopsy[50]. Thus, Src signaling network may

contribute to PCa progression via exosomes. Although the authors did not investigate possible Cav1 presence in this exosomes, it is a quite promising observation since the alterations of Cav1 observed by us and others during PCa progression, maybe either based on direct transfer of Cav1 via those vesicles between malignant epithelial cells and stromal fibroblasts or might be fostered via the transfer of Cav1 regulating components like Src.

In summary, we demonstrate here for the first time that stromal Cav1 is a critical regulator of the sensitivity of PCa to IR in human PCa PC3 xenograft tumors with impact on tumor growth delay after local irradiation. We observed (i) increased Src expression levels in subcutanously or orthotopic PC3(−)-derived tumors as well as in PC3(−)HS5(−)-derived tumors, (ii) increased Src and Cav1 expression levels in the more radioresistant PC3(−)HS5(−)-derived tumors upon radiation, (iii) a potential Cav1 (re)-expression in Cav1-silenced or deficient prostate cancer cells *in vitro* and *in vivo*, (iv) increased Cav1 expression levels of cultured PC3(+) cells upon radiation and in particular after treatment with supernatants derived from the more radioresistant HS5(−), (v) a downregulation of Cav1 in HS5 fibroblasts upon radiation, and (vi) an upregulation of Tgfb expression in HS5(−) fibroblasts as well as increased expression levels of the corresponding Tgfb receptors in Cav1-expressing PC3(+) cells. Finally (vii) similar to the Cav1-alterations, immunoreactivity of phosphoCav1 and the Cav1 phosphorylating kinase Src clearly increased in the malignant epithelial cells of the more radioresistant higher Gleason grade human prostate adenocarcinomas which was paralleled by a more reactive Cav1-deficient tumor stroma, and thus confirms the importance of Src signaling as a potential candidate for future Cav1-mediated radiation response modulation.

Taken together, Cav1 signaling pathways in particular in stromal fibroblasts contribute to this resistance especially to radiation therapy. Our results strongly argue for a Cav1-dependent EMT in prostate cancer progression which is closely linked and thus may account for the observed radiation resistance. However up to now a detailed mechanism how Cav1(−) HS5 fibroblasts foster Cav1 upregulations or (re) expressions in malignant prostate cancer cells and thereby radiation resistance remains elusive.

In particular it is not clear how Cav1–induced (re-)expression fostered by Cav1(−) fibroblasts might promote EMT and potentially thereby radiation therapy resistance as tumors derived Cav1-expressing PC3(+) were more radiosensitive than respective tumors derived from Cav1-silenced PC3(−) cells. However the potential re-distribution of Cav1 we observed *in vivo* when we attempt to mimic the human situation by implanting Cav1(−) PC3 cells (as prostate epithelial cells were Cav1-negative when the cancer develops) coincides with increased radiation resistance. It will be further important to investigate which factors are decisive the critical stromal-epithelial Cav1 alterations during PCa progression and radiation therapy resistance, namely the observed reduction of stromal Cav1 and increased expression of epithelial Cav1. However induced, a 'simple' transfer of Cav1 from stromal fibroblasts to the epithelial cells might not be the only mechanism resulting in epithelial Cav1 (re) expressions as Cav1(−) fibroblasts *in vivo* or as supernatants derived from these cells *in vitro* foster radiation resistance of the PCa cells used here. Even more important the amount and phenotype of endogenous or co-implanted fibroblasts at the time point of irradiation remains to be investigated. Here we showed already that Cav1-silenced fibroblasts have a decreased proliferation rate *in vitro*. Even more important *in vivo* an increased immunoreactivity of the proliferation marker Pcna was predominantly detected in the malignant epithelial cells and not within the fibroblasts. Together with the findings that Cav1-silencing induced a more reactive phenotype of HS5 fibroblasts as revealed by the upregulation of the reactive fibroblasts markers Acta2 and Tagln as well as reduced Mmp2 mRNA expression levels *in vitro*, the phenotype and activation state of the fibroblasts seems to be more important than the amount of these cells within a tumor. Further studies are needed to determine this ratio between prostate cancer cells and fibroblasts in the ectopic tumors at the time of irradiation and how the observed fibroblast activation state than correlates with radiation resistance.

In future studies we finally aim to specify the role of Cav1 alterations potentially induced by the Cav1-deficient and more reactive stroma for the radiosensitivity of PCa on molecular level, in particular to identify Cav1-dependent fibroblastic secreted factors which potentially foster the observed Cav1 re-expression in the malignant epithelial cells. This is a necessary step to develop pharmacological strategies to reduce Cav1 expression or inhibit resistance-promoting Cav1-dependent signals, respectively.

Methods

Reagents and antibodies. Antibodies against alpha smooth muscle actin (ACTA2), Cav1 were from Santa Cruz (Santa Cruz, CA), against total AKT, phospho-Cav1, Ccdn1 and Src were from Cell Signaling Technology (Danvers, MA, Germany), against Tagln from Proteintech (Chicago, IL), against FAP from Abcam (Cambridge, MA), against Pcna from GeneTex (Irvine, CA) and against beta actin (clone AC-74, A2228) from Sigma-Aldrich (St. Louis, MO).

Human tumor tissue. Tissues from human prostate carcinomas were obtained during surgery according to local ethical and biohazard regulations. All experiments were performed in strict accordance with local guidelines and regulations. Resected tissue specimens were processed for pathological diagnostic routine in agreement with institutional standards and diagnoses were made based on current WHO and updated ISUP criteria[54]. All studies including human tissue samples were approved by the local ethics committee (Ethik-Kommission) of the University Hospital Essen (Nr. 10–4363). Informed consent (written form) from each patient was obtained. Human tissue samples were analyzed anonymously.

Cav1 silencing. The human prostate epithelial cell lines PC3, LNCaP and the fibroblast cell line HS5 were from ATCC (Manassas, VA). Levels of Cav1 mRNA level were down-regulated by shRNA technology[19,26]. Therefore, a lentivirus based pLentilox3.7 vector for mammalian expression was used as previously described[19]. Within 2–5 days after transduction eGFP-positive cells were sorted in a FACS Vantage cell sorter (BD Biosciences, Heidelberg, Germany).

Cell viability assay. The number of living cells was determined upon staining of the cells with the vital dye trypan blue. For this, cells were harvested with Trypsin-EDTA, re-suspended in fresh medium, diluted with trypan blue, and counted employing a Neubauer chamber.

Colony formation assay. For this long-term assay, 200–1600 cells/well were plated in 6-well plates. Radiation with indicated doses was performed using the Isovolt-320-X-ray machine (Seifert-Pantak) at 320 kV, 10 mA with a 1.65 mm aluminum filter and a distance of about 500 mm to the object being irradiated[19]. The X-ray tube operated at 90 kV (~45 keV X-rays) and the dose rate was about 3 Gy/min[55]. Plates were incubated for a total of 10 days to allow growth of single colonies. Cells were then fixed in 3.7% formaldehyde and 70% ethanol and subsequently stained with 0.05% Coomassie Brilliant Blue. Colonies ($\geq$50 cells/colony) were counted under the microscope at fivefold magnification.

Conditioned Media. Cav1-specific shRNA (shCav1) as well as control-transduced (shCtrl) HS5 cells were cultured in normal growth media until confluence. Cells were left non-irradiated or irradiated with 10 Gy, media were replaced and cells were cultured in the presence of 0.5% fetal bovine serum for 24 hours before collection of media. Control media were generated by incubating the same medium (containing 0.5% fetal bovine serum) without cells. Conditioned media were used as 1/1 mixture with normal growth medium[55].

Flow cytometry analyses. For quantification of apoptotic DNA-fragmentation (sub-G1 population), cells were incubated for 15–30 min with a staining solution containing 0.1% (w/v) sodium citrate, 50 μg/ml PI, and 0.05% (v/v) Triton X-100 (v/v) and subsequently analyzed by flow cytometry (FACS Calibur, Becton Dickinson, Heidelberg, Germany; FL-2)[19].

Mouse tumor model. Mouse xenograft tumors were generated by subcutaneous injection of 0.5×10^6 cells PC3 (+/−Cav1) either alone or mixed with 0.5×10^6 cells HS5 (+/−Cav1) cells onto the hind limb of the mice (total volume 50 μl) as previously described[19]. Up to 20 animals of each experimental group received a single subcutaneous injection of 0.5×10^6 viable cells. For radiation therapy mice were anesthetized (2% isoflurane) and tumors were exposed to a single dose of 10 Gy ±5% in 5 mm tissue depth (~1.53 Gy/min, 300 kV, filter: 0.5 mm Cu, 10 mA, focus distance: 60 cm) using a collimated beam with a XStrahl RS 320 cabinet irradiator (XStrahl Limited, Camberly, Surrey, Great Britain)[56]. For intraprostatic implantation, mice were anesthetized with ketamine (50 mg/kg) and xylazine (10 mg/kg). A low abdominal transverse incision was made and PC3 (+/−Cav1) cells (1×10^5 in 50 μl of PBS) were injected into the right and left dorsolateral lobe (25 μl per lobe) of the prostate, and the wound was closed with surgical clips. Carpofen (50 μg/10 g bodyweight) was injected subcutaneously as analgesic. Mouse experiments were carried out in strict accordance with the recommendations of the Guide for the Care and Use of Laboratory Animals of the German Government and they were approved by the Committee on the Ethics of Animal Experiments of the responsible authorities [Landesamt für Natur, Umwelt und Verbraucherschutz (LANUV), Regierungspräsidium Düsseldorf Az. 8.87–50.10.37.09.187; Az. 8.87–51.04.20.09.390].

Immunohistochemistry and immunofluorescence. Paraffin embedded tissue sections were hydrated using a descending alcohol series, incubated for 10–20 min in target retrieval solution (Dako) and incubated with blocking solution (2% FCS/PBS). After permeabilisation, sections were incubated with primary antibodies over night at 4 °C. Antigen was detected with a peroxidase-conjugated secondary antibody (1/250) and DAB staining (Dako). Nuclei were counterstained using hematoxylin. Masson´s Goldner Trichrome (TC) (Carl Roth Karlsruhe, Germany) for histological evaluation of connective tissue was performed according to the manufactures instruction. For immunofluorescence analysis, antigen was detected with an anti-rabbit-Alexa488 and anti-rat-Alexa555-conjugated secondary antibody (1/500). Hoechst 33342 (Invitrogen, Karlsruhe, Germany) was used for nuclei staining. Specimens were analyzed by confocal microscopy.

Western blot. Whole cell lysates were generated by scraping cells into ice-cold RIPA-P buffer (150 mmol/L NaCl, 1% NP40, 0.5% sodium-desoxycholate, 0.1% sodium-dodecylsulfate, 50 mmol/L Tris/HCL pH 8, 10 mmol/L NaF, 1 mmol/L Na_3VO_4), supplemented with complete Protease-Inhibitor-Cocktail (Roche) and performing 2–3 freeze-thaw cycles. Protein samples (50–100 μg total protein) were subjected to SDS-PAGE electrophoresis and Western blots were done as previously described using the indicated antibodies[57].

Statistical Analysis. If not otherwise indicated, data were obtained from 3 independent experiments with at least 3 mice each. Statistical significance was evaluated by 1-way ANOVA followed by Tukey's or Bonferroni multiple comparisons post-hoc test and set at the level of $P \leq 0.05$. Data analysis was performed with Prism 5.0 software (GraphPad, La Jolla, California).

References

1. Singh, S. R., Rameshwar, P. & Siegel, P. Targeting tumor microenvironment in cancer therapy. *Cancer letters*, doi: 10.1016/j.canlet.2016.04.009 (2016).
2. Sun, Y. Tumor microenvironment and cancer therapy resistance. *Cancer letters*, doi: 10.1016/j.canlet.2015.07.044 (2015).
3. Cheng, C. J. *et al.* MicroRNA silencing for cancer therapy targeted to the tumour microenvironment. *Nature* **518,** 107–110, doi: 10.1038/nature13905 (2015).
4. Masuda, S. & Izpisua Belmonte, J. C. The microenvironment and resistance to personalized cancer therapy. *Nature reviews. Clinical oncology* **10,** doi: 10.1038/nrclinonc.2012.127-c1 (2013).
5. Swartz, M. A. *et al.* Tumor microenvironment complexity: emerging roles in cancer therapy. *Cancer research* **72,** 2473–2480, doi: 10.1158/0008-5472.CAN-12-0122 (2012).
6. Yang, H. *et al.* Mechanosensitive caveolin-1 activation-induced PI3K/Akt/mTOR signaling pathway promotes breast cancer motility, invadopodia formation and metastasis *in vivo*. *Oncotarget* **7,** 16227–16247, doi: 10.18632/oncotarget.7583 (2016).

7. El-Gendi, S. M., Mostafa, M. F. & El-Gendi, A. M. Stromal caveolin-1 expression in breast carcinoma. Correlation with early tumor recurrence and clinical outcome. *Pathology oncology research: POR* **18,** 459–469, doi: 10.1007/s12253-011-9469-5 (2012).
8. Koo, J. S., Park, S., Kim, S. I., Lee, S. & Park, B. W. The impact of caveolin protein expression in tumor stroma on prognosis of breast cancer. *Tumour biology: the journal of the International Society for Oncodevelopmental Biology and Medicine* **32,** 787–799, doi: 10.1007/s13277-011-0181-6 (2011).
9. Nassar, Z. D., Hill, M. M., Parton, R. G. & Parat, M. O. Caveola-forming proteins caveolin-1 and PTRF in prostate cancer. *Nature reviews. Urology* **10,** 529–536, doi: 10.1038/nrurol.2013.168 (2013).
10. Ayala, G. *et al.* Loss of caveolin-1 in prostate cancer stroma correlates with reduced relapse-free survival and is functionally relevant to tumour progression. *The Journal of pathology* **231,** 77–87, doi: 10.1002/path.4217 (2013).
11. Freeman, M. R., Yang, W. & Di Vizio, D. Caveolin-1 and prostate cancer progression. *Advances in experimental medicine and biology* **729,** 95–110, doi: 10.1007/978-1-4614-1222-9_7 (2012).
12. Shan, T. *et al.* Loss of stromal caveolin-1 expression: a novel tumor microenvironment biomarker that can predict poor clinical outcomes for pancreatic cancer. *PloS one* **9,** e97239, doi: 10.1371/journal.pone.0097239 (2014).
13. Gumulec, J. *et al.* Caveolin-1 as a potential high-risk prostate cancer biomarker. *Oncology reports* **27,** 831–841, doi: 10.3892/or.2011.1587 (2012).
14. Tahir, S. A. *et al.* Development of an immunoassay for serum caveolin-1: a novel biomarker for prostate cancer. *Clinical cancer research: an official journal of the American Association for Cancer Research* **9,** 3653–3659 (2003).
15. Thompson, T. C. *et al.* The role of caveolin-1 in prostate cancer: clinical implications. *Prostate cancer and prostatic diseases* **13,** 6–11, doi: 10.1038/pcan.2009.29 (2010).
16. Sotgia, F. *et al.* Caveolin-1 and cancer metabolism in the tumor microenvironment: markers, models, and mechanisms. *Annual review of pathology* **7,** 423–467, doi: 10.1146/annurev-pathol-011811-120856 (2012).
17. Goetz, J. G., Lajoie, P., Wiseman, S. M. & Nabi, I. R. Caveolin-1 in tumor progression: the good, the bad and the ugly. *Cancer metastasis reviews* **27,** 715–735, doi: 10.1007/s10555-008-9160-9 (2008).
18. Tahir, S. A. *et al.* Serum caveolin-1, a biomarker of drug response and therapeutic target in prostate cancer models. *Cancer biology & therapy* **14,** 117–126, doi: 10.4161/cbt.22633 (2013).
19. Klein, D. *et al.* Endothelial Caveolin-1 regulates the radiation response of epithelial prostate tumors. *Oncogenesis* **4,** e148, doi: 10.1038/oncsis.2015.9 (2015).
20. Kannan, A. *et al.* Caveolin-1 promotes gastric cancer progression by up-regulating epithelial to mesenchymal transition by crosstalk of signalling mechanisms under hypoxic condition. *Eur J Cancer* **50,** 204–215, doi: 10.1016/j.ejca.2013.08.016 (2014).
21. Williams, T. M. & Lisanti, M. P. Caveolin-1 in oncogenic transformation, cancer, and metastasis. *American journal of physiology. Cell physiology* **288,** C494–506, doi: 10.1152/ajpcell.00458.2004 (2005).
22. Quest, A. F., Gutierrez-Pajares, J. L. & Torres, V. A. Caveolin-1: an ambiguous partner in cell signalling and cancer. *Journal of cellular and molecular medicine* **12,** 1130–1150, doi: 10.1111/j.1582-4934.2008.00331.x (2008).
23. Cordes, N. *et al.* Human pancreatic tumor cells are sensitized to ionizing radiation by knockdown of caveolin-1. *Oncogene* **26,** 6851–6862, doi: 10.1038/sj.onc.1210498 (2007).
24. Hehlgans, S. & Cordes, N. Caveolin-1: an essential modulator of cancer cell radio-and chemoresistance. *American journal of cancer research* **1,** 521–530 (2011).
25. Hehlgans, S. *et al.* Caveolin-1 mediated radioresistance of 3D grown pancreatic cancer cells. *Radiotherapy and oncology: journal of the European Society for Therapeutic Radiology and Oncology* **92,** 362–370, doi: 10.1016/j.radonc.2009.07.004 (2009).
26. Barzan, D., Maier, P., Zeller, W. J., Wenz, F. & Herskind, C. Overexpression of caveolin-1 in lymphoblastoid TK6 cells enhances proliferation after irradiation with clinically relevant doses. Strahlentherapie und Onkologie: Organ der Deutschen Rontgengesellschaft … [*et al*] **186,** 99–106, doi: 10.1007/s00066-010-2029-1 (2010).
27. Joniau, S. & Van Poppel, H. Localized prostate cancer: can we better define who is at risk of unfavourable outcome? *BJU international* **101** Suppl 2, 5–10 (2008).
28. Ganswindt, U. *et al.* Combination of celecoxib with percutaneous radiotherapy in patients with localised prostate cancer - a phase I study. *Radiat Oncol* **1,** 9, doi: 10.1186/1748-717X-1-9 (2006).
29. Kawamorita, N. *et al.* Radical prostatectomy for high-risk prostate cancer: biochemical outcome. *International journal of urology: official journal of the Japanese Urological Association* **16,** 733–738, doi: 10.1111/j.1442-2042.2009.02352.x (2009).
30. Ploussard, G. *et al.* Impact of positive surgical margins on prostate-specific antigen failure after radical prostatectomy in adjuvant treatment-naive patients. *BJU international* **107,** 1748–1754, doi: 10.1111/j.1464-410X.2010.09728.x (2011).
31. Pascal, L. E. *et al.* Gene expression down-regulation in $CD90^+$ prostate tumor-associated stromal cells involves potential organ-specific genes. *BMC cancer* **9,** 317, doi: 10.1186/1471-2407-9-317 (2009).
32. Orr, B. *et al.* Identification of stromally expressed molecules in the prostate by tag-profiling of cancer-associated fibroblasts, normal fibroblasts and fetal prostate. *Oncogene* **31,** 1130–1142, doi: 10.1038/onc.2011.312 (2012).
33. Dakhova, O. *et al.* Global gene expression analysis of reactive stroma in prostate cancer. *Clinical cancer research: an official journal of the American Association for Cancer Research* **15,** 3979–3989, doi: 10.1158/1078-0432.CCR-08-1899 (2009).
34. Hanahan, D. & Weinberg, R. A. The hallmarks of cancer. *Cell* **100,** 57–70 (2000).
35. Hanahan, D. & Weinberg, R. A. Hallmarks of cancer: the next generation. *Cell* **144,** 646–674, doi: 10.1016/j.cell.2011.02.013 (2011).
36. Bhowmick, N. A., Neilson, E. G. & Moses, H. L. Stromal fibroblasts in cancer initiation and progression. *Nature* **432,** 332–337, doi: 10.1038/nature03096 (2004).
37. Schlomm, T. *et al.* Molecular cancer phenotype in normal prostate tissue. *European urology* **55,** 885–890, doi: 10.1016/j.eururo.2008.04.105 (2009).
38. Ellem, S. J., De-Juan-Pardo, E. M. & Risbridger, G. P. *In vitro* modeling of the prostate cancer microenvironment. *Advanced drug delivery reviews*, doi: 10.1016/j.addr.2014.04.008 (2014).
39. Dakhova, O., Rowley, D. & Ittmann, M. Genes upregulated in prostate cancer reactive stroma promote prostate cancer progression *in vivo*. *Clinical cancer research: an official journal of the American Association for Cancer Research* **20,** 100–109, doi: 10.1158/1078-0432.CCR-13-1184 (2014).
40. Barron, D. A. & Rowley, D. R. The reactive stroma microenvironment and prostate cancer progression. *Endocrine-related cancer* **19,** R187–204, doi: 10.1530/ERC-12-0085 (2012).
41. Huber, R. M. *et al.* DNA damage induces GDNF secretion in the tumor microenvironment with paracrine effects promoting prostate cancer treatment resistance. *Oncotarget* **6,** 2134–2147, doi: 10.18632/oncotarget.3040 (2015).
42. Gilbert, L. A. & Hemann, M. T. DNA damage-mediated induction of a chemoresistant niche. *Cell* **143,** 355–366, doi: 10.1016/j.cell.2010.09.043 (2010).
43. Sun, Y. *et al.* Treatment-induced damage to the tumor microenvironment promotes prostate cancer therapy resistance through WNT16B. *Nature medicine* **18,** 1359–1368, doi: 10.1038/nm.2890 (2012).
44. Shukla, S. *et al.* Activation of PI3K-Akt signaling pathway promotes prostate cancer cell invasion. *International journal of cancer. Journal international du cancer* **121,** 1424–1432, doi: 10.1002/ijc.22862 (2007).
45. Edwards, J. Src kinase inhibitors: an emerging therapeutic treatment option for prostate cancer. *Expert opinion on investigational drugs* **19,** 605–614, doi: 10.1517/13543781003789388 (2010).
46. Rice, L., Lepler, S., Pampo, C. & Siemann, D. W. Impact of the SRC inhibitor dasatinib on the metastatic phenotype of human prostate cancer cells. *Clinical & experimental metastasis* **29,** 133–142, doi: 10.1007/s10585-011-9436-2 (2012).

47. Zimnicka, A. M. *et al.* Src-dependent phosphorylation of caveolin-1 Tyr14 promotes swelling and release of caveolae. *Molecular biology of the cell*, doi: 10.1091/mbc.E15-11-0756 (2016).
48. Nethe, M. & Hordijk, P. L. A model for phospho-caveolin-1-driven turnover of focal adhesions. *Cell adhesion & migration* **5,** 59–64 (2011).
49. Desgrosellier, J. S. & Cheresh, D. A. Integrins in cancer: biological implications and therapeutic opportunities. *Nature reviews. Cancer* **10,** 9–22, doi: 10.1038/nrc2748 (2010).
50. DeRita, R. M. *et al.* c-Src, Insulin-Like Growth Factor I Receptor, G-Protein-Coupled Receptor Kinases and Focal Adhesion Kinase Are Enriched into Prostate Cancer Cell Exosomes. *Journal of cellular biochemistry*, doi: 10.1002/jcb.25611 (2016).
51. Bailey, K. M. & Liu, J. Caveolin-1 up-regulation during epithelial to mesenchymal transition is mediated by focal adhesion kinase. *The Journal of biological chemistry* **283,** 13714–13724, doi: 10.1074/jbc.M709329200 (2008).
52. Liang, W. *et al.* CAV-1 contributes to bladder cancer progression by inducing epithelial-to-mesenchymal transition. *Urologic oncology* **32,** 855–863, doi: 10.1016/j.urolonc.2014.01.005 (2014).
53. Hwangbo, C. *et al.* Syntenin regulates TGF-beta1-induced Smad activation and the epithelial-to-mesenchymal transition by inhibiting caveolin-mediated TGF-beta type I receptor internalization. *Oncogene* **35,** 389–401, doi: 10.1038/onc.2015.100 (2016).
54. Epstein, J. I., Allsbrook, W. C. Jr., Amin, M. B. & Egevad, L. L. The 2005 International Society of Urological Pathology (ISUP) Consensus Conference on Gleason Grading of Prostatic Carcinoma. *The American journal of surgical pathology* **29,** 1228–1242 (2005).
55. Klein, D. *et al.* Mesenchymal stem cell therapy protects lungs from radiation-induced endothelial cell loss by restoring superoxide dismutase 1 expression. *Antioxidants & redox signaling*, doi: 10.1089/ars.2016.6748 (2016).
56. Matschke, J. *et al.* Targeted Inhibition of Glutamine-Dependent Glutathione Metabolism Overcomes Death Resistance Induced by Chronic Cycling Hypoxia. *Antioxidants & redox signaling*, doi: 10.1089/ars.2015.6589 (2016).
57. Klein, D. *et al.* Wnt2 acts as a cell type-specific, autocrine growth factor in rat hepatic sinusoidal endothelial cells cross-stimulating the VEGF pathway. *Hepatology* **47,** 1018–1031, doi: 10.1002/hep.22084 (2008).

Acknowledgements

We thank Michael Groneberg for support with the irradiation of mice, Mohammed Benchellal, Inge Spratte and Eva Gau for their excellent technical assistance.

Author Contributions

A.P., J.K. and D.K. performed experiments; D.K. analysed results and made the figures; A.S., C.H., P.M. H.R. provided materials; H.R. performed the Gleasing scoring; D.K. and V.J. designed research and wrote the paper. All author reviewed and approved the manuscript. This work was supported by grants of the DFG (GRK1739/1), the BMBF (ZISS - FKZ: 02NUK024-D) and IFORES (D/107-40740).

Additional Information

Supplementary information accompanies this paper at http://www.nature.com/srep

Competing financial interests: The authors declare no competing financial interests.

How to cite this article: Panic, A. *et al.* Progression-related loss of stromal Caveolin 1 levels fosters the growth of human PC3 xenografts and mediates radiation resistance. *Sci. Rep.* **7**, 41138; doi: 10.1038/srep41138 (2017).

Publisher's note: Springer Nature remains neutral with regard to jurisdictional claims in published maps and institutional affiliations.

Supplementary Information

Progression-related loss of stromal Caveolin 1 levels fosters the growth of human PC3 xenografts and mediates radiation resistance

Andrej Panic[1,2,#], Julia Ketteler[1,#], Henning Reis[3], Ali Sak[4], Carsten Herskind[5], Patrick Maier[5], Herbert Rübben[2], Verena Jendrossek[1,*] and Diana Klein[1,*]

[1]Institute of Cell Biology (Cancer Research), University of Duisburg-Essen, University Hospital, Virchowstrasse 173, 45122 Essen, Germany.
[2]Department of Urology and Urooncology, University of Duisburg-Essen, University Hospital, Essen, Hufelandstr. 55, 45122 Essen, Germany
[3]Institut of Pathology, University of Duisburg-Essen, University Hospital, Hufelandstr. 55, 45122 Essen, Essen, Germany.
[4]Department of Radiotherapy, University of Duisburg-Essen, University Hospital, Hufelandstr. 55, 45122 Essen, Germany
[5]Department of Radiation Oncology, University Hospital, Medical Faculty Mannheim, Heidelberg University, Theodor-Kutzer-Ufer 1-3, 68167 Mannheim, Germany

[#] equal contribution
* shared senior authorship

Supplementary Figures

Supplementary Figure S1

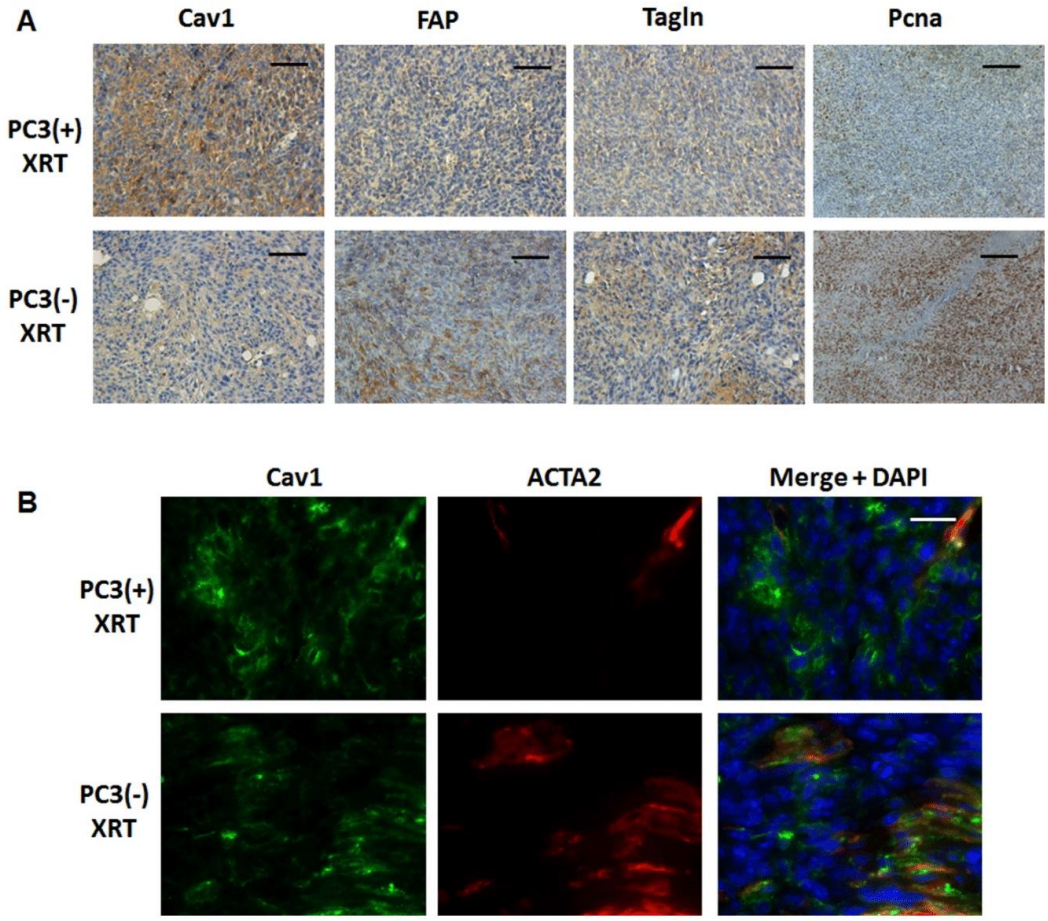

Supplementary Figure S1 | Radiation treatment of prostate tumors grown from Cav1-silenced PC3 cells were accompanied by a more reactive tumor stroma. (A) Tumors derived from PC3(-) as well as from PC3(+) control cells with normal Cav1 expression with radiation treatment (10Gy) were removed when tumor volumes reached a critical size (15-20 days after tumor irradiation) and were then subjected to immunohistochemistry with the indicated antibodies. Representative images are shown. Sections were counterstained using hematoxylin. Magnification Cav1, FAP, Tagln 20x; Pcna 10x. (B) Subcutaneously grown tumors were further analysed by immunofluorescence and confocal microscopy. Tumor stroma was stained for smooth muscle actin (ACTA2; red) and Cav1 (green). Representative images from at least three independent experiments are shown. Magnification 63x (scale bar 50µm).

Supplementary Figure S2

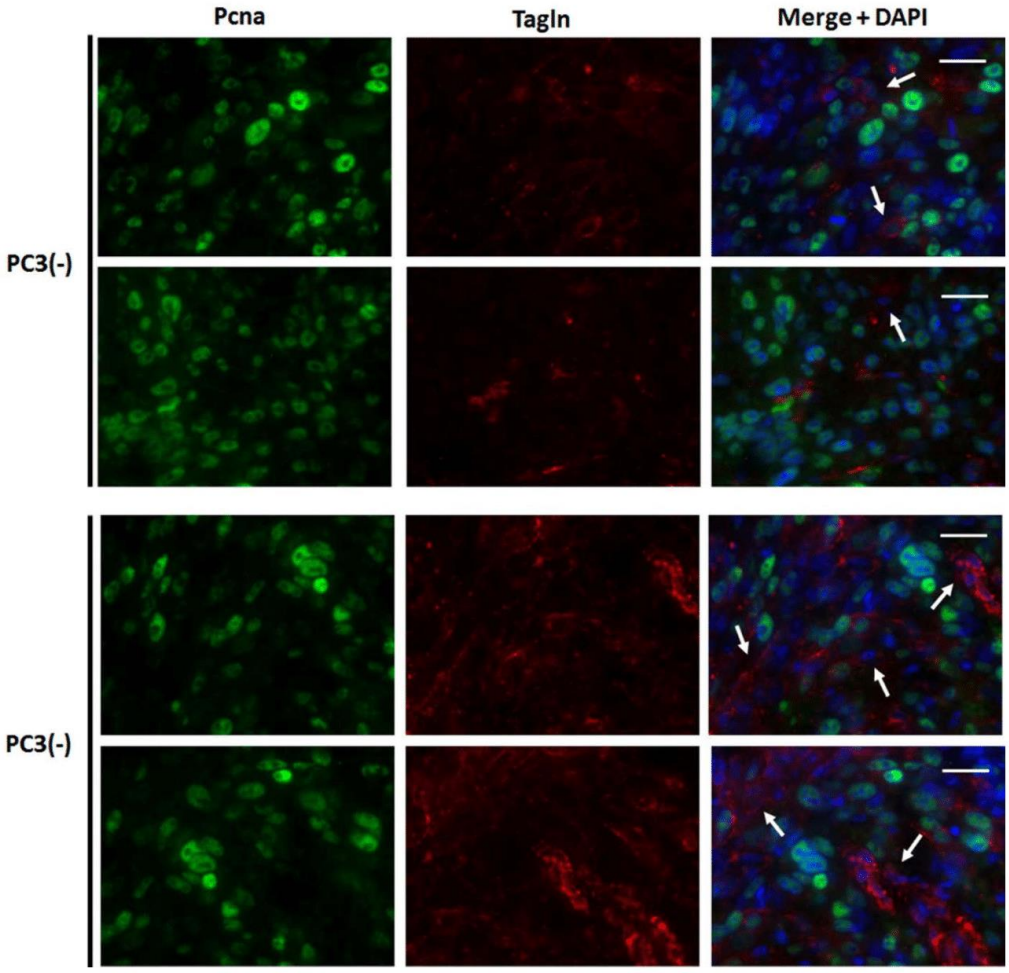

Supplementary Figure S2 | Proliferation was mainly restricted to the malignant epithelial cells. Tumors derived from PC3(-) as well as from PC3(+) control cells with normal Cav1 expression were removed when tumor volumes reached a critical size (8-14 days after implantation) and were analysed by immunofluorescence and confocal microscopy. Sections were stained for the proliferation marker Pcna (green) and tumor stroma was visualized by TagIn-immunoreactivity (red). Representative images are shown. Arrows point towards Pcna-negative stromal cells which were immunoreactive for TagIn. Magnification 63x (scale bar 25µm).

Supplementary Figure S3

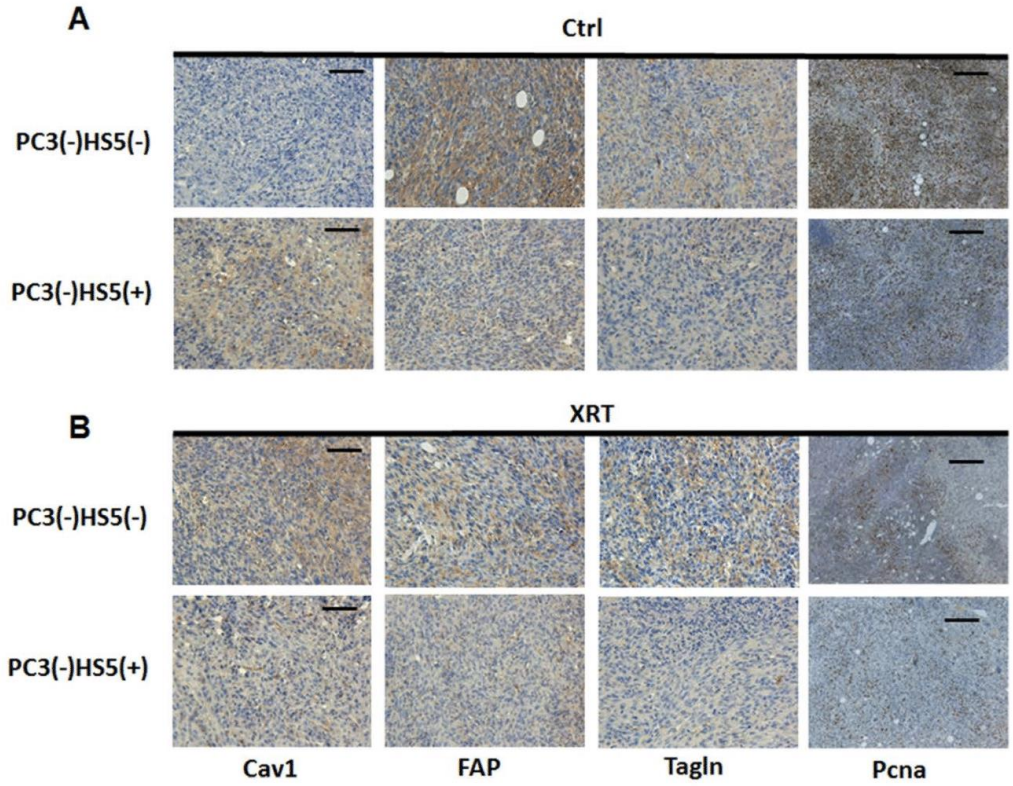

Supplementary Figure S3 | Radiation-induced Cav1 alterations mimicked the human situation: a more reactive tumor stroma potentially supports the resistance to radiation treatment. (A) Tumors derived from shCav1 PC3(-) cells in combination with Cav1-silenced HS5(-) fibroblasts or control transfected Cav1-expressing HS5(+) fibroblasts with or without radiation treatment (10Gy) (B) were removed when tumor volumes reached a critical size (12-22 days after tumor irradiation) and were then subjected to immunohistochemistry with the indicated antibodies. Representative images are shown. Sections were counterstained using hematoxylin. Magnification Cav1, FAP, Tagln 20x; Pcna 10x.

Supplementary Figure S4

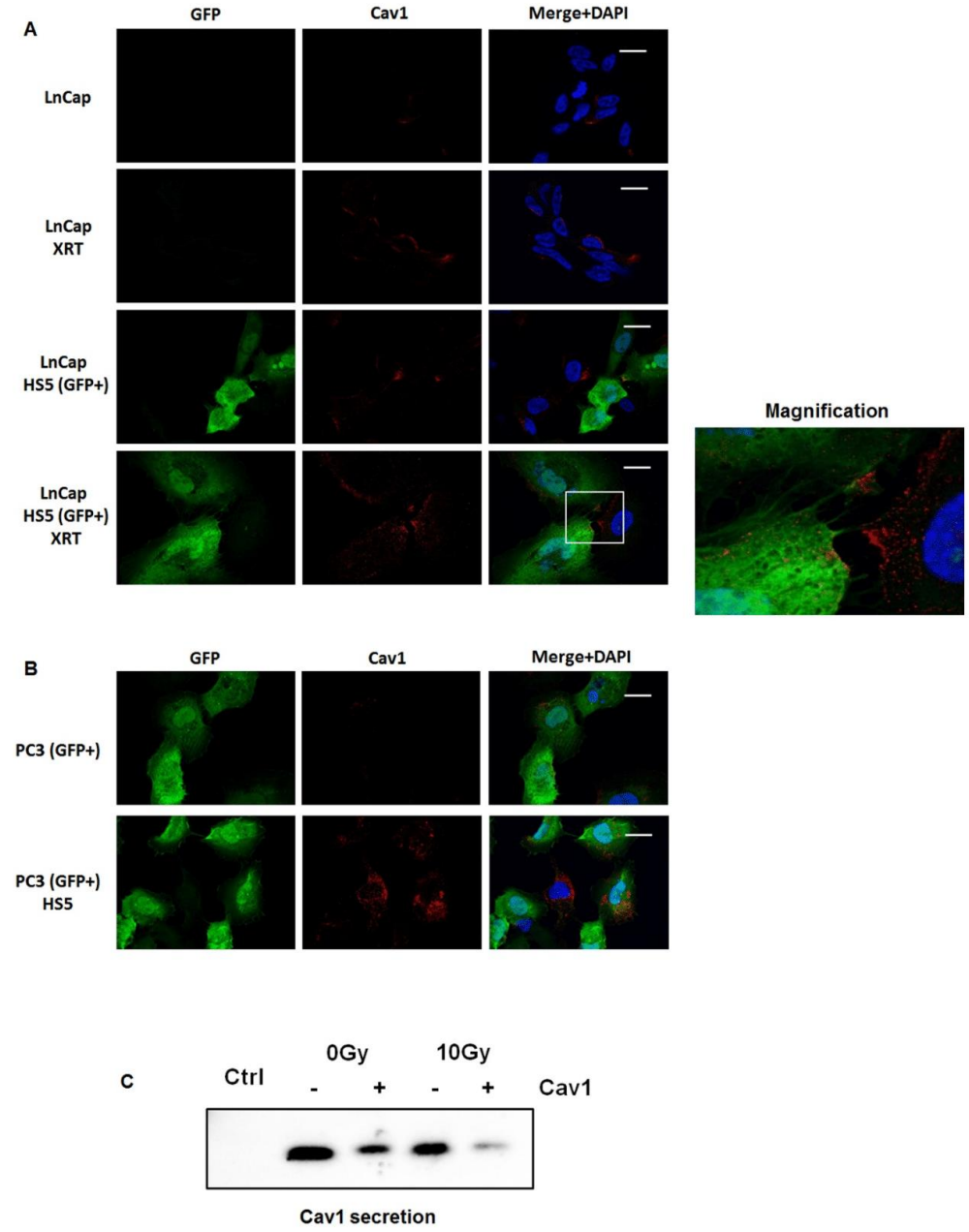

Supplementary Figure S4 | Co-culture of Cav1-expressing HS5 fibroblasts with Cav1-silenced PC3 or Cav-deficient LNCaP malignant epithelial cells yields Cav1-positive cancer cells. (A) Cav1 expression and localization was analyzed in LNCaP cells co-cultured with GFP-expressing (shCtrl)-transfected HS5 fibroblasts by immunofluorescence (red). (B) Cav1 expression was further analyzed in Cav1-silenced and GFP-expressing (shCav1-

transfected) PC3 cell co-cultures with normal (non-transfected**)** HS5 fibroblasts. Nuclei were stained in blue. Representative images from three independent experiments are shown. Magnification 63x (scale bar 25μm). (C) Cav1 secretion was further determined in cell culture supernatants derived from Cav1-silenced HS5(-) or control transfected Cav1-expressing HS5(+) fibroblasts with or without radiation treatment (10Gy) using Western blot analysis. Equal protein amounts (100 μg) were loaded.

Supplementary Figure S5

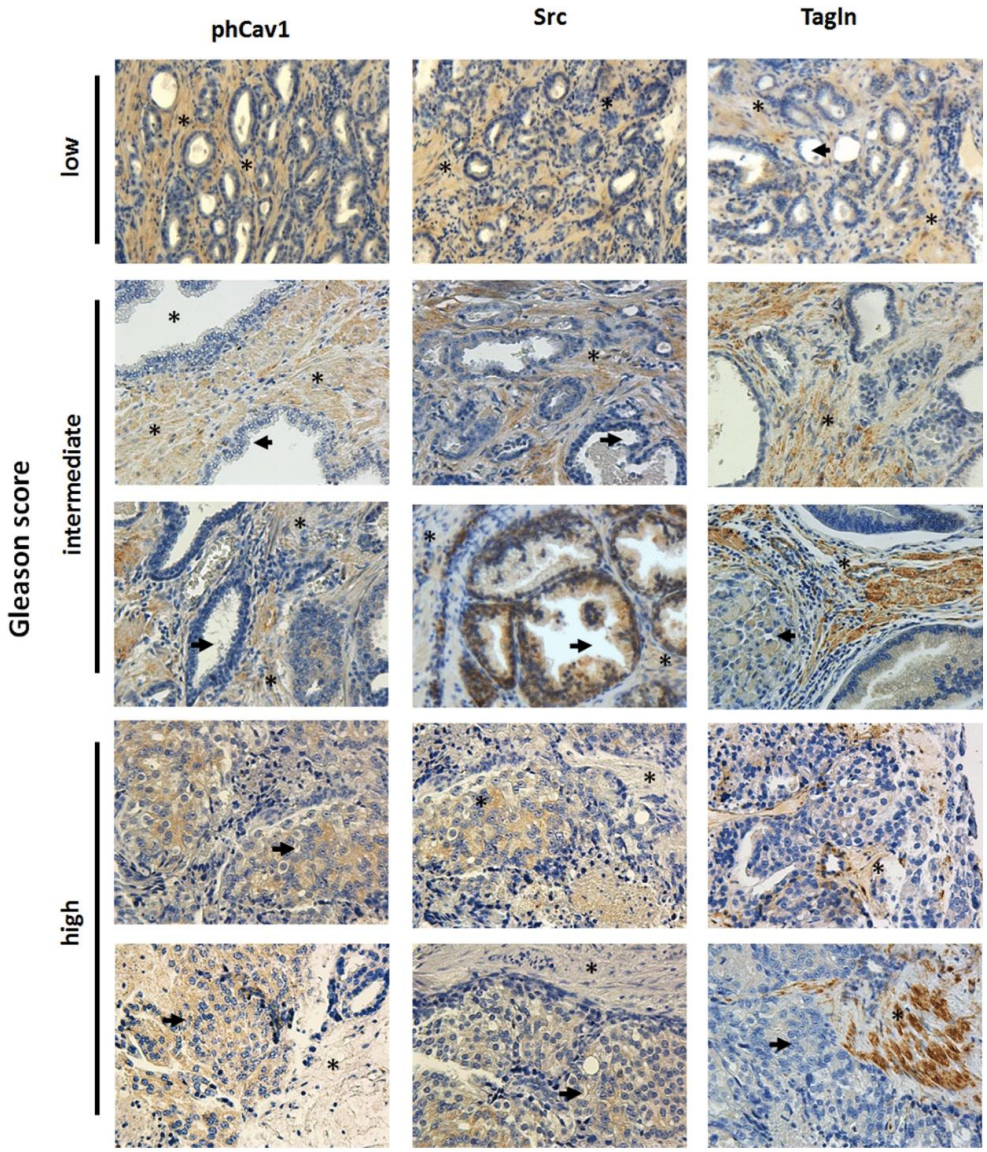

Supplementary Figure S5 | Immunohistological analysis of Cav1 expressions in human prostate tumor tissues (higher magnification photographs). Paraffin-sections of human prostate tumors were stained for the indicated antibodies. Gleason grading scores used to evaluate prognosis of men with prostate cancer were divided into low (1+1, 2+2), intermediate (3+3, 4+3) and high scores (4+5) according to the sum of the primary and secondary Gleason patterns in whole resection specimens. Sections were counterstained using hematoxylin. Representative images are shown. Magnification 40x.

Full Gels

Supplementary Figure S6

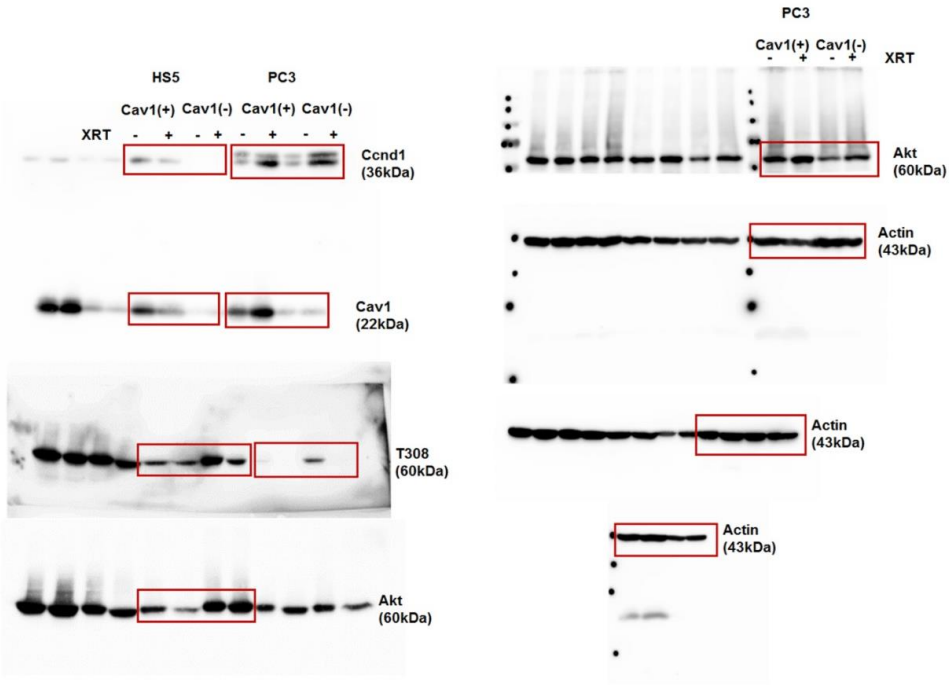

Supplementary Figure S6 | Full gels of cropped gels (emphasized by a red rectangle) as shown in Figure 1C and 5C. Cav1 protein levels were detected by Western blot. Equal protein amounts (50 µg, whole cell lysate) were loaded. Beta-actin was included as a loading control.

Supplementary Figure S7

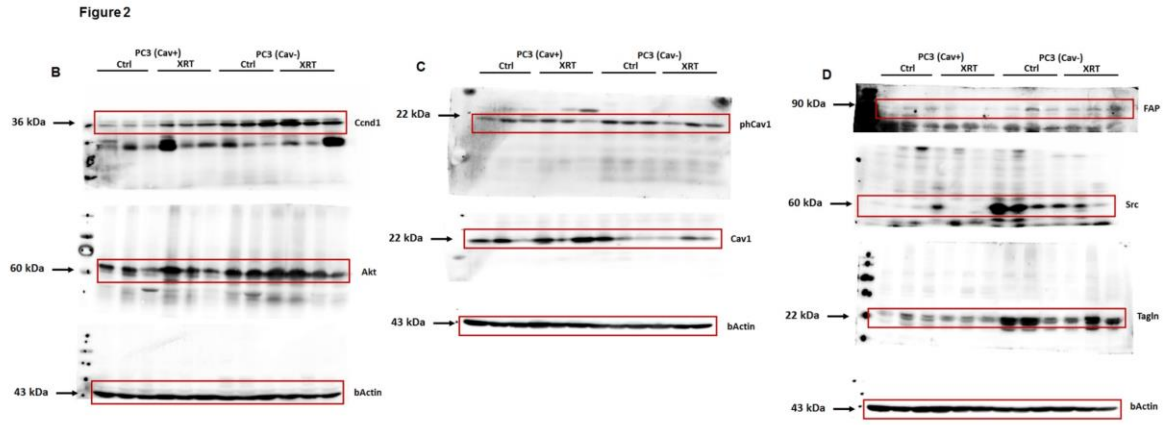

Supplementary Figure S7 | Full gels of cropped gels (emphasized by a red rectangle) as shown in Figure 2B-D. Indicated protein levels were detected by Western blot. Equal protein amounts (50 µg, whole cell lysate) were loaded. Beta-actin was included as a loading control. The Ccnd1 gel (first gel in B) was first probed with a different antibody (~20kDa).

Supplementary Figure S8

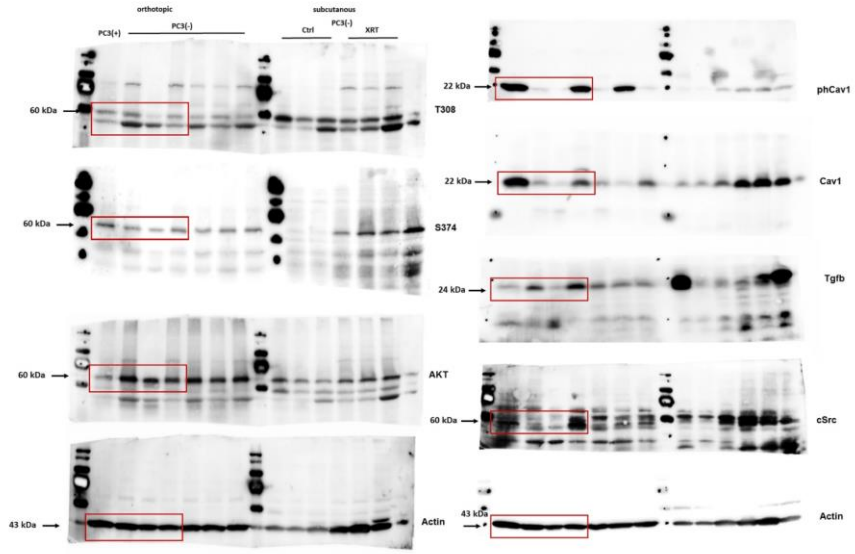

Supplementary Figure S8 | Full gels of cropped gels (emphasized by a red rectangle) as shown in Figure 4B. Indicated protein levels were detected by Western blot. Equal protein amounts (50 µg, whole cell lysate) were loaded. Beta-actin was included as a loading control.

Supplementary Figure S9

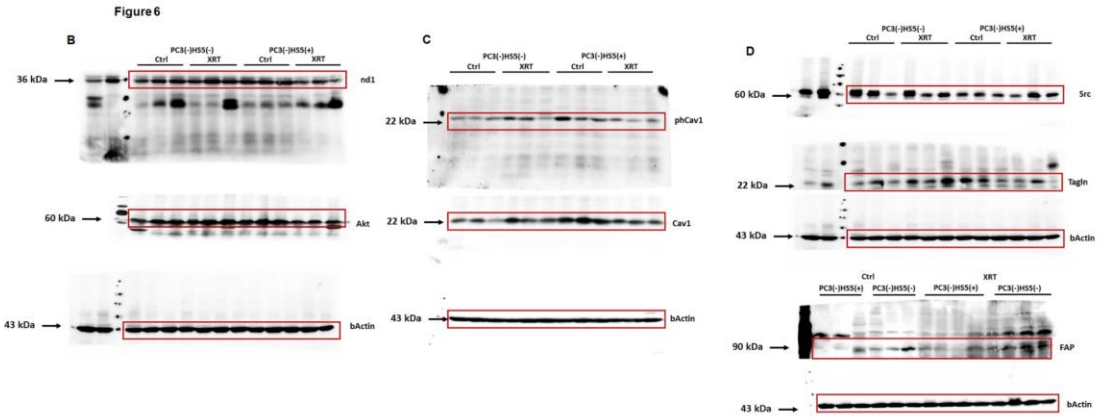

Supplementary Figure S9 | Full gels of cropped gels (emphasized by a red rectangle) as shown in Figure 6B-D. Indicated protein levels were detected by Western blot. Equal protein amounts (50 µg, whole cell lysate) were loaded. Beta-actin was included as a loading control.

Supplementary Figure S10

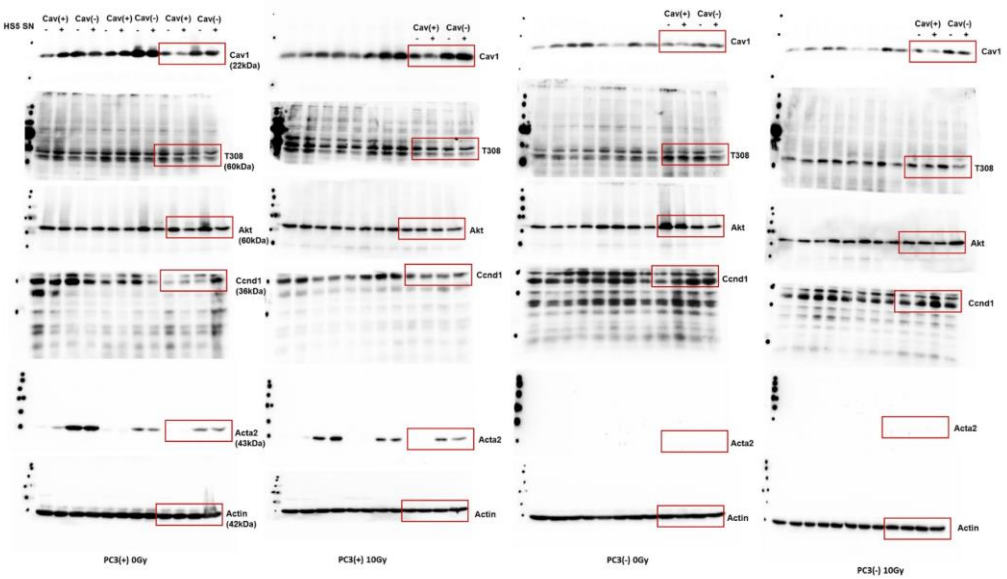

Supplementary Figure S10 | Full gels of cropped gels (emphasized by a red rectangle) as shown in Figure 7A. Indicated protein levels were detected by Western blot. Equal protein amounts (50 µg, whole cell lysate) were loaded. Beta-actin was included as a loading control.

5.4 Progression-related Loss of Stromal Caveolin 1 Levels Mediates Radiation Resistance in Prostate Carcinoma via the Apoptosis Inhibitor TRIAP1.

Cumulative thesis of Ms Julia Ketteler

Author contributions

Title of publication: Progression-Related Loss of Stromal Caveolin 1 Levels Mediates Radiation Resistance in Prostate Carcinoma via the Apoptosis Inhibitor TRIAP1.

Authors: Ketteler J, Panic A, Reis H, Wittka A, Maier P, Herskind C, Yagüe E, Jendrossek V, Klein D.

Jorunal of Clinical Medicine 2019, *8*, 348, doi: 10.3390/jcm8030348

Contributions:

- Conception – 40 %: planning experimens, proposing hypothesis
- Experimental work – 75 %: experiments for Figure 1 a, b and c, Figure 2, Figure 3, Figure 4 a and c
- Data analysis - 70 %: Figure 1 a, Figure 2, Figure 3, Figure 4 a, prepared Figures 1 - 4
- species identification: not applicable
- Statistical analysis – 75 %: Figure 1, 2 and 3
- Writing the manuscript - 50 %: writing first draft of the manuscript (all sections), proof reading
- Revising the manuscript – 50 %: critical proof-reading, additional figure preparation

Unterschrift Doktorand/in

Unterschrift Betreuer/in

Journal of
Clinical Medicine

MDPI

Article

Progression-Related Loss of Stromal Caveolin 1 Levels Mediates Radiation Resistance in Prostate Carcinoma via the Apoptosis Inhibitor TRIAP1

Julia Ketteler [1], Andrej Panic [1,2], Henning Reis [3], Alina Wittka [1], Patrick Maier [4], Carsten Herskind [4], Ernesto Yagüe [5], Verena Jendrossek [1] and Diana Klein [1,*]

1 Institute of Cell Biology (Cancer Research), University of Duisburg-Essen, University Hospital, Virchowstrasse 173, 45122 Essen, Germany; Julia.Ketteler@uk-essen.de (J.K.); Andrej.Panic@uk-essen.de (A.P.); Alina.Wittka@uk-essen.de (A.W.); Verena.Jendrossek@uk-essen.de (V.J.)
2 Department of Urology and Urooncology, University of Duisburg-Essen, University Hospital, Essen, Hufelandstr. 55, 45122 Essen, Germany
3 Institute of Pathology, University of Duisburg-Essen, University Hospital, Hufelandstr. 55, 45122 Essen, Germany; henning.reis@uk-essen.de
4 Department of Radiation Oncology, University Medical Center Mannheim, Medical Faculty Mannheim, Heidelberg University, Theodor-Kutzer-Ufer 1-3, 68167 Mannheim, Germany; Patrick.Maier@medma.uni-heidelberg.de (P.M.); Carsten.Herskind@medma.uni-heidelberg.de (C.H.)
5 Cancer Research Center, Division of Cancer, Imperial College London, Hammersmith Hospital Campus, London W12 0NN, UK; ernesto.yague@imperial.ac.uk
* Correspondence: Diana.Klein@uk-essen.de; Tel.: +49-201-723-83342; Fax: +49-201-723-5904

Received: 10 February 2019; Accepted: 6 March 2019; Published: 12 March 2019

Abstract: Tumour resistance to chemo- and radiotherapy, as well as molecularly targeted therapies, limits the effectiveness of current cancer treatments. We previously reported that the radiation response of human prostate tumours is critically regulated by CAV1 expression in stromal fibroblasts and that loss of stromal CAV1 expression in advanced tumour stages may contribute to tumour radiotherapy resistance. Here we investigated whether fibroblast secreted anti-apoptotic proteins could induce radiation resistance of prostate cancer cells in a CAV1-dependent manner and identified TRIAP1 (TP53 Regulated Inhibitor of Apoptosis 1) as a resistance-promoting CAV1-dependent factor. TRIAP1 expression and secretion was significantly higher in CAV1-deficient fibroblasts and secreted TRIAP1 was able to induce radiation resistance of PC3 and LNCaP prostate cancer cells *in vitro*, as well as of PC3 prostate xenografts derived from co-implantation of PC3 cells with TRIAP1-expressing fibroblasts *in vivo*. Immunohistochemical analyses of irradiated PC3 xenograft tumours, as well as of human prostate tissue specimen, confirmed that the characteristic alterations in stromal-epithelial CAV1 expression were accompanied by increased TRIAP1 levels after radiation in xenograft tumours and within advanced prostate cancer tissues, potentially mediating resistance to radiation treatment. In conclusion, we have determined the role of CAV1 alterations potentially induced by the CAV1-deficient, and more reactive, stroma in radio sensitivity of prostate carcinoma at a molecular level. We suggest that blocking TRIAP1 activity and thus avoiding drug resistance may offer a promising drug development strategy for inhibiting resistance-promoting CAV1-dependent signals.

Keywords: Caveolin-1; TP53-regulated inhibitor of apoptosis 1; tumour stroma; tumour microenvironment; fibroblast; CAF; resistance; prostate cancer; radiotherapy

1. Introduction

Cancer therapeutic resistance occurs through many different mechanisms, including specific genetic and epigenetic changes in the cancer cell itself and/or the respective microenvironment.

The tumour stroma is now recognized as a key player in cancer cell invasiveness, progression and therapy resistance [1–3]. Activated fibroblasts (cancer associated fibroblasts, CAF) are capable of preventing cancer cell apoptosis and induce proliferation, as well as invasion, of surrounding cancer cells via direct stroma-tumour interactions by secreting extracellular matrix components, growth factors and matrix metalloproteinases, among others [4]. Although the exact mechanisms of fibroblast activation remain elusive, the activation or repression of specific genes or proteins within stromal cells has also been correlated with clinical outcome. Within that scenario, the membrane protein Caveolin-1 (CAV1) came into focus as it is highly expressed in many tumours and high CAV1 levels in tumour cells, as well as the downregulation of stromal CAV1, were shown to correlate with cancer progression, invasion and metastasis and thus, a worse clinical outcome [4,5]. Loss of stromal CAV1 can even be used as a prognostic marker, for example, in breast and prostate cancer patients [6–9]. Data on the CAV1-dependent epithelia-stroma crosstalk indicates that stromal CAV1 possesses tumour-suppressor properties, whereas loss of stromal CAV1 fosters malignant epithelial cell resistance by evading apoptosis [5,10]. Stromal loss of CAV1 is particularly prominent in epithelial prostate cancer, where loss of CAV1 in the stroma correlates with high Gleason score, presence of metastasis and pronounced resistance to chemotherapy and radiotherapy [6,8,11,12]. However, a detailed mechanism explaining how CAV1-deficient fibroblasts foster therapy resistance of malignant prostate cancer cells remains elusive. An improved understanding of the molecular basis of resistance will inevitably lead to the clinical assessment of rational drug combinations in selected patient populations.

An important mechanism by which cancer cells acquire drug resistance is by apoptosis evasion [3] and apoptosis inhibiting proteins have been described in both the development of cancer [13] and drug resistance [14]. TP53-regulated inhibitor of apoptosis 1 (TRIAP1, also known as p53-inducible cell-survival factor, p53CSV) is a small, 76 amino acids long, evolutionary conserved protein [15]. TRIAP1 was first characterized as a p53-inducible cell survival factor [16]. A genetic screen further identified TRIAP1 as a pathway-specific regulator of the cellular response to p53 activation [17]. Mechanistically, TRIAP1 modulates the apoptotic pathways through interaction with HSP70, inhibition of the interaction of cytochrome c with the apoptotic protease activating factor 1 and activation of the downstream caspase-9, thus resulting in increased resistance by inhibiting apoptosis and permitting DNA damage repair [15,16].

In this study, we aimed at determining the role of CAV1 alterations potentially induced by stromal CAV1-deficiency for the radio sensitivity of prostate cancer on molecular level and identified the apoptosis inhibitor TRIAP1 as a CAV1-dependent fibroblastic secreted factor, fostering radio resistance of malignant prostate epithelial cells.

2. Material and Methods

2.1. Reagents and Antibodies

Antibodies against CAV1 (N-20: sc-894) and XIAP1 (H-202: sc-11426) were from Santa Cruz (Santa Cruz, CA, USA), against CCND1 (92G2: #2978) and GFP (D5.1: #2956) from Cell Signalling Technology (Denvers, MA, Germany), against PCNA (PC10: GTX20029) from GeneTex (Irvine, CA, USA), against TRIAP1 from ProteinTech Group [15351-1-AP, (WB) Rosemont, IL, USA] and LSBio [LS-C346398-100, (Histology) Seattle, WA, USA), against SURVIVIN (NB500-201) from Novus Biologicals (Centennial, CO, USA) and against β-actin (clone AC-74, A2228) from Sigma-Aldrich (St. Louis, MO, USA). The rabbit anti human ASA antibody BE#3 was previously described [18] and the goat anti ASM antibody was kindly provided by Prof. K. Sandhoff (Bonn, Germany) [19].

2.2. Cell Culture Conditions

The human prostate cancer cell lines PC3, DU145 and LNCaP, the human skin fibroblast cell line HS5 and the human prostate fibroblast cell line WPMY-1 were from ATCC (Manassas, VA, USA) and cultured in RPMI Medium (Gibco, ThermoFisher, Waltham, MA, USA) supplemented with 10% foetal

bovine serum and 100 U/mL Penicillin/Streptomycin under standard cell culture conditions (37 °C, 5% CO_2, 95% humidity) and passaged every 3–4 days. CAV1 mRNA levels were down-regulated in indicated cells using shRNA technology as previously described [11,20,21]. For transient transfection of cells, human TRIAP1 cDNA with a C-terminal GFP-tag cloned into pCMV6-AC-GFP was used [15]. For selection of transfected cells, 500 µg/mL G418/Neomycin (Merck/Millipore, Darmstadt, Germany) was used.

2.3. Irradiation of Cell Cultures

Radiation was performed using the Isovolt-320-X-ray machine (Seifert-Pantak) at 320 kV, 10 mA with a 1.65 mm aluminium filter and a distance of about 500 mm to the object being irradiated [21]. The X-ray tube operated at 90 kV (~45 keV X-rays) and the dose rate was about 3 Gy/min [22].

2.4. Colony Formation Assay

The long-term survival assay was carried out by seeding 250 cells/well to 15.000 cells/well in a 6-well plate and irradiation at 0, 2, 4 and 6 Gy [11,21]. The plates were left to grow for 10 days into single colonies before they were fixed in 3.7% Formaldehyde (in PBS) and 70% Ethanol. Colonies were stained with 0.05% Coomassie Brilliant Blue for 1.5–3 h. Colonies (≥50 cells) were counted at fivefold magnification under the microscope.

2.5. Flow Cytometry Analysis

To measure and quantify the DNA-fragmentation (apoptotic sub-G1 population), as well as to quantify the cell cycle phases, cells were incubated for 30 min at RT with a staining solution containing 0.1% (*w*/*v*) sodium citrate, 50 µg/mL PI and 0.05% (*v*/*v*) Triton X-100 (*v*/*v*). Afterwards they were analysed by flow cytometry (FACS Calibur, Becton Dickinson, Heidelberg, Germany; FL-2).

2.6. Western Blotting

Generation of whole cell lysates was carried out by scraping cells off into ice-cold RIPA buffer (150 mmol/L NaCl, 1% NP40, 0.5% sodium-deoxycholate, 0.1% sodium-dodecylsulfate, 50 mmol/L Tris/HCl, pH 8, 10 mmol/L NaF, 1 mmol/L Na3VO4) supplemented with Protease-Inhibitor cocktail (Roche). After 2–3 freeze and thaw cycles the protein content of the lysates was measured by using DC™ Protein Assay (Bio-Rad). 50 µg to 100 µg of protein were loaded onto SDS-PAGE electrophoresis. Western blots were done as previously described [11,21] and the indicated antibodies were used to detect protein expression.

2.7. Real-Time Reverse Transcription PCR (qRT-PCR)

RNA was isolated using RNeasy Mini Kit (74106, Qiagen, Hilden, Germany) according to the manufacturer's instruction and as previously described [11,22]. Expression levels were normalized to the reference gene (β-actin; set as 1) and were shown as relative quantification. Specific primers were designed using Primer 3 [23] based on available NCBI nucleotide CDS sequences. Cross-reaction of primers was excluded by comparison of the sequence of interest with the NCBI database (Blast 2.2, U.S. National Centre for Biotechnology Information, Bethesda, MD) and all primers used were intron-spanning. PCR products are 200-300 bp in size. qRT-PCR was carried out using specific oligonucleotide primers (s sense, as antisense; TRIAP1s AGGATTTCGCAAGTCCAGAA, TRIAP1as GCTGATTCCACCCAAGTAT; TAGLNs TCCAGACTGTTGACCTCTTTGA, TAGLNas CCTCTCCGC TCTAACTGATGAT; ACTA2s GCCGAGATCTCACTGACTACCT, ACTA2as TGATGCTGTTGTAGGTG GTTTC; TGFB1s CCCACAACGAAATCTATGACAA, TGFB1as AACTCCGGTGACATCAAAAGAT; LAMP1s CCTGCCTTTAAAGCTGCCAA; LAMP1as CACCTTCCACCTTGAAAGCC; LAMP2s ACC ACTGTGCCATCTCCTAC, LAMP2as TGCCTGTGGAGTGAGTTGTA; ACTINs GGCACCACACTTT CTACAATGA, ACTINas TCTCTTTAATGTCACGCACGAT) as previously described [11,22].

2.8. Conditioned Media

Cells were cultured in normal growth media until confluence. Cells were left non-irradiated or irradiated with 10 Gy, media were replaced and cells cultured in the presence of 0.5% foetal bovine serum for 48 h before collection of media. Control media were generated by incubating the same medium (containing 0.5% foetal bovine serum) without cells. Conditioned media were used as 1/1 mixture with normal growth medium [11,22].

2.9. Mouse Tumour Model

Mouse xenograft tumours were generated by subcutaneous injection of 0.5×10^6 PC3 cells (+/−CAV1) either alone or mixed with 0.5×10^6 WMPY-1 cells (+/−TRIAP1) onto the hind limb of male NMRI nude mice (total volume 50 µL) as previously described [11,21]. Animals of each experimental group received a single subcutaneous injection. For radiation therapy mice were anesthetized (2% isoflurane) and tumours were exposed to a single dose of 10 Gy ± 5% in 5 mm tissue depth (~1.53 Gy/min, 300 kV, filter: 0.5 mm Cu, 10 mA, focus distance: 60 cm) using a collimated beam with an XStrahl RS 320 cabinet irradiator (XStrahl Limited, Camberly, Surrey, Great Britain). Mouse experiments were carried out in strict accordance with the recommendations of the Guide for the Care and Use of Laboratory Animals of the German Government and they were approved by the Committee on the Ethics of Animal Experiments of the responsible authorities [Landesamt für Natur, Umwelt und Verbraucherschutz (LANUV), Regierungspräsidium Düsseldorf Az.8.87-50.10.37.09.187; Az.8.87-51.04.20.09.390; Az.84-02.04.2015.A586].

2.10. Human Tumour Tissue

Tissues from human prostate carcinomas were obtained during surgery according to local ethical and biohazard regulations. All experiments were performed in strict accordance with local guidelines and regulations. Resected tissue specimens were processed for pathological diagnostic routine in agreement with institutional standards and diagnoses were made based on current WHO and updated ISUP criteria [11,21]. All studies including human tissue samples were approved by the local ethics committee (Ethik-Kommission) of the University Hospital Essen (Nr. 10-4363 and 10-4051). Human tissue samples were analysed anonymously.

2.11. Immunohistochemistry and Immunofluorescence

Immunohistochemistry was performed on 4 µm slides of formalin-fixed and paraffin-embedded prostate tissues after performing a descending alcohol-series and incubation for 10 min to 20 min in target retrieval solution (Dako, Agilent, Santa Clara, CA, USA) [11]. After blocking of the slides with 2% NGS/PBS sections were incubated with primary antibodies o/n at 4 °C. Antigen were detected with horseradish-peroxidase conjugated secondary antibodies (1:250) and developed with DAB (Dako). Nuclei were counterstained using haematoxylin.

2.12. Statistical Analysis

If not otherwise indicated, data were obtained from 3 independent experiments with at least 2–3 mice each. Total mice numbers were stated in the figure legends. Statistical significance was evaluated by 1- or 2-way ANOVA followed by Tukey's or Bonferroni multiple comparisons post-hoc test and set at the level of $p \leq 0.05$. Data analysis was performed with Prism 5.0 software (GraphPad, La Jolla, CA, USA).

3. Results

3.1. Radioresistant (CAV1-Silenced) Fibroblasts Express and Secrete Anti-Apoptotic TRIAP1

We previously reported that CAV1-deficient fibroblasts foster radiation resistance of malignant prostate epithelial cells resulting in decreased apoptosis rates *in vitro* and *in vivo*, most likely via a paracrine mechanism of action [11]. Because we hypothesized that fibroblasts could allocate CAV1-dependent apoptosis inhibiting proteins to the tumour cells, we investigated the presence and expression levels of well-known resistance-associated anti-apoptotic proteins in stromal HS5 fibroblasts being either proficient [HS5(+)] for CAV1 or CAV1-deficient [HS5(-)] achieved by a shRNA-mediated knock-down (Figure 1). Of note, CAV1-silenced HS5 fibroblasts expressed significantly higher levels of TRIAP1 at both protein (Figure 1A) and mRNA level (Figure 1B). In addition, an increased CAV1-dependent TRIAP1 secretion was confirmed in cell culture supernatants of CAV1-silenced HS5 fibroblasts, which was accompanied by increased levels of lysosomal enzymes (acid sphingomyelinase, ASM and arylsulfatase A, ASA), which might be indicative for lysosomal exocytosis (Figure 1C).

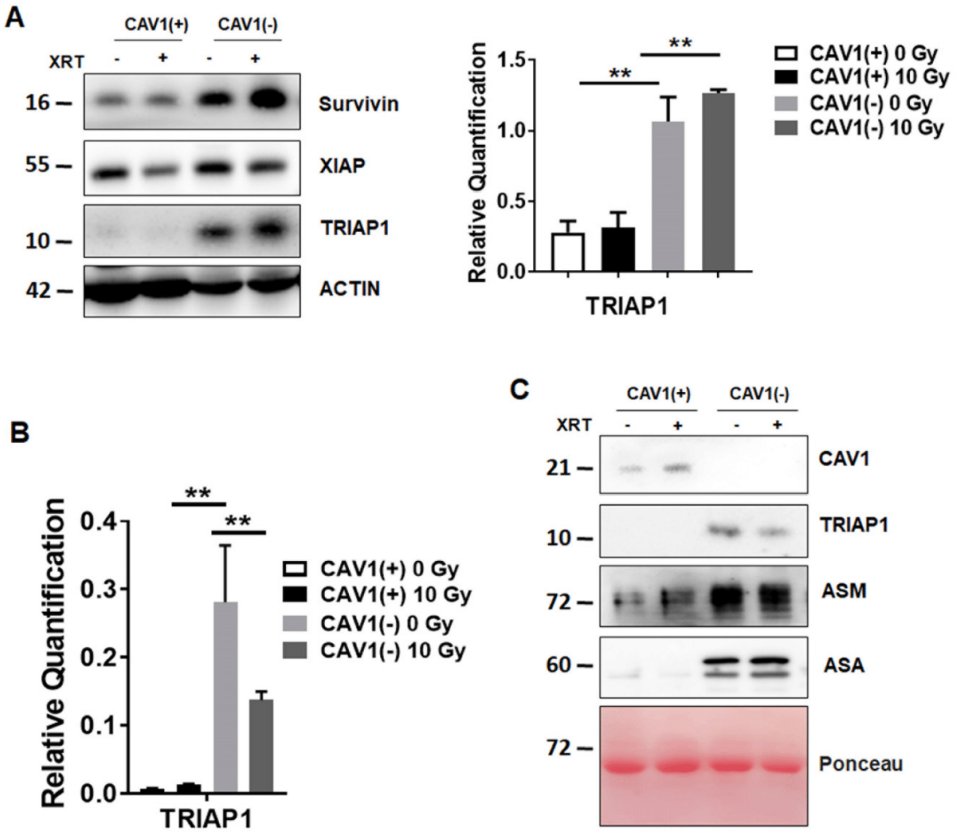

Figure 1. Radiation-resistant Caveolin-1 (CAV1)-silenced fibroblasts differentially express and secrete the apoptosis inhibiting protein TP53-regulated inhibitor of apoptosis 1 (TRIAP1).

Thus, increased expression and secretion of TRIAP1 by CAV1-silenced fibroblasts suggests that secreted TRIAP1 and then internalized by neighbouring prostate cancer cells, might account for the induced radiation resistance of these cells.

(A) Protein expression levels of apoptosis inhibiting proteins survivin, XIAP (X-linked inhibitor of apoptosis protein) and TRIAP1 were determined in CAV1-proficient [Cav1(+)] and CAV1-silenced [Cav1(-)] HS5 fibroblasts. Indicated proteins were analysed in whole protein lysates 96 h after radiation with 10 Gy by western blot analysis. Representative blots are shown. For TRIAP1 quantification, blots were analysed by densitometry and the respective signal was normalized to that from β-actin (n = 3–4 for each group). *p*-values were indicated: * $p \leq 0.05$, ** $p < 0.01$ by one-way ANOVA followed by post-hoc Tukey's test.

(B) qRT-PCR quantifications of TRIAP1 mRNA levels were performed 96 h post irradiation and shown as relative expression to β-actin mRNA. Data shown represent mean values ± SEM from 4 independent samples per group, each measured in duplicate. * $p \leq 0.05$, ** $p \leq 0.01$, by one-way ANOVA followed by post-hoc Tukey's test.

(C) TRIAP1 and lysosomal enzymes (ASM, acid sphingomyelinase and ASA, arylsulfatase A) secretion were further determined in cell culture supernatants derived from CAV1-silenced HS5(-) or control transfected CAV1-expressing HS5(+) fibroblasts with or without radiation treatment (10 Gy) using western blot analysis. Equal protein amounts (100 µg) were loaded. Ponceau S staining of transferred proteins was included as loading control.

3.2. Ectopic TRIAP1 Expression in Prostate Carcinoma Cells Induces Radiation Resistance

We previously have shown that cell culture supernatants of CAV1-silenced HS5 fibroblasts were able to induce radiation resistance of PC3 and LNCaP cells by decreased apoptosis [11]. We then investigated if the induced resistance of prostate cancer cells, after treatment with supernatants derived from CAV1-proficient or -deficient fibroblasts, led to higher TRIAP1 levels (not shown). However, no increased TRIAP1 levels were detectable in PC3, DU145 or LNCaP prostate carcinoma cells upon supernatants treatment most likely because the amount of tumour cell internalized TRIAP1 which was secreted from fibroblasts did not pass the threshold level of detection by western blot analysis. To provide the proof of principle that TRIAP1 mediates radiation resistance, the prostate cancer cells PC3 (p53 null), DU145 (p53 mutant) and LNCaP (p53 wild type) were transiently transfected with an expression vector encoding for human GFP-tagged TRIAP1 (Figure 2A). Empty vector transfected cells served as a control. Ectopic TRIAP1 expression resulted in decreased subG1 levels in PC3 and LNCaP cells 48 h after radiation with 10 Gy and thus increased resistance to radiation treatment. However, DU145 cells were not affected. Increased TRIAP1-levels were confirmed by western blot analysis (Figure 2B). Cell cycle analysis further revealed that ectopic TRIAP1 expression resulted in a slightly diminished G0/G1 subpopulation in PC3 cells upon radiation, while the proportion of cells in the G2/M phase increased (Figure 2C). The cell cycle of DU145 prostate carcinoma cells after TRIAP1 transfection was not affected upon radiation. Similar to PC3 cells, more TRIAP1-transfected LNCaP cells were in the G2/M phase after radiation as compared to control transfected cells. The proportions of respective cells in the S and <4n phase were rather low and not affected (not shown).

These results indicate that ectopic TRIAP1 expression mediates radiation resistance in a cell-type dependent manner and suggest that resistant prostate cancer cells will have an increased proliferation potential.

(A) Prostate cancer cells were transiently transfected with an expression vector encoding for human TRIAP1-GFP. Empty vector served as control. 24 h after transfection cells were irradiated with 0 or 10 Gy. The degree of apoptosis was quantified measuring the SubG1 fraction after radiation by flow cytometry analysis after additional 48 h of culture. Data shown represent mean values ± SEM from 4–5 independent samples per group measured in duplicates each. * $p \leq 0.05$, by two-tailed students *t*-test.

(B) Efficiency of TRIAP1-GFP expressions as analysed by Western blots. Representative blots from 3-4 independent experiments are shown. β-actin is used as a loading control. As additional control (Ctrl) mock transfected cells, which underwent the transfection procedure without an expression vector were shown.

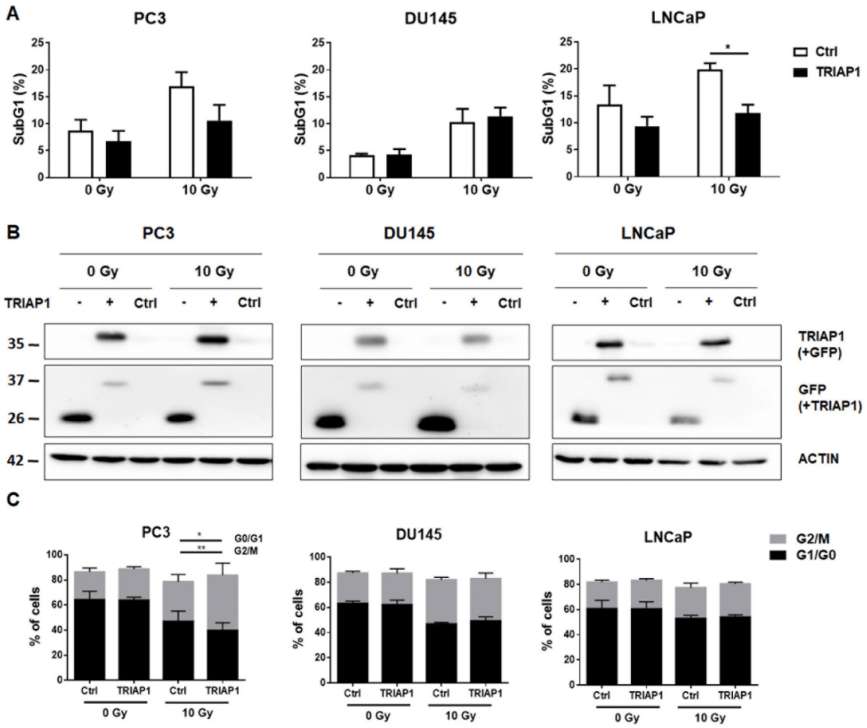

Figure 2. Ectopic TRIAP1 expression in prostate carcinoma cells results in radiation resistance.

(C) Cell cycle analysis of TRIAP1-GFP transfected prostate cancer cell lines was performed using Nicoletti/PI staining and flow cytometry. Empty vector transfected cells served as control. Data represent mean values ± SEM from 3–5 independent samples per group measured in duplicates each. ** $p \leq 0.01$, by two-way ANOVA followed by post-hoc Tukey's test.

3.3. Generation of Stromal Prostate Fibroblasts with Stable TRIAP1 Expression

Prior to investigating whether TRIAP1 derived from a reactive tumour stroma might account for the radiation resistance observed in PC3 xenografts *in vivo* [11], we assessed the suitability of another fibroblast cell type, prostate fibroblasts (WPMY-1) derived from healthy donors, to more closely mimic the human situation in future *in vivo* experiments (Figure 3).

Compared to normal HS5 fibroblasts, WPMY-1 prostate fibroblasts expressed less endogenous CAV1-expression levels (Figure 3A). Quantitative Real Time RT-PCR analysis of TRIAP1 expression levels as well as of reactive fibroblasts markers (ACTA2 and TAGLN) and tumour-promoting EMT factor transforming growth factor β (TGFB1) in WPMY-1 fibroblasts (+/− XRT) confirmed the more reactive phenotype of WPMY-1 with a less pronounced CAV1-content and furthermore of irradiated WPMY-1 fibroblasts (Figure 3B). In line with previous findings [11], colony formation assays indicated that WPMY-1 fibroblasts with a reduced CAV1 content were more resistant to radiation (Figure 3C). To further investigate a potential TRIAP1-mediated radiation resistance of prostate carcinoma cells caused by the stromal compartment, we generated TRIAP1-overexpressing WPMY-1 fibroblasts via transfection of WPMY-1 with an expression vector encoding for human TRIAP1 tagged with GFP (Figure 3D). Stably transfected and TRIAP1-GFP-sorted cells (via flow cytometry) were successfully generated. Increased TRIAP1 expression was confirmed by western blot analysis. It is worth noting that TRIAP1-overexpression did not alter CAV1 expression levels (Figure 3D). Ectopic TRIAP1 expression resulted in a significant reduced subG1 population upon radiation, which confirmed the

resistant phenotype of TRIAP1-GFP expressing prostate fibroblasts (Figure 3E). TRIAP1 secretion from TRIAP1-GFP-expressing cells was confirmed by western blot analysis from cell culture supernatants and revealed an increased secretion upon radiation (Figure 3F).

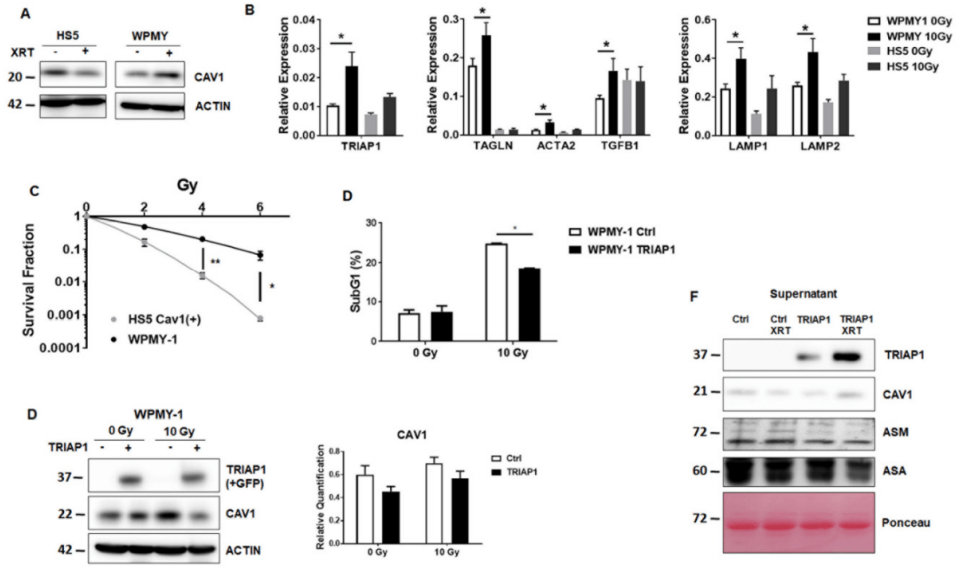

Figure 3. Characterization of the human prostate fibroblast cell line WPMY-1.

(A) CAV1 expression levels analysed by western blot in normal HS5 and prostate WPMY-1 fibroblasts, with or without radiation treatment with 10 Gy (96 h post irradiation). β-actin was included as loading control. Representative blots of at least three different experiments are shown.

(B) qRT-PCR quantifications of TRIAP1 mRNA levels, as well as reactive fibroblast markers, were performed 96 h post irradiation and shown as relative expression to β-actin mRNA. Data shown represent mean values ± SEM from 4-6 independent samples per group measured in duplicate each. * $p \leq 0.05$, ** $p \leq 0.01$, by two-way ANOVA followed by post-hoc Tukey's test.

(C) Colony formation assay of HS5 and WPMY-1 cells. Following irradiation (0–8 Gy) cells were further incubated for 10 days. Data show the surviving fractions from three independent experiments measured in triplicates each (means ± SD). *** $p \leq 0.005$, **** $p \leq 0.001$ by two-tailed students *t*-test.

(D) The degree of apoptosis was quantified measuring the SubG1 fraction 48 h after radiation by flow cytometry. Data shown indicate mean values ± SEM from 3 independent samples per group measured in duplicates each. * $p \leq 0.05$, by two-way ANOVA followed by post-hoc Tukey's test.

(E) WPMY-1 prostate fibroblasts were transfected with a TRIAP1-GFP encoding plasmid or empty vector in the control, selected with G418 and sorted via flow cytometry to select GFP-expressing cells. Expression levels of TRIAP1-GFP and CAV1 were confirmed by western blot analyses, with or without 10 Gy irradiations. Band signal intensity was quantified by densitometry and normalized to that from β-actin. Data represent mean ± SEM from three independent experiments. *p*-values were indicated: ** $p < 0.01$; *** $p \leq 0.005$ by two-way ANOVA followed by post-hoc Tukey's test.

(F) TRIAP1-GFP secretion in cell culture supernatants derived from TRIAP1-GFP or control, transfected WPMY-1 fibroblasts with or without radiation treatment (10 Gy) determined by western blot analysis. CAV1, ASM and ASA secretion levels were also investigated. Equal protein amounts (100 μg) were loaded. Ponceau S staining of transferred proteins was included as loading control.

3.4. TRIAP1-Expressing Stromal Fibroblasts Mediate Radiation Resistance

Next, we asked whether fibroblastic tumour stroma-derived TRIAP1 accounts for an increased radiation resistance in PC3 xenograft tumours [11]. To mimic the human situation we performed subcutaneous transplantations onto the hind limb of NMRI nude mice by injecting CAV1-silenced PC3(-) tumour cells in combination with control-transfected or TRIAP1-GFP-expressing WPMY-1 prostate fibroblasts (Figure 4). Prostate xenografts were implanted onto the hind limb of NMRI nude mice and were irradiated locally with a single dose of 10 Gy when the tumour reached a size of about 100 mm3 (around day 3). Tumour growth was determined by measuring the tumour volume 3 times a week (Figure 4A). Either co-implantation with WPMY-1 cells, control or TRIAP1-transfected, did not change tumour growth. The tumour growth delay after radiation was significantly decreased in PC3(-)-derived tumours co-implanted with TRIAP1-expressing WPMY-1. These tumours showed a significantly increased growth after radiation treatment when compared to PC3(-)-derived tumours co-implanted with control-transfected WPMY-1 as demonstrated by the reduced time to reach a four-fold tumour volume (Figure 2B). Immunohistochemistry using the proliferation marker PCNA (proliferating cell nuclear antigen) antibody further confirmed an increase in the proliferation rate of PC3(-) xenografts when co-implanted with TRIAP1-GFP expressing fibroblasts and a significantly decreased sensitivity to radiation treatment (Figure 4C). Thus, in line with the *in vitro* results, TRIAP1 derived from stromal fibroblasts is able to induce radiation resistance of prostate tumours.

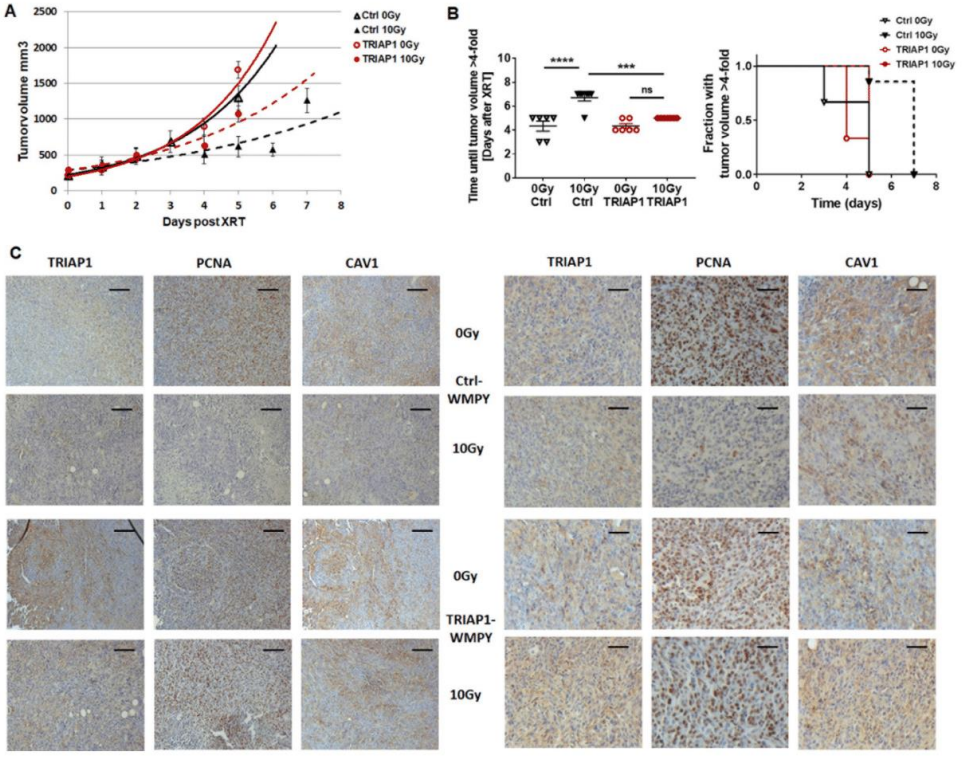

Figure 4. TRIAP1 expression in fibroblasts fosters radiation resistance in tumours derived from PC3 CAV1(-) cells.

(A) PC3 CAV1(-) cells were subcutaneously injected with either TRIAP1-expressing WPMY-1 or control-transfected fibroblasts (0.5×10^6 cells in total, ratio1/1) into the hind limb of NMRI nude mice. One set of animals from each group received a single tumour radiation dose of 10 Gy once its growth

was easily detected (around day 3). Tumour volume was determined at indicated time points using a sliding calliper. Data are presented as mean +/− SEM from 3 independent experiments (26 mice in total: Ctrl 0 Gy n = 6; Ctrl 10 Gy n = 7; TRIAP1 0 Gy n = 6; TRIAP1 10 Gy n = 7).

(B) Tumour growth (*left panel*) and respective computed median growth delay (*right panel*) were determined as time (days) until a four-fold tumour volume was reached. *** $p < 0.005$; **** $p < 0.001$ by one-way ANOVA followed by post-hoc Tukey's test.

(C) Immunohistochemical analysis of TRIAP1, PCNA and CAV1 in isolated PC3 xenograft tumours. Sections were counterstained using haematoxylin. Representative images are shown. Magnification 200×, scale bar 50 µm (left panel), magnification 400×, scale bar 20 µm (right panel).

3.5. Human Advanced Prostate Cancer Specimens Were Characterized by an Increased TRIAP1-Immunoreactivity Indicating Radiation Resistance

As loss of stromal CAV1 is paralleled by a radiation-resistance promoting reactive tumour stroma in human prostate tissue specimens [11,21], we decided to investigate TRIAP1 expression levels, as well as the respective stromal-epithelial TRIAP1 distribution, in human prostate tissue specimens by immunohistochemistry. TRIAP1 expression in prostate epithelial cells increased with higher Gleason scores, that is, lower tumour differentiation (Figure 5). Furthermore, stromal cells of tumour samples tended to be more intensively stained in cases with higher Gleason grade (Figure 5). These results indicate that increased, potentially fibroblast-derived, TRIAP1 has implications for prostate carcinoma progression and therapy resistance.

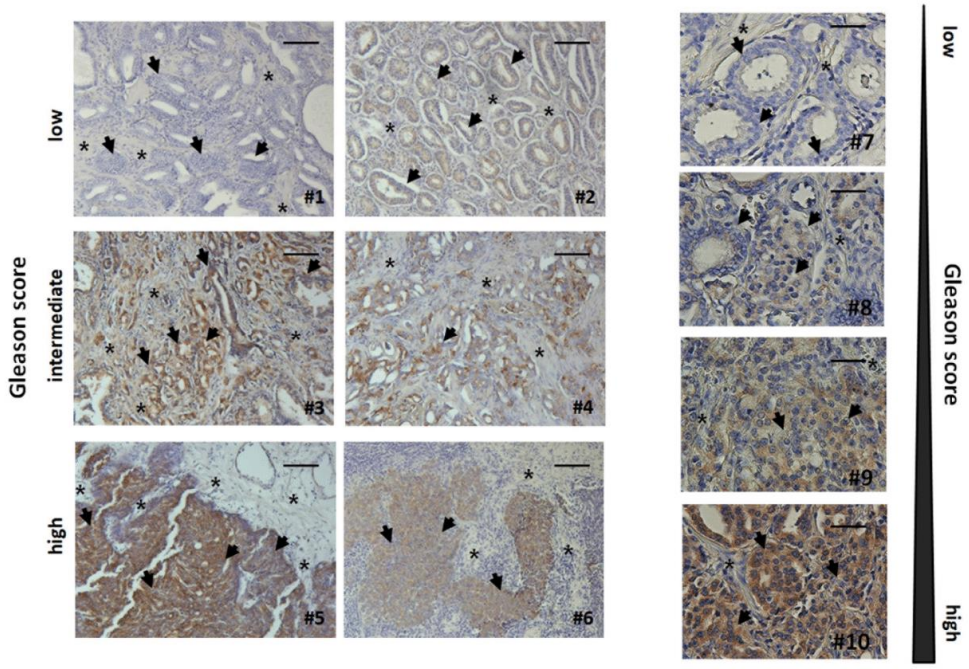

Figure 5. Immunohistochemical analysis of TRIAP1 expression levels in human prostate cancer tissues.

Paraffin-sections of human prostate cancers were stained for TRIAP1. Gleason grading scores were divided into low (Gleason Score ≥ 6, Grade group 1), intermediate (Gleason Score 7 (a/b), Grade groups 2 & 3) and high scores (Gleason Score ≥ 8, Grade groups 4 & 5). Asterisks mark stromal compartments and bold arrows point to epithelial structures. Sections were counterstained

using haematoxylin. Representative images are shown. Magnification 200x. Right panel: higher magnification images: 400x.

4. Discussion

Tumours are able to diversify their microenvironment and consequently the altered, more reactive tumour microenvironment can modulate the response of tumours to therapy treatment [24–28]. Herein, activated stromal cells and in particular activated fibroblasts/CAF can mediate therapy resistance of malignant epithelial cells in a CAV1-dependent fashion [4,5,29,30].

CAV1-dependent stromal-epithelial crosstalk in tumours with the potential to induce resistance includes processes such as autophagy or the 'reverse Warburg effect' [31,32]. For example, a more reactive stromal phenotype following a decrease of CAV1 expression by lysosomal degradation in fibroblasts was observed when cancer cells induced oxidative stress in the tumour-microenvironment [33]. In turn, downregulation of CAV1 in fibroblasts leads to increased oxidative metabolism in cancer cells, fostering cell resistance [29]. Importantly, extrinsic factors from the microenvironment and in particular from activated fibroblasts/CAF, may drive resistance in a non-tumour cell autonomous mechanism [34,35]. In line with these findings, we have recently shown that CAV1-deficient fibroblasts mediate radiation resistance of human prostate carcinoma cells *in vitro* and *in vivo* and that the decrease in cell death after radiation treatment is mediated though a paracrine mechanism of action [11]. However, the exact resistance-promoting effectors, as well as the role of CAV1-dependent fibroblast-derived factors, remained elusive. We therefore hypothesized that fibroblast-derived inhibitors of apoptosis proteins could mediate cell death resistance upon radiation. Here we show that TRIAP1 is highly expressed in stromal fibroblasts in a CAV1-dependent manner. *In vitro*, an ectopic expression of TRIAP1 leads to a cell specific increased radiation resistance in p53-deficient PC3 and p53-wildtype LNCaP prostate cancer cells, whereas p53-mutant DU145 cells do not gain any radiation resistance. Conformingly and mimicking the human situation more precisely, induced over-expression of TRIAP1 in human prostate fibroblasts leads to induced radiation resistance. Further on, TRIAP1-expressing stromal fibroblasts mediate radiation resistance *in vivo* when respective cells are co-implanted with CAV1-deficient PC3 tumour cells.

The underlying mechanism by which fibroblast-derived TRIAP1 is secreted and subsequently taken up by adjacent cancer cells and/or shuttled between the stromal and the tumour cells needs to be investigated further. TRIAP1 secretion in fibroblasts with a reduced CAV1-content is paralleled by the presence of lysosomal exocytosis related proteins and enzymes, such as ASM, ASA and LAMP proteins. This indicates that fibroblasts with a reduced CAV1 content bear a higher lysosomal exocytosis activity compared to fibroblasts containing normally high amounts of CAV1. It is known that the process and regulation of lysosomal exocytosis is largely changed upon tumour progression and in transformed cells [36]. Released lysosomal hydrolases, such as cathepsins D and B, play a role in tumour growth invasion and angiogenesis [37]. LAMP2 contributes to resistance, as the so called lysosomal cell death induced by anti-cancer drugs is decreased when LAMP2 is overexpressed in fibroblasts [38]. In addition, ASM is down-regulated in several carcinomas, for example, head and neck cancer and gastrointestinal carcinoma cancer cells, leading to a destabilized lysosomal environment in combination with an anti-apoptotic adaptation by decreased ceramide production [36]. Lysosomal exocytosis in cancer cells has been suggested to facilitate the entrapment and clearance of chemotherapeutics and provide an additional line of resistance [39].

As intrinsic drug resistance might be caused, at least in part, by factors secreted by the tumour microenvironment, it is thus imperative to dissect the tumour-microenvironment interactions which may reveal important mechanisms underlying drug resistance [35,39].

Interestingly, immunohistological analysis of TRIAP1 in advanced human prostate cancer reveals increased TRIAP1 immunoreactivity in the malignant epithelial cells of the more radioresistant higher Gleason grade adenocarcinomas. This highlights fibroblast-derived TRIAP1 as a potential candidate for future CAV1-mediated radiation response modulation. TRIAP1 is also involved in prostate cancer

bone metastasis [40] and sensitivity to doxorubicin in breast cancer cells [15]. In ovarian cancer cells, increased TRIAP1 levels correlate with increased proliferation, a decrease in apoptosis and overall tumour progression [41]. TRIAP1 is also found to be upregulated in multiple myeloma [42], and, in patients with nasopharyngeal carcinoma, TRIAP1 overexpression correlates with a poor survival rate [43]. Experimental knockdown of TRIAP1, by expression of micro RNA miR-320b, is able to induce apoptosis by mitochondrial deregulating mechanisms, such as cytochrome C release and membrane potential alterations [15,43].

In summary, we have specified the role of CAV1 alterations potentially induced by CAV1-deficient and more reactive, stroma in radio sensitivity of prostate carcinoma at molecular level. We have identified apoptosis inhibitor TRIAP1 as a stromal-derived factor with the potential to induce cancer cell resistance. We suggest that blocking TRIAP1 activity and avoiding drug resistance may offer a promising drug development strategy to inhibit resistance-promoting CAV1-dependent signals.

Author Contributions: J.K., A.P., A.W. and D.K. performed experiments; J.K., D.K. analysed results and made the figures; C.H., P.M., E.Y. and H.R. provided materials; H.R. performed the Gleasing scoring; D.K. and V.J. designed research, J.K. and D.K. wrote the paper and E.Y. performed language corrections. All authors reviewed and approved the manuscript. This work was supported by grants of the DFG (GRK1739/1; GRK1739/2) and the BMBF (02NUK024-D).

Acknowledgments: We thank Mohammed Benchellal and Eva Gau for their excellent technical assistance. We acknowledge support by the Open Access Publication Fund of the University of Duisburg-Essen.

Conflicts of Interest: The authors state that there are no personal or institutional conflict of interest.

References

1. Bissell, M.J. Thinking in three dimensions: Discovering reciprocal signaling between the extracellular matrix and nucleus and the wisdom of microenvironment and tissue architecture. *Mol. Biol. Cell* **2016**, *27*, 3205–3209. [CrossRef] [PubMed]
2. Bissell, M.J.; Hines, W.C. Why don't we get more cancer? A proposed role of the microenvironment in restraining cancer progression. *Nat. Med.* **2011**, *17*, 320–329. [CrossRef] [PubMed]
3. Hanahan, D.; Weinberg, R.A. Hallmarks of cancer: The next generation. *Cell* **2011**, *144*, 646–674. [CrossRef] [PubMed]
4. Chen, D.; Che, G. Value of caveolin-1 in cancer progression and prognosis: Emphasis on cancer-associated fibroblasts, human cancer cells and mechanism of caveolin-1 expression (Review). *Oncol. Lett.* **2014**, *8*, 1409–1421. [CrossRef]
5. Ketteler, J.; Klein, D. Caveolin-1, cancer and therapy resistance. *Int. J. Cancer* **2018**. [CrossRef]
6. Di Vizio, D.; Morello, M.; Sotgia, F.; Pestell, R.G.; Freeman, M.R.; Lisanti, M.P. An absence of stromal caveolin-1 is associated with advanced prostate cancer, metastatic disease and epithelial Akt activation. *Cell Cycle* **2009**, *8*, 2420–2424. [CrossRef]
7. Witkiewicz, A.K.; Dasgupta, A.; Sotgia, F.; Mercier, I.; Pestell, R.G.; Sabel, M.; Kleer, C.G.; Brody, J.R.; Lisanti, M.P. An absence of stromal caveolin-1 expression predicts early tumor recurrence and poor clinical outcome in human breast cancers. *Am. J. Pathol.* **2009**, *174*, 2023–2034. [CrossRef]
8. Ayala, G.; Morello, M.; Frolov, A.; You, S.; Li, R.; Rosati, F.; Bartolucci, G.; Danza, G.; Adam, R.M.; Thompson, T.C.; et al. Loss of caveolin-1 in prostate cancer stroma correlates with reduced relapse-free survival and is functionally relevant to tumour progression. *J. Pathol.* **2013**, *231*, 77–87. [CrossRef]
9. Eliyatkin, N.; Aktas, S.; Diniz, G.; Ozgur, H.H.; Ekin, Z.Y.; Kupelioglu, A. Expression of Stromal Caveolin- 1 May Be a Predictor for Aggressive Behaviour of Breast Cancer. *Pathol. Oncol. Res.* **2018**, *24*, 59–65. [CrossRef]
10. Shan-Wei, W.; Kan-Lun, X.; Shu-Qin, R.; Li-Li, Z.; Li-Rong, C. Overexpression of caveolin-1 in cancer-associated fibroblasts predicts good outcome in breast cancer. *Breast Care* **2012**, *7*, 477–483. [CrossRef]
11. Panic, A.; Ketteler, J.; Reis, H.; Sak, A.; Herskind, C.; Maier, P.; Rubben, H.; Jendrossek, V.; Klein, D. Progression-related loss of stromal Caveolin 1 levels fosters the growth of human PC3 xenografts and mediates radiation resistance. *Sci. Rep.* **2017**, *7*, 41138. [CrossRef] [PubMed]

12. Hammarsten, P.; Dahl Scherdin, T.; Hagglof, C.; Andersson, P.; Wikstrom, P.; Stattin, P.; Egevad, L.; Granfors, T.; Bergh, A. High Caveolin-1 Expression in Tumor Stroma Is Associated with a Favourable Outcome in Prostate Cancer Patients Managed by Watchful Waiting. *PLoS ONE* **2016**, *11*, e0164016. [CrossRef]
13. Antognelli, C.; Ferri, I.; Bellezza, G.; Siccu, P.; Love, H.D.; Talesa, V.N.; Sidoni, A. Glyoxalase 2 drives tumorigenesis in human prostate cells in a mechanism involving androgen receptor and p53-p21 axis. *Mol. Carcinog.* **2017**, *56*, 2112–2126. [CrossRef]
14. Cotter, T.G. Apoptosis and cancer: The genesis of a research field. *Nat. Rev. Cancer* **2009**, *9*, 501–507. [CrossRef] [PubMed]
15. Adams, C.; Cazzanelli, G.; Rasul, S.; Hitchinson, B.; Hu, Y.; Coombes, R.C.; Raguz, S.; Yague, E. Apoptosis inhibitor TRIAP1 is a novel effector of drug resistance. *Oncol. Rep.* **2015**, *34*, 415–422. [CrossRef] [PubMed]
16. Park, W.R.; Nakamura, Y. p53CSV, a novel p53-inducible gene involved in the p53-dependent cell-survival pathway. *Cancer Res.* **2005**, *65*, 1197–1206. [CrossRef] [PubMed]
17. Andrysik, Z.; Kim, J.; Tan, A.C.; Espinosa, J.M. A genetic screen identifies TCF3/E2A and TRIAP1 as pathway-specific regulators of the cellular response to p53 activation. *Cell Rep.* **2013**, *3*, 1346–1354. [CrossRef]
18. Klein, D.; Schmandt, T.; Muth-Kohne, E.; Perez-Bouza, A.; Segschneider, M.; Gieselmann, V.; Brustle, O. Embryonic stem cell-based reduction of central nervous system sulfatide storage in an animal model of metachromatic leukodystrophy. *Gene Ther.* **2006**, *13*, 1686–1695. [CrossRef]
19. Lansmann, S.; Ferlinz, K.; Hurwitz, R.; Bartelsen, O.; Glombitza, G.; Sandhoff, K. Purification of acid sphingomyelinase from human placenta: Characterization and N-terminal sequence. *FEBS Lett.* **1996**, *399*, 227–231. [CrossRef]
20. Barzan, D.; Maier, P.; Zeller, W.J.; Wenz, F.; Herskind, C. Overexpression of caveolin-1 in lymphoblastoid TK6 cells enhances proliferation after irradiation with clinically relevant doses. *Strahlenther. Onkol.* **2010**, *186*, 99–106. [CrossRef]
21. Klein, D.; Schmitz, T.; Verhelst, V.; Panic, A.; Schenck, M.; Reis, H.; Drab, M.; Sak, A.; Herskind, C.; Maier, P.; et al. Endothelial Caveolin-1 regulates the radiation response of epithelial prostate tumors. *Oncogenesis* **2015**, *4*, e148. [CrossRef] [PubMed]
22. Klein, D.; Steens, J.; Wiesemann, A.; Schulz, F.C.; Kaschani, F.; Roeck, K.; Yamaguchi, M.; Wirsdorfer, F.; Kaiser, M.; Fischer, J.; et al. Mesenchymal stem cell therapy protects lungs from radiation-induced endothelial cell loss by restoring superoxide dismutase 1 expression. *Antioxid. Redox Signal.* **2016**. [CrossRef] [PubMed]
23. Koressaar, T.; Remm, M. Enhancements and modifications of primer design program Primer3. *Bioinformatics* **2007**, *23*, 1289–1291. [CrossRef]
24. Singh, S.R.; Rameshwar, P.; Siegel, P. Targeting tumor microenvironment in cancer therapy. *Cancer Lett.* **2016**. [CrossRef]
25. Sun, Y. Tumor microenvironment and cancer therapy resistance. *Cancer Lett.* **2015**. [CrossRef] [PubMed]
26. Cheng, C.J.; Bahal, R.; Babar, I.A.; Pincus, Z.; Barrera, F.; Liu, C.; Svoronos, A.; Braddock, D.T.; Glazer, P.M.; Engelman, D.M.; et al. MicroRNA silencing for cancer therapy targeted to the tumour microenvironment. *Nature* **2015**, *518*, 107–110. [CrossRef] [PubMed]
27. Masuda, S.; Izpisua Belmonte, J.C. The microenvironment and resistance to personalized cancer therapy. *Nat. Rev. Clin. Oncol.* **2013**, *10*. [CrossRef]
28. Swartz, M.A.; Iida, N.; Roberts, E.W.; Sangaletti, S.; Wong, M.H.; Yull, F.E.; Coussens, L.M.; DeClerck, Y.A. Tumor microenvironment complexity: Emerging roles in cancer therapy. *Cancer Res.* **2012**, *72*, 2473–2480. [CrossRef]
29. Wang, S.; Wang, N.; Zheng, Y.; Zhang, J.; Zhang, F.; Wang, Z. Caveolin-1: An Oxidative Stress-Related Target for Cancer Prevention. *Oxidative Med. Cell. Longev.* **2017**, *2017*, 7454031. [CrossRef]
30. Kamposioras, K.; Tsimplouli, C.; Verbeke, C.; Anthoney, A.; Daoukopoulou, A.; Papandreou, C.N.; Sakellaridis, N.; Vassilopoulos, G.; Potamianos, S.P.; Liakouli, V.; et al. Silencing of caveolin-1 in fibroblasts as opposed to epithelial tumor cells results in increased tumor growth rate and chemoresistance in a human pancreatic cancer model. *Int. J. Oncol.* **2018**. [CrossRef]
31. Martinez-Outschoorn, U.E.; Balliet, R.M.; Rivadeneira, D.B.; Chiavarina, B.; Pavlides, S.; Wang, C.; Whitaker-Menezes, D.; Daumer, K.M.; Lin, Z.; Witkiewicz, A.K.; et al. Oxidative stress in cancer associated fibroblasts drives tumor-stroma co-evolution: A new paradigm for understanding tumor metabolism, the field effect and genomic instability in cancer cells. *Cell Cycle* **2010**, *9*, 3256–3276. [CrossRef] [PubMed]
32. White, E. The role for autophagy in cancer. *J. Clin. Investig.* **2015**, *125*, 42–46. [CrossRef] [PubMed]

33. Martinez-Outschoorn, U.E.; Pavlides, S.; Whitaker-Menezes, D.; Daumer, K.M.; Milliman, J.N.; Chiavarina, B.; Migneco, G.; Witkiewicz, A.K.; Martinez-Cantarin, M.P.; Flomenberg, N.; et al. Tumor cells induce the cancer associated fibroblast phenotype via caveolin-1 degradation: Implications for breast cancer and DCIS therapy with autophagy inhibitors. *Cell Cycle* **2010**, *9*, 2423–2433. [CrossRef]
34. Hirata, E.; Girotti, M.R.; Viros, A.; Hooper, S.; Spencer-Dene, B.; Matsuda, M.; Larkin, J.; Marais, R.; Sahai, E. Intravital imaging reveals how BRAF inhibition generates drug-tolerant microenvironments with high integrin beta1/FAK signaling. *Cancer Cell* **2015**, *27*, 574–588. [CrossRef]
35. Straussman, R.; Morikawa, T.; Shee, K.; Barzily-Rokni, M.; Qian, Z.R.; Du, J.; Davis, A.; Mongare, M.M.; Gould, J.; Frederick, D.T.; et al. Tumour micro-environment elicits innate resistance to RAF inhibitors through HGF secretion. *Nature* **2012**, *487*, 500–504. [CrossRef] [PubMed]
36. Kallunki, T.; Olsen, O.D.; Jaattela, M. Cancer-associated lysosomal changes: Friends or foes? *Oncogene* **2013**, *32*, 1995–2004. [CrossRef]
37. Gocheva, V.; Zeng, W.; Ke, D.; Klimstra, D.; Reinheckel, T.; Peters, C.; Hanahan, D.; Joyce, J.A. Distinct roles for cysteine cathepsin genes in multistage tumorigenesis. *Genes Dev.* **2006**, *20*, 543–556. [CrossRef]
38. Fehrenbacher, N.; Bastholm, L.; Kirkegaard-Sorensen, T.; Rafn, B.; Bottzauw, T.; Nielsen, C.; Weber, E.; Shirasawa, S.; Kallunki, T.; Jaattela, M. Sensitization to the lysosomal cell death pathway by oncogene-induced down-regulation of lysosome-associated membrane proteins 1 and 2. *Cancer Res.* **2008**, *68*, 6623–6633. [CrossRef]
39. Zhitomirsky, B.; Assaraf, Y.G. Lysosomes as mediators of drug resistance in cancer. *Drug Resist. Updates Rev. Comment. Antimicrob. Anticancer Chemother.* **2016**, *24*, 23–33. [CrossRef]
40. Siu, M.K.; Abou-Kheir, W.; Yin, J.J.; Chang, Y.S.; Barrett, B.; Suau, F.; Casey, O.; Chen, W.Y.; Fang, L.; Hynes, P.; et al. Correction: Loss of EGFR signaling-regulated miR-203 promotes prostate cancer bone metastasis and tyrosine kinase inhibitors resistance. *Oncotarget* **2018**, *9*, 32403. [CrossRef]
41. Liu, P.; Qi, X.; Bian, C.; Yang, F.; Lin, X.; Zhou, S.; Xie, C.; Zhao, X.; Yi, T. MicroRNA-18a inhibits ovarian cancer growth via directly targeting TRIAP1 and IPMK. *Oncol. Lett.* **2017**, *13*, 4039–4046. [CrossRef] [PubMed]
42. Fook-Alves, V.L.; de Oliveira, M.B.; Zanatta, D.B.; Strauss, B.E.; Colleoni, G.W. TP53 Regulated Inhibitor of Apoptosis 1 (TRIAP1) stable silencing increases late apoptosis by upregulation of caspase 9 and APAF1 in RPMI8226 multiple myeloma cell line. *Biochim. Biophys. Acta* **2016**, *1862*, 1105–1110. [CrossRef] [PubMed]
43. Li, Y.; Tang, X.; He, Q.; Yang, X.; Ren, X.; Wen, X.; Zhang, J.; Wang, Y.; Liu, N.; Ma, J. Overexpression of Mitochondria Mediator Gene TRIAP1 by miR-320b Loss Is Associated with Progression in Nasopharyngeal Carcinoma. *PLoS Genet.* **2016**, *12*, e1006183. [CrossRef] [PubMed]

5.5 Caveolin 1 Dependency of the Acid Sphingomyelinase/Ceramide-mediated Radiation-response of Endothelial Cells in the Context of Tumor-stroma-interactions.

Cumulative thesis of Ms Julia Ketteler

Author contributions

Title of publication: Caveolin 1 Dependency of the Acid Sphingomyelinase/Ceramide-mediated Radiation-response of Endothelial Cells in the Context of Tumor-stroma-interactions

Authors: Ketteler J, Leonetti D, Veas Roy V, Wittka A, Estephan H, Maier P, Herskind C, Jendrossek V, Paris F, Klein D

Manuscript in preparation/close to submission

Contributions:

- Conception - 40 %: planning experiments, proposing hypothesis
- Experimental work – 90 %: Figures 1, 2, 3, 4, 5, S1, S2, S3 with technical support of DL (Figure 1, 5) and VVR (Figure 4 a, b, c, Supplementary Figure S1 a)
- Data analysis - 90 %: Figures 1, 2, 3, 4, 5, S1, S2, S3
- species identification: not applicable
- Statistical analysis - 100 %: Figures 1, 2, 3, 4, 5, S1, S2, S3
- Writing the manuscript – 50 %: writing first draft of the manuscript (all sections)
- Revising the manuscript: not applicable

Unterschrift Doktorand/in

Unterschrift Betreuer/in

Caveolin 1 dependency of the acid sphingomyelinase/ceramide-mediated radiation-response of endothelial cells in the context of tumor-stroma-interactions

Ketteler J[1], Leonetti D[2], Veas Roy V[1], Estephan H[2], Wittka A[1], Maier P[3], Henning Reis[4], Herskind C[3], Jendrossek V[1], Paris F[2], Klein D[1].

[1]Institute of Cell Biology (Cancer Research), University of Duisburg-Essen, University Hospital, Virchowstrasse 173, 45122 Essen, Germany.

[2]CRCINA, INSERM, CNRS, Université de Nantes, Nantes, France

[3]Department of Radiation Oncology, University Medical Center Mannheim, Medical Faculty Mannheim, Heidelberg University, Theodor-Kutzer-Ufer 1-3, 68167 Mannheim, Germany

[4]Institut of Pathology, University of Duisburg-Essen, University Hospital, Hufelandstr. 55, 45122 Essen, Essen, Germany.

Correspondence to

PD Dr. Diana Klein

Institute of Cell Biology (Cancer Research)

Medical Faculty

University of Duisburg-Essen

Virchowstr. 173

Ger-45122 Essen

Tel:+49-201-723 83342

Fax:+49-201-723 5904

E-mail: Diana.Klein@uk-essen.de

Abstract

Resistance to cancer therapy remains one of the biggest obstacles in cancer treatment. Herein the tumor microenvironment became a leading player, not just a supporting tumor compartment. In particular, endothelial cells (EC) evolved as critical determinants in tumor therapy response, especially in the context of radiation therapy (RT). The aim of the present study was to investigate how the acid sphingomyelinase (ASMase)/ceramide pathway, as an important key player in EC apoptosis upon ionizing radiation (IR) treatment, could be linked to a differential expression of the integral membrane protein Caveolin-1 (CAV1). CAV1 is known to be involved in the radio-resistance mediating tumor-stroma interactions of advanced prostate cancer. Using either CAV1-deficient or -proficient EC we show here that CAV1-deficiency accounting for increased apoptosis rates of these cells upon RT, results in an increased ASMase activity, ceramide generation and formation of large lipid platforms, finally influencing p38 MAPK signaling upon treatment with IR. In addition, the *de novo* synthesis of long and very long-chain ceramides was influenced by a differential CAV1 expression. CAV1 deficiency resulted in increased expressions of ceramide synthases (CerS) CerS5 and CerS6 that foster the generation of pro-apoptotic C16 ceramide. Using 3D co-cultures of prostate cancer cells LNCaP or PC3 in combination with CAV1-deficient or –proficient EC resulted in increased growth delays after IR when CAV1-deficient EC were co-cultured. Analysis of CAV1-proficient and -deficient PC3 prostate carcinoma cells in contrast revealed a general increased generation of C16, C24 and C24:1in the radio-resistant CAV1(+) PC3 variant, which was already associated with metastasis and therapy resistance and thus a worse clinical outcome. Increased ASMase and ceramide levels were further confirmed in advanced and therapy resistant human prostate cancer specimen. Conclusively, we show here that CAV1 expression critically regulates the generation of ceramide-dependent (re-)organization of the plasma membrane that in turn affects the radiation response of endothelial and prostate cancer cells. Thus, stromal EC-derived C16 ceramide-mediated apoptosis could be used as a potential target to scavenge radiation resistance in prostate cancer.

Keywords

Endothelium, tumor stroma, microenvironment, radiotherapy, therapy resistance, prostate cancer, caveolin-1, ceramide, acid sphingomyelinase

Introduction

Radiotherapy (RT) in cancer treatment perturbs the homeostatic interactions of organs and tissues, linking tumor cells with stromal cells and normal tissue cells (epithelial cells, fibroblasts, vascular cells) with the extracellular matrix and infiltrating immune cells (Almeida et al., 2013; Ghafoori et al., 2008; Rube et al., 2005). Among these cell types, the endothelial cells (EC) have been shown to be critical determinants of the radiation response of tumors and normal tissues (Corre et al., 2013; Klein, 2018; Klein et al., 2015; Paris et al., 2001; Wiesemann et al., 2019). Acute vascular damage resulting in vascular dysfunction associated with edema, increased immune cell extravasation and metastasis, as well as EC apoptosis upon RT contribute to those radiation responses (Klein, 2018; Korpela and Liu, 2014; Lafargue et al., 2017). Indeed, microvascular EC of small vessels and microvessels, including newly-formed angiogenic blood vessels turned out to be particularly sensitive to ionizing radiation (IR) (Fajardo, 2005; Garcia-Barros et al., 2003; Lafargue et al., 2017; Wiesemann et al., 2019; Zeng et al., 2008).

Mechanistically, it was shown, that the p38 MAPK signaling pathway is essential in the endothelial cellular response to stress stimuli, including IR (Corre et al., 2017). Activation of the p38 MAPK pathway by RT was shown to result in endothelial barrier dysfunction (Li et al., 2015). Likewise, VEGF-induced VEGFR2-dependent p38 phosphorylation fostered EC migration as well as tube formation (pro-angiogenic phenotype) (Gee et al., 2010; Wiesemann et al., 2019). In contrast, RT-induced p38 activation in EC was shown to depress AKT levels resulting in apoptotic signaling. The RT-induced p38 MAPK pathway mediating EC apoptosis was further linked to acid sphingomyelinase (ASMase)/ ceramide signaling and plasma membrane reorganization (Niaudet et al., 2017). Mechanistically, radiation treatment induced a deep reorganization of the plasma membrane with the formation of large lipid platforms at the cell surface, accompanied by the activation of the enzyme ASMase and the generation of ceramide, finally resulting in the radiation-induced activation of p38 MAPK and apoptosis (Niaudet et al., 2017).

The integral membrane protein Caveolin-1 (CAV1) is heterogeneously expressed on various cell types, including adipocytes, fibroblasts, smooth muscle cells, pneumocytes, mammary epithelial cells and EC (Chidlow and Sessa, 2010; Sotgia et al., 2012; Xu et al., 2017). Herein, CAV1 is the major structural component of plasma membrane caveolae, non-planar specialized cholesterol and sphingolipids-enriched

microdomains (lipid rafts) with a size of 50-100 nm that form a vesicular invagination in the membrane and are involved in vesicular trafficking through endocytosis and cholesterol homeostasis (Glenney and Soppet, 1992; Karen G. Rothberg, 1992). In cancer therapy, CAV1 gained attraction because it was found that CAV1 expression levels highly increase in the malignant epithelial cells of many solid tumors in advanced tumor stages. These increased CAV1 levels correlated with tumor progression, invasion and metastasis, as well as therapy resistance (Chen and Che, 2014; Ketteler and Klein, 2018; Ketteler et al., 2019). In parallel, a loss of stromal CAV1 can be observed which is associated with a worse clinical outcome, e.g. in prostate and breast cancer patients (Ayala et al., 2013; Dolores Di Vizio, 2009; Karam et al., 2007; Witkiewicz et al., 2009), and therefore could be used as a prognostic marker. However, the vascular compartment was spared from those CAV1 alterations.
The association between CAV1 in EC and the response to RT was already established: Lowering CAV1 levels in tumor EC may be suited to improve the outcome of radiation therapy in prostate cancer, because a reduction of CAV1 levels increased the radiation-induced EC death and decreased survival of clonogenic endothelial cells *in vitro* and *in vivo* and thus had an impact on tumor growth delay after local irradiation (Klein et al., 2015). The CAV1-deficient blood vessels and respective EC were characterized by a less stabilized, proangiogenic phenotype that facilitates tumor growth (Dewever et al., 2007; Klein et al., 2015; Lin et al., 2007). Of note, these CAV1-deficient EC were more sensitive to RT in prostate tumors, which finally led to a more pronounced growth delay of tumors upon irradiation (Klein et al., 2015). Even in normal tissues, angiogenic EC were shown to be more apoptosis-prone, finally resulting in severe EC loss and increased tissue toxicity upon RT (Wiesemann et al., 2019).

The aim of the present study was to investigate how the CAV1-dependent radiation response of stromal EC can be linked to the signaling mediated by ceramide-enriched platforms that in turn lead to the activation of downstream signaling molecules launching the apoptotic process. Furthermore, it was investigated how those CAV1-dependent signaling pathways in EC affect the radiation response of adjacent prostate cancer cells. Understanding the crosstalk between tumor cells and the host-derived tumor microvasculature and thus, potentially targeting CAV1 in tumors, may offer a novel strategy for reducing cancer therapy resistance and improving clinical outcomes.

Results

Reduction of CAV1 levels in EC increased the ASMase activity resulting in ceramide generation and stabilization in a time-dependent manner upon IR

As EC with reduced CAV1 expression levels were more sensitive to IR and thus apoptosis-prone and EC apoptosis in turn is dependent on the early generation of ceramide, we investigated the activity of ASMase upon IR treatment in the EC line AS-M5 in combination with shRNA knock-down of CAV1 expression (Figure 1). Although total ASMase protein levels were detected in similar amounts in CAV1-proficient [CAV1(+)] and CAV1-deficient [CAV1(-)] AS-M5 EC, a significantly increased activity of the enzyme was detected in CAV1(-) EC (Figure 1A, B). Shortly after IR treatment, CAV1(+) EC showed a time-dependent significant increase in ASMase activities, whereas 30 min after IR treatment ASMase activity levels were decreasing to control levels (Figure 1B). In CAV1(-) EC, a continuous increase in ASMase activity upon irradiation was observed, which decreased less dramatically than activity levels in CAV1(+) EC (Figure 1B). The CAV1-dependent generation of ceramide via ASMase cleavage and quantification of the different ceramide species was analyzed using liquid chromatography in combination with mass spectrometry (Figure 1C-E). EC have been described to abundantly express ceramide species C16, C24 and C24:1, which was confirmed in both AS-M5 CAV1-variants (Figure 1C). Levels of respective ceramide species (C24 and C24:1) were significantly increased in CAV1-deficient EC In addition, similar C18 and C22 ceramide species were found in AS-M5 EC independent of the CAV1 expression levels. Following IR, a rapid accumulation of ceramide was observed (Figure 1D, E). At extremely short time points after IR (1-15 min) total ceramide levels (not shown) as well as levels of the prominent species C24 and C24:1 were promptly enhanced. Herein, ceramide generation reached a maximum 5 min after treatment. In CAV1(+) EC, these increased ceramide levels were reduced to control levels 30 min after IR (Figure 1D). In contrast, CAV1(-) cells steadily generated ceramide at longer time points measures (15 min and 30 min) (Figure 1E). Levels of the known apoptosis mediator C16 were changed in a similar fashion, although the alteration by IR was not significant (Figure 1D, E). Therefore, we hypothesized that CAV1-deficiency leads to a defective homeostasis of ceramide generation and subsequent reduction upon stress induction by IR. Beside the ceramide generation via hydrolysis of sphingomyelin by ASMase, ceramides were synthesized by a family of six mammalian ceramide synthases (CerS). Each CerS is known to produce a subset of ceramides that differ in their fatty acyl chain length, which in turn have distinct roles in inducing cell death and

survival. We therefore investigated expression levels of the six CerS in CAV1(+) and CAV1(-) EC using quantitative Real Time RT-PCR (Supplementary Figure S1). Expression levels of CerS2, CerS4, CerS5 and CerS6 were observed in both EC variants and further induced upon IR. While CerS5 and CerS6, which account for ceramides with fatty acyl chain length up to C16, were expressed in both cell types at similar levels, CAV1(+) EC showed increased basal expression levels of CerS2 and CerS4 (accounting for very long ceramides up to C22-C24) (Supplementary Figure S1). In line with previously shown results of increased apoptosis levels in CAV1(-) EC upon IR (Klein et al., 2015), CAV1-deficient EC showed increased ROS-levels after IR (not shown). These data strongly suggest that the CAV1-dependent levels of different ceramide species have an impact on cellular response of EC to IR, and that the elevated C16 ceramide levels together with increased C24 levels (resulting ratios in Supplementary Figure S1) in CAV1(-) EC account for increased radiosensitivity of those cells.

CAV1-deficiency increased the formation of plasma membrane lipid raft domains and associated p38 MAPK signaling upon IR

Next ceramide-induced plasma membrane remodeling was investigated by immunofluorescence (Figure 2). The lipid raft component glycosphingolipid GM1, as visualized with a fluorescent-tagged cholera toxin β subunit (purple), showed agglutination and polarization of GM1 from discrete structures to large membrane platforms in CAV1(+) EC cells 10 min after IR treatment (Figure 2A, B). In line with the previous findings, an augmented GM1 clustering and thus the presence of large lipid platforms could be observed in CAV1-deficient EC either with or without IR (Figure 2A, B). Around 70% of CAV1(-) AS-M5 EC already contained lipid platforms without IR, which was approximately the number of platforms/ signalosomes CAV1(+) EC could reach10-30 min after IR (Figure 2B). Next, we investigated if lipid platform formation co-localized with CAV1 expression in the CAV1-proficient EC (Figure 2C). CAV1 positive signal (red) was shown to be localized partly at the plasma membrane, but some expression could also be found in the cytoplasm. However, elevated GM1 staining was clearly present in around 40% of the cells without overlapping CAV1 staining. Conformingly, CAV1 was not localized to those lipid platforms, although the presence of CAV1 in the plasma membrane influenced their formation (Figure 2C). The ceramide-induced large platforms were further connected to p38 MAPK activation and apoptosis (Figure 3). Although p38 signaling was not affected by a differential

CAV1 content in the EC significantly, HSP27 levels were elevated in CAV1(-) AS-M5 independently of stress induction by irradiation (Figure 3). In line with the previously reported increased apoptosis levels in CAV1(-) EC upon IR, CAV1(-) EC showed here significantly reduced HSP27 levels upon IR, while the more radio-resistant CAV1-expressing EC show increased HSP27 levels upon IR (Figure 3). This discrepancy could point to a deregulated signaling in AS-M5 CAV1(-) cells which might be due to constantly expressed lipid platforms and altered activated signaling. No influence of CAV1 on the DNA damage and DNA damage response in EC upon IR was observed as revealed by similar phosphorylated γ-H2AX foci (markers of DNA double strand breaks) and respective kinetics (data not shown). Conclusively, these results indicated that ceramide-induced large lipid platforms resulting from radiation favor p38 MAPK activation as well as apoptotic cell death depending on CAV1.

CAV1-dependent ceramide generation was paralleled by an increased response to IR of prostate cancer cells directly co-cultured with EC

We next investigated, if and how radiation of EC with a differential CAV1 content affects the radiation response of adjacent prostate cancer cells. Therefore, EC were directly co-cultured (3D) with LNCaP and PC3 prostate cancer cells as spheroids embedded in growth-factor-reduced Matrigel and treated with IR (Figure 4A). The LNCaP cells in combination with AS-M5 CAV1(-) cells showed a tendency of accelerated growth in control conditions, which is in line with an increased proliferation capacity in a CAV1(-) background that had been previously described. However, radiation treatment induced a significant growth delay of the spheroids containing LNCaP cells and CAV1(-) EC. IR treatment of co-cultures of LNCaP with CAV1(+) EC resulted in no significant growth inhibition. An increased radiation response was determined for 3D-spheroids containing PC3 cells and CAV1(-) EC (Figure 4A). (will be added: spheroids with PC3 n=3 plus statistics) Interestingly, the direct contact between the EC and the tumor cells seems to be important, because cultivation of prostate cancer cell lines with conditioned medium collected from control or irradiated CAV1(+) and CAV1(-) AS-M5 EC was not sufficient to induce tumor cell death (subG1) or tumor cell cycle alterations 48 hours after treatment (Figure 4B) In addition, an attempt at inducing tumor cell apoptosis by exogenous ceramide treatment (C16) failed to induce apoptosis and cell cycle alterations in different prostate cancer cells (Figure 4C) (will be added: PC3 with C16 induction n=3).

As the chain length of biologically active ceramides serves as an important regulatory factor for inducing cell death or survival, we investigated (analogously to the EC analyzed above) the CAV1-dependent ceramide species in either CAV1-proficient [CAV1(+)] and CAV1-deficient [CAV1(-)] PC3 prostate cancer cells (Figure 5). C16, C22, C24 and C24:1 were expressed by the PC3 cells, whereas the C16, C24 and C24:1 ceramide species were significantly increased in the more radio-resistant CAV1-expressing PC3 prostate carcinoma cells (Figure 5A). The latter one accounts for an increased C24/C24:1 ratio in the radio-sensitive CAV1(-) PC3 (Figure 5B). In line with these findings, the decreased ceramide levels of CAV1-deficient EC were paralleled by a decreased ASMase activity (Figure 5C). In accordance with the previously shown increased apoptosis levels of CAV1(-) PC3 cells upon IR (Panic et al., 2017), CAV1-deficient PC3 show increased ROS-levels after IR (not shown). As compared to the CAV1-dependent ceramide species detected in EC (Figure 1C), PC3 ceramide levels were generally higher (Supplemental Figure S2), and in particular the ceramide levels of the C16, C22 and C24:1 species in the radio-resistant CAV1-expressing PC3 cells. Conclusively, the different expression levels of the distinct ceramide species resulting from the co-culture of EC and prostate carcinoma cells with a differential CAV1 content, in particular the levels of C16, C24 and C24:1 are decisive for the radiation response, whereas the increased levels of C24 ceramides might account for the increased radio-resistance of CAV1-expressing PC3 cells.

Human advanced prostate cancer specimens were characterized by an increased ceramide-immunoreactivity indicating radiation resistance

As an increase in epithelial CAV1 (together with a loss of stromal CAV1) has been linked to radiation resistance (Ketteler et al., 2019; Panic et al., 2017), we decided to investigate ceramide and ASMase together with CAV1 expression levels, as well as the respective stromal-epithelial distributions, in human prostate tissue specimens by immunohistochemistry (Figure 6). Ceramide as well as ASMase immunoreactivity was increased in the CAV1-positive malignant epithelial cells of advanced prostate cancer specimen. Furthermore, the CAV1-deficient fibroblastic compartment of tumor samples tended to be less intensely stained for ceramide and ASMase in cases with higher Gleason grade. Of note, the CAV1-expressing EC are ceramide and ASMase-positive and remain so upon tumor progression (Figure 6). Although we were not able to distinguish the different ceramide species in the tumor specimen, the compassion of the different ceramide species as analyzed by mass spectrometry confirmed that

the increased C24 and C24:1 ceramide species and particularly in the more radio-resistant CAV1(+) PC3 and CAV1(-) fibroblasts, which resemble the critical CAV1 shift in advanced prostate specimen, have implications for prostate carcinoma progression and therapy resistance and might scavenge the effect of C16 apoptosis induction (Supplemental Figure S3).

Discussion

The sensitivity of the vascular compartment to IR has been closely linked to the tumor response to RT(Chen et al., 2013; Garcia-Barros et al., 2003; Klein et al., 2015; Potiron et al., 2013; Roe et al., 2012). Herein, EC apoptosis was shown to depend on the early generation of sphingolipid ceramide by ASMase (Bonnaud et al., 2007). Directly after IR exposure, ASMase, usually located in lysosomes, translocates to the plasma membrane resulting in the generation of ceramide by hydrolyzing sphingomyelin. Ceramide in turn induces plasma membrane remodeling leading to the formation of large lipid platforms as effective signalosomes and thereby activation of a p38 MAPK dependent apoptotic pathway (Corre et al., 2017; Niaudet et al., 2017). Here we show that CAV1 is critically involved in that pathway. The CAV1-enriched smooth invaginations of the plasma membrane (caveolae) usually form a subdomain of lipid rafts, so-called caveolin-enriched membrane fractions, that function as signaling organizing centers and platforms by modulating specific signals that are temporally and spatially controlled (Caliceti et al., 2014; Lajoie and Nabi, 2010; Yu et al., 2005). For example, the major angiogenic growth factor VEGFR2/ KDR, turned out to be partially localized in caveolae and VEGFR2/KDR binding to CAV1 significantly decreased its ability to become activated (Caliceti et al., 2014). After VEGF stimulation, VEGFR2/ KDR shifts to non-raft plasma membrane portions resulting in the activation of its tyrosine kinase via phosphorylation and genomic instability via the increased production of ROS (Caliceti et al., 2014). This matches our previous finding, when we reported that CAV1-deficieny resulted in an increased angiogenic phenotype of EC (Klein et al., 2015).

In line with these findings we demonstrate here that CAV1-deficiency in EC, which was previously shown to result in a stimulated, angiogenic EC phenotype, increased the formation of plasma membrane signalosomes and associated p38 MAPK signaling (Figure 7). Furthermore, the increased apoptosis induction upon IR was accompanied by an enhanced ceramide generation based on an increase in ASMase activity in

CAV1-deficient EC. Ceramide in turn was already shown to displace cholesterol from lipid rafts and to decrease the association of the cholesterol binding protein CAV1 (Yu et al., 2005). On the other hand, we show here that a reduction of endothelial CAV1 resulted in increased formation of lipid platforms in respective cells, which is most likely due to enhanced ASMase activity and thus increased ceramide generation. Quantification of the different ceramide species using LC-MS revealed that EC expressed the ceramide species C16, C24 and C24:1 differentially, particularly in response to IR, which further correlated with the CAV1-dependent expressions of different CerS. CerS1 is known to preferentially biosynthesize C18 and C20 ceramide, CerS2 and CerS4 generate very-long-chain fatty acid-containing ceramides (C22-C26), and CerS5 and CerS6 are mostly responsible for the generation of C12-C16 ceramides (Mullen et al., 2012; Ponnusamy et al., 2010). Accordingly, we show here that CerS2, CerS4, CerS5 and CerS6 were expressed in both EC variants, and was further induced upon IR. While CerS5 and CerS6 were expressed in both cell types at similar levels, CAV1(-) EC showed decreased basal expression levels of CerS2 and CerS4 which generate very long ceramides (up to C22-C24). In line with these expression levels, CAV1(-) EC showed a decreased ceramide C24/C24:1 ratio, which, together with elevated C16 ceramide levels, might account for the increased radio-sensitivity of those cells. Several studies already suggested that the equilibrium between the chain lengths of ceramides is important with respect to their cellular effects and especially for regulating cell death. Herein, a shift from very-long-chain ceramides (C22–C26) to long-chain ceramides (C14–C20) increases apoptosis susceptibility and apoptosis rates (Hartmann et al., 2012; Kurz et al., 2019; Ponnusamy et al., 2010; Rudd and Devaraj, 2018). In addition, saturation of the very-long-chain ceramides seems to play a determinant role in apoptosis induction, as the ceramide-enriched membrane platforms were preferentially formed by saturated ceramides prior to activation of the apoptosis pathways (Rudd and Devaraj, 2018).

In general, the apoptotic pathway (intrinsic activation) is initiated by the permeabilization of the mitochondrial outer membrane followed by cytochrome c release and caspase activation. Inhibition of CerS was shown to inhibit caspase 3/7 activation and thus apoptosis, which is indicative for a ceramide function downstream of mitochondria but upstream of caspase activation, possibly through controlling mitochondrial outer membrane permeabilization (Mullen et al., 2012). Mechanistically, ceramides were found to form channels in mitochondrial membranes, and these ceramide channels were regulated by Bcl2 family proteins and dihydroceramide

(Stiban and Perera, 2015). The efficiency of ceramide-mediated membrane permeabilization was shown to depend on the ceramide species, whereas C16 ceramide turned out to permeabilize the membrane most potently. Of note, very-long-chain ceramides, in particular C24, reduced the potency of C16-mediated membrane permeabilization and thus apoptosis execution (Stiban and Perera, 2015). In line with these findings we show here, that apoptosis-prone CAV1-deficient EC were characterized by increased C16 ceramide levels.

One of our initial hypotheses was that lowering the CAV1 content particularly in EC could increase the radiation response of tumors which were characterized by increased CAV1 expression levels (Klein et al., 2015). Silencing of CAV1 in–cancer cells itself was already shown to sensitize lymphoblastoid TK6 to radiation-induced apoptosis (Barzan et al., 2010). Similarly, a reduction of CAV1 resulted in reduced cell adhesion, proliferation and survival of pancreatic cancer cell lines after exposure to IR (Cordes et al., 2007; Hehlgans and Cordes, 2011; Hehlgans et al., 2009). Notably in prostate cancer, which is characterized by increased CAV1 expression levels in malignant epithelial cells at advanced radio-resistant disease stages, a reduction of CAV1 aiming at radio-sensitization seemed to be a promising option (Klein et al., 2015; Panic et al., 2017). Of note, we show now that radiation treatment induced a significant growth delay of–prostate cancer cells when co-cultured with CAV1-deficient EC. Although being decisive for advanced tumor growth and cancer progression, the tumor vasculature acts not separately, but in conformity with a heterogeneous tumor stroma that is now recognized as a key player in cancer cell invasiveness, progression and therapy resistance (Bissell, 2016; Bissell and Hines, 2011; Hanahan and Weinberg, 2011). Especially in prostate cancer, it is now widely accepted that a reactive tumor stroma significantly contributes to growth, malignant progression and RT resistance (Ketteler and Klein, 2018; Ketteler et al., 2019; Panic et al., 2017; Schlomm et al., 2009). Upon progression, a characteristic shift in CAV1 expression levels was observed, where CAV1 expressions increased in epithelial cancer cells while CAV1 expressions decreased in the tumor stroma, most notably in prostate cancer fibroblasts.

Therefore, we investigated here the CAV1-dependent expression of ceramide species in prostate cancer cells and fibroblasts. Although C16, C22, C24 and C24:1 were shown to be expressed in PC3 cells, the C16, C24 and C24:1 ceramide species were significantly increased in the more radio-resistant CAV1-expressing PC3 prostate carcinoma cells whereas C24 levels accounted for an increased C24/C24:1 ratio,

which was shown to counteract the apoptosis-inducing effects of C16 in CAV1-deficient PC3 cells. On the other hand, a shift in sphingolipid composition from C24 to C16 was shown to increase the susceptibility to apoptosis in HeLa cells (Sassa et al., 2012). Herein, it was speculated that changes in the composition of sphingolipid chain length affect the susceptibility of respective cells to stimuli-induced apoptosis by affecting the properties of cell membranes, such as lipid micro-domains, e.g. raft formation (Sassa et al., 2012). Increases in C16 ceramide levels (generated via CerS) were further shown to play a role during apoptosis induced by androgen ablation in androgen-dependent LNCaP prostate cancer cells (Eto et al., 2003).

Beside the expression levels of each cell type in a certain cellular mass like a tumor, the concentration and distribution of certain ceramide species is crucial for apoptosis induction in response (Blaess et al., 2015). Exogenous ceramide species, either derived from cellular secretion or exogenously added, can in turn modify the composition/concentrations of endogenous ceramide species or that of adjacent cells which then might alter associated signaling such as apoptosis. Thus, we could show here that advanced prostate cancer specimen were characterized by increased ceramide as well as ASMase amounts in the CAV1-positive malignant epithelial cells. Using CAV1(+) EC, CAV1(-) PC3 together with CAV1(+) HS5 fibroblasts as a model combination for the CAV1 status of the respective cells found in healthy and low grade prostate carcinoma, and CAV1(+) EC, CAV1(+) PC3 together with CAV1(-) fibroblasts as a model combination for advanced tumor stages, it becomes clear that the very-long-chain ceramides are expressed in higher amounts in each respective more radio-resistant CAV1 variant. In particular, the increased levels of C24 and C24:1 in CAV1(+) PC3 and CAV1(-) fibroblasts may account for the absent apoptosis usually mediated by C16 ceramide either derived from irradiated CAV1(+) EC or CAV1(-) PC3 cells which were shown to upregulate CAV1 upon IR, and/or with CAV1(+) fibroblasts that were shown to downregulate CAV1 upon IR (Ketteler et al., 2019; Panic et al., 2017).

Ceramides or combinations of the different ceramide species have even been proposed as specific disease biomarkers that could be detected in diseased tissue and body fluids (Kurz et al., 2019). In particular cancer elevated levels of ceramides (C16:0, C24:0 and C24:1) in malignant breast tumor tissues as compared with benign and normal tissues indicated that an increase in distinct ceramides correlated with the development of breast cancer (Schiffmann et al., 2009). In ovarian cancer, elevated levels of ceramides (C16:0, C22:0 and C24:0) were shown to be predictive in patients compared to healthy controls and patients with benign cancer conditions (Kozar et al.,

2018). C16:0, C24:0, and C24:1 were elevated in colorectal cancer and correlated here with prognosis and clinical outcome, whereas ceramide C18:0 and C20:0 were found to be reduced in colorectal cancer tissue compared to non-tumor tissue (Chen et al., 2015). Increased ceramide generation based on increased ASMase expression resulted in apoptotic cell death in human lymphoblasts (Santana et al., 1996). Besides mitochondrial outer membrane permeabilization, reduced mitochondrial membrane potential and apoptosis, certain ceramides were associated with decreased mitochondrial respiratory chain (MRC) activity, oxidative phosphorylation, increased reactive oxygen species (ROS) production and oxidative stress (Kogot-Levin and Saada, 2014). In particular C16-ceramide and/or sphinganine was suggested to induce ROS formation through the modulation (inhibition) of mitochondrial complex IV activity, resulting in chronic oxidative stress (Zigdon et al., 2013). Finally, CerS and ASMase seem to co-operate to produce pro-apoptotic ceramide as revealed by either the knockdown of ASMase or the knockdown/ inhibition of CerS6 in glioblastoma multiform cells that reduced ceramide generation, blocked cytosolic calcium elevations, induced ROS generation and finally apoptosis (Yacoub et al., 2010).

Overall, a balance between synthesis and metabolism of sphingomyelin/ ceramide through multiple enzymes determines intracellular ceramide levels. Herein, targeting CerS for therapeutic interventions in human diseases in which the ceramide acyl chain length is altered gained attraction (Park et al., 2014). An upregulation of CerS4 and CerS6, which results in the generation of C16- and C18-ceramides, in human colon and breast cancer cells induced mitochondrial damage and apoptosis (Hartmann et al., 2012). In contrast, overexpression of CerS2, which results in the generation of very-long-chain fatty acids, failed to induce apoptosis. Again, the equilibrium between the various ceramide species is key to instruct the cell to initiate the apoptotic machinery, because although co-overexpression of CerS2 with CerS4 or CerS6 led to a marked increase in total ceramide levels, it had no apoptotic effect in colon cancer cells (Hartmann et al., 2013).

Differential expression levels of ceramides were also crucial for cancer cell sensitivity to chemotherapeutic agents and radiation (Mullen et al., 2012; Verlekar et al., 2018). A decrease in C16 ceramide in colon adenocarcinoma cells, achieved by a knockdown of CerS6, protected the cells from tumor necrosis factor-related apoptosis-inducing ligand (White-Gilbertson et al., 2009). While CerS6-dependent C16 ceramide increased the sensitivity of breast carcinoma cells to TNF-related apoptosis-induced ligand mediated cell death induction, CerS6-dependent C16 ceramide generation

increased tumor development and growth, suggesting anti-apoptotic properties in human head and neck squamous cell carcinoma cells (Hernandez-Corbacho et al., 2015; Senkal et al., 2011). CerS6 overexpression further sensitized a variety of cancer cells to cell death induced by the combined treatment with the multi-kinase inhibitor sorafenib and the histone deacetylase inhibitor vorinostat (Walker et al., 2009).

In particular, IR was shown to increase the p53-dependent expression of CerS5 (but not CerS6) which mediated the cell death-mediating radiation response in human lymphoblastoid cells (El-Assaad et al., 2003; Panjarian et al., 2008). CerS5 and CerS6 were shown to promote cell death via C16 ceramide which was related to IR induced C16-CerS activity in mitochondria-associated membranes (Mesicek et al., 2010). In contrast, overexpression of CerS2 that usually generates very-long-chain fatty acid-containing ceramides (C22-C26) delayed the IR-induced apoptosis. Especially in response to radiation, CerS6-generated C16 ceramide induced BAX-mediated apoptosis (Lee et al., 2011). CerS6-generated C16 ceramide was identified as a transcriptional target of p53 that fostered apoptosis in response to non-genotoxic stress in human lung cancer cells (White-Gilbertson et al., 2009). Increased levels of CerS6-generated C16 ceramide were further assessed in lung and oral cancer tissues as compared to healthy controls (Suzuki et al., 2016; Suzuki et al., 2019). Using lung cancer cells, these observations were confirmed, when CerS6-generated C16 ceramide contributed to the pro-apoptotic cellular response after genotoxic stress and induced then p53 protein activation (Fekry et al., 2016). Thus, different ceramide species have distinct roles in inducing cancer cell death and survival that is dependent on the context and/or tissue or cell type (Ogretmen, 2018).

Conclusively, ceramides are important messengers aiming at apoptosis induction that might also be generated in response to signaling through CD95-Fas/Apo1, tumor necrosis factor alpha, and cancer therapy like chemotherapeutic agents and in particular IR. Upon pro-inflammatory or pro-apoptotic stimulation and most importantly upon radiation, ceramides either generated from ASMase that catalyze the breakdown of phospho-sphingolipid sphingomyelin or generated by *de novo* synthesis via CerS, are highly bioactive lipid-mediators. Here we showed that this ceramide generation is critically influenced by the membrane protein CAV1. As stated above, different ceramide species, in particular their respective N-acyl chain length were shown to affect the functions of ceramides (Mullen et al., 2012). CAV1-expression levels in the different stromal cells as well as malignant epithelial cells of a tumor can change, e.g. upon tumor progression and/or therapy- induction, and thus affect their cellular fate. In

prostate cancer, the critical stromal-epithelial CAV1-shift is accompanied by a shift to higher ceramide levels overall and particularly to more very-long-chain ceramide species (C24) that finally affect the respective cell survival upon IR. Thus, ceramides or synthetic, metabolically stabilized and more rigid analogs that bear the potential of being pro-apoptotic (e.g. C16) may be useful as anti-cancer agents (Blaess et al., 2015). Interestingly, even in prostate cancer the use of agents that elevate ceramide levels as novel chemotherapeutic agents was suggested (Samsel et al., 2004). Here, B13, an inhibitor of acid ceramidase, which in turn resulted in increased ceramide concentrations, was an inducer of cell death by apoptosis in cultured prostate cancer cells. The induction of apoptosis was further paralleled by a drop in glutathione levels in response to B13 (Samsel et al., 2004). In addition, B13 sensitized tumors to the effects of IR, resulting in a significant reduction of tumor volume and weight after combined treatment (Samsel et al., 2004).

These studies, together with the results we presented here, suggest that targeting the ceramide pathways may be a novel treatment strategy for radiation-resistant prostate cancer.

Material and Methods

Materials

Prior to treatment, cells were starved in medium containing 0.1 % FCS overnight. Exogenous C16 Ceramide (Enzo Life Sciences, France) was solved in 100 % EtOH and added after radiation treatment. CAV1 antibody was from Santa Cruz (Santa Cruz, CA; 1:1000 WB, 1:100 IF), antibodies targeting p-p38, p38, p-HSP27, HSP27 and Ceramide were purchased from Cell Signaling Technology (Danvers, MA; all 1:1000 WB). Antibody for beta actin (clone AC-74, A2228) was from Sigma-Aldrich (St. Louis, MO). The goat anti ASM antibody was kindly provided by Prof. K. Sandhoff (Bonn, Germany) (Lansmann et al., 1996).

Cell Cultures

The prostate cancer cell lines LNCaP, PC3 and 22RV1, as well as the fibroblast cell line HS5 were cultured in RPMI 1640 medium (Gibco, ThermoFisher, Waltham, MA, USA) supplemented with 10 % fetal calf serum (FCS) and 100 U Penicillin/Streptomycin (Sigma Aldrich, St. Louis, MO, USA) at 37°C, 5 % CO2 and 95 % humidity. Endothelial cells AS-M5 were cultured in Medium 199 (Gibco, ThermoFisher, Waltham, MA, USA) supplemented with 20 % FCS, 100U Penicillin/ Streptomycin and 15 mg Endothelial Cell Growth Supplement (Sigma) at similar conditions. Cells were passaged 2-3 times per week. CAV1 levels in AS-M5, HS5 and PC3 cells were downregulated by lentiviral transduced shRNA as previously described and labelled with green-fluorescent protein (GFP) (Panic et al., 2017).

Irradiation

Irradiation of samples was done in an Isovolt-320-X-ray machine (Seifert-Pantak) at 320 kV, 10 mA and a 1,65 mm aluminum filter at a distance of 50 cm. The dose rate was approximately 3 Gy/min with an energy of the tube of 90 kV (~ 45 keV X-rays). Irradiation for LC-MS, ASMase activity and LLP staining was performed with a 160 kV irradiator (CP160 Faxitron Xray, USA) at a dose rate of 1.48 Gy/min.

Flow cytometry measurements

Apoptotic cells (sub-G1 fraction) and cell cycle phases were analyzed by using Nicoletti/Propidium Iodide staining (PI; 0.1% sodium citrate(w/v), 50 µg/mL PI (v/v) and 0.05 % Triton X-100 (v/v)) as previously described (Riccardi and Nicoletti, 2006). Cells were stained for 30 min in the dark and subsequently measured with flow cytometer FACS Calibur (BD, Heidelberg, Germany, FL2). Analysis was done using FlowJo software.

Conditioned Medium

Cells were grown until 80 % confluency in normal growth medium, irradiated with 10 Gy or control irradiated and cultured for 48 h in low FCS medium (2 %). Supernatant was taken and centrifuged to separate dead cells. Control medium was incubated with 2 % FCS in culture conditions without cells. Conditioned medium was used 1/1 with normal growth medium for experiments.

Liquid chromatography – Mass Spectrometry (LC-MS) for Ceramide quantification

Extraction of lipids was performed by using Chloroform/Methanol (1/2, v/v) and LC-MS was done as previously described (Croyal et al., 2018). The assay was performed on a HP 1100 series liquid chromatography (Agilent) in line with an electrospray ion mass spectrometer Esquire 4.5 series (BD). Different ceramide species were analyzed with an UptiSphere 5ODB column and the integration of respective species was done using QuantAnalysis software (BD). Samples contained an internal standard (C17:1) which was used as a loading control.

ASMase activity assay

ASMase activity was quantified with BODIPY Sphingomyelin (Invitrogen). 1 µg of lysed protein sample was used and incubated with fluorescent sphingomyelin overnight at 37°C that was subsequently cleaved of ASMase to BODIPY ceramide. Reaction was stopped using a mixture of chloroform/methanol (1/1, v/v) and after centrifugation the organic phase containing the lipids was evaporated with nitrogen. Separation of the

lipids was performed using a Thin-Layer-Chromatography (TLC) silica membrane in chloroform/methanol (95/5, v/v) (Whatman, UK). After drying, the plate was analyzed with chemo luminescence and ASMase activity determined from the relation of BODIPY ceramide to sphingomyelin.

Western blotting

After treatment, cells were scraped in ice-cold RIPA buffer (150 mmol/L NaCl, 1% NP40, 0.5% sodium-desoxycholate, 0.1% sodium-dodecylsulfate, 50 mmol/L Tris/HCL pH 8, 10 mmol/L NaF, 1 mmol/L Na3VO4) containing complete Protease inhibitor cocktail (Roche). 2-3 thaw/freeze cycles were performed before subjecting whole cell lysates to SDS-gel electrophoresis as previously described (Klein et al., 2008).

Large lipid platform (GM1) staining

Cells were seeded on cover slips and treated after overnight culture. Lipid platforms were stained by using 0.1 mM Alexa Fluor 647nm conjugated cholera toxin B subunit for 45 min as described before (Niaudet et al., 2017). All steps were carried out on ice until cells were fixed with 4 % PFA for 20 min. After blocking with 10 % BSA for 20 min, co-staining with CAV1 was performed in a dilution of 1:100 in blocking buffer for 1h. Samples were mounted with GoldProlong containing DAPI (ThermoFisher) to visualize nuclei and pictures were taken with a Leica confocal microscope.

Staining of Human Tumor Tissue

Immunohistology and immunofluorescence staining was performed on formalin-fixed and paraffin-embedded slides of human prostate cancer samples as previously described (Ketteler et al., 2019; Panic et al., 2017). Samples were prepared by using a descending alcohol series and incubation with target retrieval solution (Dako). Afterwards slides were blocked with a 2% FCS/PBS blocking solution to reduce unspecific interactions and primary antibodies were incubated overnight at 4°C. Antigens were detected either by Horseradish-peroxidase conjugated secondary antibodies and DAB-staining (IHC) or fluorescently labelled secondary antibodies. Nuclei were counterstained with hematoxylin or DAPI.

Real time (RT) qPCR

RNA was isolated by using RNeasy Mini Kit (Qiagen, Hilden, Germany) after manufacturer's instructions. 1 µg of cDNA was used and expression levels of the indicated genes were compared to housekeeping gene beta-actin (set as 1). The following primer sequences were used: CerS1 for: CCTCCAGCCCAGAGAT, rev: AGAAGGGGTAGTCGGTG; CerS2 for: CCAGGTAGAGCGTTGGTT, rev: CCAGGGTTTATCCACAATGAC; CerS3 for: CCTGGCTGCTATTAGTCTGAT, rev: TCACGAGGGTCCCACT; CerS4 for: GCAAGGATTTCAAGGAGCAG, rev: AACAGCAGCACCAGAGAG; CerS5 for: CAAGTATCAGCGGCTCTGT, rev: ATTATCTCCCAACTCTCAAAGA; CerS6 for: AAGCAACTGGACTGGGATGTT, rev: AATCTGACTCCGTAGGTAAATACA; β-ACTIN for: TCCATCATGAAGTGTGACGT, rev: GAGCAATGATCTTGATCTTCAT. RT-qPCR was performed in an Agilent Aria cycler.

Spheroid Culture

PC3 or LNCaP cells were co-cultured with AS-M5 CAV1(+) or CAV1(-) cells in hanging drops for 24h (1/1, NGM/Methylcellulose). Afterwards, spheroids were plated in NGM with growth-factor reduced Matrigel (1/2). Pictures were taken directly and 48h after treatment at 10x magnification. Size was measured and calculated using ImageJ software.

Statistical analysis

If not otherwise indicated, results were obtained of at least three different experiments and analyzed using either one-way or two-way ANOVA followed by post-hoc Tukey's test or Student's t-test with Welch's correction. For statistical analysis GraphPad Prism 7 software was used (LaJolla, CA).

Acknowledgements

We thank Mohammed Benchellal and Eva Gau for their excellent technical assistance.

Author Contributions Statement

J.K., D.L., V.V.R., A.W. and D.K. performed experiments; J.K. D.K. analysed results and made the figures; C.H., P.M., and H.R. provided materials; H.R. performed the Gleason scoring; V.J., F.P. and D.K. designed research, V.J., D.K. performed fund raining, J.K., F.P. and D.K. wrote the paper. All authors reviewed and approved the manuscript. This work was supported by grants of the DFG (GRK1739/1; GRK1739/2), and the BMBF (02NUK024-D).

Conflict of Interest Statement

The authors state that there are no personal or institutional conflicts of interest.

Figure legends

Figure 1

ASMase activity and Ceramide generation is increased in CAV1(-) EC in a time-dependent manner after IR. (**A**) Whole cell lysates of irradiated (10 Gy) and control (0 Gy) AS-M5 CAV1(+) and CAV1(-) cells were used for Western blot analysis of ASMase and CAV1 protein expression 48h upon IR. β-ACTIN was used as a loading control. Representative images were taken from 3 different experiments. (**B**) ASMase enzymatic activity was measured in AS-M5 CAV1(+) and CAV1(-) cells in control conditions (n=13). CAV1(-) activity is shown in relation to CAV1(+) cells, that was set at 1. Further on, ASMase enzymatic activity was analyzed after 10 Gy IR. ASMase activity is shown in relation to CAV1(+) unirradiated samples (set as 1) 5 min, 15 min and 30 min after IR treatment (n= 3-4). Statistical analysis was performed by using one-way ANOVA (*) or Student's t-test (#), error bars are shown in SEM. P-values indicate * $p<0.05$, *** $p<0.001$ and ## $p<0.01$, ### $p<0.001$. (**C**) Overview of all detected ceramide species by LC-MS in AS-M5 CAV1(+) and CAV1(-) cells (n=3, SEM). Statistical analysis was done by using two-way ANOVA followed by post-hoc Tukey's multiple comparison. (**D**) Timeline of ceramide species C16, C24 and C24:1 generated by AS-M5 CAV1(+) cells after IR treatment. Samples were taken 1 min, 5 min, 15 min and 30 min after 10 Gy irradiation. All control (ctrl) samples were pooled (n=3, SD). Statistical analysis was done by using Student's t-Test with Welch's correction. (**E**) Timeline of ceramide species C16, C24 and C24:1 generated by CAV1(-) AS-M5 after 10 Gy irradiation (n=3, SD). Samples were taken at indicated time points. Statistical analysis was done by using Student's t-Test with Welch's correction. P-values (C-E) indicate * $p<0.05$, ** $p<0.01$, *** $p<0.001$, **** $p<0.0001$.

Figure 2

Large lipid platform (LLP) formation is elevated in CAV1(-) AS-M5 cells independently of stress induction. (**A**) Large lipid platform formation in AS-M5 CAV1(+) and CAV1(-) cells was visualized with Cholera toxin B-subunit (purple) which binds Ganglioside GM1. AS-M5 cells were lentiviral transduced with a GFP-tag (green) and the nucleus is stained with DAPI (blue). Representative images of three individual experiments are shown (upper part). Cells were irradiated with 10 Gy and stained 10 min afterwards with Cholera toxin B-subunit (purple). Cells are labelled in green and nucleus is stained with DAPI (blue) (lower part). (**B**) Quantification of LLP formation

was done by counting positive cells of control irradiated (0 Gy) and irradiated (10 Gy) cells. The graph shows LLP formation 10 min and 30 min after IR. In total at least 50 cells/condition were quantified (n=3, SEM). Statistical analysis was performed with two-way ANOVA followed by post-hoc Tukey's test. P-value indicates **** $p<0.0001$. (**C**) Co-staining of LLP (purple) and CAV1 (red) was performed. A representative image of control irradiated (0 Gy) CAV1(+) AS-M5 cells is shown. Cells are labelled in green and nucleus was stained with DAPI (blue). Scale bar indicates 50 µm in all pictures.

Figure 3

CAV1(-) EC express higher levels of HSP27 which are downregulated after IR treatment. (**A**) Whole cell lysates were used for Western blot analysis of the p38/MAPK pathway by detecting the involved proteins p-p38, p38, p-HSP27 and HSP27 in control and 10 Gy irradiated cells 5 min and 30 min after treatment. Additionally, CAV1 expression levels were measured at the same time points. β-ACTIN was used as a loading control. Representative blots of three individual experiments are shown. (**B**) Relative quantification of the indicated protein expression levels was performed (n=3). Band signal intensity was quantified by densitometry and normalized to β-ACTIN. Error bars are shown in SD and statistical analysis was performed by two-way ANOVA followed by post-hoc Tukey's multiple comparison. P-values indicate * $p<0.05$, ** $p<0.01$.

Figure 4

Paracrine signaling of AS-M5 CAV1(-) is not sufficient to induce apoptosis, whereas a direct interaction with prostate cancer cells fosters growth reduction and radio-sensitivity. (**A**) PC3 cells (top) and LNCaP cells (bottom) were co-cultured with AS-M5 CAV1(+) or CAV1(-) cells in hanging drops for 24 h. After formation of spheroids, cells were plated in a growth factor-reduced Matrigel- medium mixture (1:2, v/v) and irradiated at 10 Gy. Pictures were taken at the time of irradiation (0 h) and 48 h later. Scale bar relates to 50 µm. Representative images are shown from three individual experiments where at least 10 spheroids/condition were measured. Statistical analysis was performed by two-way ANOVA followed by post-hoc Tukey's test (n=3, SEM). P-values indicate ** $p<0.01$, **** $p<0.0001$. (**B**) Prostate cancer cells were cultivated with AS-M5 supernatant (control or 10 Gy irradiated) for 48 h in control and irradiated (10 Gy) conditions. Cell cycle phases and apoptotic cells (subG1) were analyzed by flow cytometry (channel FL-2). Graphs consist of data from three

individual experiments with SD shown. (**C**) Prostate cancer cells were starved overnight (0.1% FCS) and subsequently treated with 5 or 10 µM C16 ceramide and treated with irradiation (10 Gy). After 48 h cells were harvested and cell cycle phases and apoptotic cells (subG1) were analyzed using flow cytometry (channel FL-2). Graphs show data from three individual experiments with SD as error bars.

Figure 5

The radiation resistant CAV1(+) PC3 cells show higher levels of total ceramide whereas ASMase-activity is similar. (**A**) Different expression of ceramide species was measured by LC-MS in CAV1(+) and CAV1(-) PC3 prostate cancer cells. Bars represent three individual experiments with SEM as standard error. Statistical analysis was performed using two-way ANOVA followed by post-hoc Sidak's test. P-values indicate * $p<0.05$, **** $p<0.0001$. (**B**) The ratios of C16 to C24, C16 to C24:1 and C24 to C24:1 ceramide were calculated in CAV1(+) and CAV1(-) PC3 cells. Results are shown of three individual experiments with SEM. Statistical analysis was performed using Student's t-test with Welch's correction. P-value indicates **** $p< 0.0001$. (**C**) ASMase activity of differential CAV1-expressing PC3 cells was measured at control conditions. Activity is shown in relation to CAV1(+) cells set as 1 (n=3, SD).

Figure 6

Immunohistological analysis of CAV1, ASMase and ceramide expression levels in human prostate cancer tissues. Paraffin-sections of human prostate cancers were stained for the indicated antibodies using either IHC (**A**) or immunofluorescence (**B**). Gleason grading scores were divided into low (Gleason Score ≥6, Grade group 1), intermediate (Gleason Score 7 (a/b), Grade groups 2 & 3) and high scores (Gleason Score ≥8, Grade groups 4 & 5). Asterisks mark stromal compartments and bold arrows point to epithelial structures. Sections were counterstained using hematoxylin. Representative images are shown. Magnification 40x (phase contrast); 630x (immunofluorescence).

Figure 7

Schematic overview of CAV1-dependency on the ASMase/ceramide pathway induction in EC. Left: Under normal conditions in EC (CAV1(+), upper panel) ASMase is located in lysosomes and translocated to the plasma membrane upon stress induction by IR. Proper translocation is presumably facilitated by CAV1-abundant

regions. IR (lower panel) leads to rapidly increased ASMase activity and ceramide generation (specifically of C16 and C24), which goes along with formation of LLP and altered signal transduction. Degeneration of ceramide takes place after 15 – 30 min and apoptosis induction can be avoided. Further on, co-culture of EC CAV1(+) and prostate cancer cells leads to survival upon treatment with IR. Additionally, *de novo* synthesis of long chain C24 by CerS2 and CerS4 is elevated in CAV1(+) EC presumably leading to scavenging of apoptosis inducing C16. **Right:** CAV1 downregulation or absence in EC leads to a permanently activated and upregulated ASMase activity that may be due to improper localization at the plasma membrane. Activated ASMase facilitates increased generation of ceramide and specifically C16 and C24 ceramide species are upregulated. A stable formation of large lipid platforms alters ceramide-dependent signaling of the p38/MAPK pathway. *De novo* synthesis of ceramide is lowered compared to AS-M5 CAV1(+) EC, especially in CerS2 and CerS4, which are important for the synthetization of long chain ceramides. Co-culture of CAV1(-) AS-M5 with prostate cancer cells led to an elevated proliferation of the tumor cells. Upon stress induction by IR (lower panel), ceramide accumulates and generation is stabilized which fosters apoptosis induction and EC death, presumably by differential regulation of the p38/MAPK pathway. Our results indicate that elevated apoptosis in CAV1(-) ECs influences tumor cell survival and growth in a negative manner when co-cultured with prostate cancer cells. Additionally, *de novo* synthesis of C24 by CerS2 is lowered in comparison to the radio-resistant CAV1(+) variant.

References

Almeida, C., Nagarajan, D., Tian, J., Leal, S.W., Wheeler, K., Munley, M., Blackstock, W., and Zhao, W. (2013). The role of alveolar epithelium in radiation-induced lung injury. PLoS One 8, e53628.

Ayala, G., Morello, M., Frolov, A., You, S., Li, R., Rosati, F., Bartolucci, G., Danza, G., Adam, R.M., Thompson, T.C., et al. (2013). Loss of caveolin-1 in prostate cancer stroma correlates with reduced relapse-free survival and is functionally relevant to tumour progression. The Journal of pathology 231, 77-87.

Barzan, D., Maier, P., Zeller, W.J., Wenz, F., and Herskind, C. (2010). Overexpression of caveolin-1 in lymphoblastoid TK6 cells enhances proliferation after irradiation with clinically relevant doses. Strahlentherapie und Onkologie : Organ der Deutschen Rontgengesellschaft [et al] 186, 99-106.

Bissell, M.J. (2016). Thinking in three dimensions: discovering reciprocal signaling between the extracellular matrix and nucleus and the wisdom of microenvironment and tissue architecture. Molecular biology of the cell 27, 3205-3209.

Bissell, M.J., and Hines, W.C. (2011). Why don't we get more cancer? A proposed role of the microenvironment in restraining cancer progression. Nature medicine 17, 320-329.

Blaess, M., Le, H.P., Claus, R.A., Kohl, M., and Deigner, H.P. (2015). Stereospecific induction of apoptosis in tumor cells via endogenous C16-ceramide and distinct transcripts. Cell Death Discov 1, 15013.

Bonnaud, S., Niaudet, C., Pottier, G., Gaugler, M.H., Millour, J., Barbet, J., Sabatier, L., and Paris, F. (2007). Sphingosine-1-phosphate protects proliferating endothelial cells from ceramide-induced apoptosis but not from DNA damage-induced mitotic death. Cancer Res 67, 1803-1811.

Caliceti, C., Zambonin, L., Rizzo, B., Fiorentini, D., Vieceli Dalla Sega, F., Hrelia, S., and Prata, C. (2014). Role of plasma membrane caveolae/lipid rafts in VEGF-induced redox signaling in human leukemia cells. BioMed research international 2014, 857504.

Chen, D., and Che, G. (2014). Value of caveolin-1 in cancer progression and prognosis: Emphasis on cancer-associated fibroblasts, human cancer cells and mechanism of caveolin-1 expression (Review). Oncology letters 8, 1409-1421.

Chen, F.H., Fu, S.Y., Yang, Y.C., Wang, C.C., Chiang, C.S., and Hong, J.H. (2013). Combination of vessel-targeting agents and fractionated radiation therapy: the role of the SDF-1/CXCR4 pathway. International journal of radiation oncology, biology, physics 86, 777-784.

Chen, L., Chen, H., Li, Y., Li, L., Qiu, Y., and Ren, J. (2015). Endocannabinoid and ceramide levels are altered in patients with colorectal cancer. Oncol Rep 34, 447-454.

Chidlow, J.H., Jr., and Sessa, W.C. (2010). Caveolae, caveolins, and cavins: complex control of cellular signalling and inflammation. Cardiovascular research 86, 219-225.

Cordes, N., Frick, S., Brunner, T.B., Pilarsky, C., Grutzmann, R., Sipos, B., Kloppel, G., McKenna, W.G., and Bernhard, E.J. (2007). Human pancreatic tumor cells are sensitized to ionizing radiation by knockdown of caveolin-1. Oncogene 26, 6851-6862.

Corre, I., Guillonneau, M., and Paris, F. (2013). Membrane signaling induced by high doses of ionizing radiation in the endothelial compartment. Relevance in radiation toxicity. Int J Mol Sci 14, 22678-22696.

Corre, I., Paris, F., and Huot, J. (2017). The p38 pathway, a major pleiotropic cascade that transduces stress and metastatic signals in endothelial cells. Oncotarget 8, 55684-55714.

Croyal, M., Kaabia, Z., Leon, L., Ramin-Mangata, S., Baty, T., Fall, F., Billon-Crossouard, S., Aguesse, A., Hollstein, T., Sullivan, D.R., et al. (2018). Fenofibrate decreases plasma ceramide in type 2 diabetes patients: A novel marker of CVD? Diabetes Metab 44, 143-149.

Dewever, J., Frerart, F., Bouzin, C., Baudelet, C., Ansiaux, R., Sonveaux, P., Gallez, B., Dessy, C., and Feron, O. (2007). Caveolin-1 is critical for the maturation of tumor blood vessels through the regulation of both endothelial tube formation and mural cell recruitment. The American journal of pathology 171, 1619-1628.
Dolores Di Vizio, M.M., Federica Sotgia, Richard G. Pestell, Michael R. Freeman, and Michael P. Lisanti, (2009). An absence of stromal caveolin-1 is associated with advanced prostate cancer, metastatic disease and epithelial Akt activation. Cell cycle.
El-Assaad, W., Kozhaya, L., Araysi, S., Panjarian, S., Bitar, F.F., Baz, E., El-Sabban, M.E., and Dbaibo, G.S. (2003). Ceramide and glutathione define two independently regulated pathways of cell death initiated by p53 in Molt-4 leukaemia cells. The Biochemical journal 376, 725-732.
Eto, M., Bennouna, J., Hunter, O.C., Hershberger, P.A., Kanto, T., Johnson, C.S., Lotze, M.T., and Amoscato, A.A. (2003). C16 ceramide accumulates following androgen ablation in LNCaP prostate cancer cells. Prostate 57, 66-79.
Fajardo, L.F. (2005). The pathology of ionizing radiation as defined by morphologic patterns. Acta oncologica 44, 13-22.
Fekry, B., Jeffries, K.A., Esmaeilniakooshkghazi, A., Ogretmen, B., Krupenko, S.A., and Krupenko, N.I. (2016). CerS6 Is a Novel Transcriptional Target of p53 Protein Activated by Non-genotoxic Stress. The Journal of biological chemistry 291, 16586-16596.
Garcia-Barros, M., Paris, F., Cordon-Cardo, C., Lyden, D., Rafii, S., Haimovitz-Friedman, A., Fuks, Z., and Kolesnick, R. (2003). Tumor response to radiotherapy regulated by endothelial cell apoptosis. Science 300, 1155-1159.
Gee, E., Milkiewicz, M., and Haas, T.L. (2010). p38 MAPK activity is stimulated by vascular endothelial growth factor receptor 2 activation and is essential for shear stress-induced angiogenesis. Journal of cellular physiology 222, 120-126.
Ghafoori, P., Marks, L.B., Vujaskovic, Z., and Kelsey, C.R. (2008). Radiation-induced lung injury. Assessment, management, and prevention. Oncology (Williston Park) 22, 37-47; discussion 52-33.
Glenney, J.R., Jr., and Soppet, D. (1992). Sequence and expression of caveolin, a protein component of caveolae plasma membrane domains phosphorylated on tyrosine in Rous sarcoma virus-transformed fibroblasts. Proceedings of the National Academy of Sciences of the United States of America 89, 10517-10521.
Hanahan, D., and Weinberg, R.A. (2011). Hallmarks of cancer: the next generation. Cell 144, 646-674.
Hartmann, D., Lucks, J., Fuchs, S., Schiffmann, S., Schreiber, Y., Ferreiros, N., Merkens, J., Marschalek, R., Geisslinger, G., and Grosch, S. (2012). Long chain ceramides and very long chain ceramides have opposite effects on human breast and colon cancer cell growth. The international journal of biochemistry & cell biology 44, 620-628.
Hartmann, D., Wegner, M.S., Wanger, R.A., Ferreiros, N., Schreiber, Y., Lucks, J., Schiffmann, S., Geisslinger, G., and Grosch, S. (2013). The equilibrium between long and very long chain ceramides is important for the fate of the cell and can be influenced by co-expression of CerS. The international journal of biochemistry & cell biology 45, 1195-1203.
Hehlgans, S., and Cordes, N. (2011). Caveolin-1: an essential modulator of cancer cell radio- and chemoresistance. Am J Cancer Res 1, 521-530.
Hehlgans, S., Eke, I., Storch, K., Haase, M., Baretton, G.B., and Cordes, N. (2009). Caveolin-1 mediated radioresistance of 3D grown pancreatic cancer cells. Radiother Oncol 92, 362-370.
Hernandez-Corbacho, M.J., Canals, D., Adada, M.M., Liu, M., Senkal, C.E., Yi, J.K., Mao, C., Luberto, C., Hannun, Y.A., and Obeid, L.M. (2015). Tumor Necrosis Factor-alpha (TNFalpha)-induced Ceramide Generation via Ceramide Synthases Regulates Loss of Focal Adhesion

Kinase (FAK) and Programmed Cell Death. The Journal of biological chemistry 290, 25356-25373.
Karam, J.A., Lotan, Y., Roehrborn, C.G., Ashfaq, R., Karakiewicz, P.I., and Shariat, S.F. (2007). Caveolin-1 overexpression is associated with aggressive prostate cancer recurrence. Prostate 67, 614-622.
Karen G. Rothberg, J.E.H., William C. Donzell, Yun-Shu Ying,'John R. Glenney, and Richard G. W. Anderson (1992). Caveolin a protein component of caveolae membrane coats. Cell.
Ketteler, J., and Klein, D. (2018). Caveolin-1, cancer and therapy resistance. Int J Cancer 143, 2092-2104.
Ketteler, J., Panic, A., Reis, H., Wittka, A., Maier, P., Herskind, C., Yague, E., Jendrossek, V., and Klein, D. (2019). Progression-Related Loss of Stromal Caveolin 1 Levels Mediates Radiation Resistance in Prostate Carcinoma via the Apoptosis Inhibitor TRIAP1. J Clin Med 8.
Klein, D. (2018). The Tumor Vascular Endothelium as Decision Maker in Cancer Therapy. Frontiers in oncology 8, 367.
Klein, D., Demory, A., Peyre, F., Kroll, J., Augustin, H.G., Helfrich, W., Kzhyshkowska, J., Schledzewski, K., Arnold, B., and Goerdt, S. (2008). Wnt2 acts as a cell type-specific, autocrine growth factor in rat hepatic sinusoidal endothelial cells cross-stimulating the VEGF pathway. Hepatology 47, 1018-1031.
Klein, D., Schmitz, T., Verhelst, V., Panic, A., Schenck, M., Reis, H., Drab, M., Sak, A., Herskind, C., Maier, P., et al. (2015). Endothelial Caveolin-1 regulates the radiation response of epithelial prostate tumors. Oncogenesis 4, e148.
Kogot-Levin, A., and Saada, A. (2014). Ceramide and the mitochondrial respiratory chain. Biochimie 100, 88-94.
Korpela, E., and Liu, S.K. (2014). Endothelial perturbations and therapeutic strategies in normal tissue radiation damage. Radiat Oncol 9, 266.
Kozar, N., Kruusmaa, K., Bitenc, M., Argamasilla, R., Adsuar, A., Goswami, N., Arko, D., and Takac, I. (2018). Metabolomic profiling suggests long chain ceramides and sphingomyelins as a possible diagnostic biomarker of epithelial ovarian cancer. Clin Chim Acta 481, 108-114.
Kurz, J., Parnham, M.J., Geisslinger, G., and Schiffmann, S. (2019). Ceramides as Novel Disease Biomarkers. Trends Mol Med 25, 20-32.
Lafargue, A., Degorre, C., Corre, I., Alves-Guerra, M.C., Gaugler, M.H., Vallette, F., Pecqueur, C., and Paris, F. (2017). Ionizing radiation induces long-term senescence in endothelial cells through mitochondrial respiratory complex II dysfunction and superoxide generation. Free Radic Biol Med 108, 750-759.
Lajoie, P., and Nabi, I.R. (2010). Lipid rafts, caveolae, and their endocytosis. International review of cell and molecular biology 282, 135-163.
Lansmann, S., Ferlinz, K., Hurwitz, R., Bartelsen, O., Glombitza, G., and Sandhoff, K. (1996). Purification of acid sphingomyelinase from human placenta: characterization and N-terminal sequence. FEBS letters 399, 227-231.
Lee, H., Rotolo, J.A., Mesicek, J., Penate-Medina, T., Rimner, A., Liao, W.C., Yin, X., Ragupathi, G., Ehleiter, D., Gulbins, E., et al. (2011). Mitochondrial ceramide-rich macrodomains functionalize Bax upon irradiation. PloS one 6, e19783.
Li, L., Hu, J., He, T., Zhang, Q., Yang, X., Lan, X., Zhang, D., Mei, H., Chen, B., and Huang, Y. (2015). P38/MAPK contributes to endothelial barrier dysfunction via MAP4 phosphorylation-dependent microtubule disassembly in inflammation-induced acute lung injury. Scientific reports 5, 8895.
Lin, M.I., Yu, J., Murata, T., and Sessa, W.C. (2007). Caveolin-1-deficient mice have increased tumor microvascular permeability, angiogenesis, and growth. Cancer research 67, 2849-2856.

Mesicek, J., Lee, H., Feldman, T., Jiang, X., Skobeleva, A., Berdyshev, E.V., Haimovitz-Friedman, A., Fuks, Z., and Kolesnick, R. (2010). Ceramide synthases 2, 5, and 6 confer distinct roles in radiation-induced apoptosis in HeLa cells. Cell Signal 22, 1300-1307.
Mullen, T.D., Hannun, Y.A., and Obeid, L.M. (2012). Ceramide synthases at the centre of sphingolipid metabolism and biology. Biochem J 441, 789-802.
Niaudet, C., Bonnaud, S., Guillonneau, M., Gouard, S., Gaugler, M.H., Dutoit, S., Ripoche, N., Dubois, N., Trichet, V., Corre, I., et al. (2017). Plasma membrane reorganization links acid sphingomyelinase/ceramide to p38 MAPK pathways in endothelial cells apoptosis. Cell Signal 33, 10-21.
Ogretmen, B. (2018). Sphingolipid metabolism in cancer signalling and therapy. Nat Rev Cancer 18, 33-50.
Panic, A., Ketteler, J., Reis, H., Sak, A., Herskind, C., Maier, P., Rubben, H., Jendrossek, V., and Klein, D. (2017). Progression-related loss of stromal Caveolin 1 levels fosters the growth of human PC3 xenografts and mediates radiation resistance. Sci Rep 7, 41138.
Panjarian, S., Kozhaya, L., Arayssi, S., Yehia, M., Bielawski, J., Bielawska, A., Usta, J., Hannun, Y.A., Obeid, L.M., and Dbaibo, G.S. (2008). De novo N-palmitoylsphingosine synthesis is the major biochemical mechanism of ceramide accumulation following p53 up-regulation. Prostaglandins & other lipid mediators 86, 41-48.
Paris, F., Fuks, Z., Kang, A., Capodieci, P., Juan, G., Ehleiter, D., Haimovitz-Friedman, A., Cordon-Cardo, C., and Kolesnick, R. (2001). Endothelial apoptosis as the primary lesion initiating intestinal radiation damage in mice. Science 293, 293-297.
Park, J.W., Park, W.J., and Futerman, A.H. (2014). Ceramide synthases as potential targets for therapeutic intervention in human diseases. Biochim Biophys Acta 1841, 671-681.
Ponnusamy, S., Meyers-Needham, M., Senkal, C.E., Saddoughi, S.A., Sentelle, D., Selvam, S.P., Salas, A., and Ogretmen, B. (2010). Sphingolipids and cancer: ceramide and sphingosine-1-phosphate in the regulation of cell death and drug resistance. Future Oncol 6, 1603-1624.
Potiron, V.A., Abderrahmani, R., Clement-Colmou, K., Marionneau-Lambot, S., Oullier, T., Paris, F., and Supiot, S. (2013). Improved functionality of the vasculature during conventionally fractionated radiation therapy of prostate cancer. PloS one 8, e84076.
Riccardi, C., and Nicoletti, I. (2006). Analysis of apoptosis by propidium iodide staining and flow cytometry. Nat Protoc 1, 1458-1461.
Roe, K., Mikalsen, L.T., van der Kogel, A.J., Bussink, J., Lyng, H., Ree, A.H., Marignol, L., and Olsen, D.R. (2012). Vascular responses to radiotherapy and androgen-deprivation therapy in experimental prostate cancer. Radiat Oncol 7, 75.
Rube, C.E., Uthe, D., Wilfert, F., Ludwig, D., Yang, K., Konig, J., Palm, J., Schuck, A., Willich, N., Remberger, K., et al. (2005). The bronchiolar epithelium as a prominent source of pro-inflammatory cytokines after lung irradiation. International journal of radiation oncology, biology, physics 61, 1482-1492.
Samsel, L., Zaidel, G., Drumgoole, H.M., Jelovac, D., Drachenberg, C., Rhee, J.G., Brodie, A.M., Bielawska, A., and Smyth, M.J. (2004). The ceramide analog, B13, induces apoptosis in prostate cancer cell lines and inhibits tumor growth in prostate cancer xenografts. Prostate 58, 382-393.
Santana, P., Pena, L.A., Haimovitz-Friedman, A., Martin, S., Green, D., McLoughlin, M., Cordon-Cardo, C., Schuchman, E.H., Fuks, Z., and Kolesnick, R. (1996). Acid sphingomyelinase-deficient human lymphoblasts and mice are defective in radiation-induced apoptosis. Cell 86, 189-199.
Sassa, T., Suto, S., Okayasu, Y., and Kihara, A. (2012). A shift in sphingolipid composition from C24 to C16 increases susceptibility to apoptosis in HeLa cells. Biochim Biophys Acta 1821, 1031-1037.

Schiffmann, S., Sandner, J., Birod, K., Wobst, I., Angioni, C., Ruckhaberle, E., Kaufmann, M., Ackermann, H., Lotsch, J., Schmidt, H., et al. (2009). Ceramide synthases and ceramide levels are increased in breast cancer tissue. Carcinogenesis 30, 745-752.
Schlomm, T., Hellwinkel, O.J., Buness, A., Ruschhaupt, M., Lubke, A.M., Chun, F.K., Simon, R., Budaus, L., Erbersdobler, A., Graefen, M., et al. (2009). Molecular cancer phenotype in normal prostate tissue. European urology 55, 885-890.
Senkal, C.E., Ponnusamy, S., Manevich, Y., Meyers-Needham, M., Saddoughi, S.A., Mukhopadyay, A., Dent, P., Bielawski, J., and Ogretmen, B. (2011). Alteration of ceramide synthase 6/C16-ceramide induces activating transcription factor 6-mediated endoplasmic reticulum (ER) stress and apoptosis via perturbation of cellular Ca2+ and ER/Golgi membrane network. The Journal of biological chemistry 286, 42446-42458.
Sotgia, F., Martinez-Outschoorn, U.E., Howell, A., Pestell, R.G., Pavlides, S., and Lisanti, M.P. (2012). Caveolin-1 and cancer metabolism in the tumor microenvironment: markers, models, and mechanisms. Annual review of pathology 7, 423-467.
Stiban, J., and Perera, M. (2015). Very long chain ceramides interfere with C16-ceramide-induced channel formation: A plausible mechanism for regulating the initiation of intrinsic apoptosis. Biochim Biophys Acta 1848, 561-567.
Verlekar, D., Wei, S.J., Cho, H., Yang, S., and Kang, M.H. (2018). Ceramide synthase-6 confers resistance to chemotherapy by binding to CD95/Fas in T-cell acute lymphoblastic leukemia. Cell death & disease 9, 925.
Walker, T., Mitchell, C., Park, M.A., Yacoub, A., Graf, M., Rahmani, M., Houghton, P.J., Voelkel-Johnson, C., Grant, S., and Dent, P. (2009). Sorafenib and vorinostat kill colon cancer cells by CD95-dependent and -independent mechanisms. Molecular pharmacology 76, 342-355.
White-Gilbertson, S., Mullen, T., Senkal, C., Lu, P., Ogretmen, B., Obeid, L., and Voelkel-Johnson, C. (2009). Ceramide synthase 6 modulates TRAIL sensitivity and nuclear translocation of active caspase-3 in colon cancer cells. Oncogene 28, 1132-1141.
Wiesemann, A., Ketteler, J., Slama, A., Wirsdorfer, F., Hager, T., Rock, K., Engel, D.R., Fischer, J.W., Aigner, C., Jendrossek, V., et al. (2019). Inhibition of Radiation-Induced Ccl2 Signaling Protects Lungs from Vascular Dysfunction and Endothelial Cell Loss. Antioxid Redox Signal 30, 213-231.
Witkiewicz, A.K., Dasgupta, A., Sotgia, F., Mercier, I., Pestell, R.G., Sabel, M., Kleer, C.G., Brody, J.R., and Lisanti, M.P. (2009). An absence of stromal caveolin-1 expression predicts early tumor recurrence and poor clinical outcome in human breast cancers. Am J Pathol 174, 2023-2034.
Xu, H., Zhang, L., Chen, W., Xu, J., Zhang, R., Liu, R., Zhou, L., Hu, W., Ju, R., Lee, C., et al. (2017). Inhibitory effect of caveolin-1 in vascular endothelial cells, pericytes and smooth muscle cells. Oncotarget 8, 76165-76173.
Yacoub, A., Hamed, H.A., Allegood, J., Mitchell, C., Spiegel, S., Lesniak, M.S., Ogretmen, B., Dash, R., Sarkar, D., Broaddus, W.C., et al. (2010). PERK-dependent regulation of ceramide synthase 6 and thioredoxin play a key role in mda-7/IL-24-induced killing of primary human glioblastoma multiforme cells. Cancer research 70, 1120-1129.
Yu, C., Alterman, M., and Dobrowsky, R.T. (2005). Ceramide displaces cholesterol from lipid rafts and decreases the association of the cholesterol binding protein caveolin-1. Journal of lipid research 46, 1678-1691.
Zeng, L., Ou, G., Itasaka, S., Harada, H., Xie, X., Shibuya, K., Kizaka-Kondoh, S., Morinibu, A., Shinomiya, K., and Hiraoka, M. (2008). TS-1 enhances the effect of radiotherapy by suppressing radiation-induced hypoxia-inducible factor-1 activation and inducing endothelial cell apoptosis. Cancer science 99, 2327-2335.

Zigdon, H., Kogot-Levin, A., Park, J.W., Goldschmidt, R., Kelly, S., Merrill, A.H., Jr., Scherz, A., Pewzner-Jung, Y., Saada, A., and Futerman, A.H. (2013). Ablation of ceramide synthase 2 causes chronic oxidative stress due to disruption of the mitochondrial respiratory chain. J Biol Chem 288, 4947-4956.

Figures

Figure 1

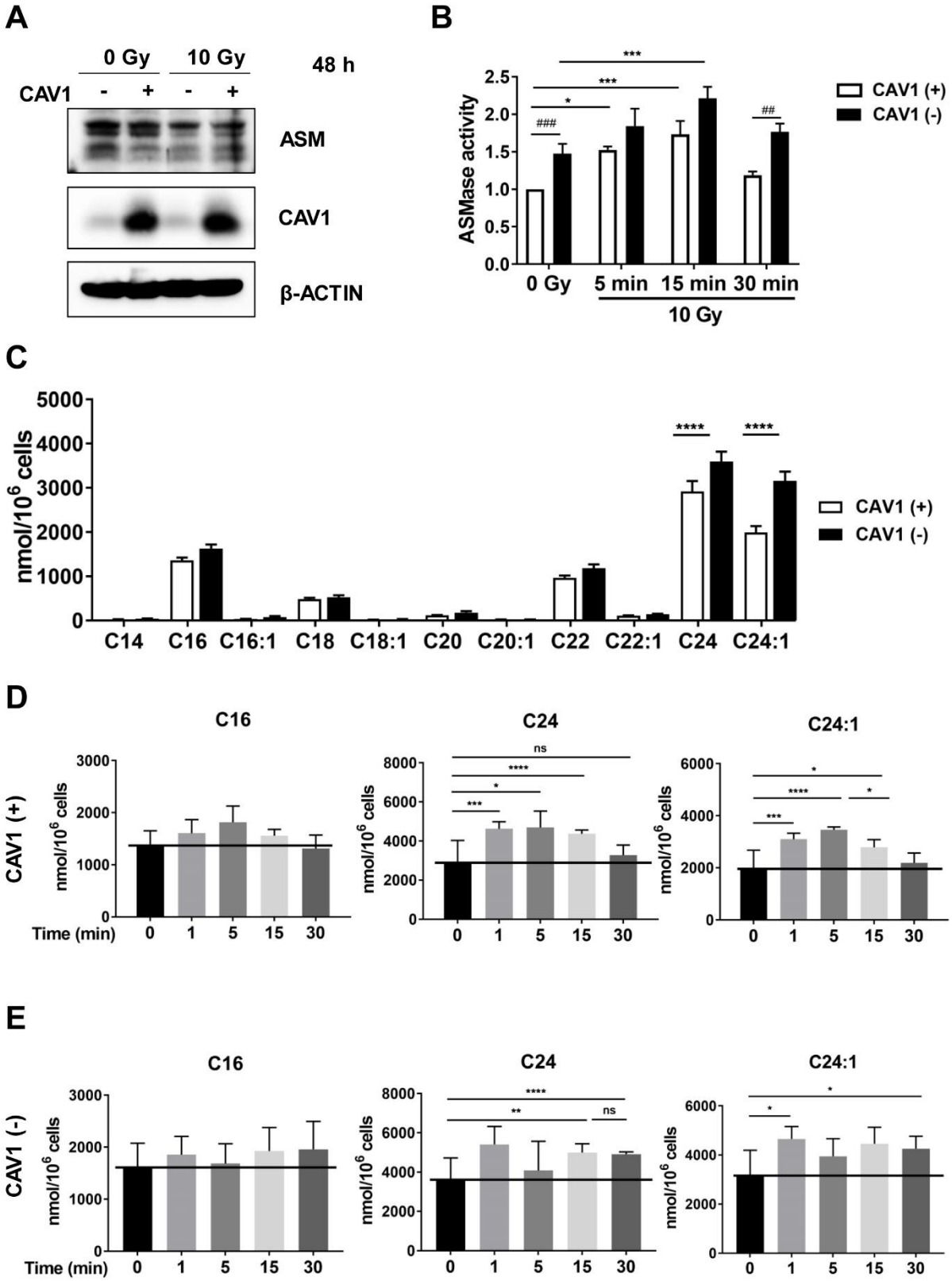

Figure 2

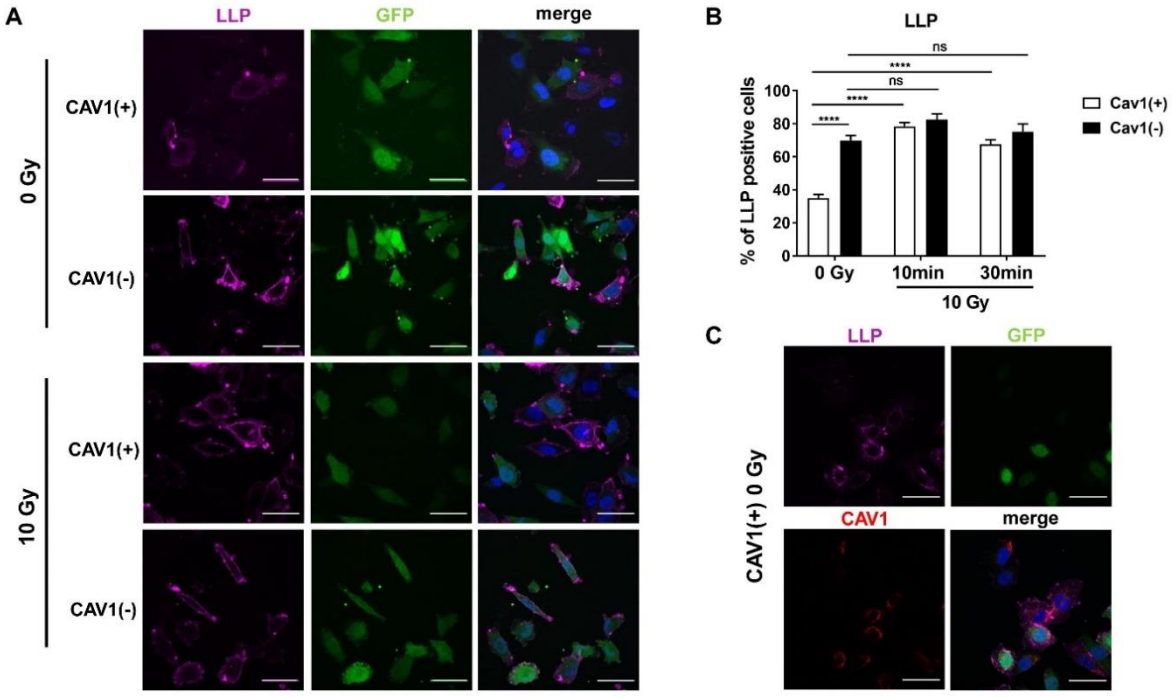

Figure 3

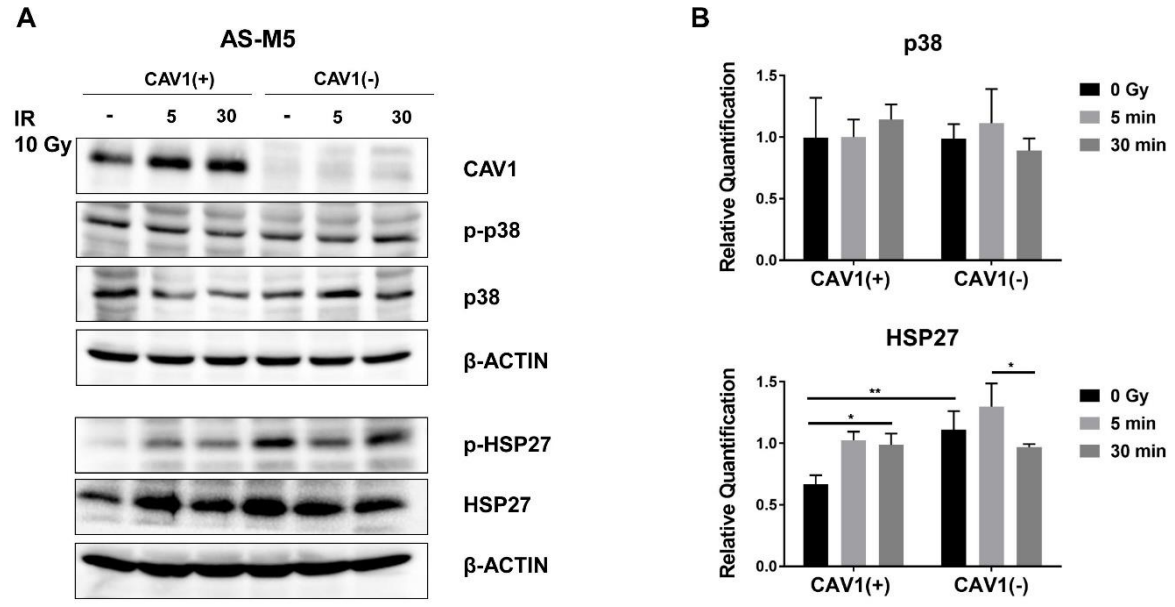

Figure 4

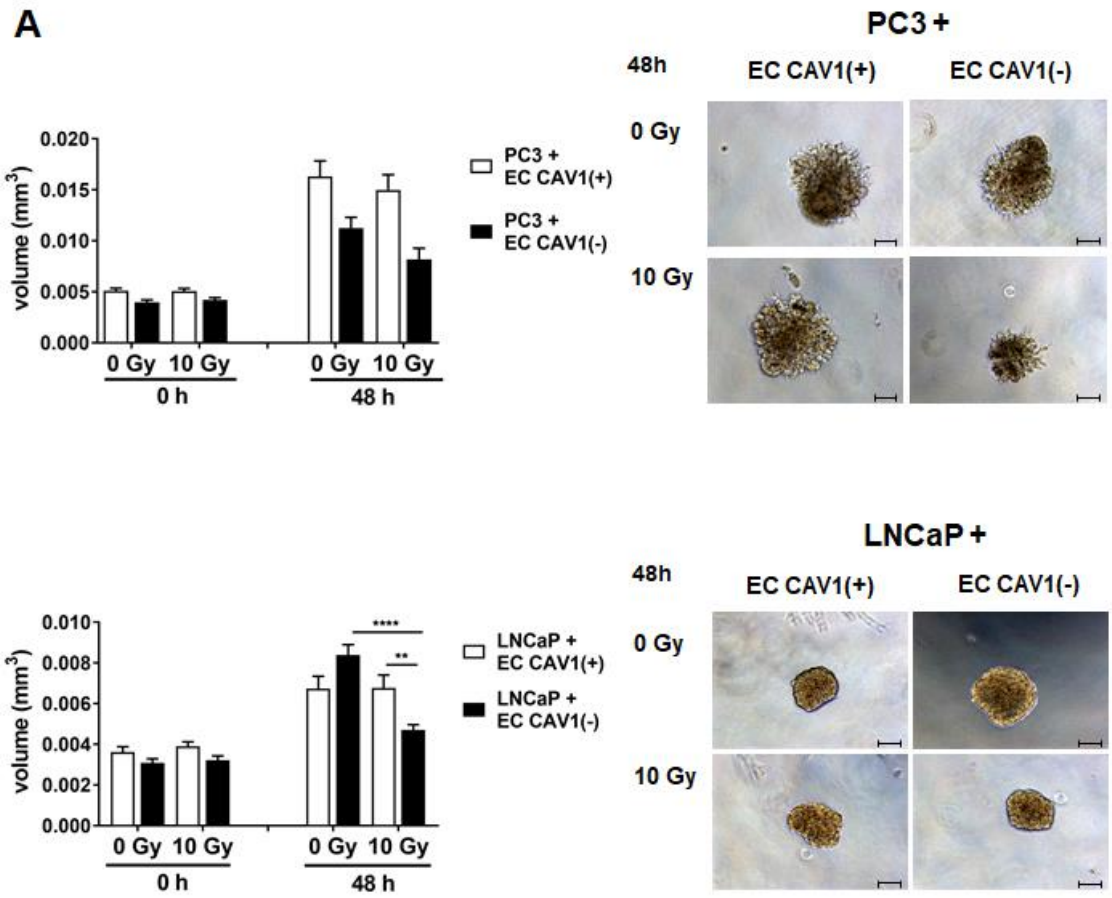
A
PC3 +
48h
EC CAV1(+)
EC CAV1(-)
0 Gy
10 Gy
volume (mm3)
0.020
0.015
0.010
0.005
0.000
PC3 + EC CAV1(+)
PC3 + EC CAV1(-)
0 Gy 10 Gy
0 h
0 Gy 10 Gy
48 h
LNCaP +
48h
EC CAV1(+)
EC CAV1(-)
0 Gy
10 Gy
volume (mm3)
0.010
0.008
0.006
0.004
0.002
0.000
****
**
LNCaP + EC CAV1(+)
LNCaP + EC CAV1(-)
0 Gy 10 Gy
0 h
0 Gy 10 Gy
48 h

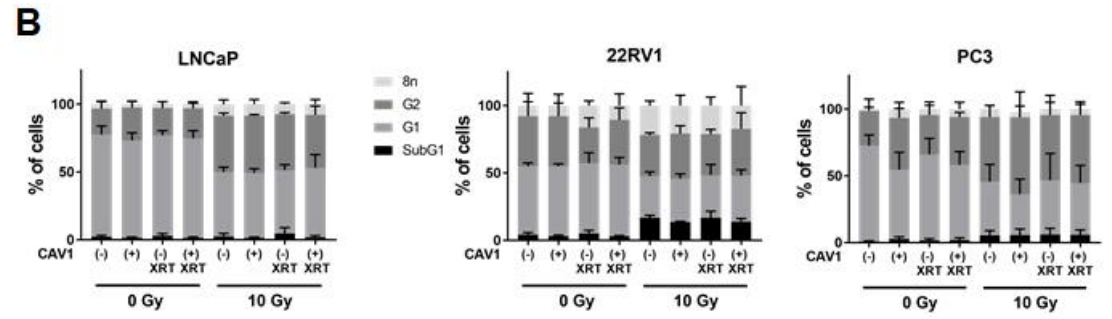
B
LNCaP
22RV1
PC3
% of cells
100
50
0
8n
G2
G1
SubG1
CAV1
(-) (+) (-) XRT (+) XRT
0 Gy
10 Gy

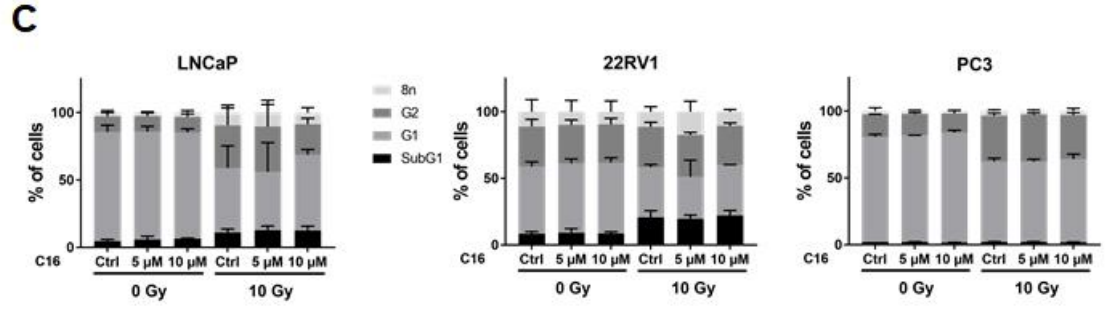
C
LNCaP
22RV1
PC3
% of cells
100
50
0
8n
G2
G1
SubG1
C16
Ctrl 5 µM 10 µM
0 Gy
10 Gy

Figure 5

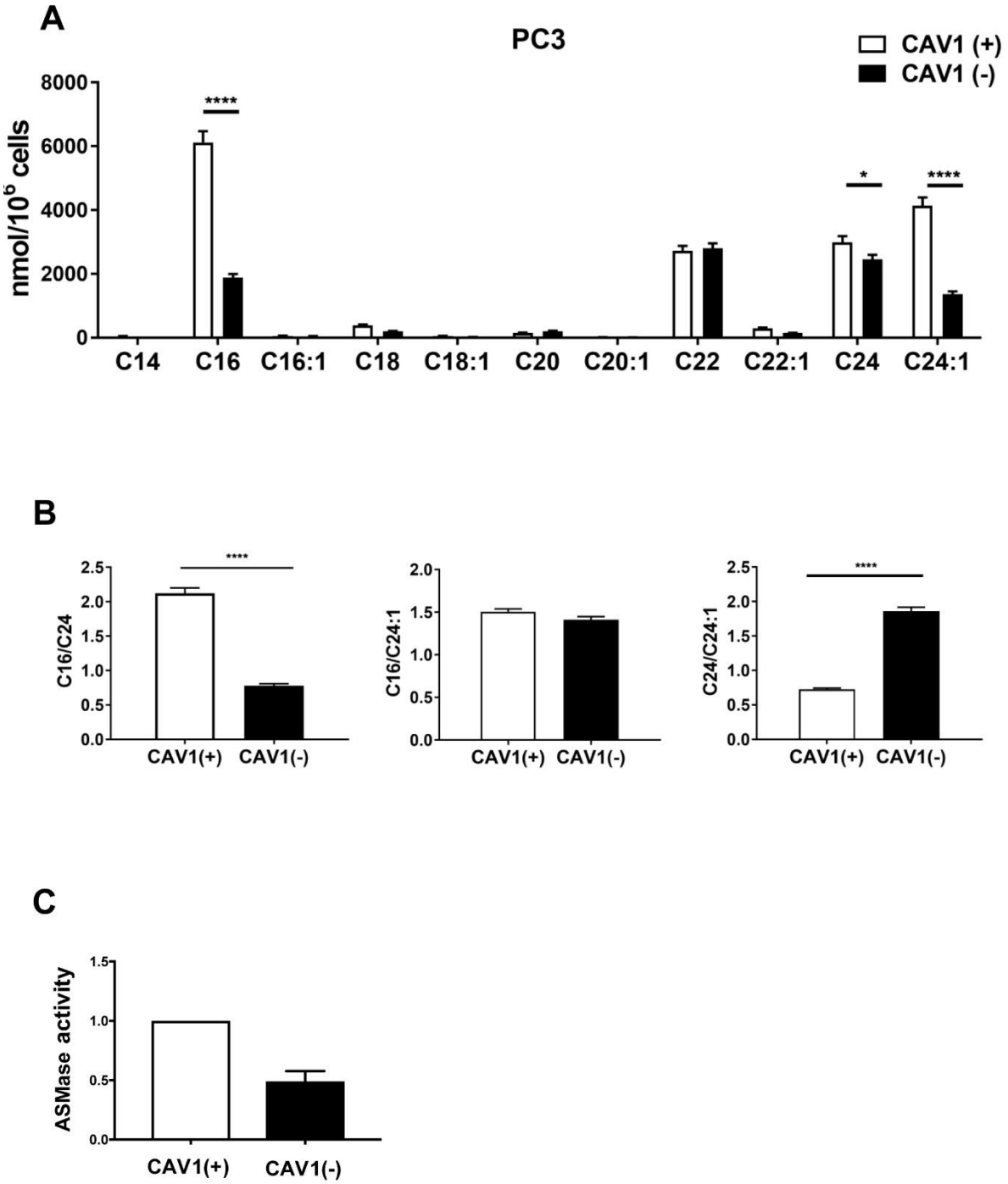
A
PC3
CAV1 (+)
CAV1 (-)
nmol/10^6 cells
8000
6000
4000
2000
0
****
*
****
C14
C16
C16:1
C18
C18:1
C20
C20:1
C22
C22:1
C24
C24:1
B
C16/C24
C16/C24:1
C24/C24:1
CAV1(+)
CAV1(-)
C
ASMase activity
CAV1(+)
CAV1(-)

Figure 6

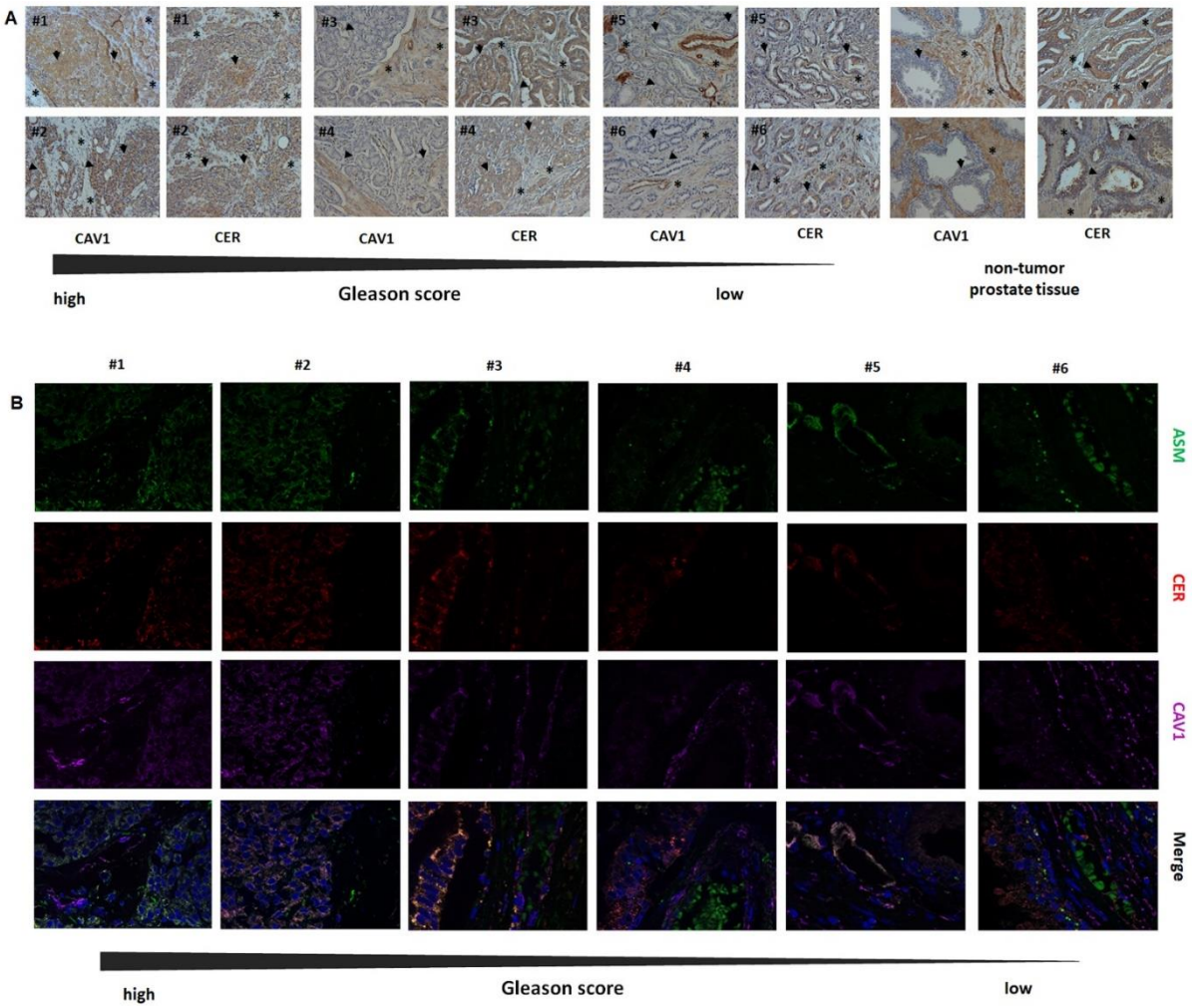

Figure 7

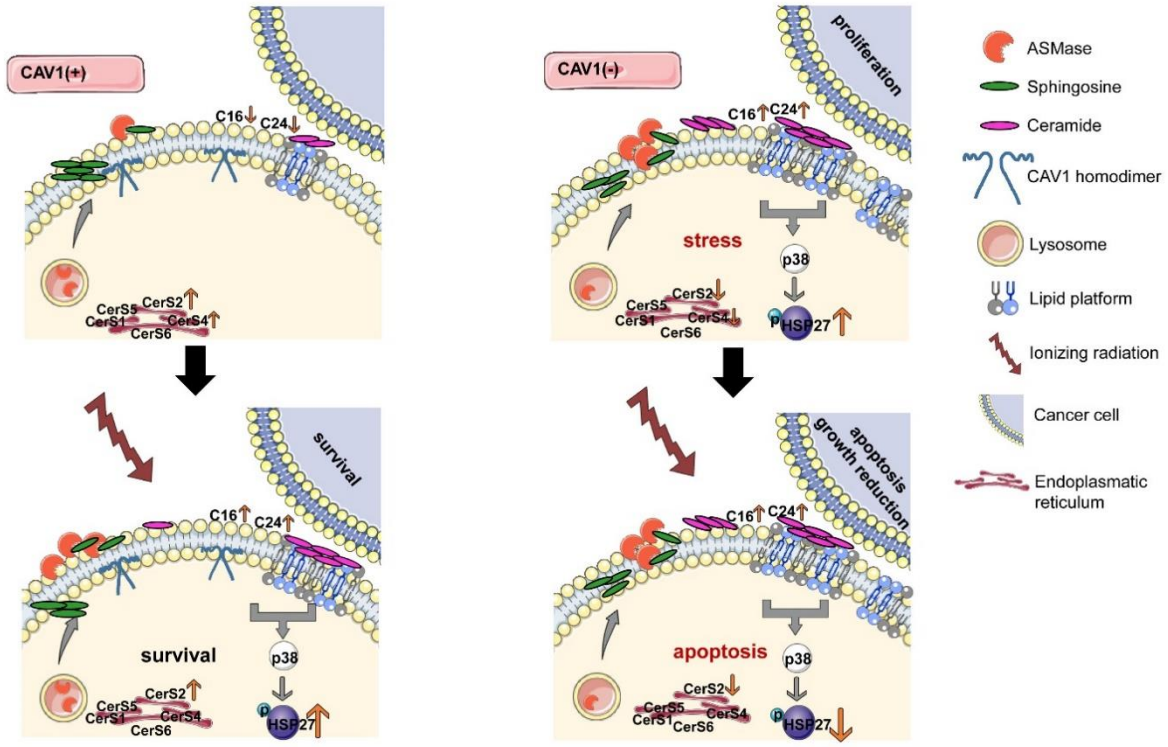

Supplemental Data

Supplemental Figure 1

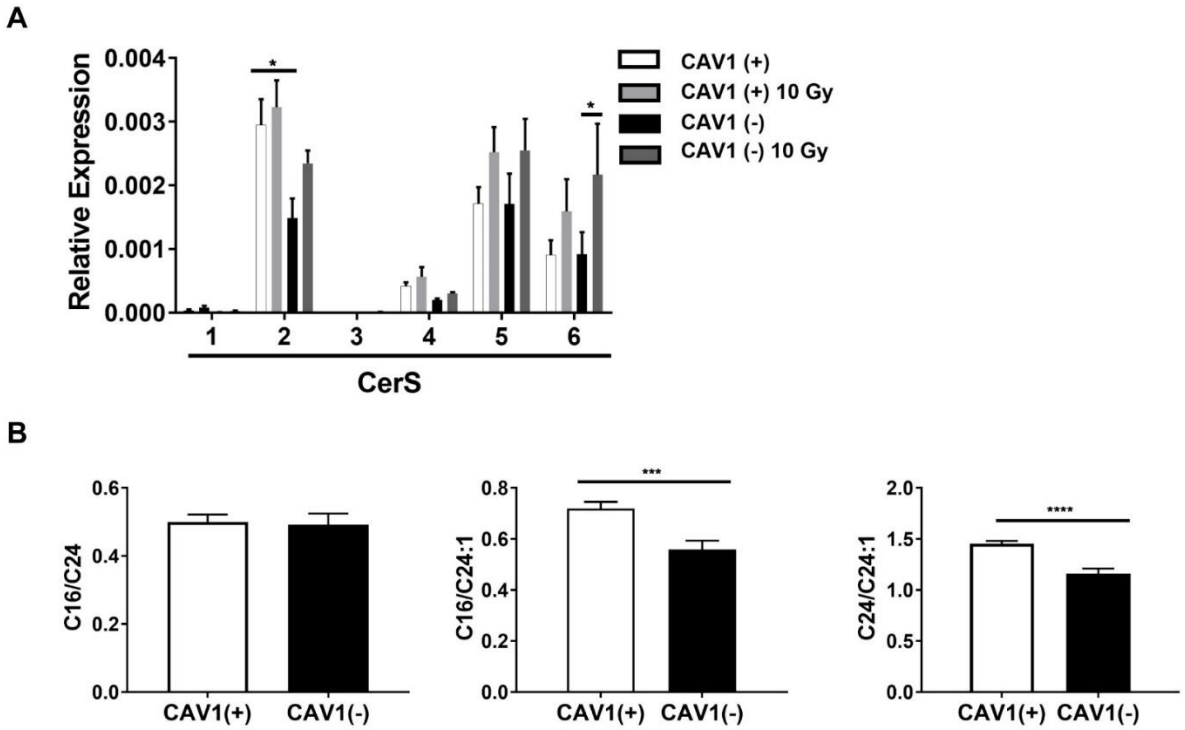

Ceramide is differentially synthesized *de novo* in CAV1 (+) AS-M5 cells. (**A**) RT-qPCR was performed using primers of the six known ceramide synthases (CerS1 – CerS6) in control (0 Gy) and irradiated (10 Gy, 48 h) AS-M5 cells (n=4, SEM). Statistical analysis was done by using two-way ANOVA. P-value indicates * $p<0.05$. (**B**) The ratio of ceramide species C16 to C24, C16 to C24:1 and C24 to C24:1 was calculated in AS-M5 CAV1(+) and CAV1(-) cells. Control levels were pooled out of three individual experiments (n=3, SEM). Statistical significance was calculated with Tukey's student t-test with Welch's correction. P-value indicates *** $p<0.001$, **** $p<0.0001$.

Supplemental Figure S2

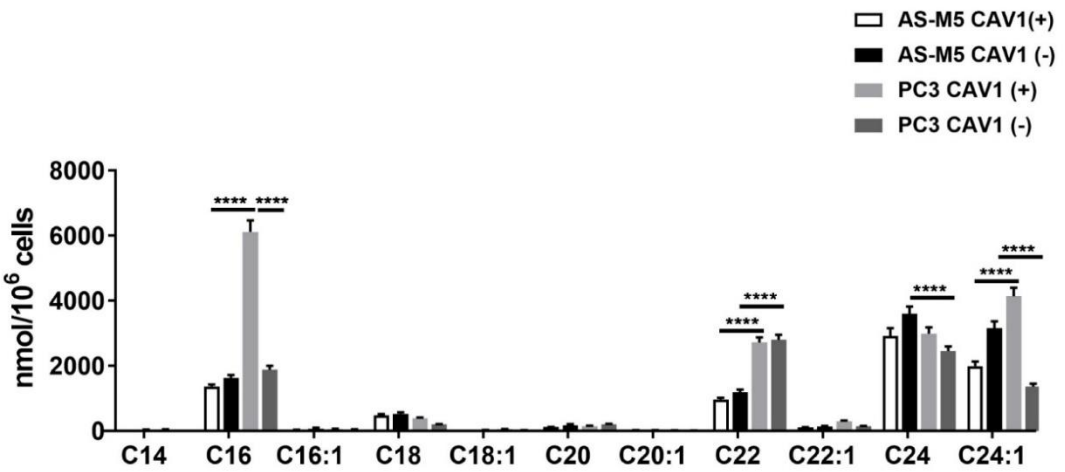

Most prominent ceramide species were significantly higher expressed in radio-resistant CAV1(+) PC3 cells compared to EC. The different ceramide species in CAV1-proficient and –deficient EC and prostate cancer cells were analyzed by LC-MS and compared next to each other. Control levels out of three individual sample sets are shown with SEM. Two-way ANOVA followed by Tukey's test was performed to confirm statistical significance. P-value indicates ****<p 0.0001.

Supplemental Figure S3

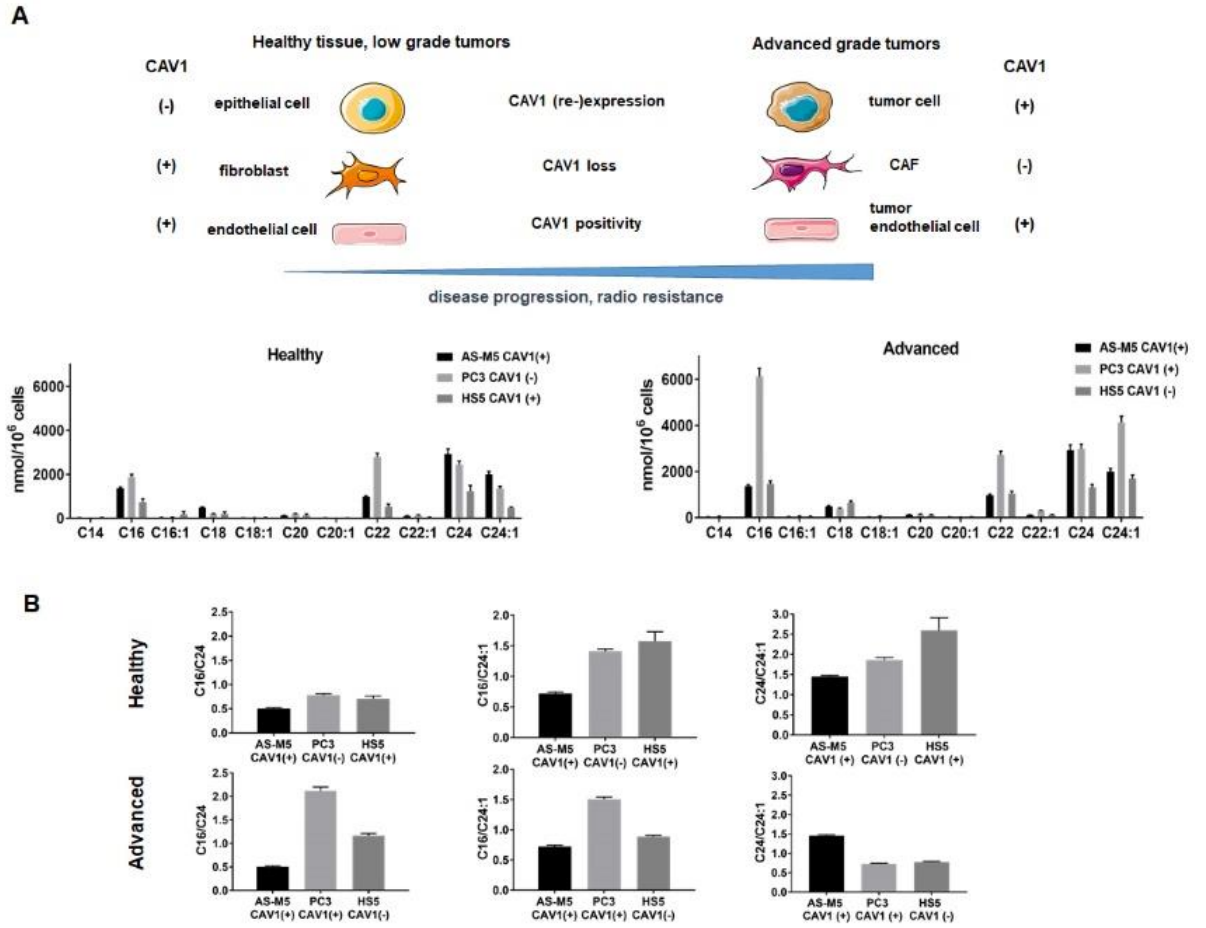

Overall ceramide levels of differential CAV1-expressing tumor and stroma cells in advanced prostate cancer are elevated. (**A**) Ceramide species of the healthy situation or low graded tumor (EC CAV1(+), PC3 CAV1(-) and HS5 CAV1(+)) and cells present in advanced prostate cancer (EC CAV1(+), PC3 CAV1(+) and HS5 CAV1(-)) were analyzed by LC-MS. Levels of three individual experiments are shown with SEM. The schematic overview emphasizes CAV1 levels in stroma and epithelial/tumor cells in each stage. (**B**) Ratios of C16 to C24, C16 to C24:1 and C24 to C24:1 in the healthy and advanced situation of prostate cancer are described. Ratios were taken out of three individual experiments and are shown with SEM.

IR is within the most prominent treatments in cancer therapy, but resistance of aggressive and advanced tumors remains as one of the biggest challenges in cancer treatment. In addition, radiation-induced normal tissue complication limits the application of curative radiation doses needed to control and/or kill all tumor cells. The tumor microenvironment evolved here as an additional important factor influencing tumor progression and therapy resistance. Thus, biological approaches concentrate on the understanding of the intrinsic or acquired resistance of advanced tumors with the aim to identify potential targets finally aiming at radio-sensitizing the tumors. Alternatively, protecting normal tissues from radiation-induced toxicity might potentially result in the use of higher, more efficient radiation doses.

Concerning a potential radio-sensitization of tumors the present thesis (publications 2-4) highlight the impact of the candidate molecule CAV1 in prostate cancer progression and the stroma-epithelial crosstalk of EC and fibroblasts.

A loss of CAV1 in the stromal compartment, namely in fibroblasts significantly impacts prostate cancer progression *in vitro* and *in vivo*. CAV1 downregulation in fibroblasts fostered tumor growth and increased radiation resistance of prostate cancer in xenograft mouse models. Conformingly, supernatant of CAV1-deficient fibroblasts protected cancer cells of IR-induced apoptosis *in vitro* (publication 2). Importantly, one CAV1-dependent secreted factor of fibroblasts was identified, namely the apoptosis inhibiting protein TRIAP1, which caused pronounced radiation resistance in prostate cancer cells *in vitro* and *in vivo* using xenograft tumors (publication 3). TRIAP1 expression levels were further increased in tissue of advanced human prostate cancer specimen, which is characterized by a loss of stromal CAV1 and increased CAV1-expressions in malignant epithelial cells.

The CAV1-dependent pathway operating in stromal cells (EC and fibroblasts) and prostate cancer cells that regulates cellular growth and apoptosis induction upon RT was further specified (publication 4). Previous work in the lab described CAV1-downregulation in ECs as a sensitizing factor for RT (84). Now it could be shown that CAV1 affects/regulates the ASMase/ceramide pathway in EC directly and upon stress induction by RT, which is a major factor mediating vascular dysfunction and regulating EC apoptosis. With respect to the tumor-stroma interactions, stroma e.g. EC-derived apoptotic ceramide, would be a potential option to radio-sensitize prostate cancer cells. Of note, the differential CAV1-expression levels as found in advanced prostate

carcinomas and dependent ceramide species counteract the stromal derived ceramide actions.

Taken together, the present thesis investigated two important aspects of RT: radioprotection of the normal tissue and radio-sensitization of tumors. These studies gained insight in stroma-epithelial crosstalk causing therapy resistance and identify molecular targets to possibly improve the outcome of RT.

6. Discussion

6.1 Radiation-induced Normal Tissue Toxicity

In the present thesis, new insights of radiation-induced normal tissue toxicity and the influence of CAV1-dependent stromal-epithelial crosstalk on RT resistance were given. Radiation-induced EC loss and vascular dysfunction in the lung could be restored by inhibiting the SASP factor CCL2. C57BL/6 WT mice or CCR2-KO mice were treated with whole thorax irradiation (WTI). Here, CCR2-deficiency led to decreased EC loss and associated radiation-induced lung fibrosis. Treatment with the CCL2 specific inhibitor Bindarit (BIN) furthermore decreased CCL2 expression after WTI, stabilized vascular function and reduced seeding of lung metastasis. Thus, CCL2 signaling inhibition is a promising option for vascular protection from IR in the normal tissue.

Normal tissue toxicity is one of the limiting factors of RT and can lead to acute and chronic complications, as well as secondary malignancies of the patient (23). Therefore, protectors or protective signaling of the normal tissue are under current investigations in order to facilitate the application of higher, potentially curative IR doses. Herein, EC play an important role due to their capacity in building up and maintaining the organ's functional (micro-) vascular structure. IR was shown to destroy the homeostatic network of resident parenchymal, mesenchymal and EC. This facilitates infiltration by immune cells and thereby causes acute and/or chronic inflammation (1, 25). Additionally, the function of EC can be affected upon IR treatment due to oxidative stress or altered signaling of tumor cells, as for example secretion of the chemokine CCL2 (8, 36, 86). CCL2 has been shown to be secreted by senescent resident epithelial cells upon irradiations. Part of this thesis concentrated on the inhibition of CCL2 signaling and its impact on the response of resident EC in the normal tissue. Acute and chronic inflammation is especially important in sensitive tissue such as the lung. Therefore, WTI was used in a C57BL/6 mice model. Here, it was shown that inhibition of CCL2 by using the specific inhibitor BIN restored EC morphology and limited metastasis formation in the lung. Apoptosis-dependent EC loss upon IR treatment facilitates a leaky environment and hereby promotes tumor cell migration and extravasation (90). Deficiency in the CCL2 receptor CCR2 resulted in decreased EC loss, lung metastasis and fibrosis formation. Therefore, targeting of SASP factors secreted by senescent epithelial cells could be a potential treatment strategy to prevent

acute and chronic immune cell infiltration that in turn could lead to short and long term effects such as lung fibrosis. Moreover, evidence for pro-tumorigenic properties of CCL2 emerged recently. CCL2 promotes proliferation and metastasis in nasopharyngeal carcinoma and can be used as a prognostic marker in breast and pancreatic cancer to only name a few examples (31, 101, 119, 161). Thus, targeting the CCL2/CCR2 axis could not only protect the normal tissue but has properties to sensitize tumor cells to drug therapy.

Of note, the membrane protein CAV1 was already linked to normal tissue toxicity. Although the work presented in this thesis was independent of CAV1, it was shown before that it also has influence on normal tissue toxicity. Generation of $CAV1^{(-/-)}$ mice was used to define the influence of caveolae and CAV1 on normal tissue. Disruption of the CAV1 gene led to an absence of caveolae in EC and epithelial cells in all organs. Moreover, those animals tend to develop lung fibrosis accompanied by an uncontrolled proliferation of EC (47, 140). Additionally, vascular dysfunction was observed in those mice, linking CAV1 to be an important mediator of EC maintenance and cell proliferation control in lung tissue (47, 140). Further on, CAV1 controls the signaling of eNOS with its CSD and prevents NO production (59). In line, $CAV1^{(-/-)}$ animals showed a decreased vasoconstrictor response leading to physical weakness due to NO overproduction. Moreover, increased NO induces oxidative stress which leads to CAV1 downregulation and reduced palmitoylation in EC (123, 133). Thus, signaling mediated by CAV1 and caveolae trafficking is well known to influence normal tissue response and its targeting could be a potential risk for damaging normal tissue upon treatment by inducing fibrosis and oxidative stress. Future work of the group will address how a differential CAV1 regulation affects normal tissue toxicity and particularly, how CAV1 is regulated in EC upon radiation and if this can be linked to the radiation-induced dysfunction and EC loss observed in the present studies.

6.2 Impact of CAV1 on Stromal-Epithelial Crosstalk

Various solid human tumors are characterized by an overexpression of CAV1 and CAV1 was shown to be decisive for chemo- and RT resistance (83). Thus, CAV1 downregulation was thought to be a potential mediator for increasing radio-sensitivity of tumors (10, 35, 70). But recent studies showed that the tumor microenvironment has to be taken into account as well. The role of stromal cells in tumor progression and

response to therapy has been investigated thoroughly but a deeper understanding of mechanisms of action is critical to reduce tumor therapy resistance. CAV1-dependent regulations of tumor-stroma interactions could be linked to alterations in therapy response before and it has been suggested as a potential therapeutic target to improve therapy outcome (35, 70, 71, 84). However, part of this thesis demonstrated that there is a potential risk of targeting CAV1 to sensitize tumors to therapy. Although, CAV1(-) PC3 cells showed decreased clonogenic survival upon IR *in vitro*, xenograft and orthotopical implanted tumors derived from PC3 CAV1(-) cells displayed increased tumor growth and RT resistance (publication 2). These tumors were accompanied by an elevated reactive tumor stroma and a CAV1 (re-)expression in malignant epithelial cells. Similar findings were detected in mice with a CAV1-deficient background. Tumors derived of MPR31-4 prostate cancer cells grew significantly faster in CAV1$^{(-/-)}$ mice (84). Based on those findings, a closer look on a modulator of radiation resistance that too has an impact on stromal-epithelial crosstalk was taken: CAV1. It was previously described in the lab, that CAV1 content influences EC radiation sensitivity and a CAV1-deficient background favors tumor growth *in vivo*. Therefore, investigating how the loss of CAV1 in tumor stroma affects the radiation response was the next step to unravel another part of the stromal-epithelial crosstalk.

Here, it was shown that loss of CAV1 in HS5 fibroblasts increased radiation resistance and tumor growth in a direct manner and therefore mediated radiation resistance of prostate cancer xenografts. Moreover, a paracrine secretion of CAV1(-) fibroblasts was sufficient to protect prostate cancer cells *in vitro*. Additionally, those fibroblasts showed increased expression levels of CAF markers, such as TGF-β and α-SMA. *Ex vivo* analysis of prostate tumor tissue revealed a more reactive tumor stroma correlating with decreased CAV1 expression in fibroblasts of advanced prostate tumor samples. Of note, TRIAP1 (TP-53 regulated inhibitor of apoptosis 1) as a CAV1-dependent secreted factor of fibroblasts was identified and thus is a potential mediator of the previously described radiation resistance. TRIAP1 was shown to be highly expressed in CAV1-downregulated fibroblasts and most important it was secreted exclusively by those. Additionally, prostate cancer xenograft models of NMRI nude mice revealed increased radiation resistance when implanted with TRIAP1 overexpressing fibroblasts. Finally, histologic staining of TRIAP1 was elevated in advanced human prostate cancer tissues.

In line with these results, tumor growth of implanted Lewis-lung carcinoma cells was exceeded as well in CAV1$^{(-/-)}$ mice, compared to WT (103). Thus, there is a potential risk of targeting CAV1 to improve the outcome of therapy. However, since CAV1 secretion of prostate cancer cells was shown to be linked to increased cell growth and angiogenesis, attempts of blocking CAV1 secretion by using polyclonal antibodies were promising (91, 168, 175) and inhibition of CAV1-secretion impaired tumor cell growth. Nevertheless, results of the present thesis and others show that a CAV1-deficient tumor stroma contributes to therapy resistance (17, 18, 83). Prostate tumor xenografts implanted with CAV1-downregulated HS5 fibroblasts were characterized by increased tumor growth and significantly higher resistance to IR, as well as an elevated activated tumor stroma. Furthermore, CAV1 levels in tumors derived of PC3 (-) HS5 (-) were significantly increased after single radiation treatment. Analysis of the tumors revealed an increased proliferation and survival signaling by elevated levels of CyclinD1 and AKT after IR. Those results were confirmed by increased CAV1 and transgelin expression in high Gleason Score human prostate tumor tissues. Therefore, it was clearly shown that loss of CAV1 in stromal cells regulates stromal-epithelial crosstalk by (re-)expression of CAV1 in malignant epithelial cells having an impact on tumor progression and therapy resistance. Of note, as described beforehand, a switch of CAV1 expression from benign to advanced prostate cancer occurs in epithelial cells (from CAV1(-) to CAV1(+)) and fibroblasts of the tumor microenvironment (from CAV1(+) to CAV1(-)). Thus, importance of the critical shift of CAV1 expression alterations in the tumor stroma and epithelial cells has to be evaluated and prevention could be used as a potential target fostering therapy sensitivity.

Mechanistically, degradation of CAV1 in fibroblasts is mediated by lysosomes (109). There is evidence, that lysosomal degradation is mediated of cancer cells themselves or via induction of oxidative stress in their microenvironment. Moreover, this seems to be a critical step for the induction of a CAF phenotype (110, 156). Herein, studies showed that loss of CAV1 in the tumor stroma could be used as a prognostic marker for autophagy and oxidative stress (155). Lysosomal degradation of CAV1 in fibroblasts can be successfully counteracted by using lysosome inhibitors (109). Moreover, not only the loss of CAV1 in tumor stroma is important but also the mechanism behind the (re-)expression of CAV1 in malignant epithelial cells has to be unraveled. CAV1 expression is either upregulated by a direct transfer between cells or by CAV1-expression regulating proteins. Results of the present thesis show that there

are junctions formed between CAV1-deficient LNCaP cells and HS5 CAV1(+) fibroblasts, where CAV1 proteins are involved and/or transferred as revealed by immunofluorescent analysis. LNCaP cells close to CAV1(+) fibroblasts also expressed CAV1 upon IR treatment *in vitro*. Therefore, it was speculated or seems likely that CAV1 transfer and the respective content could be facilitated due to the fusion as extracellular vesicles or exosomes derived from adjacent fibroblasts. Exosomes secreted by the tumor microenvironment and tumor cells itself have been shown to play an important role in tumor progression and metastasis (6, 136). Recently, cSRC - a CAV1 related molecule - has been identified to be packed in exosomes released by prostate cancer cells (40). cSRC is an important mediator of CAV1 Y14 phosphorylation, but also CAV1 itself binds SRC protein and inhibits the enzyme's basal activity (95, 96). Here, it was shown that radio-resistant tumors of xenograft models displayed elevated SRC levels, which in turn affect the more IR resistant phenotype and tumor progression because SRC is known as a pro-proliferative protein. Constitutive activation of SRC is associated with transformation of normal cells (167). Together with its direct interaction partner focal adhesion kinase (FAK), it was shown to promote invasion and migration (171). Moreover, also CAV1 itself was identified as content of extracellular vesicles in breast cancer cells. Extracellular vesicles containing CAV1 were taken up by cells lacking CAV1 expression. The uptake subsequently led to migration and invasion of those cells (26). Further on, it has been shown that prostate cancer cell lines secrete vesicles containing CAV1 that can affect tumor cells, EC and fibroblasts in the microenvironment to promote invasion and metastasis formation (44). Therefore, targeting the formation, release or uptake of extracellular vesicles containing CAV1 or CAV1-expression regulating proteins could be one possible option to prevent the critical CAV1 switch in advanced cancer cells and the tumor microenvironment.

6.3 CAV1-dependent Signaling in Fibroblasts of the Tumor Microenvironment

Transformed and activated fibroblasts lacking CAV1 have been correlated with more aggressive disease and increased therapy resistance in various types of cancer (83). Therefore, we aimed to identify CAV1-dependent secreted factors of fibroblasts that are able to modulate therapy resistance within the tumor. One of the hallmarks of cancer is the escape from apoptosis induction (64). Therefore, well-known proteins

involved in apoptosis were investigated in a CAV1-dependent manner. The apoptosis inhibitor TRIAP1 was identified (publication 3) as a factor that is mainly secreted by CAV1-deficient HS5 fibroblasts and its overexpression in fibroblasts mediated radiation resistance in *in vitro* and *in vivo* models. Several mechanisms of CAF-mediated tumor promotion have been reported, wherein autophagy, senescence and oxidative metabolic changes were pointed out. The results of this thesis add more evidence for regulation of apoptosis to those hallmarks of cancer and its surrounding microenvironment mediated in part by CAFs. TRIAP1, also known as p53CSV, has recently been identified as a new member of the inhibitor of apoptosis (IAP) family (127). TRIAP1 is directly activated by p53 upon genotoxic stress and DNA damage induction and therefore part of the p53-dependent cell survival pathway. It can then bind to HSP70 which consequently binds apoptotic protease activating factor 1 (APAF1) and thereby inhibits Caspase-9 activation (127). Moreover, TRIAP1 has been identified as a pathway-specific regulator of p53-activation (3). It is upregulated in ovarian and nasopharyngeal cancer, as well as multiple myeloma cell lines and silencing of TRIAP1 leads to elevated apoptosis levels in these cells (55, 97, 106). However, until today there is not much known about this protein and only few publications highlight its influence on cell survival. As an apoptosis inhibitor it is likely to have an impact on tumor cell survival and therapy resistance and could therefore be a possible target to sensitize tumors to RT. Here, it was shown that advanced prostate cancer tissue samples displayed increased TRIAP1 expression levels which could indicate radiation resistance mediated by CAV1-dependent secretion of stromal cells. However, the mechanism behind the secretion and whether TRIAP1 is transported in vesicles remains elusive.

Downregulation of CAV1 in transforming fibroblasts is mediated by lysosomal degradation. Results of this thesis show, that upon IR CAV1 expression levels decreased in CAV1(+) HS5 fibroblasts which could be associated with an induction of phenotype transformation. Of note, DNA-damaging chemotherapeutic agents were found to induce DRAM (damage-regulated autophagy mediator) which in turn mediated autophagy and CAV1 degradation via lysosomes (38, 111). This could explain the observations after IR induced DNA damage and the subsequent decrease of CAV1 in the fibroblasts model. Moreover, lysosomal endocytosis and secretion of required proteins, such as ASMase, ASA and LAMP2 was enhanced in CAV1(-) fibroblasts pointing to a possible transfer supporting autophagy/lysosomal activity in cancer cells. This has been shown to promote aggressiveness and cancer progression

(173, 176). Autophagy induction was also associated with tumor cells evading apoptosis, which could have supported the tumor-promoting and radiation resistant phenotype of the prostate cancer xenograft model (173). Of note, other lysosomal related proteases, the family of cathepsins, have been linked to CAV1 expression and tumor progression. Cathepsin B was located at caveolae in colorectal carcinoma cells in a CAV1 dependent manner and was associated with invasion (29). Cathepsin D and L were also already associated with cancer progression and metastasis in ovarian and breast cancer and might be a possible CAV1-dependent factor localized in caveolae (45, 135). Conclusively, CAV1-dependent factors secreted by fibroblasts either by lysosomal exocytosis or exosomes are promising targets for therapeutically approaches to inhibit the characteristic stromal-epithelial CAV1 shift upon prostate cancer progression that is supposed to account for RT resistance.

6.4 CAV1-dependent Signaling in EC

As already stated, EC play an important role for tumor formation and growth because of their ability to build up the vasculature for oxygen and nutrient supply of the tumor. Moreover, vascular leakage due to EC loss facilitates invasion and metastasis. It has been shown that CAV1 expression influences several pathways and mediates radiation resistance of EC. According to those results, a CAV1-dependent pathway influencing EC radiation outcome was aimed to be unraveled, to paint a broader picture of stromal-epithelial crosstalk in advanced prostate carcinoma. Therefore, a pathway that takes part in the plasma membrane and is likely to be influenced by CAV1 expression was addressed. The ASMase/ceramide pathway is known to be particularly active in EC and likely enough CAV1 expression affected the pathway in a direct manner, as well as in a radiation-dependent manner. ASMase activity was increased in the radio-sensitive CAV1-downregulated EC, which was in line with an elevated ceramide generation and formation of large lipid platforms. Moreover, a direct interaction of CAV1-downregulated EC with prostate cancer cells resulted in decreased growth of spheroids after IR, pointing to enhanced cell apoptosis and/or impaired growth capacities. CAV1-downregulation in the EC line AS-M5 resulted in increased apoptosis levels and decreased clonogenic survival upon IR treatment (84). This was accompanied by a less stabilized vasculature in prostate cancer xenograft models grown in CAV1$^{(-/-)}$ mice. However, the mechanism of CAV1-dependent apoptosis induction remained elusive. In the present thesis, the ASMase/ceramide

pathway was shown to be regulated in part by CAV1 expression in AS-M5 EC. CAV1 affected the pathway in a basal and stress-induced manner. CAV1 downregulation led to an increased ASMase enzymatic activity, ceramide generation and formation of large lipid platforms. Moreover, treatment with IR induced a stabilization of ceramide generation that affected signaling and could be linked to elevated apoptosis induction through the p38/MAPK pathway (118). Niaudet et al. recently described impaired p38-dependent AKT signaling in EC after IR treatment leading to apoptosis induction (118). However, it was also shown here that CAV1 affects *de novo*-synthesis of ceramide next to the sphingomyelin-dependent pathway. The effects of different ceramide species on cell processes have been evaluated extensively, but until today many species-dependent processes remain elusive. The ceramide species C18, for example, was associated with cancer cell apoptosis upon chemotherapeutic treatment (9), whereas C16 expression could be connected to tumor progression in head and neck squamous cell carcinoma (HNSCC) (80, 151). There are many open questions about the influence of ceramide in cancer treatment and more research is needed to unravel the specific processes. However, it was shown here that CAV1-dependent ceramide increase in EC of the tumor microenvironment upon IR leads to impaired growth and presumably increased apoptosis in culture with prostate cancer cells *in vitro*. Moreover, it was demonstrated that CAV1-dependent ASMase/ceramide signaling seems to be cell type specific.

CAV1 expression in EC could also be linked to increased effectiveness of chemotherapeutic agent gemcitabine in pancreatic adenocarcinoma (22). Herein, treatment with gemcitabine led to elevated levels of CAV1 in EC which facilitated transport of a combinational chemotherapeutic to the cancer cells (22). This study highlights that also CAV1 expression levels and therapy outcome in EC are dependent of tumor type and stage. Here, it was shown that radio-resistant CAV1(+) PC3 cells expressed high levels of very-long-chain ceramides C24 and C24:1. Those very-long-chain ceramides and the ratio were already associated with delayed apoptosis induction, whereas a shift to shorter ceramide species (C16) increased the sensitivity of cells to apoptosis (52, 149). Additionally, very-long-chain ceramides were shown to scavenge the apoptosis-inducing effect of exogenous or stroma secreted C16 ceramide (19). Therefore, C16 ceramide that is potentially secreted by EC of the tumor microenvironment is scavenged by the high levels of C24 and C24:1 in the radio-resistant CAV1(+) cancer cells.

The initial idea was to downregulate EC CAV1 expression to improve IR response but the tumor stroma, in particular CAV1-deficient fibroblasts/CAFs have to be critically reviewed due to their tumor and resistance promoting effects. Therefore, a simple CAV1 targeting is not a therapeutic option. Conclusively, the present data gained insight into how differential CAV1 expression levels result in the observed differences in the RT response (Figure 5). The C16-induced p38-related apoptosis induction might be counteracted by a differential ceramide synthase (CerS) synthesis. The ratio of the most prominent ceramide species C16, C24 and C24:1 seems to be important and dependent on ASMase activity and *de novo* synthesis by CerS. Therefore, increasing C16, either exogenously added or endogenously elevated, could be a promising therapeutic option to (re-)sensitize advanced prostate tumors to IR.

Finally, to unravel the link between CAV1 and normal tissue toxicity, the CAV1-dependent ceramide signaling will be investigated in normal tissues by using EC and normal epithelial cells in future work.

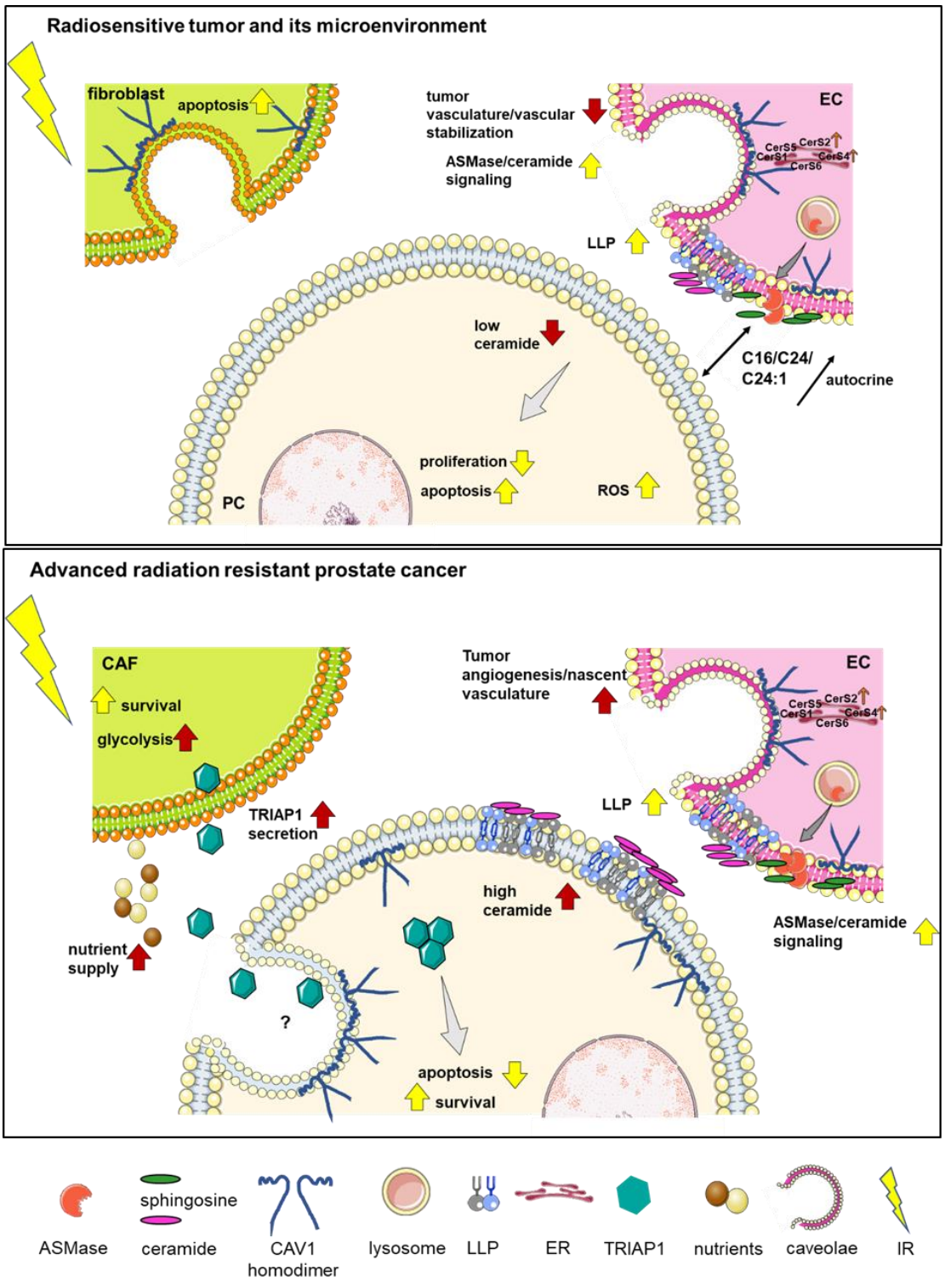

Figure 5: Scheme of the present findings about the stromal-epithelial crosstalk in the radio-sensitive (up) and radio-resistant (down) CAV1-distributions of prostate cancer. Upper panel: Radio-sensitive or low-grade prostate cancers show a positive immunoreactivity of EC (CAV1(+) EC), CAV1(+) fibroblasts and CAV1(-) cancer cells. Fibroblast and cancer cells are more apoptosis prone upon IR. With respect to the advanced situation (below) a “simple” downregulation (as favor for PC3 and EC) seems not to be a good therapeutic option. Lower panel: Advanced and radio-resistant prostate cancers were characterized by a prominent switch of CAV1 expression: CAV1(+) EC, CAV1(-) fibroblasts/CAFs, CAV1(+) cancer cells. This switch is associated with increased expression/secretion of the anti-apoptotic TRIAP1, which subsequently protects malignant prostate cells from IR-induced apoptosis. Furthermore, CAFs supply tumor cells with nutrients such as lactate or pyruvate. Moreover, the increased C16/C24:1 ratio in prostate cancer cells and EC presumably rescues the tumor from C16-induced apoptosis signaling.

7. References

1 Almeida C, Nagarajan D, Tian J, Leal SW, Wheeler K, Munley M, Blackstock W, Zhao W. The role of alveolar epithelium in radiation-induced lung injury. PLoS One 2013; 8: e53628.

2 Ando T, Ishiguro H, Kimura M, Mitsui A, Mori Y, Sugito N, Tomoda K, Mori R, Harada K, Katada T, Ogawa R, Fujii Y, Kuwabara Y. The overexpression of caveolin-1 and caveolin-2 correlates with a poor prognosis and tumor progression in esophageal squamous cell carcinoma. Oncol Rep 2007; 18: 601-609.

3 Andrysik Z, Kim J, Tan AC, Espinosa JM. A genetic screen identifies TCF3/E2A and TRIAP1 as pathway-specific regulators of the cellular response to p53 activation. Cell Rep 2013; 3: 1346-1354.

4 Anscher MS, Chen L, Rabbani Z, Kang S, Larrier N, Huang H, Samulski TV, Dewhirst MW, Brizel DM, Folz RJ, Vujaskovic Z. Recent progress in defining mechanisms and potential targets for prevention of normal tissue injury after radiation therapy. Int J Radiat Oncol Biol Phys 2005; 62: 255-259.

5 Ayala G, Morello M, Frolov A, You S, Li R, Rosati F, Bartolucci G, Danza G, Adam RM, Thompson TC, Lisanti MP, Freeman MR, Vizio DD. Loss of caveolin-1 in prostate cancer stroma correlates with reduced relapse-free survival and is functionally relevant to tumour progression. J Pathol 2013; 231: 77-87.

6 Azmi AS, Bao B, Sarkar FH. Exosomes in cancer development, metastasis, and drug resistance: a comprehensive review. Cancer Metastasis Rev 2013; 32: 623-642.

7 Bailar JC, 3rd, Mellinger GT, Gleason DF. Survival rates of patients with prostatic cancer, tumor stage, and differentiation--preliminary report. Cancer Chemother Rep 1966; 50: 129-136.

8 Baker DG, Krochak RJ. The response of the microvascular system to radiation: a review. Cancer Invest 1989; 7: 287-294.

9 Baran Y, Salas A, Senkal CE, Gunduz U, Bielawski J, Obeid LM, Ogretmen B. Alterations of ceramide/sphingosine 1-phosphate rheostat involved in the regulation of resistance to imatinib-induced apoptosis in K562 human chronic myeloid leukemia cells. J Biol Chem 2007; 282: 10922-10934.

10 Barzan D, Maier P, Zeller WJ, Wenz F, Herskind C. Overexpression of caveolin-1 in lymphoblastoid TK6 cells enhances proliferation after irradiation with clinically relevant doses. Strahlenther Onkol 2010; 186: 99-106.

11 Baskar R, Lee KA, Yeo R, Yeoh KW. Cancer and radiation therapy: current advances and future directions. Int J Med Sci 2012; 9: 193-199.

12 Baudrand R, Gupta N, Garza AE, Vaidya A, Leopold JA, Hopkins PN, Jeunemaitre X, Ferri C, Romero JR, Williams J, Loscalzo J, Adler GK, Williams GH, Pojoga LH. Caveolin 1 Modulates Aldosterone-Mediated Pathways of Glucose and Lipid Homeostasis. J Am Heart Assoc 2016; 5.

13 Begg AC, Stewart FA, Vens C. Strategies to improve radiotherapy with targeted drugs. Nat Rev Cancer 2011; 11: 239-253.

14 Bentzen SM. Preventing or reducing late side effects of radiation therapy: radiobiology meets molecular pathology. Nat Rev Cancer 2006; 6: 702-713.

15 Bhide SA, Nutting CM. Recent advances in radiotherapy. BMC Med 2010; 8: 25.

16 Bhowmick NA, Neilson EG, Moses HL. Stromal fibroblasts in cancer initiation and progression. Nature 2004; 432: 332-337.

17 Bissell MJ, Hines WC. Why don't we get more cancer? A proposed role of the microenvironment in restraining cancer progression. Nat Med 2011; 17: 320-329.

18 Bissell MJ. Thinking in three dimensions: discovering reciprocal signaling between the extracellular matrix and nucleus and the wisdom of microenvironment and tissue architecture. Mol Biol Cell 2016; 27: 3205-3209.

19 Blaess M, Le HP, Claus RA, Kohl M, Deigner HP. Stereospecific induction of apoptosis in tumor cells via endogenous C16-ceramide and distinct transcripts. Cell Death Discov 2015; 1: 15013.
20 Bonnaud S, Niaudet C, Legoux F, Corre I, Delpon G, Saulquin X, Fuks Z, Gaugler MH, Kolesnick R, Paris F. Sphingosine-1-phosphate activates the AKT pathway to protect small intestines from radiation-induced endothelial apoptosis. Cancer Res 2010; 70: 9905-9915.
21 Bonuccelli G, Casimiro MC, Sotgia F, Wang C, Liu M, Katiyar S, Zhou J, Dew E, Capozza F, Daumer KM, Minetti C, Milliman JN, Alpy F, Rio MC, Tomasetto C, Mercier I, Flomenberg N, Frank PG, Pestell RG, Lisanti MP. Caveolin-1 (P132L), a common breast cancer mutation, confers mammary cell invasiveness and defines a novel stem cell/metastasis-associated gene signature. Am J Pathol 2009; 174: 1650-1662.
22 Borsoi C, Leonard F, Lee Y, Zaid M, Elganainy D, Alexander JF, Kai M, Liu YT, Kang Y, Liu X, Koay EJ, Ferrari M, Godin B, Yokoi K. Gemcitabine enhances the transport of nanovector-albumin-bound paclitaxel in gemcitabine-resistant pancreatic ductal adenocarcinoma. Cancer Lett 2017; 403: 296-304.
23 Braunstein S, Nakamura JL. Radiotherapy-induced malignancies: review of clinical features, pathobiology, and evolving approaches for mitigating risk. Front Oncol 2013; 3: 73.
24 Bray F, Ferlay J, Soerjomataram I, Siegel RL, Torre LA, Jemal A. Global cancer statistics 2018: GLOBOCAN estimates of incidence and mortality worldwide for 36 cancers in 185 countries. CA Cancer J Clin 2018; 68: 394-424.
25 Brush J, Lipnick SL, Phillips T, Sitko J, McDonald JT, McBride WH. Molecular mechanisms of late normal tissue injury. Semin Radiat Oncol 2007; 17: 121-130.
26 Campos A, Salomon C, Bustos R, Diaz J, Martinez S, Silva V, Reyes C, Diaz-Valdivia N, Varas-Godoy M, Lobos-Gonzalez L, Quest AF. Caveolin-1-containing extracellular vesicles transport adhesion proteins and promote malignancy in breast cancer cell lines. Nanomedicine (Lond) 2018; 13: 2597-2609.
27 Carmeliet P, Jain RK. Molecular mechanisms and clinical applications of angiogenesis. Nature 2011; 473: 298-307.
28 Cassoni P, Senetta R, Castellano I, Ortolan E, Bosco M, Magnani I, Ducati A. Caveolin-1 expression is variably displayed in astroglial-derived tumors and absent in oligodendrogliomas: concrete premises for a new reliable diagnostic marker in gliomas. Am J Surg Pathol 2007; 31: 760-769.
29 Cavallo-Medved D, Mai J, Dosescu J, Sameni M, Sloane BF. Caveolin-1 mediates the expression and localization of cathepsin B, pro-urokinase plasminogen activator and their cell-surface receptors in human colorectal carcinoma cells. J Cell Sci 2005; 118: 1493-1503.
30 Cerezo A, Guadamillas MC, Goetz JG, Sanchez-Perales S, Klein E, Assoian RK, del Pozo MA. The absence of caveolin-1 increases proliferation and anchorage-independent growth by a Rac-dependent, Erk-independent mechanism. Mol Cell Biol 2009; 29: 5046-5059.
31 Chen CH, Su LJ, Tsai HT, Hwang CF. ELF-1 expression in nasopharyngeal carcinoma facilitates proliferation and metastasis of cancer cells via modulation of CCL2/CCR2 signaling. Cancer Manag Res 2019; 11: 5243-5254.
32 Cheng ZJ, Singh RD, Marks DL, Pagano RE. Membrane microdomains, caveolae, and caveolar endocytosis of sphingolipids. Mol Membr Biol 2006; 23: 101-110.
33 Cho DS, Yim H, Cho KS, Hong SJ, Cho NH, Kim SI, Ahn HS, Kim SJ. Impact of caveolin-1 expression on the prognosis of transitional cell carcinoma of the upper urinary tract. J Korean Med Sci 2008; 23: 296-301.
34 Chung AS, Ferrara N. Developmental and pathological angiogenesis. Annu Rev Cell Dev Biol 2011; 27: 563-584.

35 Cordes N, Frick S, Brunner TB, Pilarsky C, Grutzmann R, Sipos B, Kloppel G, McKenna WG, Bernhard EJ. Human pancreatic tumor cells are sensitized to ionizing radiation by knockdown of caveolin-1. Oncogene 2007; 26: 6851-6862.
36 Corre I, Guillonneau M, Paris F. Membrane signaling induced by high doses of ionizing radiation in the endothelial compartment. Relevance in radiation toxicity. Int J Mol Sci 2013; 14: 22678-22696.
37 Couet J, Li S, Okamoto T, Ikezu T, Lisanti MP. Identification of peptide and protein ligands for the caveolin-scaffolding domain. Implications for the interaction of caveolin with caveolae-associated proteins. J Biol Chem 1997; 272: 6525-6533.
38 Crighton D, Wilkinson S, O'Prey J, Syed N, Smith P, Harrison PR, Gasco M, Garrone O, Crook T, Ryan KM. DRAM, a p53-induced modulator of autophagy, is critical for apoptosis. Cell 2006; 126: 121-134.
39 Delaney G, Jacob S, Featherstone C, Barton M. The role of radiotherapy in cancer treatment: estimating optimal utilization from a review of evidence-based clinical guidelines. Cancer 2005; 104: 1129-1137.
40 DeRita RM, Zerlanko B, Singh A, Lu H, Iozzo RV, Benovic JL, Languino LR. c-Src, Insulin-Like Growth Factor I Receptor, G-Protein-Coupled Receptor Kinases and Focal Adhesion Kinase are Enriched Into Prostate Cancer Cell Exosomes. J Cell Biochem 2017; 118: 66-73.
41 Deshmane SL, Kremlev S, Amini S, Sawaya BE. Monocyte chemoattractant protein-1 (MCP-1): an overview. J Interferon Cytokine Res 2009; 29: 313-326.
42 Dewever J, Frerart F, Bouzin C, Baudelet C, Ansiaux R, Sonveaux P, Gallez B, Dessy C, Feron O. Caveolin-1 is critical for the maturation of tumor blood vessels through the regulation of both endothelial tube formation and mural cell recruitment. Am J Pathol 2007; 171: 1619-1628.
43 Di Vizio D, Morello M, Sotgia F, Pestell RG, Freeman MR, Lisanti MP. An absence of stromal caveolin-1 is associated with advanced prostate cancer, metastatic disease and epithelial Akt activation. Cell Cycle 2009; 8: 2420-2424.
44 Di Vizio D, Morello M, Dudley AC, Schow PW, Adam RM, Morley S, Mulholland D, Rotinen M, Hager MH, Insabato L, Moses MA, Demichelis F, Lisanti MP, Wu H, Klagsbrun M, Bhowmick NA, Rubin MA, D'Souza-Schorey C, Freeman MR. Large oncosomes in human prostate cancer tissues and in the circulation of mice with metastatic disease. Am J Pathol 2012; 181: 1573-1584.
45 Dian D, Heublein S, Wiest I, Barthell L, Friese K, Jeschke U. Significance of the tumor protease cathepsin D for the biology of breast cancer. Histol Histopathol 2014; 29: 433-438.
46 Dittmann K, Mayer C, Kehlbach R, Rodemann HP. Radiation-induced caveolin-1 associated EGFR internalization is linked with nuclear EGFR transport and activation of DNA-PK. Mol Cancer 2008; 7: 69.
47 Drab M, Verkade P, Elger M, Kasper M, Lohn M, Lauterbach B, Menne J, Lindschau C, Mende F, Luft FC, Schedl A, Haller H, Kurzchalia TV. Loss of caveolae, vascular dysfunction, and pulmonary defects in caveolin-1 gene-disrupted mice. Science 2001; 293: 2449-2452.
48 Duregon E, Senetta R, Pittaro A, Verdun di Cantogno L, Stella G, De Blasi P, Zorzetto M, Mantovani C, Papotti M, Cassoni P. CAVEOLIN-1 expression in brain metastasis from lung cancer predicts worse outcome and radioresistance, irrespective of tumor histotype. Oncotarget 2015; 6: 29626-29636.
49 Engelman JA, Wykoff CC, Yasuhara S, Song KS, Okamoto T, Lisanti MP. Recombinant expression of caveolin-1 in oncogenically transformed cells abrogates anchorage-independent growth. J Biol Chem 1997; 272: 16374-16381.
50 Engelman JA, Zhang XL, Galbiati F, Lisanti MP. Chromosomal localization, genomic organization, and developmental expression of the murine caveolin gene family (Cav-

1, -2, and -3). Cav-1 and Cav-2 genes map to a known tumor suppressor locus (6-A2/7q31). FEBS Lett 1998; 429: 330-336.
51 Epstein JI, Allsbrook WC, Jr., Amin MB, Egevad LL, Committee IG. The 2005 International Society of Urological Pathology (ISUP) Consensus Conference on Gleason Grading of Prostatic Carcinoma. Am J Surg Pathol 2005; 29: 1228-1242.
52 Eto M, Bennouna J, Hunter OC, Hershberger PA, Kanto T, Johnson CS, Lotze MT, Amoscato AA. C16 ceramide accumulates following androgen ablation in LNCaP prostate cancer cells. Prostate 2003; 57: 66-79.
53 Fang K, Fu W, Beardsley AR, Sun X, Lisanti MP, Liu J. Overexpression of caveolin-1 inhibits endothelial cell proliferation by arresting the cell cycle at G0/G1 phase. Cell Cycle 2007; 6: 199-204.
54 Ferlay J, Colombet M, Soerjomataram I, Mathers C, Parkin DM, Pineros M, Znaor A, Bray F. Estimating the global cancer incidence and mortality in 2018: GLOBOCAN sources and methods. Int J Cancer 2019; 144: 1941-1953.
55 Fook-Alves VL, de Oliveira MB, Zanatta DB, Strauss BE, Colleoni GW. TP53 Regulated Inhibitor of Apoptosis 1 (TRIAP1) stable silencing increases late apoptosis by upregulation of caspase 9 and APAF1 in RPMI8226 multiple myeloma cell line. Biochim Biophys Acta 2016; 1862: 1105-1110.
56 Frank PG, Pavlides S, Cheung MW, Daumer K, Lisanti MP. Role of caveolin-1 in the regulation of lipoprotein metabolism. Am J Physiol Cell Physiol 2008; 295: C242-248.
57 Galbiati F, Volonte D, Liu J, Capozza F, Frank PG, Zhu L, Pestell RG, Lisanti MP. Caveolin-1 expression negatively regulates cell cycle progression by inducing G(0)/G(1) arrest via a p53/p21(WAF1/Cip1)-dependent mechanism. Mol Biol Cell 2001; 12: 2229-2244.
58 Garcia-Barros M, Paris F, Cordon-Cardo C, Lyden D, Rafii S, Haimovitz-Friedman A, Fuks Z, Kolesnick R. Tumor response to radiotherapy regulated by endothelial cell apoptosis. Science 2003; 300: 1155-1159.
59 Garcia-Cardena G, Fan R, Stern DF, Liu J, Sessa WC. Endothelial nitric oxide synthase is regulated by tyrosine phosphorylation and interacts with caveolin-1. J Biol Chem 1996; 271: 27237-27240.
60 Garcia-Cardena G, Martasek P, Masters BS, Skidd PM, Couet J, Li S, Lisanti MP, Sessa WC. Dissecting the interaction between nitric oxide synthase (NOS) and caveolin. Functional significance of the nos caveolin binding domain in vivo. J Biol Chem 1997; 272: 25437-25440.
61 Ghafoori P, Marks LB, Vujaskovic Z, Kelsey CR. Radiation-induced lung injury. Assessment, management, and prevention. Oncology (Williston Park) 2008; 22: 37-47; discussion 52-33.
62 Goetz JG, Minguet S, Navarro-Lerida I, Lazcano JJ, Samaniego R, Calvo E, Tello M, Osteso-Ibanez T, Pellinen T, Echarri A, Cerezo A, Klein-Szanto AJ, Garcia R, Keely PJ, Sanchez-Mateos P, Cukierman E, Del Pozo MA. Biomechanical remodeling of the microenvironment by stromal caveolin-1 favors tumor invasion and metastasis. Cell 2011; 146: 148-163.
63 Hanahan D, Weinberg RA. The hallmarks of cancer. Cell 2000; 100: 57-70.
64 Hanahan D, Weinberg RA. Hallmarks of cancer: the next generation. Cell 2011; 144: 646-674.
65 Hannun YA, Linardic CM. Sphingolipid breakdown products: anti-proliferative and tumor-suppressor lipids. Biochim Biophys Acta 1993; 1154: 223-236.
66 Hannun YA. The sphingomyelin cycle and the second messenger function of ceramide. J Biol Chem 1994; 269: 3125-3128.
67 Hannun YA, Luberto C. Ceramide in the eukaryotic stress response. Trends Cell Biol 2000; 10: 73-80.

68 Hart PC, Ratti BA, Mao M, Ansenberger-Fricano K, Shajahan-Haq AN, Tyner AL, Minshall RD, Bonini MG. Caveolin-1 regulates cancer cell metabolism via scavenging Nrf2 and suppressing MnSOD-driven glycolysis. Oncotarget 2016; 7: 308-322.
69 Hayashi K, Matsuda S, Machida K, Yamamoto T, Fukuda Y, Nimura Y, Hayakawa T, Hamaguchi M. Invasion activating caveolin-1 mutation in human scirrhous breast cancers. Cancer Res 2001; 61: 2361-2364.
70 Hehlgans S, Eke I, Storch K, Haase M, Baretton GB, Cordes N. Caveolin-1 mediated radioresistance of 3D grown pancreatic cancer cells. Radiother Oncol 2009; 92: 362-370.
71 Hehlgans S, Cordes N. Caveolin-1: an essential modulator of cancer cell radio-and chemoresistance. Am J Cancer Res 2011; 1: 521-530.
72 Hill MM, Bastiani M, Luetterforst R, Kirkham M, Kirkham A, Nixon SJ, Walser P, Abankwa D, Oorschot VM, Martin S, Hancock JF, Parton RG. PTRF-Cavin, a conserved cytoplasmic protein required for caveola formation and function. Cell 2008; 132: 113-124.
73 Ho CC, Kuo SH, Huang PH, Huang HY, Yang CH, Yang PC. Caveolin-1 expression is significantly associated with drug resistance and poor prognosis in advanced non-small cell lung cancer patients treated with gemcitabine-based chemotherapy. Lung Cancer 2008; 59: 105-110.
74 Holler V, Buard V, Gaugler MH, Guipaud O, Baudelin C, Sache A, Perez Mdel R, Squiban C, Tamarat R, Milliat F, Benderitter M. Pravastatin limits radiation-induced vascular dysfunction in the skin. J Invest Dermatol 2009; 129: 1280-1291.
75 Hossain MB, Shifat R, Johnson DG, Bedford MT, Gabrusiewicz KR, Cortes-Santiago N, Luo X, Lu Z, Ezhilarasan R, Sulman EP, Jiang H, Li SS, Lang FF, Tyler J, Hung MC, Fueyo J, Gomez-Manzano C. TIE2-mediated tyrosine phosphorylation of H4 regulates DNA damage response by recruiting ABL1. Sci Adv 2016; 2: e1501290.
76 Hossain MB, Shifat R, Li J, Luo X, Hess KR, Rivera-Molina Y, Puerta Martinez F, Jiang H, Lang FF, Hung MC, Fueyo J, Gomez-Manzano C. TIE2 Associates with Caveolae and Regulates Caveolin-1 To Promote Their Nuclear Translocation. Mol Cell Biol 2017; 37.
77 Hu H, Sun L, Guo C, Liu Q, Zhou Z, Peng L, Pan J, Yu L, Lou J, Yang Z, Zhao P, Ran Y. Tumor cell-microenvironment interaction models coupled with clinical validation reveal CCL2 and SNCG as two predictors of colorectal cancer hepatic metastasis. Clin Cancer Res 2009; 15: 5485-5493.
78 Jain RK. Molecular regulation of vessel maturation. Nat Med 2003; 9: 685-693.
79 Jung K, Heishi T, Khan OF, Kowalski PS, Incio J, Rahbari NN, Chung E, Clark JW, Willett CG, Luster AD, Yun SH, Langer R, Anderson DG, Padera TP, Jain RK, Fukumura D. Ly6Clo monocytes drive immunosuppression and confer resistance to anti-VEGFR2 cancer therapy. J Clin Invest 2017; 127: 3039-3051.
80 Karahatay S, Thomas K, Koybasi S, Senkal CE, Elojeimy S, Liu X, Bielawski J, Day TA, Gillespie MB, Sinha D, Norris JS, Hannun YA, Ogretmen B. Clinical relevance of ceramide metabolism in the pathogenesis of human head and neck squamous cell carcinoma (HNSCC): attenuation of C(18)-ceramide in HNSCC tumors correlates with lymphovascular invasion and nodal metastasis. Cancer Lett 2007; 256: 101-111.
81 Karam JA, Lotan Y, Roehrborn CG, Ashfaq R, Karakiewicz PI, Shariat SF. Caveolin-1 overexpression is associated with aggressive prostate cancer recurrence. Prostate 2007; 67: 614-622.
82 Kawamorita N, Saito S, Ishidoya S, Ito A, Saito H, Kato M, Arai Y. Radical prostatectomy for high-risk prostate cancer: biochemical outcome. Int J Urol 2009; 16: 733-738.
83 Ketteler J, Klein D. Caveolin-1, cancer and therapy resistance. Int J Cancer 2018; 143: 2092-2104.

84 Klein D, Schmitz T, Verhelst V, Panic A, Schenck M, Reis H, Drab M, Sak A, Herskind C, Maier P, Jendrossek V. Endothelial Caveolin-1 regulates the radiation response of epithelial prostate tumors. Oncogenesis 2015; 4: e148.
85 Klein D, Schmetter A, Imsak R, Wirsdorfer F, Unger K, Jastrow H, Stuschke M, Jendrossek V. Therapy with Multipotent Mesenchymal Stromal Cells Protects Lungs from Radiation-Induced Injury and Reduces the Risk of Lung Metastasis. Antioxid Redox Signal 2016; 24: 53-69.
86 Klein D, Steens J, Wiesemann A, Schulz F, Kaschani F, Rock K, Yamaguchi M, Wirsdorfer F, Kaiser M, Fischer JW, Stuschke M, Jendrossek V. Mesenchymal Stem Cell Therapy Protects Lungs from Radiation-Induced Endothelial Cell Loss by Restoring Superoxide Dismutase 1 Expression. Antioxid Redox Signal 2017; 26: 563-582.
87 Klein D. The Tumor Vascular Endothelium as Decision Maker in Cancer Therapy. Front Oncol 2018; 8: 367.
88 Koleske AJ, Baltimore D, Lisanti MP. Reduction of caveolin and caveolae in oncogenically transformed cells. Proc Natl Acad Sci U S A 1995; 92: 1381-1385.
89 Kolesnick RN, Kronke M. Regulation of ceramide production and apoptosis. Annu Rev Physiol 1998; 60: 643-665.
90 Korpela E, Liu SK. Endothelial perturbations and therapeutic strategies in normal tissue radiation damage. Radiat Oncol 2014; 9: 266.
91 Kuo SR, Tahir SA, Park S, Thompson TC, Coffield S, Frankel AE, Liu JS. Anti-caveolin-1 antibodies as anti-prostate cancer therapeutics. Hybridoma (Larchmt) 2012; 31: 77-86.
92 Lajoie P, Nabi IR. Regulation of raft-dependent endocytosis. J Cell Mol Med 2007; 11: 644-653.
93 Lazennec G, Richmond A. Chemokines and chemokine receptors: new insights into cancer-related inflammation. Trends Mol Med 2010; 16: 133-144.
94 Lee H, Woodman SE, Engelman JA, Volonte D, Galbiati F, Kaufman HL, Lublin DM, Lisanti MP. Palmitoylation of caveolin-1 at a single site (Cys-156) controls its coupling to the c-Src tyrosine kinase: targeting of dually acylated molecules (GPI-linked, transmembrane, or cytoplasmic) to caveolae effectively uncouples c-Src and caveolin-1 (TYR-14). J Biol Chem 2001; 276: 35150-35158.
95 Li S, Couet J, Lisanti MP. Src tyrosine kinases, Galpha subunits, and H-Ras share a common membrane-anchored scaffolding protein, caveolin. Caveolin binding negatively regulates the auto-activation of Src tyrosine kinases. J Biol Chem 1996; 271: 29182-29190.
96 Li S, Seitz R, Lisanti MP. Phosphorylation of caveolin by src tyrosine kinases. The alpha-isoform of caveolin is selectively phosphorylated by v-Src in vivo. J Biol Chem 1996; 271: 3863-3868.
97 Li Y, Tang X, He Q, Yang X, Ren X, Wen X, Zhang J, Wang Y, Liu N, Ma J. Overexpression of Mitochondria Mediator Gene TRIAP1 by miR-320b Loss Is Associated with Progression in Nasopharyngeal Carcinoma. PLoS Genet 2016; 12: e1006183.
98 Li Z, Wang N, Huang C, Bao Y, Jiang Y, Zhu G. Downregulation of caveolin-1 increases the sensitivity of drug-resistant colorectal cancer HCT116 cells to 5-fluorouracil. Oncol Lett 2017; 13: 483-487.
99 Liao JK. Linking endothelial dysfunction with endothelial cell activation. J Clin Invest 2013; 123: 540-541.
100 Liauw SL, Connell PP, Weichselbaum RR. New paradigms and future challenges in radiation oncology: an update of biological targets and technology. Sci Transl Med 2013; 5: 173sr172.
101 Lim SY, Yuzhalin AE, Gordon-Weeks AN, Muschel RJ. Targeting the CCL2-CCR2 signaling axis in cancer metastasis. Oncotarget 2016; 7: 28697-28710.

102 Lin CF, Chen CL, Lin YS. Ceramide in apoptotic signaling and anticancer therapy. Curr Med Chem 2006; 13: 1609-1616.
103 Lin MI, Yu J, Murata T, Sessa WC. Caveolin-1-deficient mice have increased tumor microvascular permeability, angiogenesis, and growth. Cancer Res 2007; 67: 2849-2856.
104 Lingwood D, Simons K. Lipid rafts as a membrane-organizing principle. Science 2010; 327: 46-50.
105 Lisanti MP, Scherer PE, Tang Z, Sargiacomo M. Caveolae, caveolin and caveolin-rich membrane domains: a signalling hypothesis. Trends Cell Biol 1994; 4: 231-235.
106 Liu P, Qi X, Bian C, Yang F, Lin X, Zhou S, Xie C, Zhao X, Yi T. MicroRNA-18a inhibits ovarian cancer growth via directly targeting TRIAP1 and IPMK. Oncol Lett 2017; 13: 4039-4046.
107 Lorusso G, Ruegg C. The tumor microenvironment and its contribution to tumor evolution toward metastasis. Histochem Cell Biol 2008; 130: 1091-1103.
108 Marathe S, Schissel SL, Yellin MJ, Beatini N, Mintzer R, Williams KJ, Tabas I. Human vascular endothelial cells are a rich and regulatable source of secretory sphingomyelinase. Implications for early atherogenesis and ceramide-mediated cell signaling. J Biol Chem 1998; 273: 4081-4088.
109 Martinez-Outschoorn UE, Pavlides S, Whitaker-Menezes D, Daumer KM, Milliman JN, Chiavarina B, Migneco G, Witkiewicz AK, Martinez-Cantarin MP, Flomenberg N, Howell A, Pestell RG, Lisanti MP, Sotgia F. Tumor cells induce the cancer associated fibroblast phenotype via caveolin-1 degradation: implications for breast cancer and DCIS therapy with autophagy inhibitors. Cell Cycle 2010; 9: 2423-2433.
110 Martinez-Outschoorn UE, Lin Z, Ko YH, Goldberg AF, Flomenberg N, Wang C, Pavlides S, Pestell RG, Howell A, Sotgia F, Lisanti MP. Understanding the metabolic basis of drug resistance: therapeutic induction of the Warburg effect kills cancer cells. Cell Cycle 2011; 10: 2521-2528.
111 Martinez-Outschoorn UE, Lisanti MP, Sotgia F. Catabolic cancer-associated fibroblasts transfer energy and biomass to anabolic cancer cells, fueling tumor growth. Semin Cancer Biol 2014; 25: 47-60.
112 Martinez-Outschoorn UE, Sotgia F, Lisanti MP. Caveolae and signalling in cancer. Nat Rev Cancer 2015; 15: 225-237.
113 Meshulam T, Simard JR, Wharton J, Hamilton JA, Pilch PF. Role of caveolin-1 and cholesterol in transmembrane fatty acid movement. Biochemistry 2006; 45: 2882-2893.
114 Meyer C, Liu Y, Kaul A, Peipe I, Dooley S. Caveolin-1 abrogates TGF-beta mediated hepatocyte apoptosis. Cell Death Dis 2013; 4: e466.
115 Mladenov E, Magin S, Soni A, Iliakis G. DNA double-strand break repair as determinant of cellular radiosensitivity to killing and target in radiation therapy. Front Oncol 2013; 3: 113.
116 Murata M, Peranen J, Schreiner R, Wieland F, Kurzchalia TV, Simons K. VIP21/caveolin is a cholesterol-binding protein. Proc Natl Acad Sci U S A 1995; 92: 10339-10343.
117 Naumov GN, Folkman J, Straume O. Tumor dormancy due to failure of angiogenesis: role of the microenvironment. Clin Exp Metastasis 2009; 26: 51-60.
118 Niaudet C, Bonnaud S, Guillonneau M, Gouard S, Gaugler MH, Dutoit S, Ripoche N, Dubois N, Trichet V, Corre I, Paris F. Plasma membrane reorganization links acid sphingomyelinase/ceramide to p38 MAPK pathways in endothelial cells apoptosis. Cell Signal 2017; 33: 10-21.
119 Noel M, O'Reilly EM, Wolpin BM, Ryan DP, Bullock AJ, Britten CD, Linehan DC, Belt BA, Gamelin EC, Ganguly B, Yin D, Joh T, Jacobs IA, Taylor CT, Lowery MA. Phase 1b study of a small molecule antagonist of human chemokine (C-C motif) receptor 2 (PF-04136309) in combination with nab-paclitaxel/gemcitabine in first-line treatment of metastatic pancreatic ductal adenocarcinoma. Invest New Drugs 2019.

120 Ogretmen B, Hannun YA. Biologically active sphingolipids in cancer pathogenesis and treatment. Nat Rev Cancer 2004; 4: 604-616.
121 Ortiz R, Diaz J, Diaz N, Lobos-Gonzalez L, Cardenas A, Contreras P, Diaz MI, Otte E, Cooper-White J, Torres V, Leyton L, Quest AF. Extracellular matrix-specific Caveolin-1 phosphorylation on tyrosine 14 is linked to augmented melanoma metastasis but not tumorigenesis. Oncotarget 2016; 7: 40571-40593.
122 Panic A, Ketteler J, Reis H, Sak A, Herskind C, Maier P, Rubben H, Jendrossek V, Klein D. Progression-related loss of stromal Caveolin 1 levels fosters the growth of human PC3 xenografts and mediates radiation resistance. Sci Rep 2017; 7: 41138.
123 Parat MO, Stachowicz RZ, Fox PL. Oxidative stress inhibits caveolin-1 palmitoylation and trafficking in endothelial cells. Biochem J 2002; 361: 681-688.
124 Parat MO, Anand-Apte B, Fox PL. Differential caveolin-1 polarization in endothelial cells during migration in two and three dimensions. Mol Biol Cell 2003; 14: 3156-3168.
125 Paris F, Fuks Z, Kang A, Capodieci P, Juan G, Ehleiter D, Haimovitz-Friedman A, Cordon-Cardo C, Kolesnick R. Endothelial apoptosis as the primary lesion initiating intestinal radiation damage in mice. Science 2001; 293: 293-297.
126 Park J, Bae E, Lee C, Yoon SS, Chae YS, Ahn KS, Won NH. RNA interference-directed caveolin-1 knockdown sensitizes SN12CPM6 cells to doxorubicin-induced apoptosis and reduces lung metastasis. Tumour Biol 2010; 31: 643-650.
127 Park WR, Nakamura Y. p53CSV, a novel p53-inducible gene involved in the p53-dependent cell-survival pathway. Cancer Res 2005; 65: 1197-1206.
128 Parton RG, Simons K. The multiple faces of caveolae. Nat Rev Mol Cell Biol 2007; 8: 185-194.
129 Parton RG, del Pozo MA. Caveolae as plasma membrane sensors, protectors and organizers. Nat Rev Mol Cell Biol 2013; 14: 98-112.
130 Paulino AC, Constine LS, Rubin P, Williams JP. Normal tissue development, homeostasis, senescence, and the sensitivity to radiation injury across the age spectrum. Semin Radiat Oncol 2010; 20: 12-20.
131 Pavlides S, Whitaker-Menezes D, Castello-Cros R, Flomenberg N, Witkiewicz AK, Frank PG, Casimiro MC, Wang C, Fortina P, Addya S, Pestell RG, Martinez-Outschoorn UE, Sotgia F, Lisanti MP. The reverse Warburg effect: aerobic glycolysis in cancer associated fibroblasts and the tumor stroma. Cell Cycle 2009; 8: 3984-4001.
132 Perry DK, Carton J, Shah AK, Meredith F, Uhlinger DJ, Hannun YA. Serine palmitoyltransferase regulates de novo ceramide generation during etoposide-induced apoptosis. J Biol Chem 2000; 275: 9078-9084.
133 Peterson TE, Poppa V, Ueba H, Wu A, Yan C, Berk BC. Opposing effects of reactive oxygen species and cholesterol on endothelial nitric oxide synthase and endothelial cell caveolae. Circ Res 1999; 85: 29-37.
134 Potente M, Gerhardt H, Carmeliet P. Basic and therapeutic aspects of angiogenesis. Cell 2011; 146: 873-887.
135 Pranjol MZ, Gutowski N, Hannemann M, Whatmore J. The Potential Role of the Proteases Cathepsin D and Cathepsin L in the Progression and Metastasis of Epithelial Ovarian Cancer. Biomolecules 2015; 5: 3260-3279.
136 Quail DF, Joyce JA. Microenvironmental regulation of tumor progression and metastasis. Nat Med 2013; 19: 1423-1437.
137 Quest AF, Leyton L, Parraga M. Caveolins, caveolae, and lipid rafts in cellular transport, signaling, and disease. Biochem Cell Biol 2004; 82: 129-144.
138 Rannou E, Francois A, Toullec A, Guipaud O, Buard V, Tarlet G, Mintet E, Jaillet C, Iruela-Arispe ML, Benderitter M, Sabourin JC, Milliat F. In vivo evidence for an endothelium-dependent mechanism in radiation-induced normal tissue injury. Sci Rep 2015; 5: 15738.
139 Rawla P. Epidemiology of Prostate Cancer. World J Oncol 2019; 10: 63-89.

140 Razani B, Engelman JA, Wang XB, Schubert W, Zhang XL, Marks CB, Macaluso F, Russell RG, Li M, Pestell RG, Di Vizio D, Hou H, Jr., Kneitz B, Lagaud G, Christ GJ, Edelmann W, Lisanti MP. Caveolin-1 null mice are viable but show evidence of hyperproliferative and vascular abnormalities. J Biol Chem 2001; 276: 38121-38138.
141 Razani B, Schlegel A, Liu J, Lisanti MP. Caveolin-1, a putative tumour suppressor gene. Biochem Soc Trans 2001; 29: 494-499.
142 Rodel F, Capalbo G, Rodel C, Weiss C. Caveolin-1 as a prognostic marker for local control after preoperative chemoradiation therapy in rectal cancer. Int J Radiat Oncol Biol Phys 2009; 73: 846-852.
143 Rollins BJ. Chemokines. Blood 1997; 90: 909-928.
144 Rothberg KG, Heuser JE, Donzell WC, Ying YS, Glenney JR, Anderson RG. Caveolin, a protein component of caveolae membrane coats. Cell 1992; 68: 673-682.
145 Rothkamm K, Lobrich M. Evidence for a lack of DNA double-strand break repair in human cells exposed to very low x-ray doses. Proc Natl Acad Sci U S A 2003; 100: 5057-5062.
146 Rube CE, Uthe D, Wilfert F, Ludwig D, Yang K, Konig J, Palm J, Schuck A, Willich N, Remberger K, Rube C. The bronchiolar epithelium as a prominent source of pro-inflammatory cytokines after lung irradiation. Int J Radiat Oncol Biol Phys 2005; 61: 1482-1492.
147 Saddoughi SA, Song P, Ogretmen B. Roles of bioactive sphingolipids in cancer biology and therapeutics. Subcell Biochem 2008; 49: 413-440.
148 Sappino AP, Schurch W, Gabbiani G. Differentiation repertoire of fibroblastic cells: expression of cytoskeletal proteins as marker of phenotypic modulations. Lab Invest 1990; 63: 144-161.
149 Sassa T, Suto S, Okayasu Y, Kihara A. A shift in sphingolipid composition from C24 to C16 increases susceptibility to apoptosis in HeLa cells. Biochim Biophys Acta 2012; 1821: 1031-1037.
150 Scherer PE, Lewis RY, Volonte D, Engelman JA, Galbiati F, Couet J, Kohtz DS, van Donselaar E, Peters P, Lisanti MP. Cell-type and tissue-specific expression of caveolin-2. Caveolins 1 and 2 co-localize and form a stable hetero-oligomeric complex in vivo. J Biol Chem 1997; 272: 29337-29346.
151 Senkal CE, Ponnusamy S, Bielawski J, Hannun YA, Ogretmen B. Antiapoptotic roles of ceramide-synthase-6-generated C16-ceramide via selective regulation of the ATF6/CHOP arm of ER-stress-response pathways. FASEB J 2010; 24: 296-308.
152 Sherborne AL, Davidson PR, Yu K, Nakamura AO, Rashid M, Nakamura JL. Mutational Analysis of Ionizing Radiation Induced Neoplasms. Cell Rep 2015; 12: 1915-1926.
153 Sloan EK, Ciocca DR, Pouliot N, Natoli A, Restall C, Henderson MA, Fanelli MA, Cuello-Carrion FD, Gago FE, Anderson RL. Stromal cell expression of caveolin-1 predicts outcome in breast cancer. Am J Pathol 2009; 174: 2035-2043.
154 Smart EJ, Graf GA, McNiven MA, Sessa WC, Engelman JA, Scherer PE, Okamoto T, Lisanti MP. Caveolins, liquid-ordered domains, and signal transduction. Mol Cell Biol 1999; 19: 7289-7304.
155 Sotgia F, Martinez-Outschoorn UE, Pavlides S, Howell A, Pestell RG, Lisanti MP. Understanding the Warburg effect and the prognostic value of stromal caveolin-1 as a marker of a lethal tumor microenvironment. Breast Cancer Res 2011; 13: 213.
156 Sotgia F, Martinez-Outschoorn UE, Howell A, Pestell RG, Pavlides S, Lisanti MP. Caveolin-1 and cancer metabolism in the tumor microenvironment: markers, models, and mechanisms. Annu Rev Pathol 2012; 7: 423-467.
157 Spiegel S, Foster D, Kolesnick R. Signal transduction through lipid second messengers. Curr Opin Cell Biol 1996; 8: 159-167.
158 Spiegel S, Merrill AH, Jr. Sphingolipid metabolism and cell growth regulation. FASEB J 1996; 10: 1388-1397.

159 Steyers CM, 3rd, Miller FJ, Jr. Endothelial dysfunction in chronic inflammatory diseases. Int J Mol Sci 2014; 15: 11324-11349.
160 Sun Y, Hu G, Zhang X, Minshall RD. Phosphorylation of caveolin-1 regulates oxidant-induced pulmonary vascular permeability via paracellular and transcellular pathways. Circ Res 2009; 105: 676-685, 615 p following 685.
161 Svensson S, Abrahamsson A, Rodriguez GV, Olsson AK, Jensen L, Cao Y, Dabrosin C. CCL2 and CCL5 Are Novel Therapeutic Targets for Estrogen-Dependent Breast Cancer. Clin Cancer Res 2015; 21: 3794-3805.
162 Tahir SA, Yang G, Ebara S, Timme TL, Satoh T, Li L, Goltsov A, Ittmann M, Morrisett JD, Thompson TC. Secreted caveolin-1 stimulates cell survival/clonal growth and contributes to metastasis in androgen-insensitive prostate cancer. Cancer Res 2001; 61: 3882-3885.
163 Tahir SA, Park S, Thompson TC. Caveolin-1 regulates VEGF-stimulated angiogenic activities in prostate cancer and endothelial cells. Cancer Biol Ther 2009; 8: 2286-2296.
164 Tahir SA, Kurosaka S, Tanimoto R, Goltsov AA, Park S, Thompson TC. Serum caveolin-1, a biomarker of drug response and therapeutic target in prostate cancer models. Cancer Biol Ther 2013; 14: 117-126.
165 Tanase CP, Dima S, Mihai M, Raducan E, Nicolescu MI, Albulescu L, Voiculescu B, Dumitrascu T, Cruceru LM, Leabu M, Popescu I, Hinescu ME. Caveolin-1 overexpression correlates with tumour progression markers in pancreatic ductal adenocarcinoma. J Mol Histol 2009; 40: 23-29.
166 Tang Z, Scherer PE, Okamoto T, Song K, Chu C, Kohtz DS, Nishimoto I, Lodish HF, Lisanti MP. Molecular cloning of caveolin-3, a novel member of the caveolin gene family expressed predominantly in muscle. J Biol Chem 1996; 271: 2255-2261.
167 Tatarov O, Mitchell TJ, Seywright M, Leung HY, Brunton VG, Edwards J. SRC family kinase activity is up-regulated in hormone-refractory prostate cancer. Clin Cancer Res 2009; 15: 3540-3549.
168 Thompson TC, Tahir SA, Li L, Watanabe M, Naruishi K, Yang G, Kadmon D, Logothetis CJ, Troncoso P, Ren C, Goltsov A, Park S. The role of caveolin-1 in prostate cancer: clinical implications. Prostate Cancer Prostatic Dis 2010; 13: 6-11.
169 Torres VA, Tapia JC, Rodriguez DA, Parraga M, Lisboa P, Montoya M, Leyton L, Quest AF. Caveolin-1 controls cell proliferation and cell death by suppressing expression of the inhibitor of apoptosis protein survivin. J Cell Sci 2006; 119: 1812-1823.
170 Tuxhorn JA, Ayala GE, Smith MJ, Smith VC, Dang TD, Rowley DR. Reactive stroma in human prostate cancer: induction of myofibroblast phenotype and extracellular matrix remodeling. Clin Cancer Res 2002; 8: 2912-2923.
171 Varkaris A, Katsiampoura AD, Araujo JC, Gallick GE, Corn PG. Src signaling pathways in prostate cancer. Cancer Metastasis Rev 2014; 33: 595-606.
172 Vilalta M, Rafat M, Giaccia AJ, Graves EE. Recruitment of circulating breast cancer cells is stimulated by radiotherapy. Cell Rep 2014; 8: 402-409.
173 Wang R, He W, Li Z, Chang W, Xin Y, Huang T. Caveolin-1 functions as a key regulator of 17beta-estradiol-mediated autophagy and apoptosis in BT474 breast cancer cells. Int J Mol Med 2014; 34: 822-827.
174 Wang Z, Dabrosin C, Yin X, Fuster MM, Arreola A, Rathmell WK, Generali D, Nagaraju GP, El-Rayes B, Ribatti D, Chen YC, Honoki K, Fujii H, Georgakilas AG, Nowsheen S, Amedei A, Niccolai E, Amin A, Ashraf SS, Helferich B, Yang X, Guha G, Bhakta D, Ciriolo MR, Aquilano K, Chen S, Halicka D, Mohammed SI, Azmi AS, Bilsland A, Keith WN, Jensen LD. Broad targeting of angiogenesis for cancer prevention and therapy. Semin Cancer Biol 2015; 35 Suppl: S224-S243.
175 Watanabe M, Yang G, Cao G, Tahir SA, Naruishi K, Tabata K, Fattah EA, Rajagopalan K, Timme TL, Park S, Kurosaka S, Edamura K, Tanimoto R, Demayo FJ, Goltsov AA, Thompson TC. Functional analysis of secreted caveolin-1 in mouse models of prostate cancer progression. Mol Cancer Res 2009; 7: 1446-1455.

176 White E. The role for autophagy in cancer. J Clin Invest 2015; 125: 42-46.
177 Wiechen K, Diatchenko L, Agoulnik A, Scharff KM, Schober H, Arlt K, Zhumabayeva B, Siebert PD, Dietel M, Schafer R, Sers C. Caveolin-1 is down-regulated in human ovarian carcinoma and acts as a candidate tumor suppressor gene. Am J Pathol 2001; 159: 1635-1643.
178 Wiechen K, Sers C, Agoulnik A, Arlt K, Dietel M, Schlag PM, Schneider U. Down-regulation of caveolin-1, a candidate tumor suppressor gene, in sarcomas. Am J Pathol 2001; 158: 833-839.
179 Williams TM, Hassan GS, Li J, Cohen AW, Medina F, Frank PG, Pestell RG, Di Vizio D, Loda M, Lisanti MP. Caveolin-1 promotes tumor progression in an autochthonous mouse model of prostate cancer: genetic ablation of Cav-1 delays advanced prostate tumor development in tramp mice. J Biol Chem 2005; 280: 25134-25145.
180 Williams TM, Lisanti MP. Caveolin-1 in oncogenic transformation, cancer, and metastasis. Am J Physiol Cell Physiol 2005; 288: C494-506.
181 Witkiewicz AK, Dasgupta A, Nguyen KH, Liu C, Kovatich AJ, Schwartz GF, Pestell RG, Sotgia F, Rui H, Lisanti MP. Stromal caveolin-1 levels predict early DCIS progression to invasive breast cancer. Cancer Biol Ther 2009; 8: 1071-1079.
182 Witkiewicz AK, Dasgupta A, Sotgia F, Mercier I, Pestell RG, Sabel M, Kleer CG, Brody JR, Lisanti MP. An absence of stromal caveolin-1 expression predicts early tumor recurrence and poor clinical outcome in human breast cancers. Am J Pathol 2009; 174: 2023-2034.
183 Wu KN, Queenan M, Brody JR, Potoczek M, Sotgia F, Lisanti MP, Witkiewicz AK. Loss of stromal caveolin-1 expression in malignant melanoma metastases predicts poor survival. Cell Cycle 2011; 10: 4250-4255.
184 Xu L, Qu X, Li H, Li C, Liu J, Zheng H, Liu Y. Src/caveolin-1-regulated EGFR activation antagonizes TRAIL-induced apoptosis in gastric cancer cells. Oncol Rep 2014; 32: 318-324.
185 Yamada E. The fine structure of the gall bladder epithelium of the mouse. J Biophys Biochem Cytol 1955; 1: 445-458.
186 Yang G, Timme TL, Frolov A, Wheeler TM, Thompson TC. Combined c-Myc and caveolin-1 expression in human prostate carcinoma predicts prostate carcinoma progression. Cancer 2005; 103: 1186-1194.
187 Zhang H, Su L, Muller S, Tighiouart M, Xu Z, Zhang X, Shin HJ, Hunt J, Sun SY, Shin DM, Chen ZG. Restoration of caveolin-1 expression suppresses growth and metastasis of head and neck squamous cell carcinoma. Br J Cancer 2008; 99: 1684-1694.
188 Zhang J, Patel L, Pienta KJ. CC chemokine ligand 2 (CCL2) promotes prostate cancer tumorigenesis and metastasis. Cytokine Growth Factor Rev 2010; 21: 41-48.
189 Zhao X, He Y, Gao J, Fan L, Li Z, Yang G, Chen H. Caveolin-1 expression level in cancer associated fibroblasts predicts outcome in gastric cancer. PLoS One 2013; 8: e59102.
190 Zhu H, Yue J, Pan Z, Wu H, Cheng Y, Lu H, Ren X, Yao M, Shen Z, Yang JM. Involvement of Caveolin-1 in repair of DNA damage through both homologous recombination and non-homologous end joining. PLoS One 2010; 5: e12055.
191 Zimnicka AM, Husain YS, Shajahan AN, Sverdlov M, Chaga O, Chen Z, Toth PT, Klomp J, Karginov AV, Tiruppathi C, Malik AB, Minshall RD. Src-dependent phosphorylation of caveolin-1 Tyr-14 promotes swelling and release of caveolae. Mol Biol Cell 2016; 27: 2090-2106.
192 Zlotnik A. Chemokines and cancer. Int J Cancer 2006; 119: 2026-2029.
193 Zlotnik A, Yoshie O, Nomiyama H. The chemokine and chemokine receptor superfamilies and their molecular evolution. Genome Biol 2006; 7: 243.
194 Zou M, Li Y, Xia S, Chu Q, Xiao X, Qiu H, Chen Y, Zheng Z, Liu F, Zhuang L, Yu S. Knockdown of CAVEOLIN-1 Sensitizes Human Basal-Like Triple-Negative Breast Cancer Cells to Radiation. Cell Physiol Biochem 2017; 44: 778-791.

195 Zundel W, Swiersz LM, Giaccia A. Caveolin 1-mediated regulation of receptor tyrosine kinase-associated phosphatidylinositol 3-kinase activity by ceramide. Mol Cell Biol 2000; 20: 1507-1514.

8. List of Abbreviations

ABL1	Abelson murine leukemia viral oncogene homolog 1
Akt	protein kinase B
APAF1	apoptotic protease activating factor 1
ASA	arylsulfatase A
ASMase	acid sphingomyelinase
ATP	adenosine triphosphate
BIN	bindarit
CAF	cancer associated fibroblast
CAV1	caveolin-1
CCL2	chemokine C-C motif ligand 2
CCR2	chemokine C-C motif receptor 2
CerS	ceramide synthase
CoA	co acetyl
CSD	caveolin-scaffolding domain
DNA-PK	DNA-dependent protein kinase
DRAM1	DNA damage-regulated autophagy modulator protein 1
DSB	double strand break
EC	endothelial cell
ECM	extracellular matrix
EGFR	epidermal growth factor receptor
EMT	epithelial mesenchymal transition
eNOS	endothelial nitric oxide synthase
FAK	focal adhesion kinase
FGF	fibroblasts growth factor
HNSCC	head and neck squamous cell carcinoma
HR	homologous recombination
HRAS	H-rat sarcoma
IAP	inhibitor of apoptosis
IL	interleukin
IR	ionizing radiation
LAMP2	lysosome-associated membrane protein 2
MAPK	mitogen-activated protein-kinase

MCP-1	monocyte chemoattractant protein-1
NHEJ	non-homologous end joining
NMRI	Naval medical research institute
NO	nitric oxide
NSCLC	non-small cell lung carcinoma
PI3K	phosphoinositide-3-kinase
PSA	prostate specific antigen
ROS	reactive oxygen species
RT	radiation therapy
SASP	senescence-associated secretory phenotype
SRC	non-receptor tyrosine kinase, sarcoma
TGFβ	transforming growth factor beta
TIE2	tyrosine kinase receptor, angiopoietin-1 receptor
TNF	tumor necrosis factor
TRIAP1	TP53-regulated inhibitor of apoptosis 1
VEGF	vascular-endothelial growth factor
WTI	whole thorax irradiation
α-SMA	alpha-smooth muscle actin

9. List of Figures

10. Acknowledgments

11. Curriculum Vitae

Der Lebenslauf ist in der Online-Version aufgrund des Datenschutzes nicht enthalten.

12. Declarations

Erklärung:

Hiermit erkläre ich, gem. § 6 Abs. (2) g) der Promotionsordnung der Fakultät für Biologie zur Erlangung der Dr. rer. nat., dass ich das Arbeitsgebiet, dem das Thema „Role of Caveolin-1 for modulating the radiation response in the context of tumor stroma interactions“ zuzuordnen ist, in Forschung und Lehre vertrete und den Antrag von Julia Ketteler befürworte und die Betreuung auch im Falle eines Weggangs, wenn nicht wichtige Gründe dem entgegenstehen, weiterführen werde.

Essen, den _____ _____

Unterschrift des Betreuers (Prof. oder PD) an der Universität Duisburg-Essen

Erklärung:

Hiermit erkläre ich, gem. § 7 Abs. (2) d) + f) der Promotionsordnung der Fakultät für Biologie zur Erlangung des Dr. rer. nat., dass ich die vorliegende Dissertation selbständig verfasst und mich keiner anderen als der angegebenen Hilfsmittel bedient, bei der Abfassung der Dissertation nur die angegeben Hilfsmittel benutzt und alle wörtlich oder inhaltlich übernommenen Stellen als solche gekennzeichnet habe.

Essen, den _____ _____

Unterschrift des/r Doktoranden/in

Erklärung:

Hiermit erkläre ich, gem. § 7 Abs. (2) e) + g) der Promotionsordnung der Fakultät für Biologie zur Erlangung des Dr. rer. nat., dass ich keine anderen Promotionen bzw. Promotionsversuche in der Vergangenheit durchgeführt habe und dass diese Arbeit von keiner anderen Fakultät/Fachbereich abgelehnt worden ist.

Essen, den _____ _____

Unterschrift des/r Doktoranden/in